Mesomorphic Organic Stable Radicals

Zhou Lu

Doctor of Philosophy

University of York

Chemistry

December 2014

Abstract

This thesis describes the preparation of new organic paramagnetic liquid crystals (PMLCs) and investigation of their properties. The radical components were introduced into the rigid core of the mesogens to enhance the short range intermolecular magnetic interactions. It was found that preparation of these mesogens is still challenging due to the difficulty in the molecular design and working with reactive radicals.

The concept of paramagnetic liquid crystals and the basic principles of EPR spectroscopy were introduced in Chapter 1. Some stable radicals which are suitable for the preparation of PMLCs are also discussed.

In Chapter 2, a new bent-shaped radical was obtained by 'click reaction'. However, it did not exhibit any liquid crystalline properties. It was found that it is not a suitable spin probe for rod-like liquid crystals possibly due to its bent core shape.

Chapter 3 describes the preparation of a series of new nitronyl and imino nitroxide radicals. Unfortunately, no liquid crystalline properties were observed. It was found that the preparation of nitronyl nitroxide is still challenging, and poor reproducibility and yield were obtained.

In Chapter 4, two new disk-shaped mesogens based on Blatter-type radical were prepared successfully. These mesogens shows the columnar phase over a large temperature range (around 100 °C). EPR study of these two mesogens suggested that the molecular alignment of these mesogens is poor in the applied magnetic field. Spin-singlet and spin-triplet dimerization were observed in these mesogens. However, no photoconductive properties were observed with these mesogens.

In Chapter 5, a new method to prepare Blatter-type radical was described and the mechanism of this reaction was investigated.

Table of Contents

List of Figures

List of Tables

Acknowledgements

I would like to thank my supervisors Dr. Victor Chechik and Dr. Isabel Saez for introducing me to the world of liquid crystals and EPR as well as their kind support during this project.

Many thanks to all the members of the Chechik group and the Materials group at the University of York. Special thanks to Dr. Robert Thatcher, Dr. Edwards Davis and Dr. Richard Mandle for helpful discussions and useful advices. Thanks Dr. Yury Gorbanev, Dr. Brendan Garrett, Andrew Grantham, Philip Groves and Sindhu Suravaram for proof reading my thesis. Thanks also to Chiara Baldasarri, Robert Smith, Thomas Newby and Kazim Naqvi for a good time together in the lab.

Thanks to Prof. Richard Bushby and Prof. Ben Whitaker for their work on alignement and ToF measurements of discotic mesogens.

Thanks to Dr. AnnMarie O'Donoghue and Jacob Grant for providing phenylhydrazine derivatives and the work on the formation of Blatter-type radical from Nitron.

I would also like to thank my friends in York and China for providing me a happy life beside chemistry during these four years.

Finally, specially thanks to my parents and my brother for all the love and support during my life.

Declaration

The work in this thesis was carried out by the author at the University of York, except where specific reference has been made to other sources. It has not been submitted for any other degree.

Chapter 1 Introduction

1.1 Liquid Crystals

Liquid crystals (LCs) are a state of matter intermediate between the conventional isotropic liquid and the crystal. The molecules in a crystal usually exhibit orientational and positional order, while the molecules in liquid diffuse randomly. The molecules in a liquid crystal are much like molecules in liquid in that they can diffuse but they maintain some degree of orientational or positional order (Figure 1.1).[1] Liquid crystal phases are commonly referred to as mesophases (*meso* comes from a Greek word meaning intermediate).

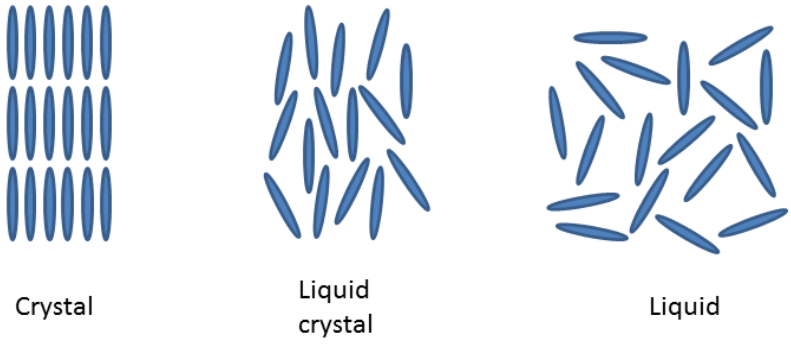

Figure 1.1 Molecular arrangement in crystal, liquid crystal and liquid.

LCs can be broadly divided into thermotropic LCs and lyotropic LCs. Thermotropic LCs change phase with temperature. When a thermotropic liquid crystal is cooled from the isotropic liquid phase, one or more mesophases can be observed. Lyotropic LCs are formed in a solvent at certain concentrations. In our work, we focus on the thermotropic LCs, which are discussed in more detail in this thesis.

1.1.1. Thermotropic LCs

When conventional crystals are heated to a certain temperature, the positional and orientational order is lost and molecules move and rotate freely in the liquid state. This temperature is called the melting point. However, for thermotropic LCs, this melting process is more complex. Upon heating, these materials lose some orientational and positional order to form stable mesophases first. At a specific higher temperature, an isotropic liquid is obtained. This temperature is called the clearing point.

1.1.1.1 Rod-like LCs (calamitic LCs)

The most common thermotropic LCs are rod-like LCs. The typical structure of these liquid crystals involves two main components (Figure 1.2). One is a rigid core, which normally consists of at least two rings (commonly phenyl rings but can also be alicyclic). These rings either connect to each other directly or by some linking groups such as an ester group. The other component is flexible chains, usually alkyl or alkoxyl chains, which are usually present at one, or both, ends of the core. In the condensed state, the rigid cores tend to pack together and flexible chains orient around the core, thereby driving the formation of mesophases.

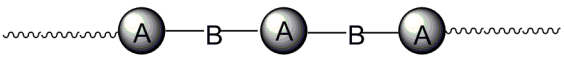

Figure 1.2 Schematic representation of typical structure of rod-like LCs; A represents ring structure, B represents linking group.

Rod-like liquid crystals usually form nematic and smectic phases. In a nematic phase (N), the molecules are arranged in a preferred direction (called the director, **n**). No positional order exists in this phase. In smectic phases, the molecules have orientational order and they also have positional order along one direction, creating layers. Different smectic phases have been

recognised, for example, smectic A (SmA) and smectic C (SmC). In the SmA phase, the molecules form layers with their long molecular axes perpendicular to the layer planes. In the SmC phase, the same layer structure is formed. However, molecules are tilted with respect to the layer planes (Figure 1.3).

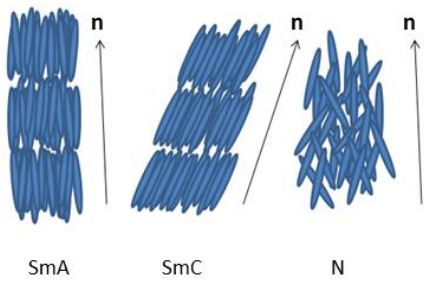

Figure 1.3 Schematic representation of SmA, SmC and N phases; arrows represent directors.

1.1.1.2 Disk-shaped LCs (discotic LCs)

Another kind of thermotropic LCs is formed by disk-shaped molecules. Like rod-like LCs, these molecules also have a rigid core and several (normally 6-9) flexible chains around the core. The overall shape of these molecules is more disk-shaped rather than rod-like. The first discotic LC **1.1** was prepared by S. Chandrasekhar and co-workers in 1977 (Figure 1.4).[2] They found that these materials exhibited liquid crystal phases in which the molecules are stacked into columns, and these columns formed 2D hexagonal arrangements (Figure 1.5). Following this discovery, the liquid crystal phases formed by these disk-shaped molecules attracted a lot of attention, followed by a vast number of publications.

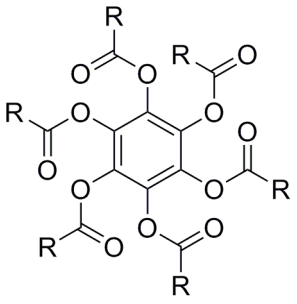

1.1

Figure 1.4 Structure of discotic liquid crystals prepared by S. Chandrasekhar and co-workers; R can vary from C_4H_9 to C_9H_{19}.[2]

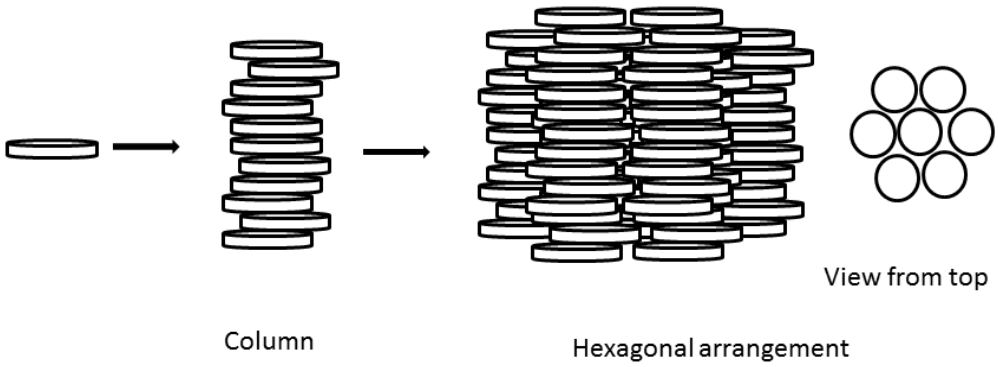

Figure 1.5 Schematic representation of discotic liquid crystals.

These disk-shaped molecules can show the discotic nematic phase (N_D) or columnar phases (Col). The molecular arrangement in N_D is similar to that of a rod-like nematic phase (Figure 1.6). The arrangement of molecules has orientational order but no long-range translational order. Two columnar phases are commonly observed with discotic liquid crystals, columnar hexagonal (Col_h) and columnar rectangular (Col_r) phase. In the Col_h phase, the columns form a hexagonal lattice; while in the Col_r phase, the molecular columns pack in a rectangular fashion (Figure 1.6).[3]

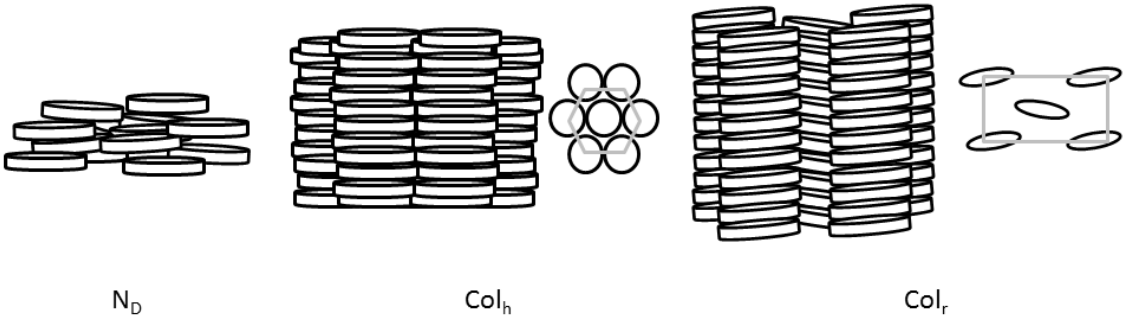

Figure 1.6 Schematic representation of N_D, Col_h and Col_r phases.

Liquid crystals can also form with other molecular architectures, such as those with a bent shape. The rigid cores of these molecules are bent-shaped rather than linear (Figure 1.7). These LCs are discussed in chapter 2.

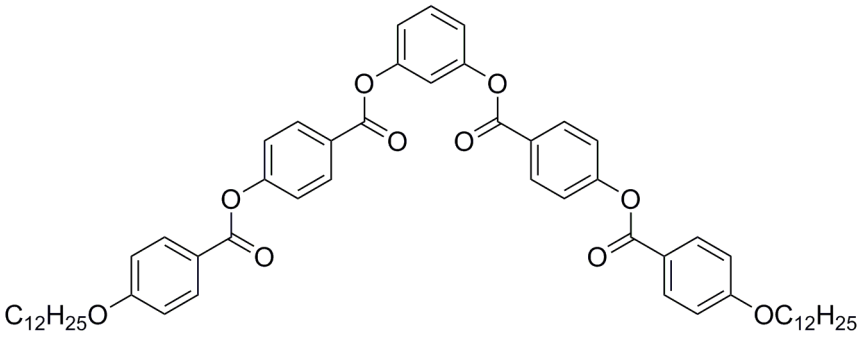

1.2

Figure 1.7 An example of bent-core liquid crystal.[4]

1.1.2 Lyotropic LCs

Unlike thermotropic LCs, lyotropic LCs are formed in a solution of amphiphilic compounds at certain concentrations and temperature. The molecules of lyotropic LCs usually contain two parts. One is hydrophilic and the other one is hydrophobic. In a very dilute solution, molecules diffuse randomly. However, when the concentration increases to a critical value, molecules will

assemble spontaneously to form micelles. In water, the hydrophobic parts of molecules will 'hide' in the core of the micelle, whereas the hydrophilic parts will be exposed to the aqueous solution. When the concentration is further increased, these self-assembled aggregates become ordered and exhibit liquid crystal phases (Figure 1.8).[5]

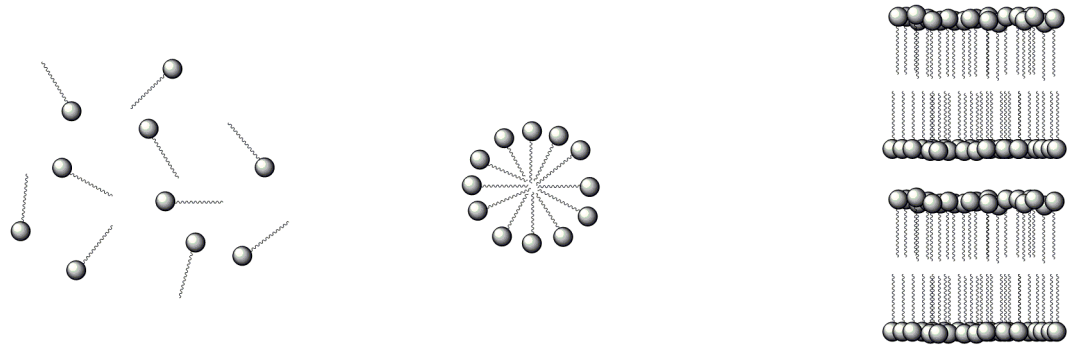

Figure 1.8 Schematic representation of lyotropic liquid crystal.

1.1.3 Paramagnetic LCs (PMLCs)

1.1.3.1 Magnetism and Paramagnetic LCs

Magnetism originates from the interactions between unpaired electrons. There are four types of these interactions: paramagnetic, ferromagnetic, antiferromagnetic and ferrimagnetic interactions.

In a paramagnetic interaction, the coupling interaction between electron spins is weak and a random distribution of electron spins is obtained because of thermal fluctuations (Figure 1.9a). A small magnetic moment is generated in the presence of a magnetic field. In a ferromagnetic interaction, the electron spins align parallel to each other, leading to a net magnetic moment (Figure 1.9b). In an antiferromagnetic interaction, the spins align antiparallel to each other

(Figure 1.9c) and in ferrimagnetic interaction, a net magnetic moment is formed from an antiparallel alignment. The magnetisation in one direction is greater than that in the other direction, leading to the net magnetic moment (Figure 1.9d).[6]

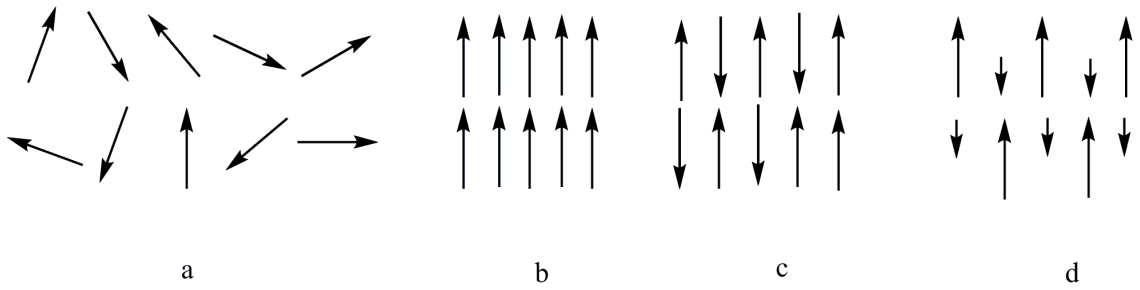

Figure 1.9 Schematic representation of different types of interaction between spins; a) paramagnetic, b) ferromagnetic, c) antiferromagnetic, d) ferrimagnetic.

Paramagnetic liquid crystals (PMLCs) have been treated as novel advanced soft materials due to their special properties, which include:

1) Molecular alignment in a weak magnetic field. Like other properties, the magnetic susceptibility of any LCs (e.g., diamagnetic or paramagnetic) is anisotropic; that is, the magnetic susceptibility is different in different directions. Therefore, molecules of LCs can be aligned by magnetic field. However, a strong magnetic field is required for the alignment of diamagnetic LCs which lack unpaired electrons. The diamagnetic susceptibility mainly arises from the core component (aromatic rings) of LCs. This small diamagnetic susceptibility results in a relatively poor response to the external magnetic field. Introducing paramagnetic components to the conventional LCs can increase the magnetic susceptibility significantly.[7] Therefore, PMLCs can be aligned by the magnetic field more easily.

2) Intermolecular magnetic interactions can be introduced into the PMLC phases. The conventional optical and electrical properties of LCs could be combined with magnetic properties of paramagnetic compounds. Therefore, unconventional magneto-optic or magneto-electric properties may be observed in LC phases.

3) Utilization as spin probes. Electron paramagnetic resonance (EPR) spectroscopy has been used to investigate the dynamic properties of LCs. However, since most conventional LCs are diamagnetic, spin probes are needed to be dissolved in LC hosts. These PMLCs could be used as spin probes to observe the dynamic behaviour of diamagnetic LCs.

Although the investigation of PMLCs is in its infancy, this new type of material has many potential applications such as smart switching devices[8], drug-delivery systems[9] and molecular electronic devices[10].

A number of PMLCs has been successfully prepared and, in general, PMLCs can be divided into two types, metallomesogens and organic mesogens. For metallomesogens, the unpaired electrons are typically located on a transition metal; while for organic mesogens, radicals (normally nitroxides) are the source of unpaired electron spins (Figure 1.10).

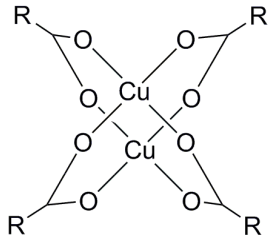

1.3 R=$C_{11}H_{23}$

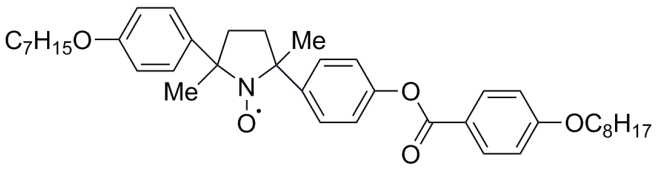

1.4

Figure 1.10 Examples of two types of PMLCs.[11,12]

1.1.3.2 Metallomesogens

Many paramagnetic transition metal ions have been used to prepare metallomesogens, such as Cu^{2+}, Fe^{3+} and Ni^{2+}. Rare-earth metal ions have also used to prepared such mesogens because these ions have large magnetic susceptibility.[13] Numerous calamitic and discotic

metallomesogens have been reported (Figure 1.11).[14-19] However, magnetic properties of metallomesogens in crystal and liquid crystal states only attracted attention after the magnetic susceptibility investigation of metallomesogen **1.3** (Figure 1.10) was carried out by A. M. Giroud-Godquin and co-workers.[20] The magnetic susceptibility of mesogen **1.3** was studied by a superconducting quantum interference device (SQUID) in temperature range 4 K-400 K. A slight drop (around 5%) of magnetic susceptibility was observed when crystal to discotic columnar phase transition occurred. Furthermore, a drop in magnetic susceptibility at the phase transition was detected when the length of alkyl chains of mesogen **1.3** was changed. This suggested that magnetic susceptibility could be a sensitive probe of phase transition.

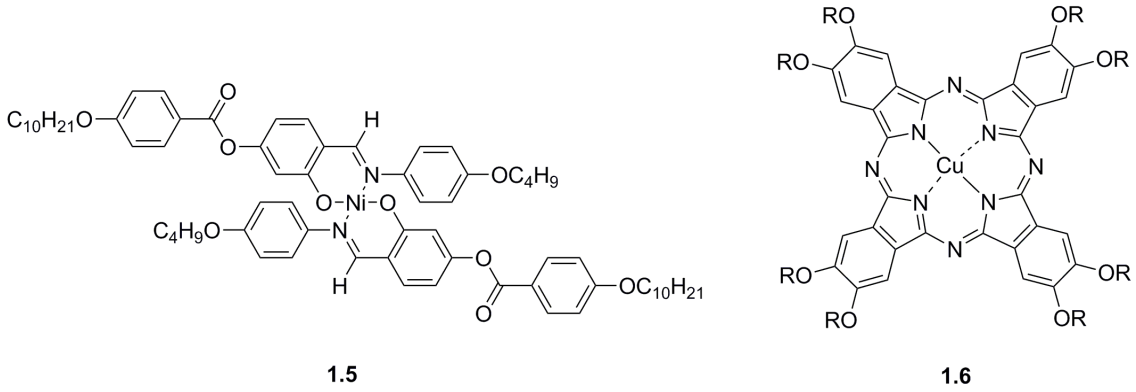

1.5 **1.6**

Figure 1.11 Examples of calamitic and discotic metallomesogens.[16,21]

In 1992, a new Fe(III) metallomesogenic complex was prepared by Y. Galyametdinov and co-workers (Figure 1.12).[22] The magnetic susceptibility of this complex was determined at temperatures of 4.2 K to 420 K. However, no drastic change of magnetic susceptibility was observed upon transition from crystal phase to SmA phase. An increase in magnetic susceptibility was observed at 395 K (around the SmA to N phase transition temperature). However, partial decomposition of this complex was observed at this temperature with an optical microscope. The change in magnetic susceptibility could therefore have arisen from decomposition of the mesogenic complex. A new Cu(II) metallomesogenic complex was prepared by S. Gehring *et al.* (Figure 1.13).[23] In this study, no change of magnetic susceptibility was observed when crystal to LC phase transition occurred.

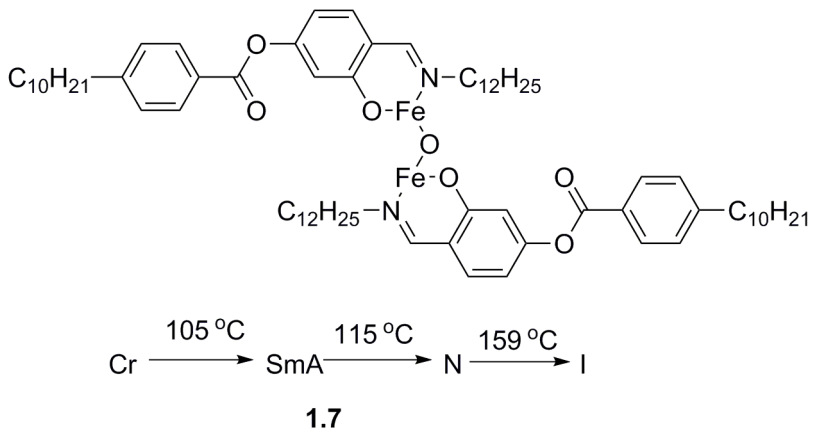

1.7

Figure 1.12 The structure of Fe(III) metallomesogenic complex.[22]

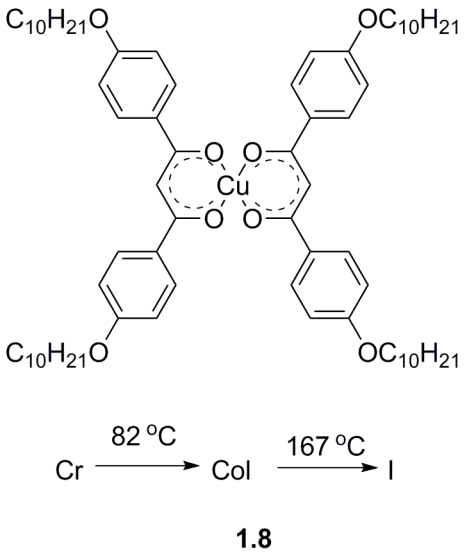

1.8

Figure 1.13 The structure of Cu(II) metallomesogen complex.[23]

The magnetic properties of PMLCs containing rare-earth metals have also been investigated. A comprehensive study of $[M(LH)_3(NO_3)_3]$ (M=Pr(III), Nd(III), Gd(III), Tb(III) and Er(III), LH is a ligand shown in Figure 1.14) type rare-earth metal containing PMLCs was carried out by K. Binnemans and co-workers.[13] For these metallomesogens, alignment of the sample was obtained in a 12000 G magnetic field. Magnetic susceptibility increased when the samples were cooled from the isotropic phase to a mesophase. The molecular alignment of these materials in the mesophase could only be observed when the sample was cooled from isotropic phase because of its high viscosity. It was found that the high viscosity of these metal complexes limits the response of these samples to magnetic field stimuli.

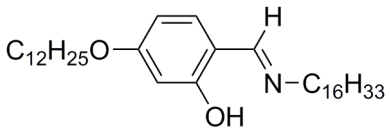

Ligand LH

Figure 1.14 Structure of ligand LH.[13]

In fact, high viscosity is a big disadvantage for most metallomesogens. In contrast, organic PMLCs often exhibit lower viscosities and low LC phase temperatures.[12]

1.1.3.3 Organic PMLCs

The other type of PMLCs is organic paramagnetic liquid crystals. The electron spins in these LCs come from organic radicals rather than metal ions. Because of the relatively high thermal and dynamic stability of nitroxide radicals (Figure 1.15), they are often used to prepare organic PMLCs.

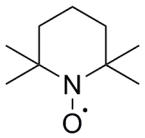

1.9

Figure 1.15 An example of stable nitroxide radical.

Unlike metallomesogens, introducing stable radicals into liquid crystals is challenging. First, the synthesis of these PMLCs is more complex than metallomesogens as even stable radicals are highly reactive. Extreme reaction conditions (high temperature, improper pH value, reducing agents, *etc.*) can destroy the radical easily. Characterisation of these species is also not straightforward (NMR spectroscopy cannot be used). Second, in order to obtain stable nitroxide radicals, the α proton of N-O group should be substituted by other groups, such as

methyl group. However, these substituents may destroy the stability of mesophases.[9]

The most straightforward method to prepare these organic PMLCs is introducing radicals into the flexible chain of a mesogen. However, only a few organic PMLCs have been successfully prepared.[12,24-38] In 1970s, several organic PMLCs were prepared by M. Dvolaitzky and co-workers (Figure 1.16).[24,26] They found that the introduction of radical components decreased the stability of mesophases. Therefore they suggested that the structural components chosen to prepare PMLCs should promote the formation of mesophases over a large temperature range. Interestingly, they found that the SmC to SmA phase transition of some organic PMLCs cannot be detected with differential scanning calorimetry (DSC). Possibly because only slight changing of molecular arrangement occurs from SmC to SmA phase. However, EPR spectra of PMLCs changed when the phase transition occurred (EPR of PMLCs is discussed in section 1.2.7). EPR spectroscopy was thus suggested to be more sensitive than DSC to detect the phase transitions for these organic PMLCs.

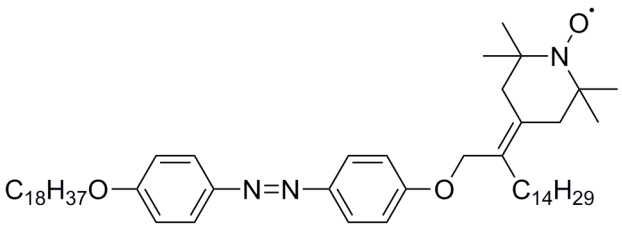

1.10

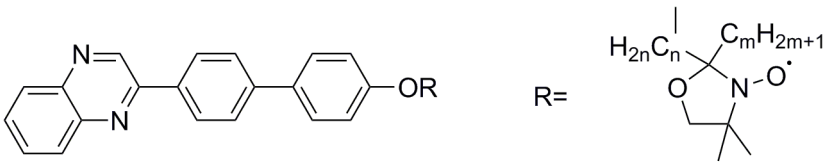

1.11a m=1, n=8
1.11b m=5, n=9
1.11c m=8, n=7

Figure 1.16 Organic PMLCs prepared by M. Dvolaitzky and co-workers.[24,26]

For all these PMLCs, the radical components are in the flexible chains and because of the free

rotation of these flexible chains, only weak magnetic interactions are observed.

In addition to rod-shaped PMLCs, a number of discotic organic radical materials have also been prepared. The first ones were prepared in 2008 by C.V. Yelamaggad and co-workers (Figure 1.17).[28] All three mesogens have large mesophase temperature ranges (more than 100 °C). Antiferromagnetic interactions were observed for these mesogens around 1 K.

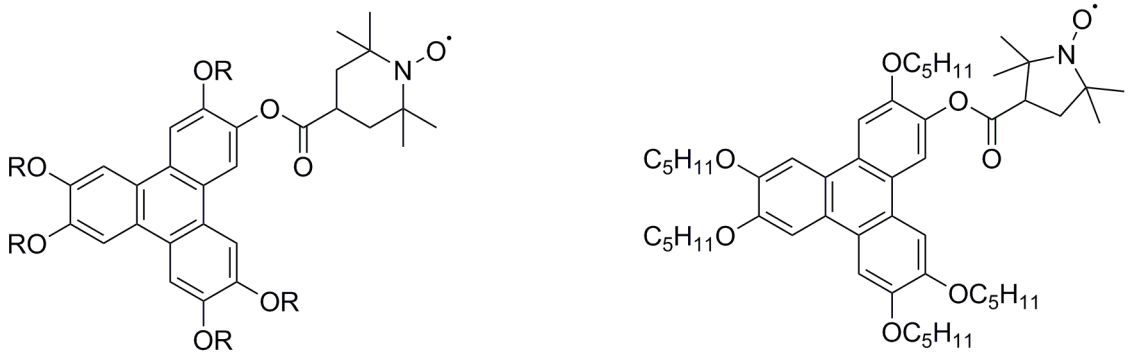

1.12a R=C_5H_{11}
1.12b R=C_6H_{13}

1.13

Figure 1.17 Discotic PMLCs prepared by C.V. Yelamaggad.[28]

A breakthrough in organic PMLCs was achieved by R. Tamura and co-workers in 2004[12], who prepared a range of organic PMLCs with the radical component in the rigid core (Figure 1.18). The magnetic susceptibilities of racemic and single enantiomer samples were measured by SQUID at 2-380 K. Interestingly, racemic sample **1.14c** and **1.14d** showed weak ferromagnetic intermolecular interactions, while other samples showed weak antiferromagnetic interactions during the first heating process from crystal phase to isotropic liquid phase. However, during the first cooling process, all samples except racemic **1.14a** showed weak antiferromagnetic intermolecular interactions. Significant change of magnetic susceptibility was observed for all samples at the crystal to LC phase transition during the first heating process. This change originated from the alignment of molecules at LC phase. Moreover, a change in the magnetic susceptibility was observed even in a magnetic field of 0.05 T, thereby suggesting that alignment of the molecules in this system can be achieved by applying a very weak magnetic field. However, the magnetic susceptibility did not change during the first cooling process.

Furthermore, no LC phase to crystal transition was observed in the DSC curve during the first cooling process due to the formation of a metastable supercooled mesophase.

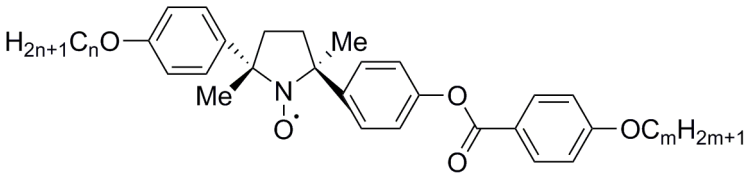

1.14a m=n=4
1.14b m=n=7
1.14c m=8, n=7
1.14d m=n=8

Figure 1.18 Organic PMLCs prepared by R. Tamura and co-workers.[12]

Compound **1.14e** was also prepared by R. Tamura and co-workers (Figure 1.19).[33] The behaviour of this mesogen in the presence of weak magnetic field was examined. A droplet of this mesogen was placed on the hot water surface in a dish (the temperature of hot water is higher than the temperature of the crystal to SmC phase transition of mesogen **1.14e**). The droplet of mesogen can be attracted by a small permanent magnet (maximum field strength 0.5 T, Figure 1.20). When hot water was cooled to a temperature below crystal to SmC phase transition temperature, the droplet of **1.14e** could not be attracted by the magnet anymore. Magnetic susceptibility increased by *ca.* 16% when the crystal to SmA phase transition occurred. The authors believed that an unusual short range ferromagnetic-like intermolecular magnetic interaction (magneto-LC effect) in the SmC phase contributes to the increased magnetic susceptibility. It was found that inhomogenous intermolecular contacts in LC phases contribute to this magneto-LC effect.[35] Ferroelectricity of mesogen (2S, 5S)-**1.14e** in chiral SmC phase was also observed.

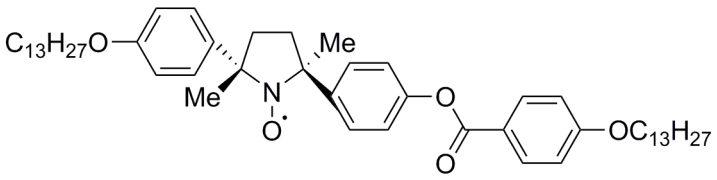

1.14e

Figure 1.19 The structure of mesogen **1.14e**.[33]

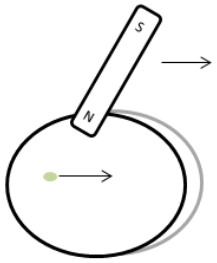

Figure 1.20 Schematic representation of a mesogen droplet attracted by a magnet.[33]

The orientational order in a mesophase decreased when the covalent bonds in the core components were replaced by hydrogen bonds.[39,40] Decreasing the orientational order in LC phases may lead to more inhomogenous intermolecular contacts which can strengthen the magneto-LC effect. In order to test this hypothesis, a hydrogen-bonded organic PMLC was prepared by R.Tamura and co-workers (Figure 1.21).[37] An abrupt decrease of magnetic susceptibility was observed when the nematic to crystal phase transition occurred. This is in agreement with the observations made for the covalently-bonded mesogen **1.14**. Furthermore, a stronger magneto-LC effect was observed in this mesogen, as expected.

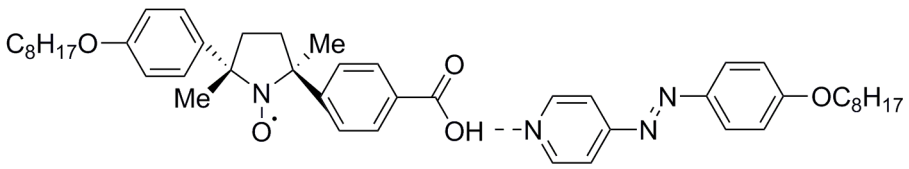

1.15

Figure 1.21 Hydrogen-bonded PMLC prepared by R. Tamura and co-workers.[37]

In our work, we focus on organic radicals, therefore EPR study of organic radicals is discussed in more detail than metal ions in the sections that follow.

1.2 Electron Paramagnetic Resonance Spectroscopy[41,42]

1.2.1 Basic Principles

A free electron has a spin angular momentum (***S***) and a spin quantum number 1⁄2. Spin quantum number can have two values, m_s = 1⁄2 or m_s = -1⁄2. Magnetic moment $\boldsymbol{\mu_e}$ depends on electron spin angular momentum and is proportional to spin angular momentum (Equation 1.1,). Here, ħ is reduced Planck constant, ϒ is gyromagnetic ratio, μ_B is the Bohr magneton.

$$\boldsymbol{\mu_e} = \hbar\, \Upsilon\, \mathbf{S} = g\, \mu_B\, \mathbf{S} \qquad (1.1)$$

In the presence of an external magnetic field (B ≠ 0), electron spins can either align parallel (α state) or antiparallel (β state) to the direction of the external magnetic field. Spin energy levels (Equation 1.2) of these two spin states are not degenerate any more, splitting into two levels. This is called Zeeman effect (Figure 1.22). The spin in the lower energy β state can absorb electromagnetic irradiation energy (hν) if it matches the energy difference between the two states (Equation 1.3) and 'jump' to the higher energy α state. Here, h is Planck constant and ν is irradiation frequency. This is the main principle of EPR spectroscopy.

$$E = -\boldsymbol{\mu_e} \bullet \mathbf{B} = g\, \mu_B\, \mathbf{S} \bullet \mathbf{B} = \pm(1/2)\, g\, |\mu_B|\, B \qquad (1.2)$$

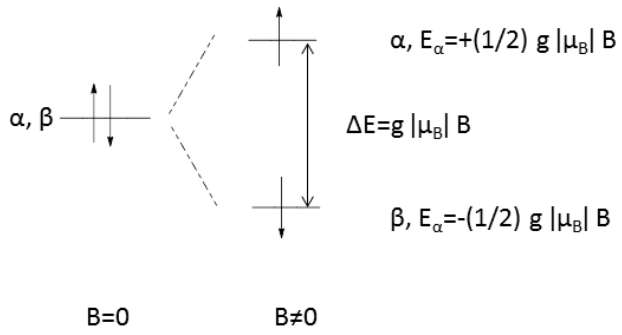

Figure 1.22 Schematic representation of Zeeman effect.

$$h\nu = E_\alpha - E_\beta = g\,|\mu_B|\,B \qquad (1.3)$$

1.2.2 Observation of Resonance

From equation 1.3, two possible method can be used to perform an EPR experiment, magnetic field sweep and microwave frequency sweep (Figure 1.23). It is technically easier to perform an EPR experiment with the field sweep method. In this work, the sample is irradiated with a microwave radiation of around 9.75 GHz (X-band).

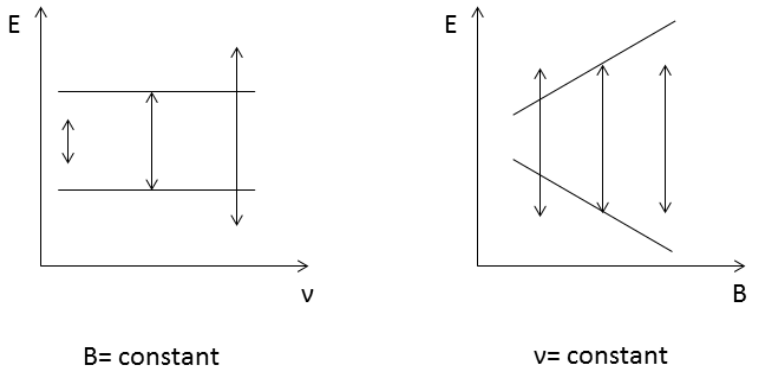

Figure 1.23 Schematic representation of two methods to perform an EPR experiment, arrows represent the energy ranges of applied microwaves.

1.2.3 Modulation Field

From equation 1.3, for an EPR experiment, an absorption spectrum should be obtained. However, a 1st derivative spectrum is recorded by an EPR spectrometer (Figure 1.24). In order to increase the signal to noise ratio, a modulation field is applied on top of the sweeping field. The output amplitude corresponds to the slope of the absorption line at the resonance field; therefore 1st derivative spectrum is obtained.

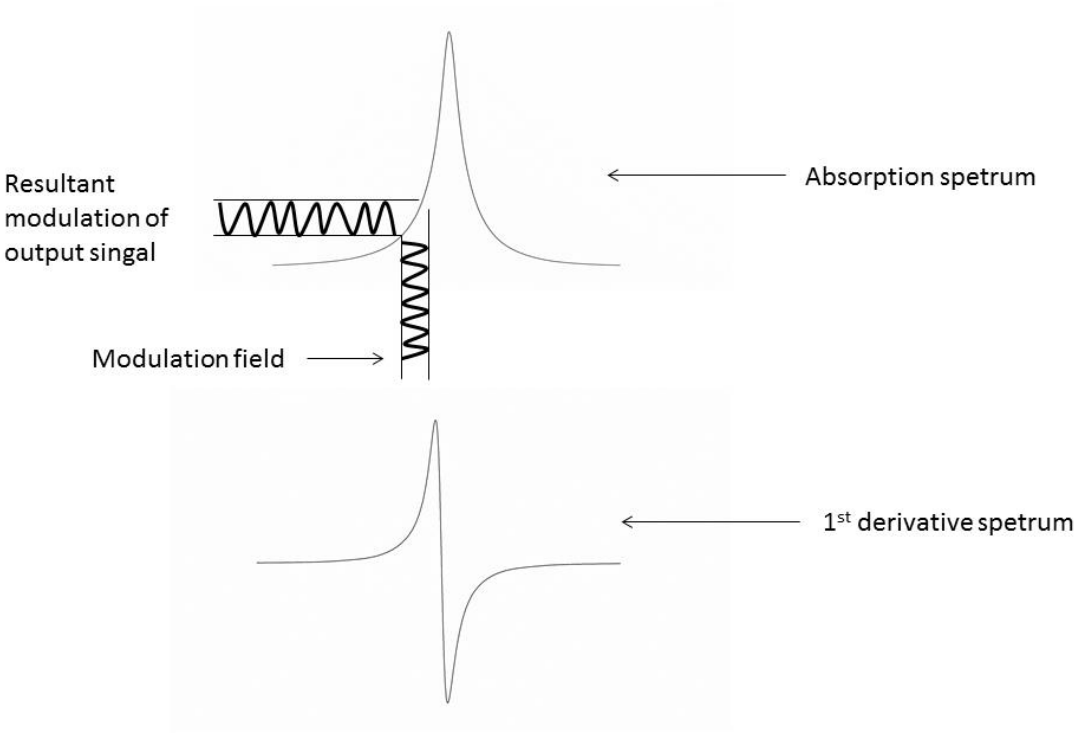

Figure 1.24 Absorption and 1st derivative spectra.

1.2.4 EPR Spectrum Parameters

Interpreting EPR spectra is important but not straightforward. The most two important parameters in an EPR spectrum are g factor and hyperfine coupling constant.

1.2.4.1 g factor

The g factor in an EPR spectrum is similar to the chemical shift in Nuclear Magnetic Resonance spectroscopy (NMR). The g factor of a paramagnetic species is different from that of free electron (g_e = 2.00232) because of the spin-orbit coupling effect. For organic radicals, spin-orbit coupling is relatively weak and therefore the g factors of these radicals are very close to that of free electron g_e.

Because of the anisotropy of spin-orbit interaction, the g value is anisotropic. For organic radicals, g value depends of the direction of magnetic field and orientation of the radicals (Figure 1.25). The g factor is a 3×3 tensor, however, a coordinate system can be found to make the matrices diagonal. Therefore, three principal values g_x, g_y and g_z are needed to describe the anisotropic g value. When an EPR spectrum of a paramagnetic species is recorded in a low viscosity solution, the anisotropy of g factor is averaged out due to the fast tumbling of the molecules and therefore, isotropic g_{iso} is observed.

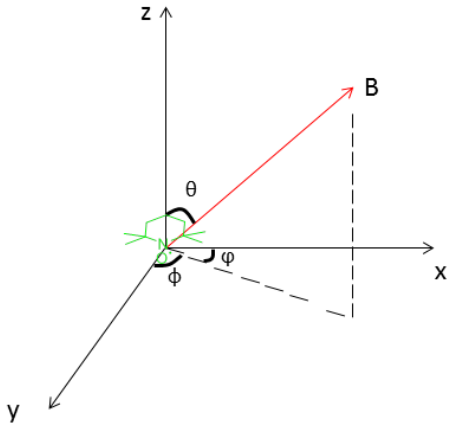

Figure 1.25 The orientation of an applied field B in the molecular axis system; nitroxide is in the xy plane.

1.2.4.2 Hyperfine interaction

The unpaired electron in a molecule interacts not only with the external magnetic field. It is also affected by the presence of the magnetic field produced by spin-active nuclei. This interaction between electron spin and nuclei is called the hyperfine interaction. It splits the EPR lines into several components. Hyperfine coupling is similar to the *J* coupling in NMR.

Nuclei have spin angular momentum and spin quantum number *I*. When the nuclear spin interacts with electron spin, it splits the electron Zeeman energy levels into 2n*I*+1 sub-levels. Because the EPR selection rule is $\Delta m_S = \pm 1$ and $\Delta m_I = 0$, the number of resulting peaks is equal to 2*I*+1. For example, for nitroxide radical, ^{14}N ($I = 1$) nucleus splits Zeeman energy levels into 3 sub-levels. Based on EPR selection rule, a 3 line EPR spectrum is observed, with the hyperfine coupling constant a_N (Figure 1.26).

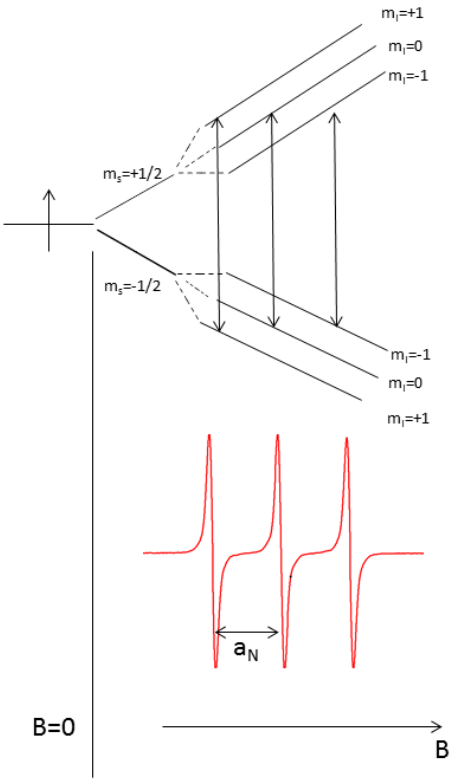

Figure 1.26 Schematic representation of hyperfine interaction.

Like the g factors, hyperfine coupling constants are 3×3 tensors. And for the same reason, only three values are needed to describe the anisotropic hyperfine coupling constant. The hyperfine interaction includes several contributions.

Fermi contact: Fermi contact originates from the non-zero electron density inside the nucleus. Only s-orbital gives a non-zero possibility of an electron being present at the position of the nucleus. The hyperfine field inside the nucleus is isotropic, and hence the contribution to the hyperfine is isotropic. The spin density distribution in the molecular orbitals can be affected by spin polarisation. The unpaired electron can align its spin with the spin in the nearest nucleus. Figure 1.27 shows the two possibilities of spin orientations for a C-H bond adjacent to the radical centre. For both of these spin orientation states, repulsive Coulomb interactions exist. However, when the electron in the C-H bond has the same spin state with the unpaired electron in the SOMO, this interaction is slightly weaker. Therefore, one spin state of the C-H bond is slightly more favourable than the other. This unbalanced distribution of spin density is called spin polarisation.

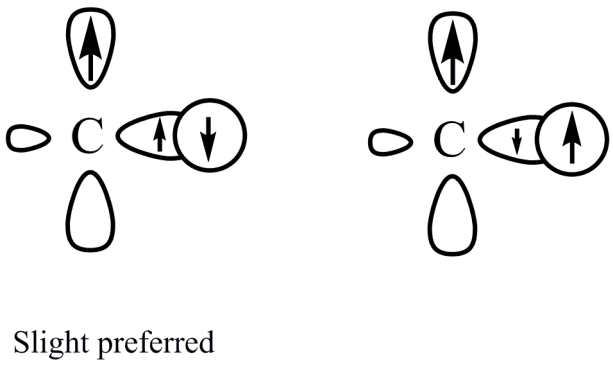

Figure 1.27 Schematic representation of two possible spin orientations for C-H bond.

Dipole-dipole interaction: Outside the nucleus, an additional magnetic field is generated by the magnetic nucleus. It is a field of a magnetic dipole. The hyperfine interaction between this field and an unpaired electron decreases with the distance (r) between the nucleus and electron. It also depends on the angle (θ) between the external field and the line joining the two dipoles (Figure 1.28).

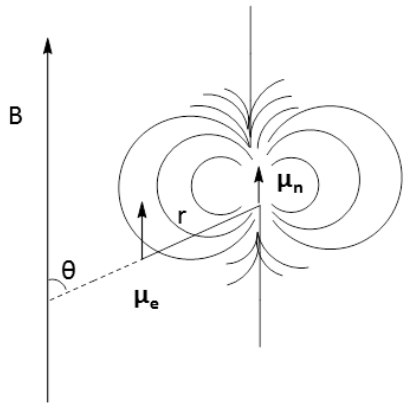

Figure 1.28 Schematic representation of dipole-dipole interaction.

Like the g factor, when a sample is in a low viscosity solution, the anisotropy of hyperfine interactions is averaged out by the fast tumbling of molecules and the isotropic hyperfine a_{iso} is observed.

1.2.5 Linewidth of EPR Spectrum

An important characteristic of an EPR spectrum is the linewidth. Normally the 1st derivative spectrum is characterized by a peak to peak linewidth ΔH_{pp} (Figure 1.29). The linewidth of a spectrum can be determined by several effects.

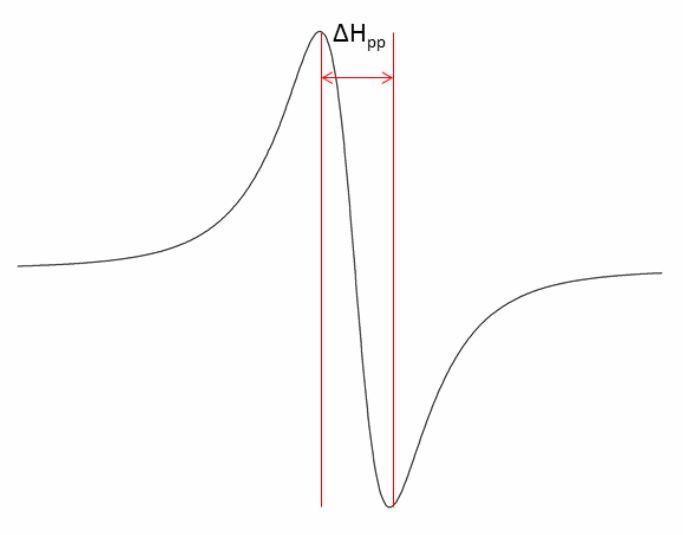

Figure 1.29 Schematic representation of linewidth in a EPR spectrum.

Electron-electron dipolar interaction: Electron spins are experiencing magnetic field generated by the electrons nearby. This interaction is anisotropic and can be averaged out to zero for rapidly tumbling molecules. The resonance field of induced spin state transition is no longer a fixed value because of the contribution of this interaction. Therefore, the EPR spectrum consists of a peak with a certain linewidth rather than a sharp line. This interaction decreases rapidly with the increased spin-spin distance. In a magnetically dilute solution, this interaction is weak. However, in a concentrated solution, line broadening can be observed.

Exchange interaction: Another factor that influences the linewidth is exchange interaction. The molecules with unpaired electron can collide with each other leading to fast relaxation. Because of reduced lifetime of spin states, line broadening is detected.

1.2.6 Dynamics

As mentioned above, anisotropic interactions could be averaged out by rapid tumbling of molecules. Therefore an isotropic EPR spectrum is obtained. For instance, for nitroxide radical, a three peaks EPR spectrum with similar height and ΔH_{pp} is observed (Figure 1.30 spectrum 1). However, in some cases, the molecular tumbling is restricted, the anisotropic effect cannot be

averaged out to zero; therefore anisotropic spectrum is obtained. The peak in high field is broadened. If the molecular tumbling is restricted further, powder pattern (e.g. radicals in frozen solution) EPR spectrum can be observed (Figure 1.30 spectrum 5).

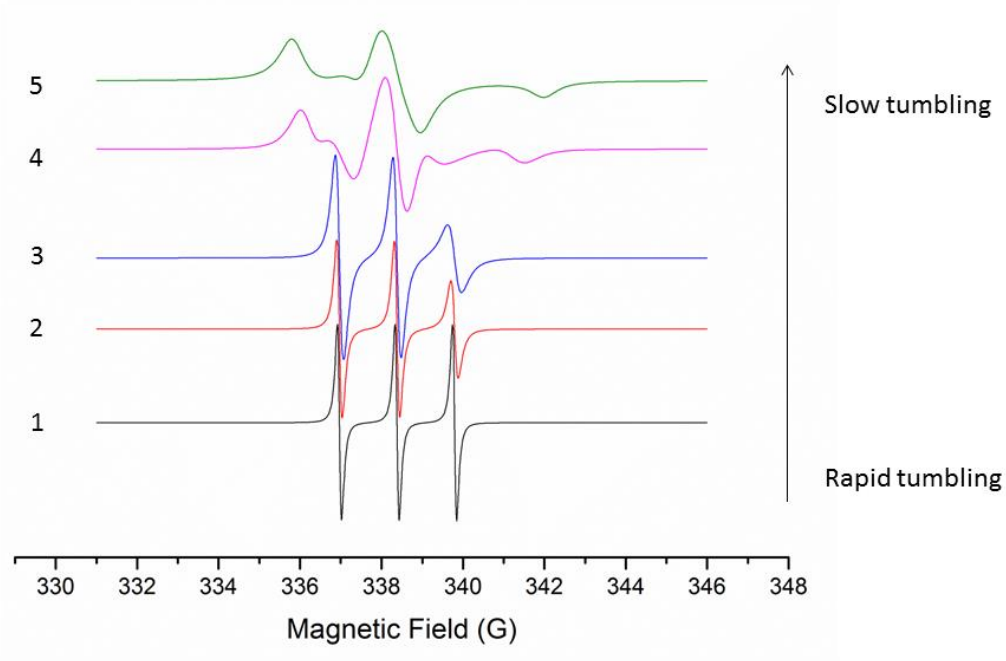

Figure 1.30 EPR spectra of nitroxide radical with different tumbling rates.

1.2.7 EPR study of Organic PMLCs

An EPR study of mesogen **1.14c** (Figure 1.18) was carried out by R. Tamura and co-workers.[12] For racemic **1.14c**, an abrupt drop of g value (from 2.0065 to 2.0052) was observed upon crystal phase to LC phase transition during the heating process. As mentioned above, g factor is anisotropic. For a pyrrolidine nitroxide radical, the g value along the N-O axis is largest g_{xx} is around 2.009, the g value along its $2p_z$ orbital axis g_{zz} is around 2.003, the g value perpendicular to both of these axis g_{yy} is around 2.006 (Figure 1.31).[43] The decrease of g value from crystal to liquid crystal arises from the increasing contribution of g_{yy} and g_{zz}. It was suggested that the molecules tend to align with the direction of the N-O axis perpendicular to the applied field (Figure 1.31). However, for non-racemic (2*S*,5*S*)-**1.14c**, g value is almost constant in chiral LC

phase and crystal phase, close to that in a solution. This suggests that alignment of molecules is not obtained in the chiral LC phase.

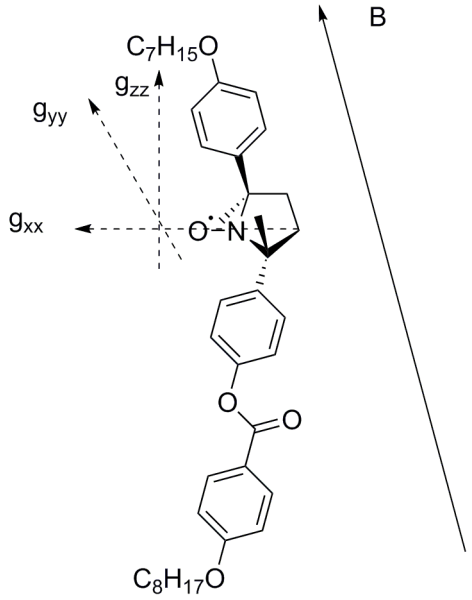

Figure 1.31 Schematic representation of molecular orientation of racemic **1.14c** in magnetic field.[12]

EPR measures the transitions between spin states and hence it measures magnetisation. Therefore the intensity of EPR signal is also proportional to the magnetic susceptibility. For instance, an increase of the intensity of the EPR signal was reported for the crystal to LC phase transition for racemic **1.14e** which is similar to the magnetic susceptibility result collected by SQUID magnetometry (section 1.1.3.3). R.Tamura and co-workers suggested that compared to SQUID magnetometry, EPR spectroscopy is a better technique to investigate the magnetic properties for organic PMLC. as it is much more sensitive and requires less sample. In addition, the contribution of diamagnetic components can be ignored, and macroscopic magnetic information is available, such as spin-spin dipole interaction.[35]

1.3 Stable radicals

Nitroxide radicals are commonly used to prepare organic PMLCs because of their excellent

thermodynamic stability. However, other stable radicals may also be used to prepare PMLCs. In this section, some stable radicals that may be suitable for the preparation of PMLCs are briefly discussed.

1.3.1 Nitroxide Radicals

The first organic nitroxide radical **1.16** was prepared by O. Piloty and B. G. Schwerin in 1901 (Figure 1.32), about 40 years before the invention of EPR spectroscopy.[44] In 1959, 2,2,6,6-tetramethyl-4-piperidone-1-oxyl (4-oxo-TEMPO) **1.17** was prepared by O. L. Lebedev and co-workers (Figure 1.32).[45] Many TEMPO derivatives have been prepared since; they are widely used in the fields of chemistry, biology and medicine (Figure 1.33).[46-49]

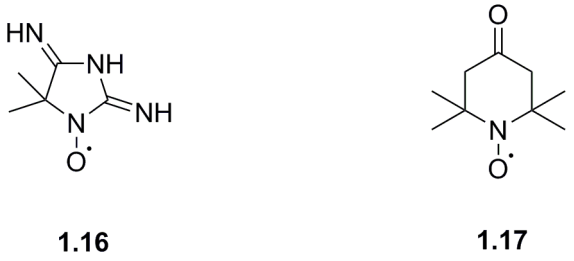

1.16 **1.17**

Figure 1.32 The structures of first nitroxide and 4-oxo-TEMPO.[45]

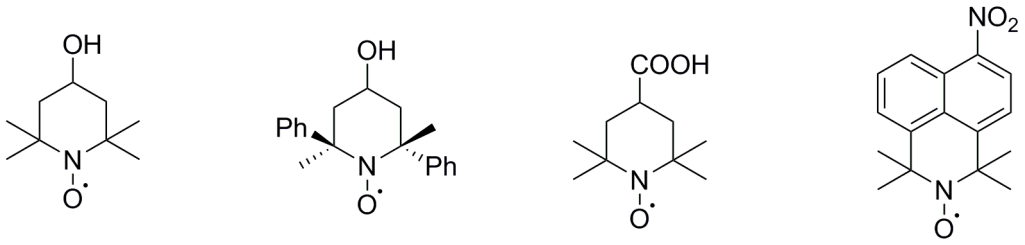

1.18 **1.19** **1.20** **1.21**

Figure 1.33 Examples of TEMPO derivatives.[46-49]

The spin density of nitroxide radicals is delocalised on N and O atoms, with slightly higher density on the O atom. The distribution of spin density can be represented by the resonance

structures of nitroxide radicals (Figure 1.34).[50] The high stability of nitroxide radicals are ascribed to the delocalisation of spin density and poor affinity for dimerisation. However, not all nitroxides are stable. A nitroxide which contains an α proton can decompose to nitrone and hydroxylamine (Figure 1.35). On the other hand, substituents in the α position can destabilise the mesophase and hence are not favourable for the preparation of PMLCs.

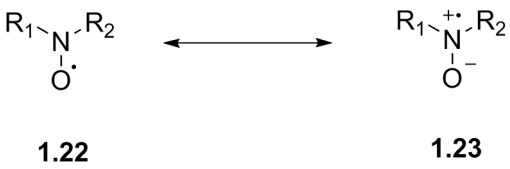

1.22 **1.23**

Figure 1.34 Resonance structures of nitroxide radicals.[50]

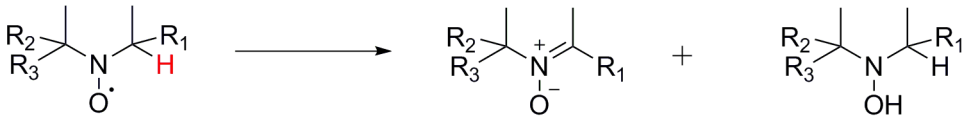

1.24 **1.25** **1.26**

Figure 1.35 Decomposition of nitroxide radicals.

1.3.2 Other Radicals

Triphenylmethyl radicals: The discovery of triphenylmethyl radical by M. Gomberg in 1900 marked the beginning of radical chemistry (Figure 1.36).[51] In a dilute and deoxygenated solution, this radical is in equilibrium with dimeric compound **1.31** (Figure 1.37).[52] The pure triphenylmethyl radical cannot be isolated. The high persistence of this radical in the absence of oxygen is ascribed to the steric protection around the C centre and resonance delocalisation.

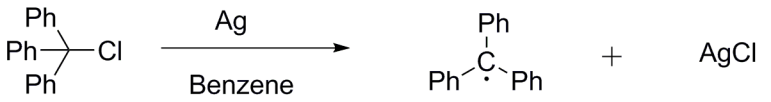

1.27 **1.28** **1.29**

Figure 1.36 Preparation of triphenylmethyl radical.[51]

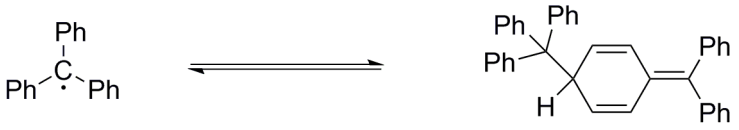

1.30 **1.31**

Figure 1.37 Dimerisation of triphenylmethyl radical.[52]

A series of triphenylmethyl radical derivatives was prepared by O. Armet and co-workers (Table 1.1).[53] They found that substituents in the aromatic rings can stabilize the radical further. These radicals can be isolated in the solid state. Then many other stable triphenylmethyl radicals were prepared.[54-57]

Table 1.1 Triphenylmethyl radical derivatives prepared by O. Armet and co-workers.

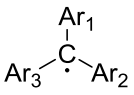

Radical	Ar_1	Ar_2	Ar_3
1.32	4H-$C_6H_2Cl_3$	4H-C_6HCl_4	4H-C_6HCl_4
1.33	3H,5H-$C_6H_2Cl_3$	C_6Cl_5	C_6Cl_5
1.34	3H,5H-$C_6H_2Cl_3$	3H,5H-$C_6H_2Cl_3$	3H,5H-$C_6H_2Cl_3$
1.35	2H-C_6HCl_4	C_6Cl_5	C_6Cl_5
1.36	2H-C_6HCl_4	2H-C_6HCl_4	C_6Cl_5

In 2009, the first organic discotic PMLC was prepared by S. Castellanos and co-workers based on the tripheylmethyl radical (Figure **1.38**).[34] This mesogen shows the Col_h phase from 300 K to 351 K, and Col_r phase was observed below 300 K. The Col_r phase to crystal phase transition was not detected by either DSC or optical microscopy because it is lower than -50 °C. A decrease in magnetic susceptibility was detected when the Col_h to Col_r phase transition occurred. Strong antiferromagnetic interaction was observed when the temperature was lowered to 20K.

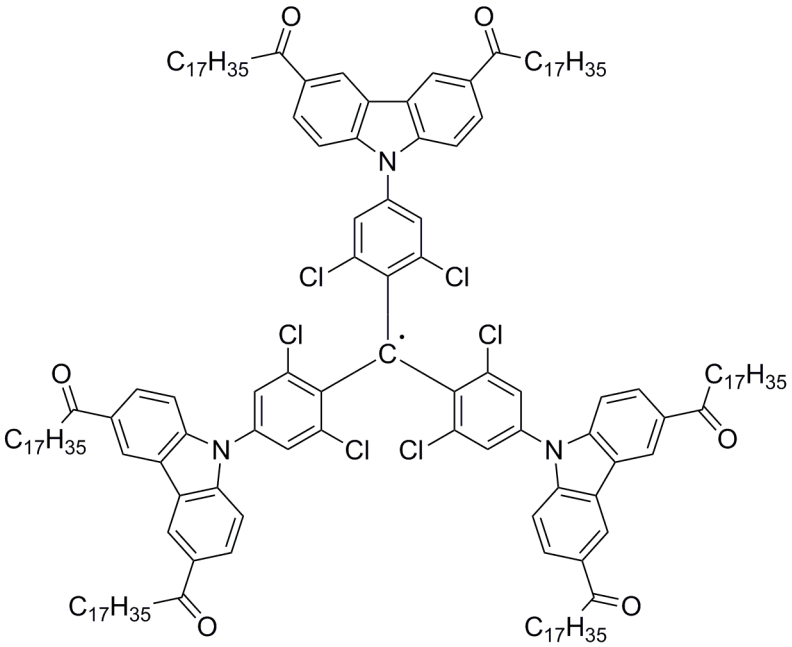

1.37

Figure 1.38 Structure of PMLC prepared by S. Castellanos.[34]

The temperature dependence of the g values of EPR spectra of **1.37** was recorded. A slight increase in g value was observed upon isotropic to Col phase transition. Polychlorotriphenylmethyl radicals have axial symmetry with anisotropic g value, g_{zz} is around 2.005, g_{xx} and g_{yy} are around 2.002. The increase of g value suggested that the molecules in Col phases tend to align along the direction of the $2p_z$ orbital of the unsaturated carbon centre parallel to the applied field.

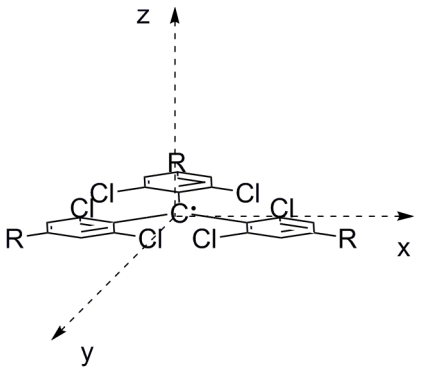

Figure 1.39 Schematic representation of polychlorotriphenylmethyl radical molecular axis system; radical is in the xy plane.[34]

Verdazyl radicals: A very short communication about verdazyl radicals was reported in 1963 by R. Kuhn and H. Trischmann.[58] These radicals gave EPR spectra of nine lines which arise from the almost equivalent hyperfine interaction of 4 N atoms. Surprisingly, no decomposition was observed when these radicals were heated in a boiling acetic acid solution. This suggested that these radicals are very stable even in the presence of acid. Dimerisation of these radicals was not observed. Similar verdazyl radicals were prepared by F. A. Neugebauer and co-workers in 1988 (Figure 1.41).[59] These radicals are very stable in the presence of air.

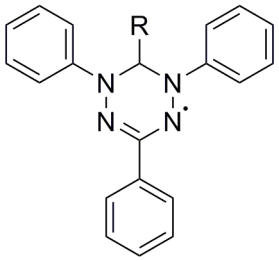

1.38 R=H
1.39 R=C_6H_5
1.40 R=*p*-BrC_6H_4

Figure 1.40 Verdazyl radical prepared by R. Kuhn and H. Trischmann.[58]

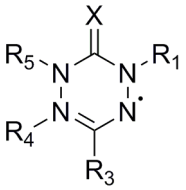

1.41 X=O, S

Figure 1.41 Verdazyl radicals prepared by F. A. Neugebauer and co-workers.[59]

Verdazyl radicals can be used as the rigid cores of discotic LCs. Possibly because of the synthetic difficulties, only a few verdazyl mesogns were reported by P. Kaszyński and co-workers (Figure 1.42, R groups are alkoxyl chains or alkylsulfanyl chains).[38,60-63] The synthesis of these LCs can be achieved in several steps (Figure 1.42). However, preparation of phenylhydrazine derivatives **1.43** and hydrazone compound **1.44** is challenging. More than 2 years were spent to prepare these verdazyl LCs. Decomposition of these LCs was observed at the temperature higher than

90 °C.

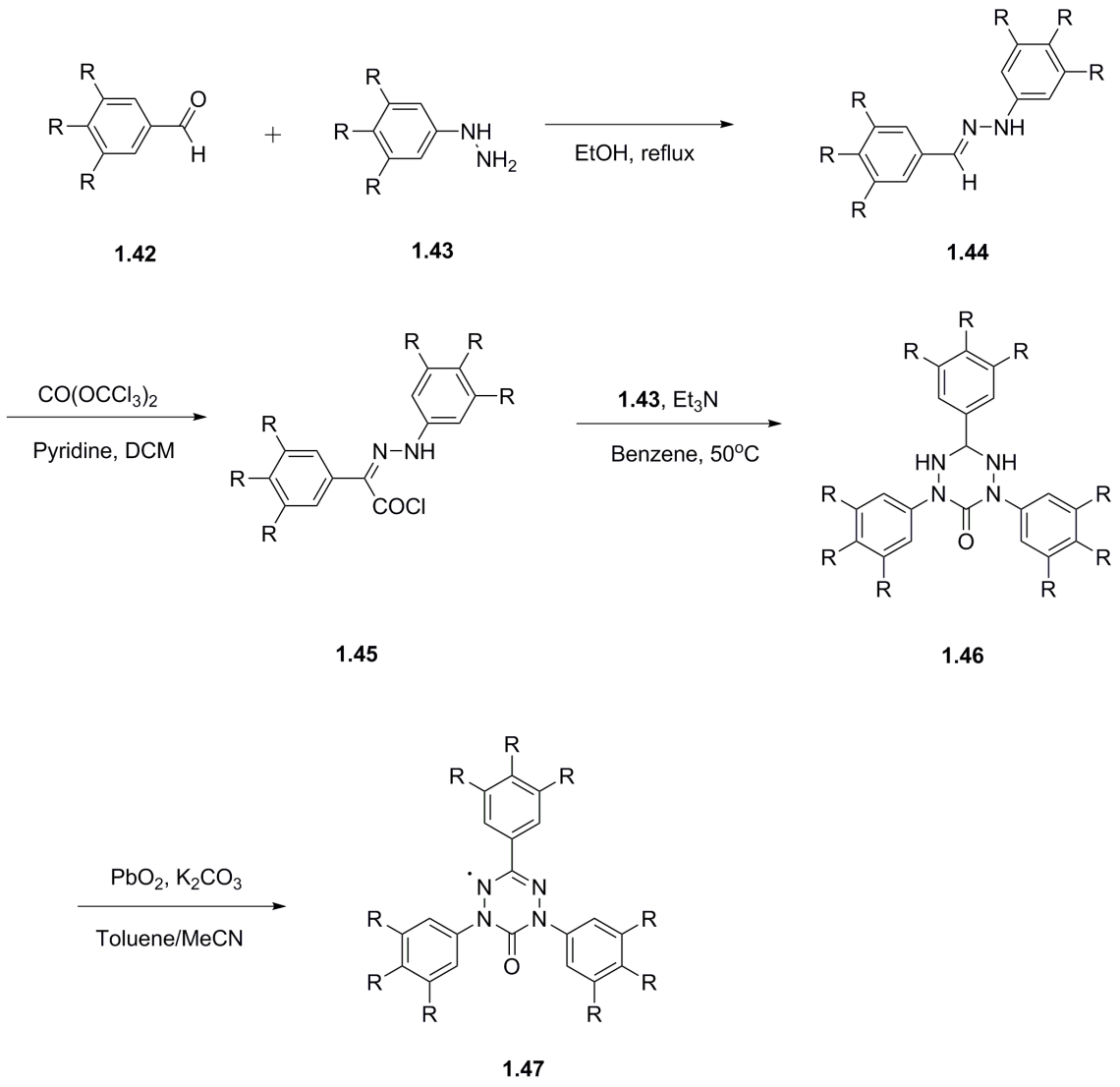

Figure 1.42 The verdazyl LCs prepared by P. Kaszyński and co-workers.[38]

Blatter's radicals: 1,2,4-Benzotriazinyl radicals (Blatter's radicals) first prepared by H. M. Blatter and H. Lukaszew in 1968 are another class of radicals which are suitable for preparation of PMLCs.[64] This will be discussed in detail in chapter 4.

1.4 Aims

Preparation of organic PMLCs is still challenging, most likely due to the difficulties with the molecular design and working with reactive radicals. Nitroxide radicals are the best choice for preparation of PMLCs because of their excellent stability. Unusual intermolecular magnetic interactions were observed with these PMLCs and the origin of these interactions has been investigated in the literature. However, the understanding of these magnetic interactions is limited. In this project, we aimed to prepare a series of organic PMLCs and investigate their magnetic properties by EPR spectroscopy to obtain a better understanding of the molecular arrangement and magnetic interactions in PMLCs. In our work, in order to enhance the intermolecular magnetic interactions, the radical components were introduced into the rigid core of PMLCs. To simplify the synthesis, the two components (mesogen and radical), were prepared separately and then coupled at the last step. The molecular design of each compound is discussed in detail in each chapter.

There are very few investigations of discotic PMLCs, especially with the radical components in the rigid core. The preparation of discotic PMLCs based on the Blatter's radical was the other aim of this project. More ordered LC phases (e.g., columnar phase) could be obtained with discotic LCs, which may strengthen the intermolecular spin-spin interactions. Introduction of stable radicals into discotic LCs can lead to materials possessing interesting electric and magnetic propreties with many potential applications.

As the characterisation of paramagnetic species is not straightforward (NMR cannot be used), high resolution Mass Spectrometry, EPR spectroscopy, thin-layer chromatography (TLC) and elemental analysis were used to characterise the target radicals. The liquid crystalline behaviour of these radicals was studied by DSC and polarised optical microscopy. Their magnetic properties were investigated by EPR spectroscopy. The photoconductive properties of discotic mesogens were studied in time of flight measurements.

Chapter 2 TEMPO-Containing Mesogen

2.1 Introduction

2.1.1 Bent-core liquid crystals

The first bent-shape liquid crystal was prepared successfully about 90 years ago (Figure 2.1).[65] However, the stability of the mesophase was not as good as that of the linear liquid crystals. The large excluded volume, which was produced by the free rotation along the long axis of bent-core liquid crystal, reduced the mesophase stability.

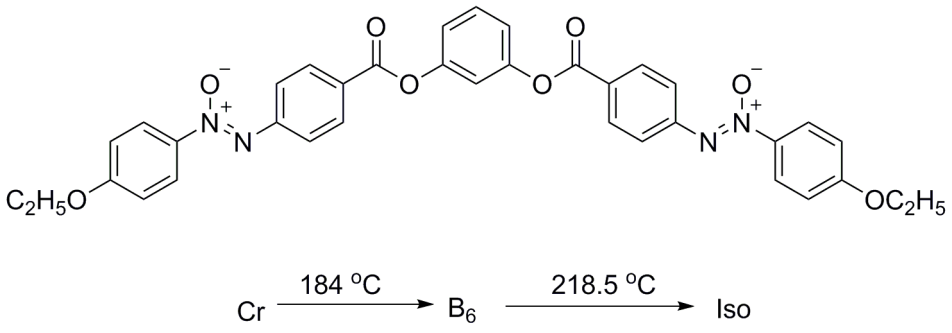

2.1

Figure 2.1 The structure of first bent-core liquid crystal.[65]

Before the polar switching of bent-core liquid crystals was discovered by T. Niori and co-workers in 1996, only a few researchers had studied this kind of liquid crystals (Figure 2.2).[66] Nowadays, not only symmetrical bent-core liquid crystals, but also numerous hockey stick shape liquid crystals have been reported (Figure 2.3).[67]

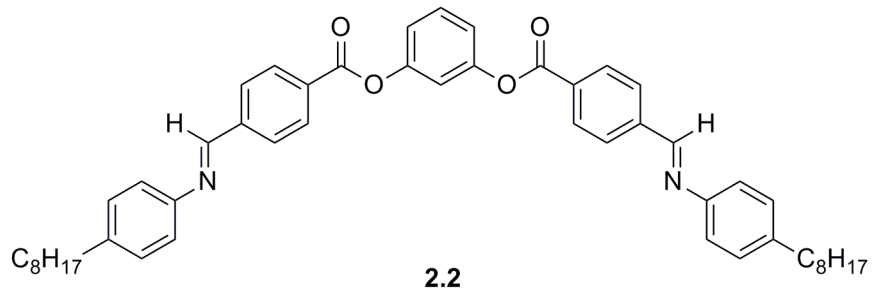

2.2

Figure 2.2 The liquid crystal prepared by T. Niori and co-workers.[66]

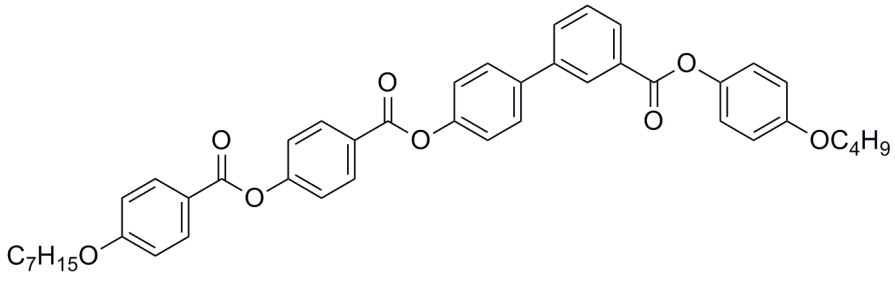

2.3

Figure 2.3 An example of hockey-stick liquid crystal.[67]

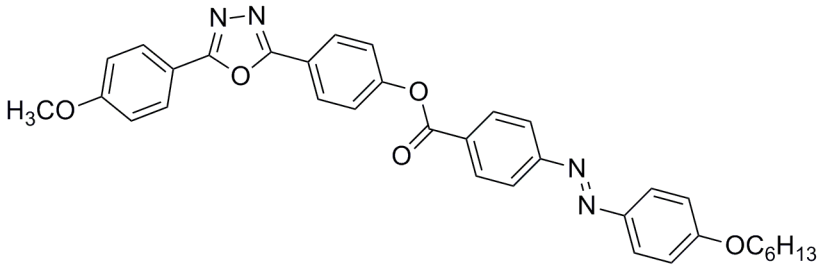

2.4

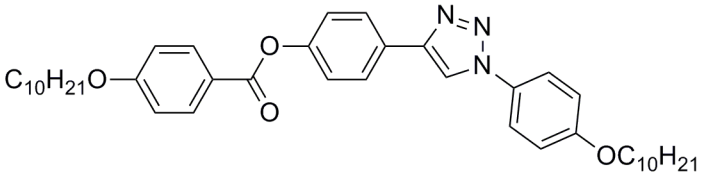

2.5

Figure 2.4 Heterocycle containing bent-core liquid crystals.[68,69]

Heterocycle containing bent-core liquid crystals have also been investigated. Oxadiazole and triazole rings have been introduced into the bent-core liquid crystals (Figure 2.4).[68-71] Because of the development of click chemistry, 1,2,3-triazole ring containing bent-core liquid crystals

attracts much attention.

2.1.2 Click chemistry in the preparation of bent core liquid crystals.

The Huisgen 1,3-dipolar cycloaddition reaction of azides and alkynes plays an important role in the field of organic synthesis (Figure 2.5). However, the high activation barrier of this reaction and poor regioselectivity limited the application of this reaction.

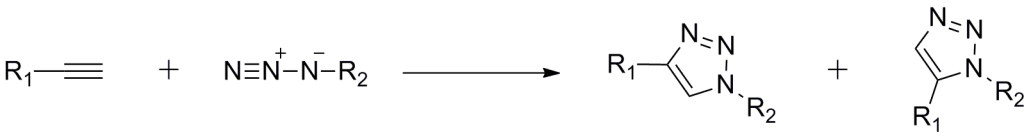

2.4 **2.5** **2.6** **2.7**

Figure 2.5 The Huisgen 1,3-dipolar cycloaddition reaction of azides and alkynes.

Fortunately, in 2001, Cu(I) catalyst was introduced to the 1,3-dipolar cycloaddition of azides and alkynes by M. Meldal and C. W. Tornøe.[72] Significant improvement of the rate and regioselectivity of this reaction was achieved.[73,74] The product **2.6** is formed regioselectively after several hours under mild reaction conditions in a high yield (> 90%). The Cu-catalysed cycloaddition reaction is not significantly affected by the substituents on azides and alkynes and the solvent.

The relevant terminal alkyne compounds could be prepared by Sonogashira coupling reaction followed by deprotection (Figure 2.6), and the azide component could be prepared by nucleophilic substituent reactions. Click chemistry is thus a good toolkit to prepare bent core liquid crystals with potentially high yield. Many triazole ring containing liquid crystals have been prepared using click chemistry (Figure 2.7).[69,75,76]

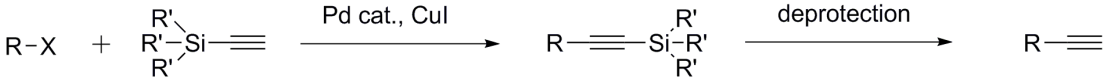

X= I, Br,Cl

Figure 2.6 Preparation of terminal alkyne using Sonogashira reaction.

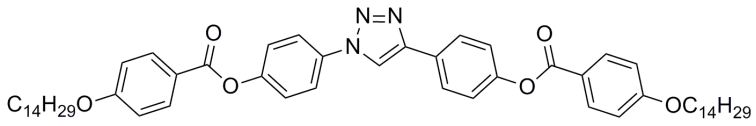

2.8

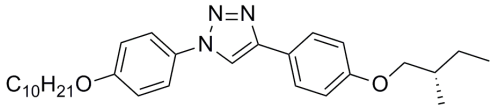

2.9

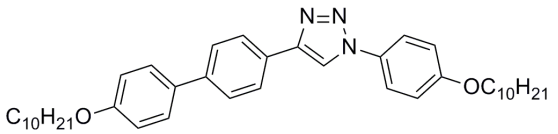

2.10

Figure 2.7 Liquid crystals prepared by click chemistry.[69,75,76]

2.1.3 Nitroxides in click chemistry

Nitroxides are commonly used as spin labels in the area of physical chemistry and biology. Usually, these labels are attached to the target compounds by an ester or an amide linkage (Figure 2.8).[77,78]

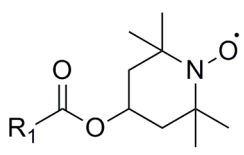

2.11

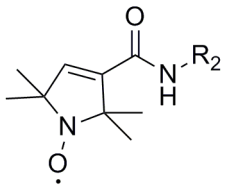

2.12

Figure 2.8 Linkages for nitroxide spin labels.[77,78]

The click reaction could be used in spin labelling chemistry because of its high yield and regioselectivity. A comprehensive study of click reaction with nitroxide derivatives was carried

out by T. Kálai and his co-workers in 2009.[79] A range of nitroxide-containing azides and alkynes was used to react with some suitably functionalized biomolecules under mild conditions (Figure 2.9). CuI was used as a catalyst for these reactions. The mixtures were left at 40 °C in DMSO for 4 h. However, the yield (30-80%) of these reactions is not very good compared to that of other click reactions. The relatively low yield of these nitroxide-containing click reactions may be explained by the relatively high reactivity of nitroxide compounds which leads to side reactions.

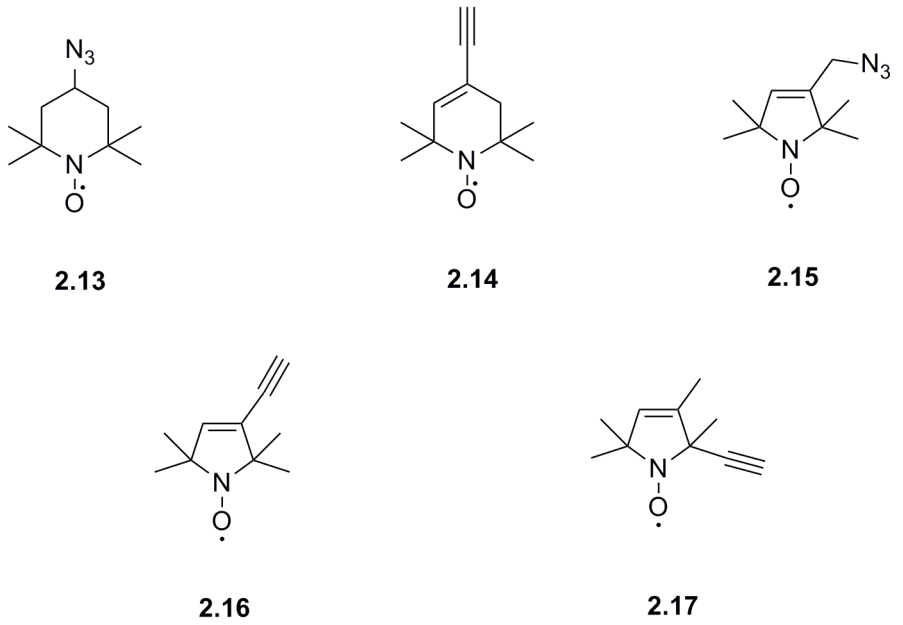

Figure 2.9 Some nitroxide containing reactants in click reaction.[79]

2.1.4 Aims

In this chapter, we aim to prepare a bent-core liquid crystal compound with nitroxide in the rigid core using click chemistry, as nitroxides are stable under the relatively mild conditions of this reaction.

2.2 Preparation of Nitroxide-containing Mesogen.

2.2.1 Design of the target mesogen

The melting point of the target mesogen should not be too high, as the decomposition of the radical occurs rapidly at high temperature. This means that the number of phenyl rings in the rigid core of the mesogen should be kept as small as possible to get a relatively low melting point target compound. However, the mesogenic stability of the compounds with a small number of aromatic rings in the core of the mesogen may be adversely affected. Usually, bent-core liquid crystals have 3 or more rings. Taking both of these factors into consideration, a target compound containing 4 rings should be suitable for our purposes (Figure 2.10).

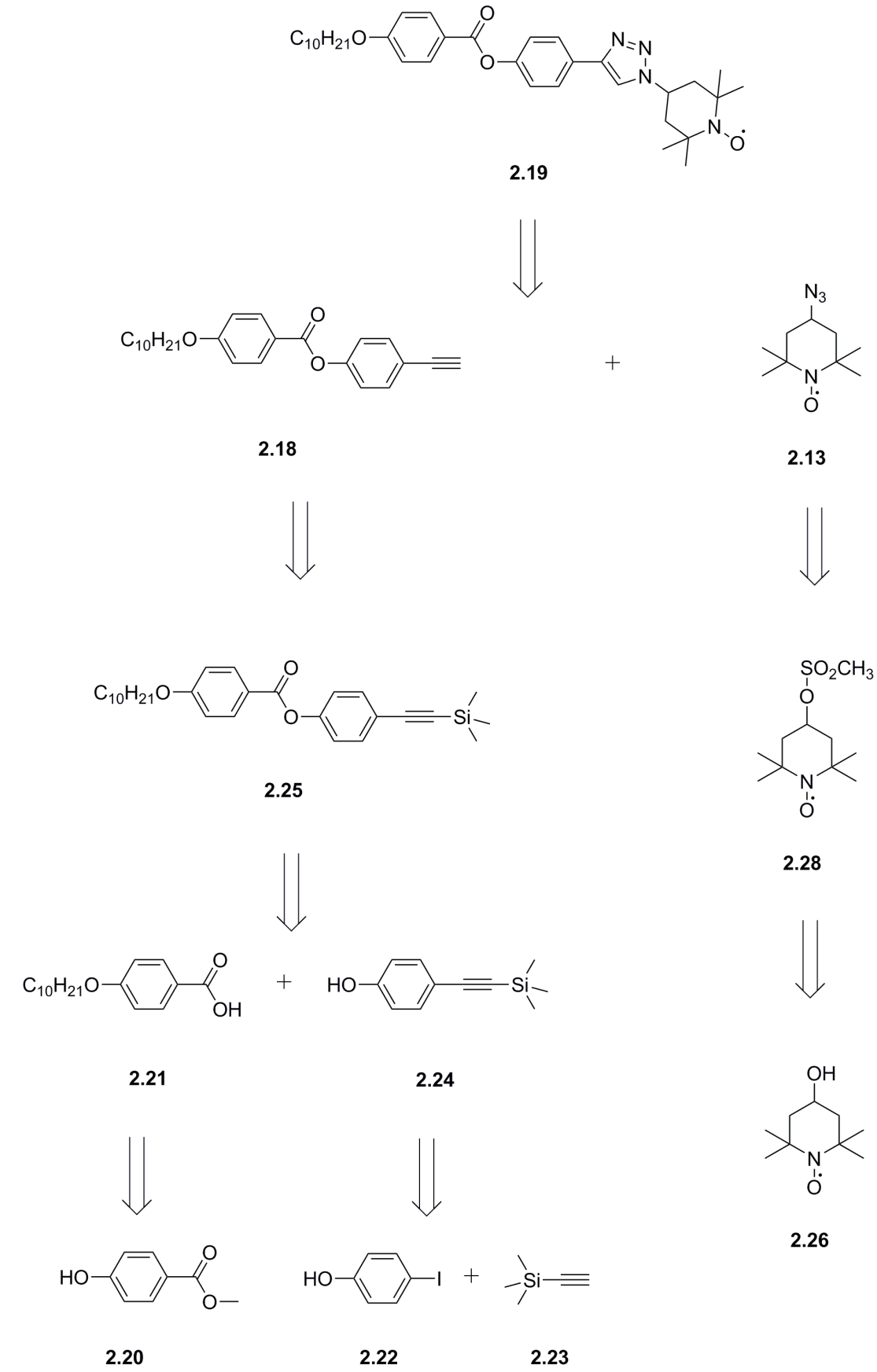

Figure 2.10 Retrosynthesis of bent-core mesogen.

TEMPO azide **2.13** is a suitable azide component that can be prepared relatively easily from commercially available 4-hydroxy TEMPO. Alkyne component **2.18** could be prepared by following the literature procedure.[80] Working with organic paramagnetic species which have relatively high reactivity is challenging and characterisation of these compounds is difficult (NMR cannot be used). Therefore, the free radical will be incorporated into the mesogen structure in the last, high yielding step (click chemistry). Mesogen **2.19** will be prepared by coupling of two components **2.13** and **2.18**.

Reaction between compounds **2.13** and **2.18** is based on click chemistry. This reaction is potentially high yielding and can tolerate a range of functional groups, but in some cases extensive optimisation is required. Development of this methodology is described in the following sections.

2.2.2 Preparation of alkyne component 2.18

Preparation of alkyne component **2.18** can be achieved by established synthetic protocols (Figure 2.11).[80] 4-Decyloxybenzoic acid **2.21** was synthesised from methyl-4-hydroxybenzoate **2.20**. 4-(Trimethylsilylethynyl)phenol **2.24** was prepared from 4-iodophenol **2.22** by Sonogashira coupling. Compound **2.25** was prepared by Steglich coupling by using *N*,*N'*-dicyclohexylcarbodiimide (DCC) and 4-dimethylaminopyridine (DMAP). 4-Ethynylphenyl-4-decyloxybenzoate **2.18** was prepared by the deprotection of 4-(trimethylsilylethynyl)phenyl 4-decyloxybenzoate **2.25** with tetrabutylammonium fluoride (TBAF).

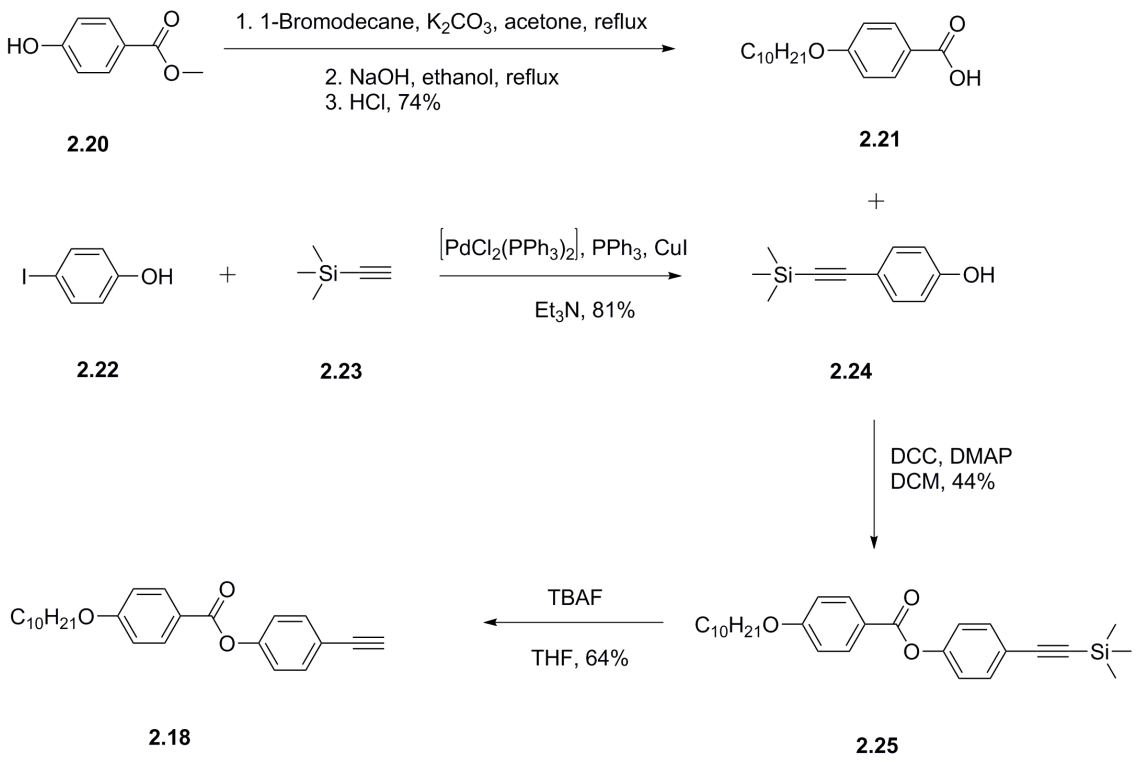

Figure 2.11 Preparation of alkyne component **2.18**.

2.2.3 Preparation of TEMPO azide 2.13

TEMPO azide was prepared from 4-hydroxy TEMPO by following the literature procedure (Figure 2.12).[81] 4-Methanesulfonyl-2,2,6,6-tetramethyl-1-piperidinyloxy radical **2.28** was obtained by reacting 4-hydroxy TEMPO with methane sulfonyl chloride **2.27** in pyridine. Nucleophilic substitution reaction of **2.28** with sodium azide in hexamethylphosphoric triamide (HMPTA) yielded TEMPO azide.

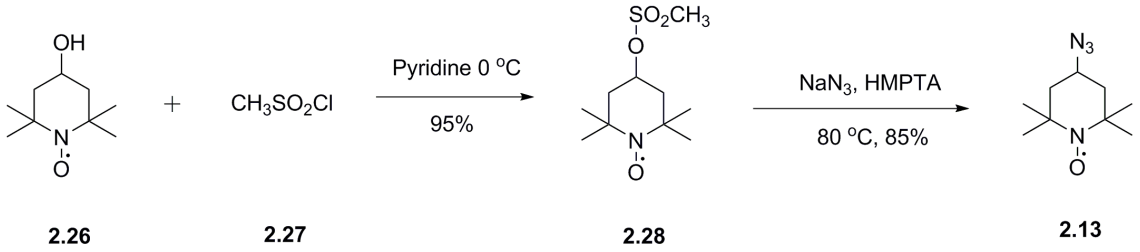

Figure 2.12 Preparation of TEMPO azide **2.13**.

2.2.4 Preparation of mesogen 2.19 using click reaction

Unfortunately, preparation of compound **2.19** from TEMPO azide **2.13** and alkyne **2.18** was not straightforward (Figure 2.13). Alkyne **2.18** and TEMPO azide **2.13** were dissolved in THF. To this solution, CuI (0.2 equiv) and diisopropylethylamine (DIPEA) were added. Then the mixture was stirred at room temperature overnight.

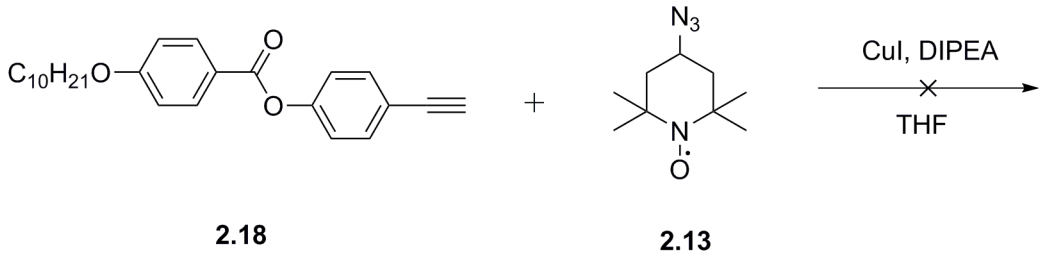

2.18 **2.13**

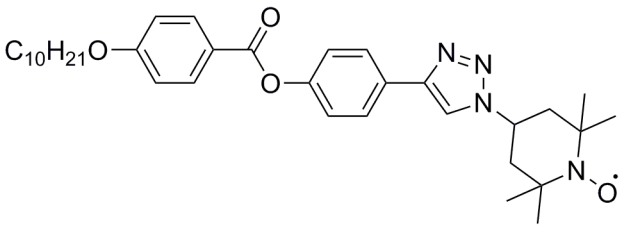

2.19

Figure 2.13 Click reaction between compound **2.13** and **2.18**.

The main EPR active product, formed in this reaction mixture, was isolated by column chromatography (Figure 2.14). However, MS analysis of this compound showed that it was not the target compound. The molecular weight of compound **2.19** is 575 g mol^{-1}, while the MS analysis of the product did not show this peak (Figure 2.15). The peaks in the MS spectrum of the purified product could not be assigned. They did not match the molecular weight of any possible intermediate.

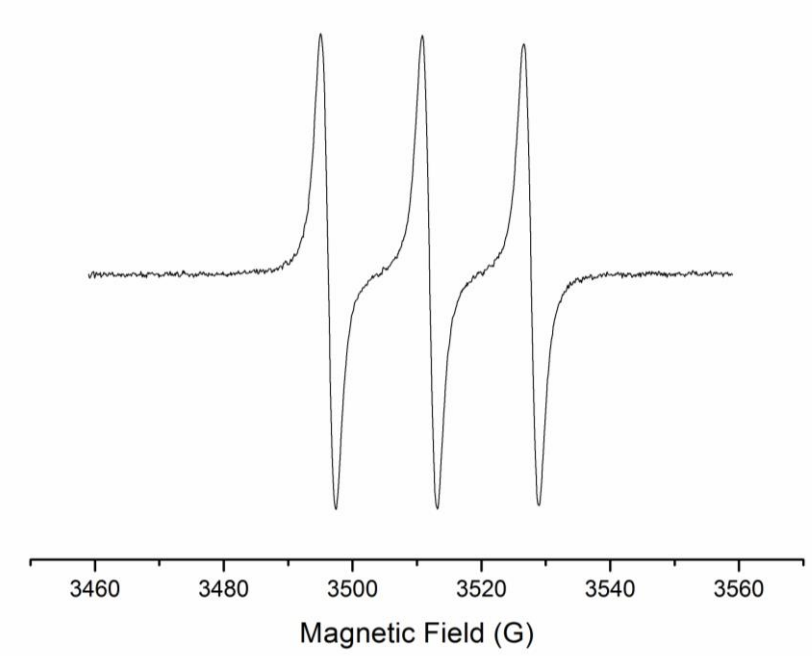

Figure 2.14 EPR spectrum of isolated product.

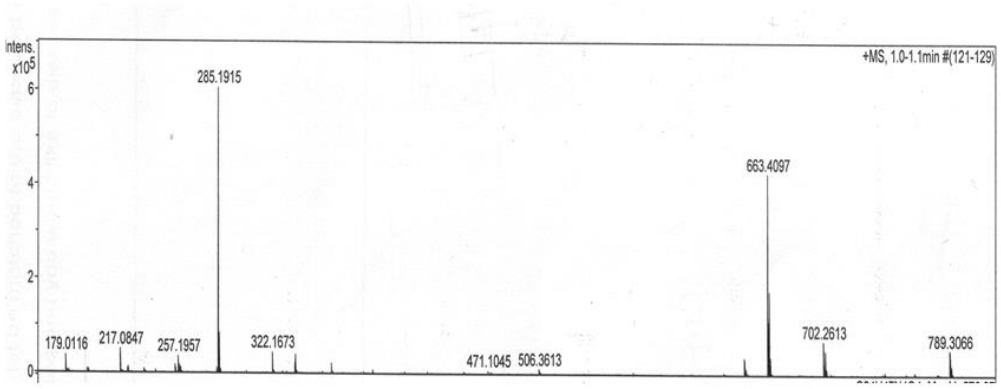

Figure 2.15 MS analysis of isolated product.

Then a new batch of this reaction was set up with 1 equivalent of CuI catalyst. The crude product was analysed by EPR and MS. Unfortunately, MS spectrum of the EPR active fraction showed a peak at m/z 663, which cannot be assigned to any reasonable product. No target product **2.19** was detected in the MS (Figure 2.16).

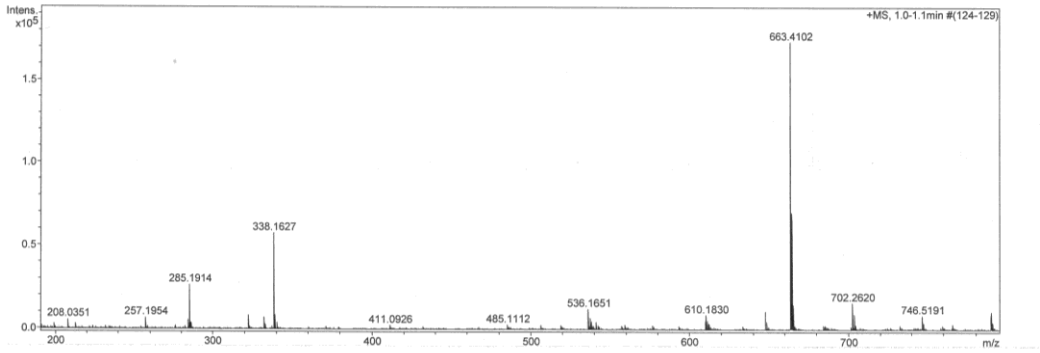

Figure 2.16 MS analysis of crude product.

A series of reactions between TEMPO azide **2.35** and alkyne **2.38** was set up in different solvents, at different temperatures, and with different amine additives (Table 2.1). The addition of amine additives can facilitate the formation of Cu-acetylide complexes which is an important intermediate in Cu-catalyzed azide-alkyne cycloaddition. When the reactants were stirred in DMSO in the presence of CuI without amine at 40 °C for 4 days, a new compound which is different from the products prepared in the first 2 reactions was detected according to TLC. Target compound **2.19** could be detected in the crude reaction mixture (Figure 2.17 and 2.18) and isolated by column chromatography.

Table 2.1 Optimisation the reaction condition

Solvent	Temperature	Amine	Target compound
THF	40 °C	Triethylamine	No
H_2O/EtOH (1:1 mixture)	reflux	Triethylamine	No
DMSO	40 °C	No	Yes

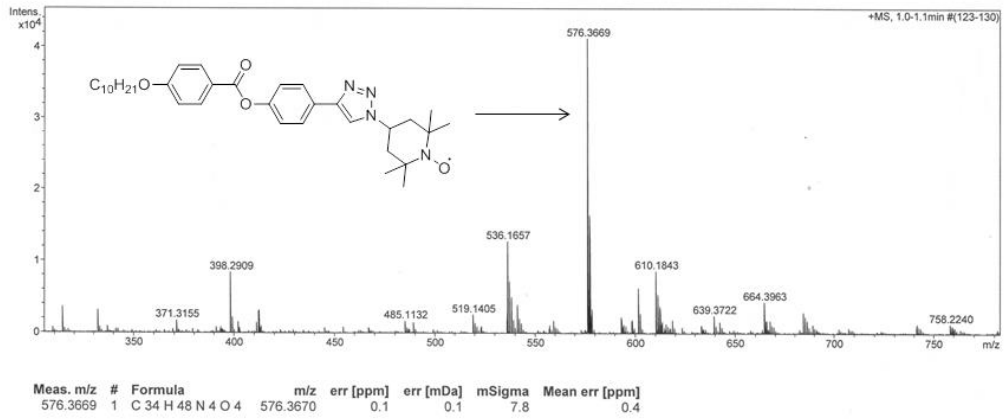

Figure 2.17 MS analysis of crude product.

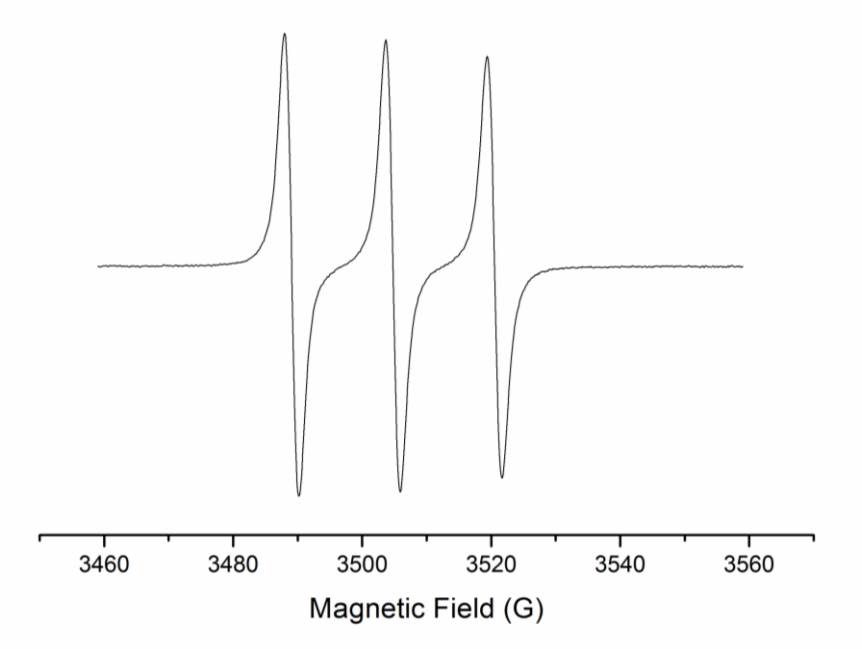

Figure 2.18 EPR spectrum of target compound **2.19**.

Unlike other click reactions, this reaction took about 4 days and the yield was not good (<40%). It was reported that the yield of TEMPO involved click chemistry is often poor; the lowest yield can be around 20%.[79,82,83] Possibly, in our reaction, the high reactivity and the steric hindrance of TEPMO azide component leads to the poor yield.

In order to test this hypothesis, alkyne component **2.18** was reacted with a non-radical azide, 1-azidocyclohexane. When 1-azidocyclohexane was reacted with alkyne **2.18**, the reaction was

complete in 48 h in 50% ethanol : water solution under reflux to give the triazole product in a 69% yield (Figure 2.19). These results suggested that click chemistry with TEMPO radical is not as straightforward as a normal click reaction.

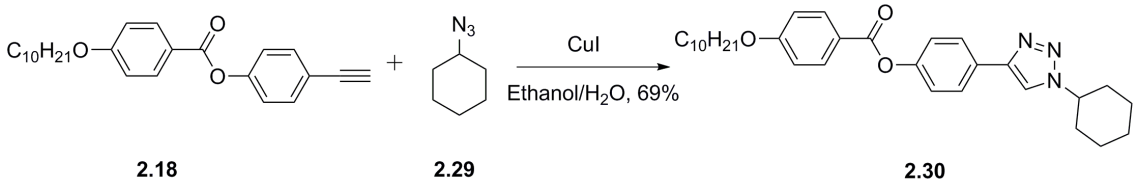

2.18 **2.29** **2.30**

Figure 2.19 The reaction of **2.18** and 1-azidocyclohexane.

J. E. Hein and V. V. Fokin suggested that CuI is not a good catalyst for the click reaction.[84] They proposed that the iodide anion could act as a bridging ligand, leading to the formation of polynuclear copper complexes. However, CuI is still commonly used in click reactions including the reactions with nitroxide-containing substrates, usually leading to target compounds in a high yield.

In summary, radical **2.19** was prepared successfully albeit in poor yield. Further optimisation of the synthesis can be carried out if this compounds shows mesogenic behaviour.

2.3 Properties of mesogen 2.19.

2.3.1 Liquid crystalline properties

The mesomorphic behaviour of **2.19** was investigated by polarised optical microscopy and DSC showing the sequence Cr 156.8 Iso liq °C. Unfortunately, **2.19** did not form liquid crystalline phases. The investigation of liquid crystals based on the 1,2,3-triazole ring, carried out by Gallardo's group, suggested that at least 3 rings are needed to obtain liquid crystalline phases.[85] **2.31** a compound with a similar structure forms the SmC and N phases (Figure 2.20). The

non-mesogenic behaviour of compound **2.19** could be explained by the lack of flexible alkyl chains on the terminal triazole rings which hampers formation of liquid crystalline phases.[76] However, introduction of a flexible chain to the TEMPO-azide component of compound **2.19** is challenging. The alkyl chains can be only introduced into the structure of TEMPO-azide by substituting a methyl group in the piperidine ring (Figure 2.21). This substituent however is a lateral group which can also be detrimental to the mesogenic stability.

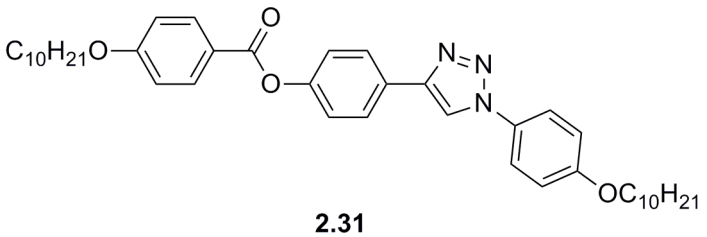

2.31

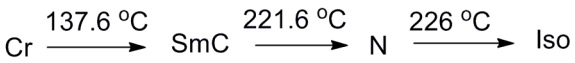

Figure 2.20 4 Rings bent-core liquid crystal compound.[85]

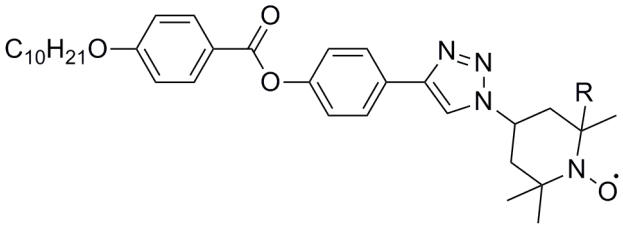

2.19'

Figure 2.21 The structure of substituted product **2.19'**.

Introduction of one more aromatic ring may increase the anisotropy of the molecule and induce mesomorphic behaviour. However, the melting point of **2.19** (156.8 °C) is already quite high. As the nitroxide radical is not stable at high temperature, high melting point is not good for our compound.

2.3.2 EPR studies in liquid crystal hosts

Although compound **2.19** did not form liquid crystalline phases, it has a potential to be used as a spin probe for studying the dynamic properties of diamagnetic liquid crystal compounds. Spin probes with a structure similar to the diamagnetic liquid crystal hosts could give precise information about dynamic properties in the mesophase.[86] Therefore, we studied the magnetic properties of mesogen **2.19** in liquid crystal hosts using EPR spectroscopy.

Liquid crystals based on 4-alkyl-4'-cyanobyphenyls (nCBs) are well studied by both experimental and computational methods. EPR studies of spin probes in these hosts have been reported.[87-90] We proposed that **2.19** can be used as a spin probe to study the dynamic properties of nCBs. In order to test this hypothesis, an EPR investigation of mesogen **2.19** in 4-octyl-4'-cyanobiphenyl (8CB, Figure 2.22) was carried out.

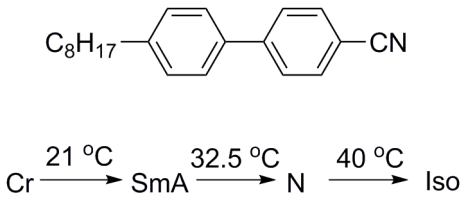

Figure 2.22 Structure and phase transition temperatures of 8CB.

A stock solution of compound **2.19** (2.3 mg) in DCM (100 ml) was prepared. 1 ml of this stock solution was added to 8CB host (200 µl). Then the solvent was removed under reduced pressure to get ca. 0.2 mM solution of compound **2.19** in 8CB. The mixture was loaded in a 1.3 mm diameter capillary tube flame sealed at the bottom. EPR spectra of this sample were recorded at various temperatures, starting from 292 K to 320 K and then cooled down to 292 K (Figure 2.23).

Anisotropic EPR spectra of compound **2.19** in 8CB were obtained (Figure 2.23). The three peaks in these spectra have different linewidth. Unlike low viscosity nitroxide solutions, the molecular tumbling of the nixtroxide in LC host is relatively slow. The relatively slow tumbling of large

molecules cause incomplete averaging of anisotropic magnetic interactions (e.g., g factor and hyperfine interaction), therefore the three peaks of these EPR spectra are not the same height (Chapter 1). A small change in effective hyperfine was observed in different phases. As the hyperfine interaction in nitroxides is dependent on the orientation of the spin probe in the magnetic field, the hyperfine constant in the direction parallel to the external magnetic field ($a_{//}$) is much larger than that in the direction perpendicular to the external magnetic field ($a_{\perp}$). When the temperature is above the isotropisation temperature, the random orientation of molecules leads to the average (e.g., isotropic) hyperfine constant. However, when the temperature is below nematic to isotropic phase transition of **2.19** in 8CB mixture, the spin probe **2.19** should be aligned in the nematic phase with the long axis of the molecule pointing in the direction of magnetic field. The decrease of hyperfine interaction constants in the liquid crystal phases should arise from the increasing contribution of $a_{\perp}$ in more ordered phase.

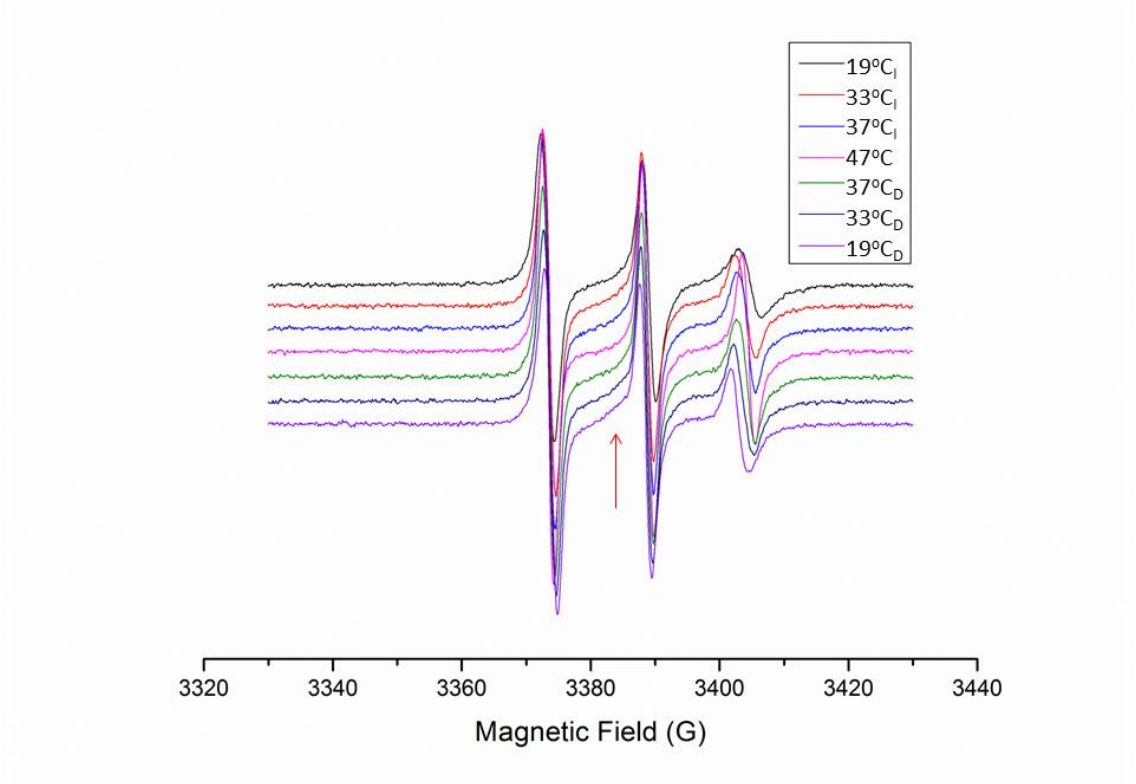

Figure 2.23 EPR spectra of compound **2.19** in 8CB; subscripts I and D represent the heating and cooling process separately.

However, the observed change of the effective hyperfine is very small (less than 1G) compared to that of the reported results, such as the EPR study of diphenyl nitroxide in 4,4'-dimethoxyazoxybenzene carried out by G. R. Luckhurst.[91] The authors reported that the nitrogen hyperfine changed from around 10G to 6G (e.g., close to $a_{\perp}$) upon nematic to isotropic transition. The small change of the effective hyperfine in our case indicates the poor alignment of spin probe **2.19** in the 8CB host. This may because probe **2.19** is bent-core, while the host 8CB is rod like. The radical component of the probe can rotate in the 8CB solution. This rotation of spin probe averages out the anisotropic hyperfine interaction further.

Alternatively, the small changes of effective hyperfine could be due to incomplete alignment of the 8CB host. Strong magnetic field should facilitate alignment of 8CB. In order to test this hypothesis, the mixture was heated to 320K then cooled down in a stronger magnetic field (8000G) to room temperature (292K). However, the effective hyperfine did not change further (Figure 2.24). It suggested that liquid crystal alignment by magnetic field at room temperature was relatively fast.

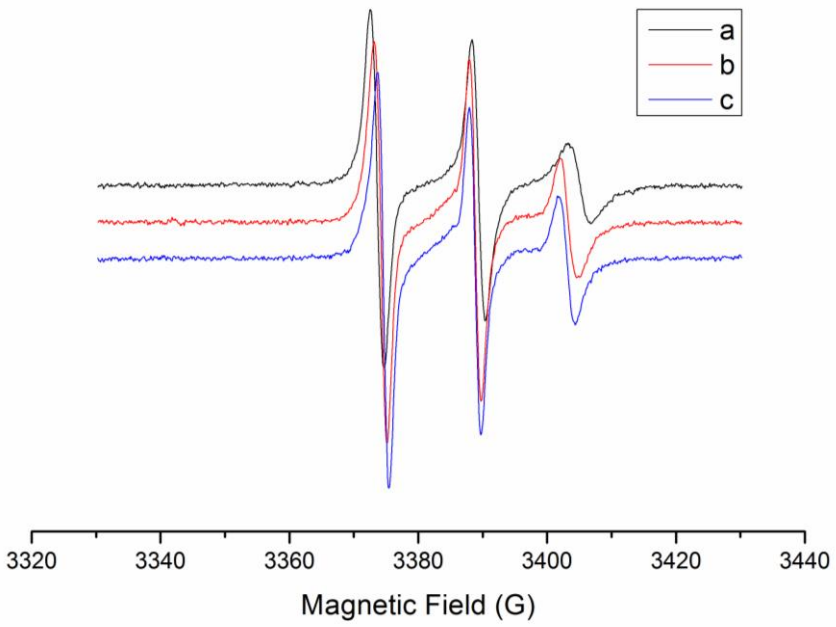

Figure 2.24 EPR spectra of 2.39 in 8CB. a) recorded directly at room temperature; b) sample heated to 320K then cooled down to room temperature in a 3400G magnetic field; c) sample heated to 320K then cooled down to room temperature in a 8000G magnetic field.

In order to check the alignment of this spin probe in other liquid crystal hosts, the probe was dissolved in E7 (a mixture of cyanobiphenyl and cyanoterphenyl compounds, Figure 2.25). E7 shows nematic phase from -10 °C to 58 °C.[92] E7 is commonly used as a liquid crystal host due to the wide temperature range in nematic phase.[93] *Ca.* 1mM solution of spin probe **2.19** in E7 host was prepared. EPR spectra of this sample were recorded at temperatures between 20 °C and 80 °C, with 5 °C intervals.

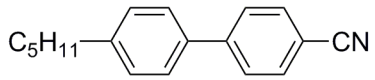

2.33

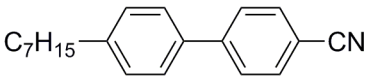

2.34

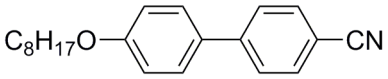

2.35

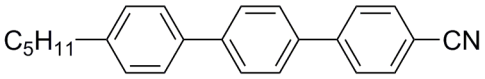

2.36

Figure 2.25 Four components of E7.

Anisotropic spectra of compound **2.19** in E7 host were obtained. Only slight change of effective hyperfine upon nematic to isotropic phase transition of E7 was observed (Figure 2.26). Again, this may due to the rotation of the bent core radical component in the host E7, averaging out the anisotropic effect.

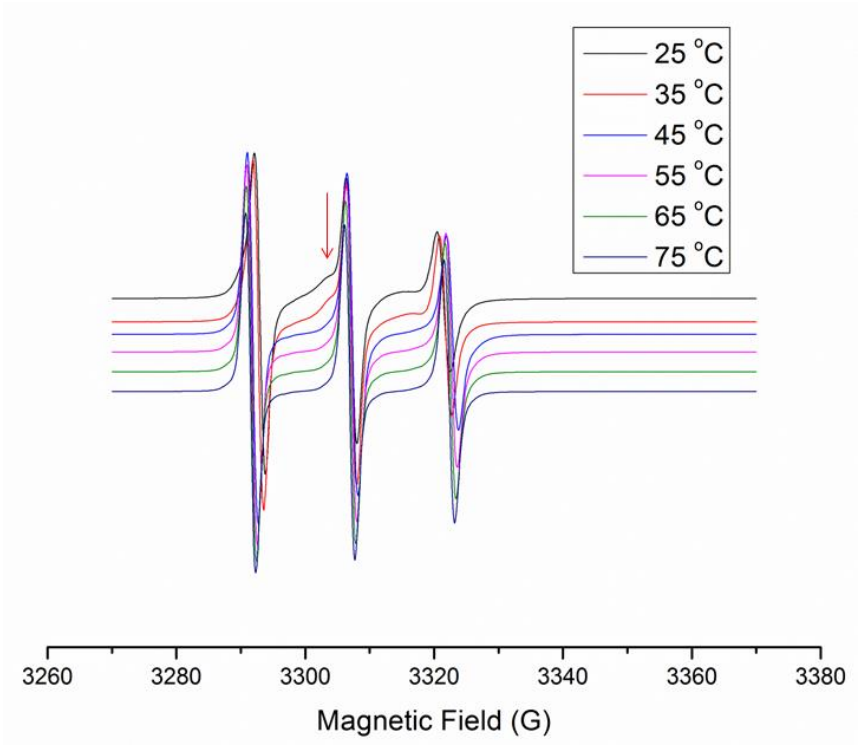

Figure 2.26 EPR spectra of **2.19** in E7 at different temperature.

Surprisingly, two paramagnetic components were found in nematic phase (the second component is shown with an arrow, Figure 2.26). Figure 2.27 shows the experimental and simulation EPR spectra of spin probe **2.19** in E7 at 25 °C. Two individual components could be obtained by simulation. These two components EPR spectra may arise from: a) paramagnetic impurity in spin probe **2.19**, b) partial aggregation of spin probe **2.19,** or c) two different orientations of **2.19** in liquid crystal hosts.

One of the two components became weaker with increasing temperature. When the temperature was above 55 °C (around the isotropisation temperature of E7), only one component was detected (Figure 2.26). When the temperature decreased to temperature below isotropic to nematic phase transition temperature, this component appeared again. This suggests that this component of EPR signal does not come from paramagnetic impurity. Moreover, no impurity was observed by other characterisation techniques, such as TLC.

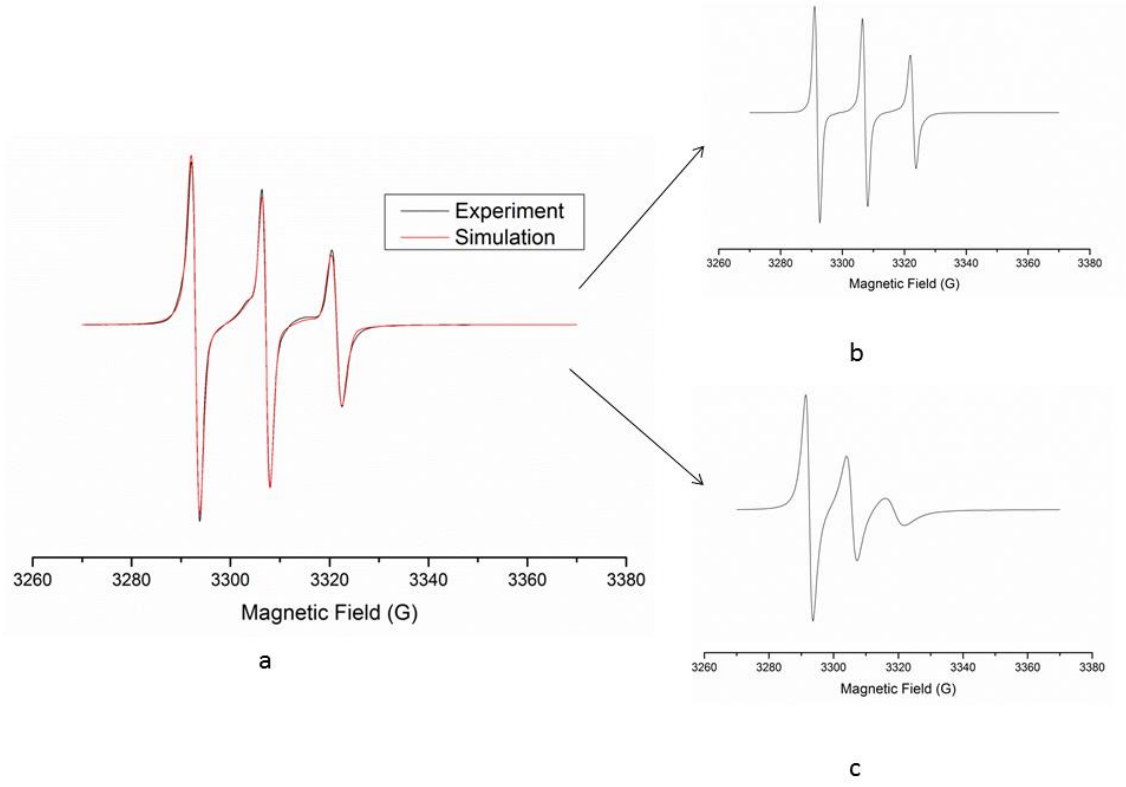

Figure 2.27 a) Experimental and simulation EPR spectrum of 2.19 in E7; b) and c) are simulation spectra of two components with a hyperfine coupling constant 14.2 G and 13.3 G respectively.

The two components EPR spectra could also originate from partial aggregation of spin probe **2.19**. Two different environments could be experienced by spin probe **2.19** because of partial aggregation leading to two components EPR spectra. In order to test this hypothesis, frozen solution spectra of spin probe **2.19** in E7 and toluene/chloroform mixture (2 : 1, this mixture forms a good glass upon freezing) were recorded. The frozen solution spectrum of TEMPO in E7 was also recorded as a control (Figure 2.28). If the nitroxides aggregated, significant line broadening of EPR spectrum would be observed due to dipole-dipole interaction which do not average out in the frozen solution (Chapter 1). Dipole-dipole interaction decreases rapidly with increasing spin-spin distance but the broadening is detectable in continuous wave EPR (cw-EPR) spectra for up to 2.5 nm interspin distances.[94,95] The aggregation of spin probe **2.19** should significantly reduce spin-spin distance leading to a broad EPR spectrum at low temperature. However, only slight difference was observed with these three spectra. It suggested that the aggregation of spin probe **2.19** did not occur.

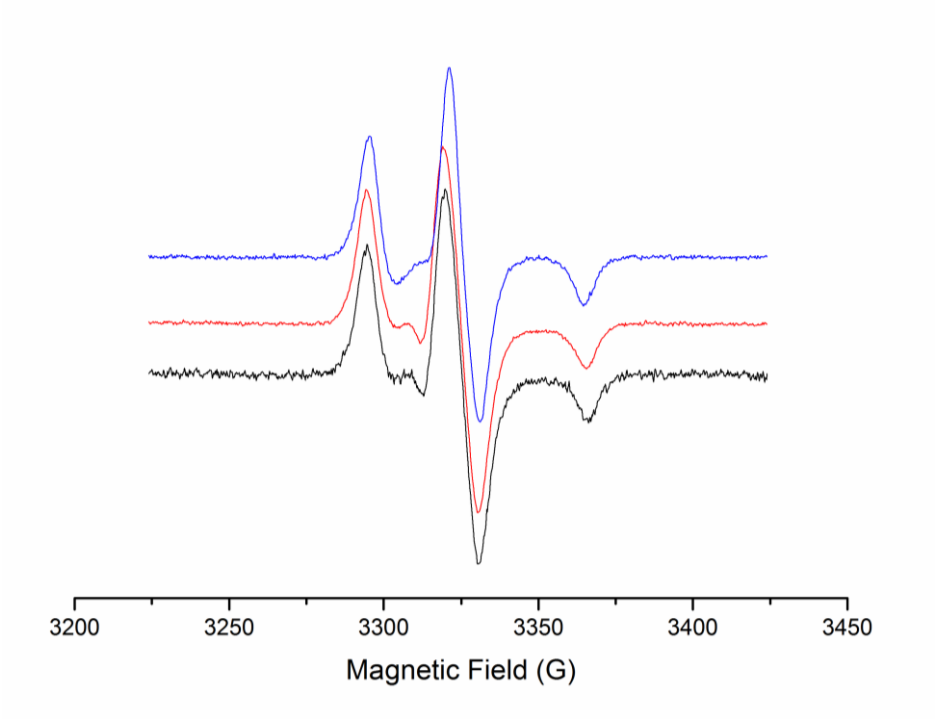

Figure 2.28 EPR spectra of spin probe **2.19** and TEMPO in E7 and toluene/chloroform mixture at 119K; blue line is **2.19** in E7; red line is **2.19** in toluene/chloroform (2 : 1) mixture; black line is TEMPO in E7.

The two components of EPR spectra could also originate from two different orientations of **2.19** in liquid crystal hosts. As the g value and hyperfine interaction are anisotropic, different orientations of **2.19** in liquid crystal hosts would result to two components EPR spectra.

In order to test whether the same phenomenon can be observed in other single component liquid crystals, spin probe **2.19** was dissolved in liquid crystal hosts **2.37** and **2.38** (Figure 2.29). 0.5% (weight percent) mixtures of **2.19** in these two liquid crystal hosts were prepared separately.

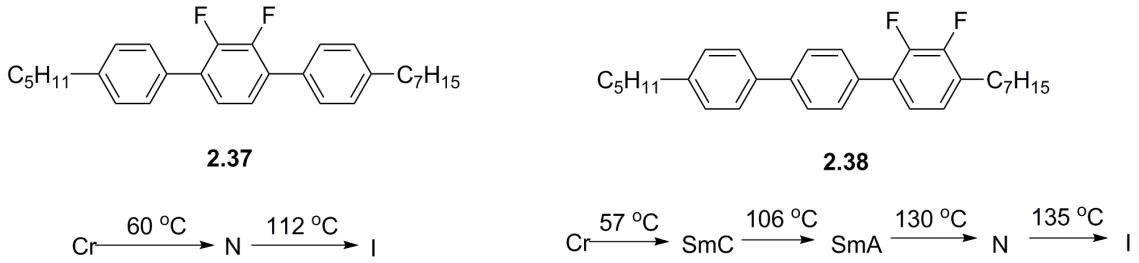

Figure 2.29 Structures and phase transition temperatures of two new liquid crystal hosts.

The EPR spectra of spin probe **2.19** in these two mixtures also showed only a small change of effective hyperfine constant upon increasing temperature (Figure 2.30 and 2.31). The second component of EPR signal was observed in the liquid crystal phase and disappeared when the temperature was above the clearing point of liquid crystal hosts.

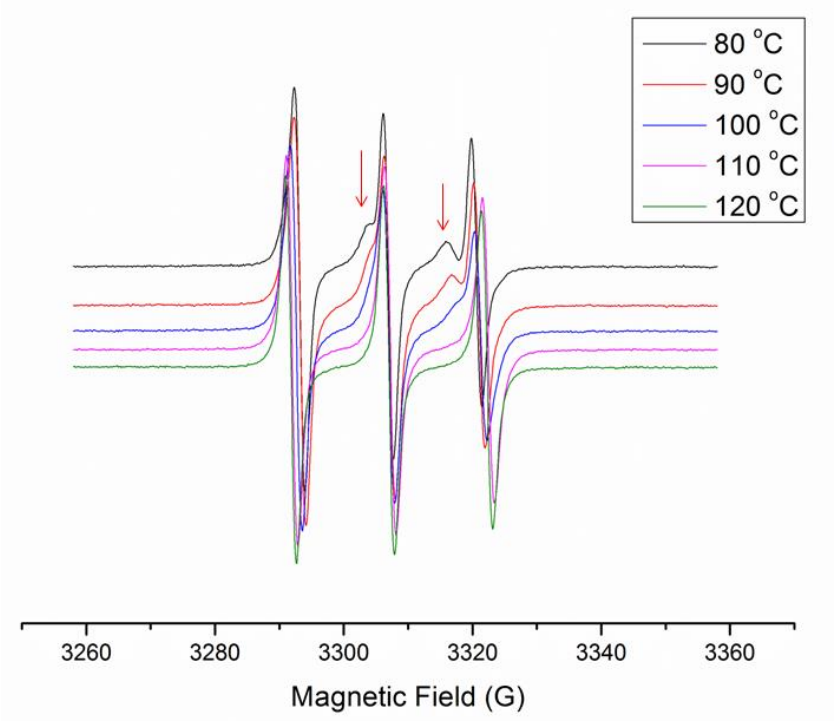

Figure 2.30 EPR spectra of **2.19** in **2.37** at different temperatures.

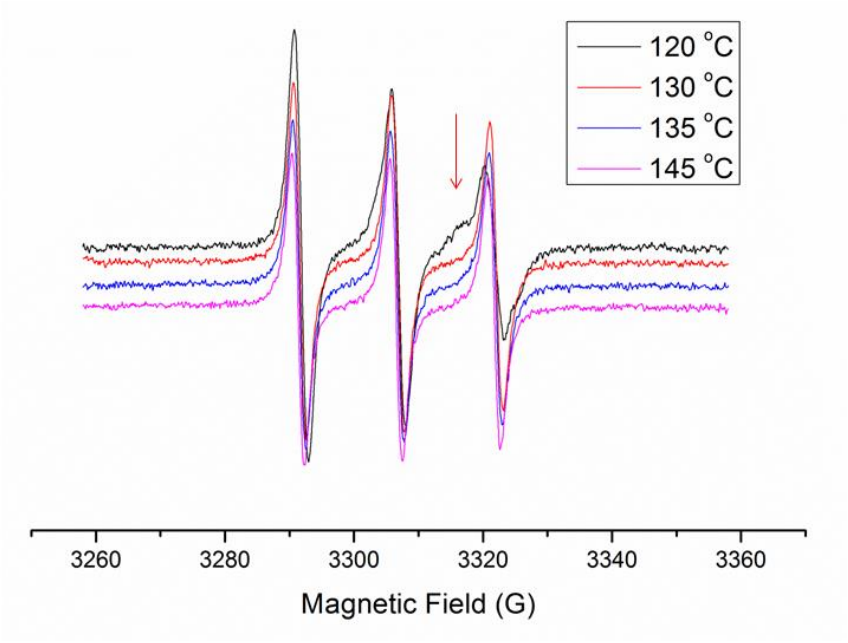

Figure 2.31 EPR spectra of **2.19** in **2.38** at different temperatures.

In summary, when compound **2.19** was mixed with different liquid crystal hosts, it was poorly aligned and EPR spectra showed the presence of two components in liquid crystal phases. The reason why two components are found in the liquid crystalline phase is not clear. One possibility is that two orientations of spin probe **2.19** exist in liquid crystal hosts.

The virtual phase transition temperature of a liquid crystal like compound (such as compound **2.19**) could be obtained from the phase diagram of a mixture of this compound with a liquid crystal host by extrapolating the liquid crystal to isotropic phase transition temperature curve (Figure 2.32). However, an attempt to build a phase diagram of a mixture of compound **2.19** with liquid crystals failed because compound **2.19** did not show complete miscibility with common liquid crystal hosts, such as 4-octoxyl-4'-cyanobiphenyl (8OCB), E44, E67 (mixture of nCBs and nOCBs) and liquid crystal **2.39** (Figure 2.33).

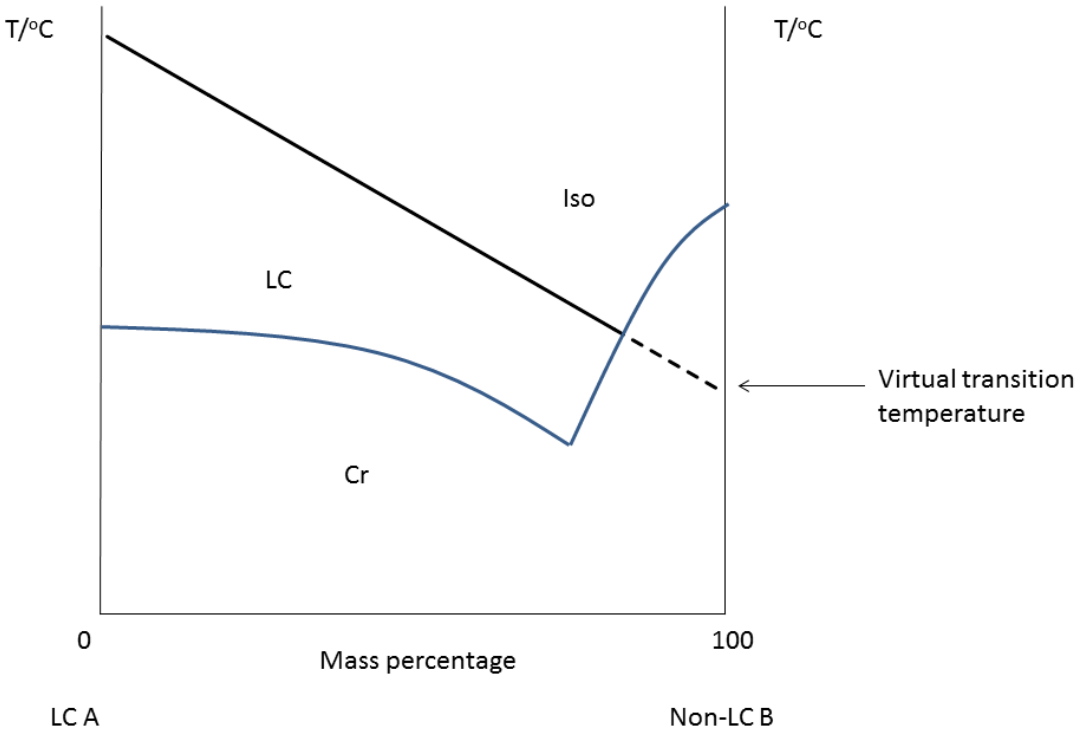

Figure 2.32 Schematic representation of phase diagram of a LC compound A and non-LC compound B; blue curve represents melting point, black curve represents clearing point.

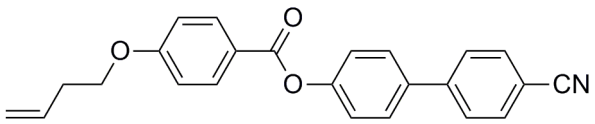

2.39

Figure 2.33 Structure of liquid crystal **2.39**.

2.4 Conclusions

A new spin probe **2.19** has been prepared using click chemistry. It did not show liquid crystalline properties, probably due to the inappropriate length to width ratio and insufficient number of alkyl chains.

The reaction between TEMPO-azide and alkyne **2.18** takes much longer than normal click reactions. Moreover, the yield of this reaction is poor. The poor yield may be due to the high reactivity of TEMPO-azide.

Addition of further aromatic rings to this compound in order to facilitate LC phase formation was considered. However, the melting point of this compound is relatively high, and introduction of more phenyl rings may increase the melting point further, which would lead to the decomposition of the radical. Another possible way to improve mesogenic behaviour is to increase the number of alkyl chains. However, alkyl chains can only be introduced in place of the methyl groups, and this may not help to improve the mesogenic stability.

EPR studies of compound **2.19** in different liquid crystal hosts suggested that the alignment of compound **2.19** in the liquid crystal matrix is poor, possibly because of the bent core shape of this compound. Two temperature dependent environments were detected in the solution of compound **2.19** in liquid crystal matrices. EPR studies of compound **2.19** in E7 and organic solvents at low temperature suggest that these two components spectra do not arise from the aggregation of compound **2.19**. It may due to the existence of two orientations of spin probe **2.19** in LCs. Poor miscibility of compound **2.19** in different liquid crystals made it difficult to build a phase diagram.

Chapter 3 Nitronyl Nitroxide Mesogens

3.1 Introduction

3.1.1 Nitronyl nitroxide

The first derivative of nitronyl nitroxide radical was prepared by E. F. Ullman and J. H. Osiecki in 1968.[96] A dark blue product was isolated when excess lead dioxide was added to a benzene solution of compound **3.1** at room temperature (Figure 3.1). Five lines with a ratio of 1 : 2 : 3 : 2 : 1 were observed in the EPR spectrum of the reaction mixture due to the coupling of electron with two equivalent nitrogen atoms (Figure 3.2). This radical could be stored in darkness at room temperature for several weeks. No decomposition was found when this radical was heated to temperature as high as its melting point (85 °C) and treated with hot aqueous alkali, while the colour of this compound changed to orange in the presence of acid.

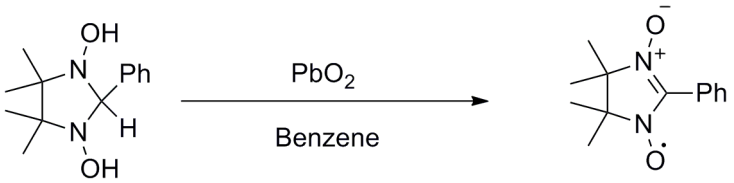

3.1 **3.2**

Figure 3.1 Preparation of nitronyl nitroxide.[96]

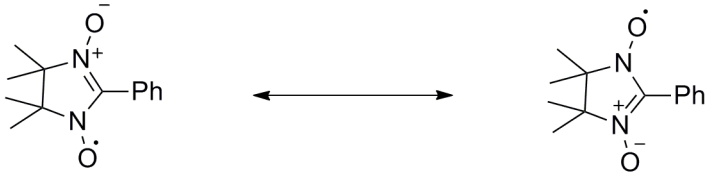

Figure 3.2 Resonant structures of nitronyl nitroxide **3.2**.

Nitronyl nitroxides attracted much attention, especially in the field of coordination chemistry. They are promising ligands for building metal ion based organic magnets. A range of metal nitronyl nitroxide complexes was prepared successfully.[97-99] In 1991, ferromagnetic coupling was observed in the bulk sample of *p*-nitrophenyl nitronyl nitroxide by M. Takahashi and co-workers at 0.65 K (Figure 3.3).[100] Since then, nitronyl nitroxide radicals have been used as building blocks for magnetic materials.

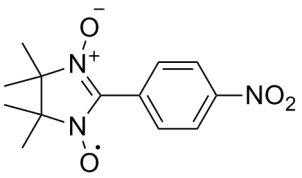

3.3

Figure 3.3 *p*-Nitrophenyl nitronyl nitroxide.[100]

3.1.2 Nitronyl nitroxide in liquid crystals

In 2002, several liquid crystalline compounds containing the nitronyl nitroxide structure unit were prepared by S. Greve and co-workers.[101] Two of them presented monotropic mesophase (Figure 3.4). On heating, compound **3.4** transforms to an isotropic liquid at 90 °C and compound **3.5** reaches the isotropic liquid at 91.5 °C. On cooling, a mesophase was observed at 36 °C for compound **3.4** and at 39 °C for compound **3.5**.

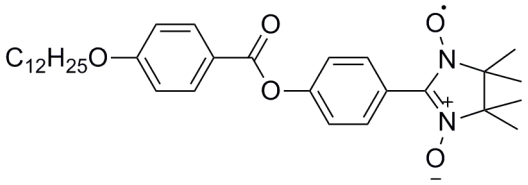

3.4

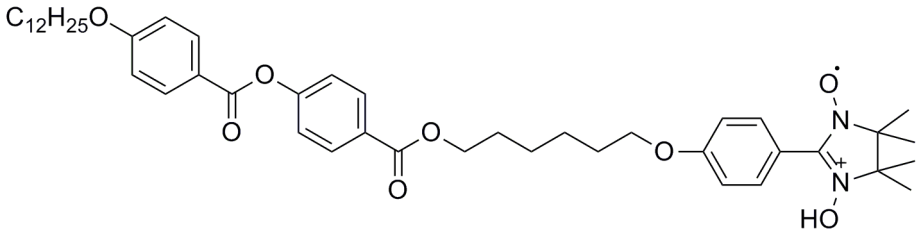

3.5

Figure 3.4 Two liquid crystalline compounds containing nitronyl nitroxide.[101]

However, the authors did not present the polarising optical microscopy textures of these two mesophases. They described these mesophases as higher order phases, rather than low order phases like nematic and smetic C phases. The mesophase of compound **3.4** was not miscible with the nematic phase of PCH7 (4-(trans-4-heptylcyclohexyl benzonitrile), while the mesophase of compound **3.5** was not miscible with the SmC phase of HOPDOB (4-hexyloxyphenyl-4-decyloxybenzoate) (Figure 3.5). The mesophase structure of these two compounds has not been determined. No further information of these two compounds was reported.

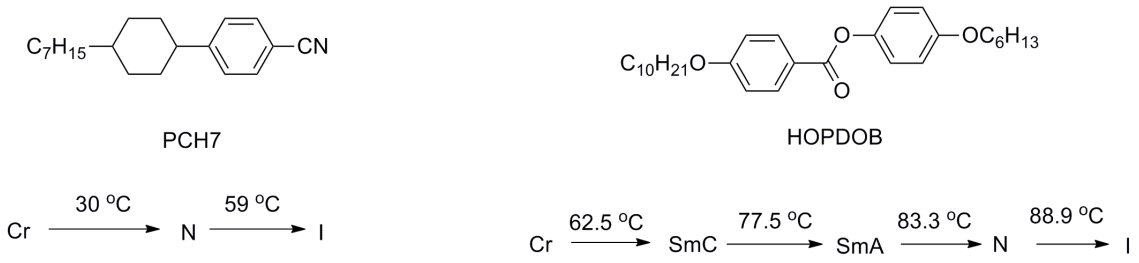

Figure 3.5 The structures and transition temperatures of PCH7 and HOPDOB.[101]

A range of nitronyl nitroxide containing liquid crystal-like compounds was prepared by S. Nakatsuji and co-workers in 2002 (Figure 3.6).[102] Unfortunately, these compounds did not form

any mesophase. Weak antiferromagnetic interaction was observed in these compounds at low temperature (lower than 0.6K).

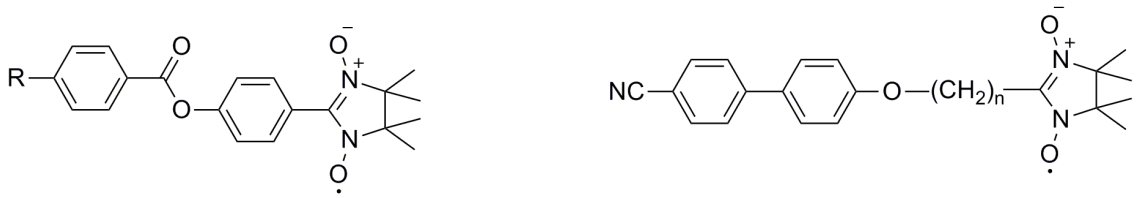

3.6a: R=C_7H_{15}
3.6b: R=C_8H_{17}

3.7a: n=9
3.7b: n=10
3.7c: n=11

Figure 3.6 Structures of nitronyl nitroxide compounds prepared by S. Nakatsuji and co-workers.[102]

To the best of our knowledge, no more reports on nitronyl nitroxide containing mesogens were published. It is still a relatively new field of paramagnetic liquid crystals.

3.1.3 Aims

In this chapter, we aim to prepare a mesogen with nitronyl nitroxide rigidly attached to an aromatic core. In order to simplify the synthetic work, *p*-hydrophenyl nitronyl nitroxide was chosen as the radical component. It can be coupled to a benzoic acid fragment using the Steglich coupling reaction.

3.2 Preparation of nitronyl nitroxide mesogen.

3.2.1 Design of the target mesogen

The melting point of compound **3.4** is 90 °C. Extending the rigid aromatic core by addition of more phenyl rings to the structure may lead to a higher melting point. Decomposition of

radicals occurs rapidly at high temperature. Our target compound should not involve too many phenyl rings. A benzoic acid involved two phenyl rings may be suitable for our target compound. S. Greve and S. Nakatsuji's work showed that two phenyl rings compounds with short alkoxyl chains do not form mesophases. Decyloxy chains may give a better chance to form mesophase (Figure 3.7).

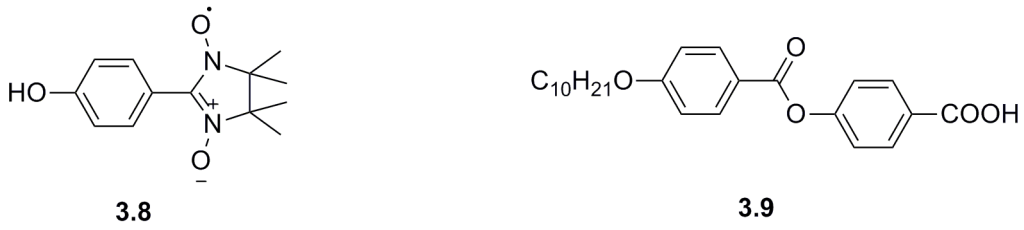

3.8 **3.9**

Figure 3.7 Two components of the target compound.

3.2.2 Preparation of compound 3.9

The 4-[[4-(decyloxy)benzoyl]oxy]benzoic acid **3.9** was prepared following literature procedure.[4] 4-(Decyloxy)benzoic acid, prepared from 4-hydroxybenzoic acid, was coupled with 4-hydroxybenzyl benzoate to obtained benzyl 4-[[4-(decyloxy)benzoyl]oxy] benzoate **3.12**. Compound **3.12** was deprotected using Pd/C catalysed hydrogenolysis to form the benzoic acid derivative **3.9** (Figure 3.8).

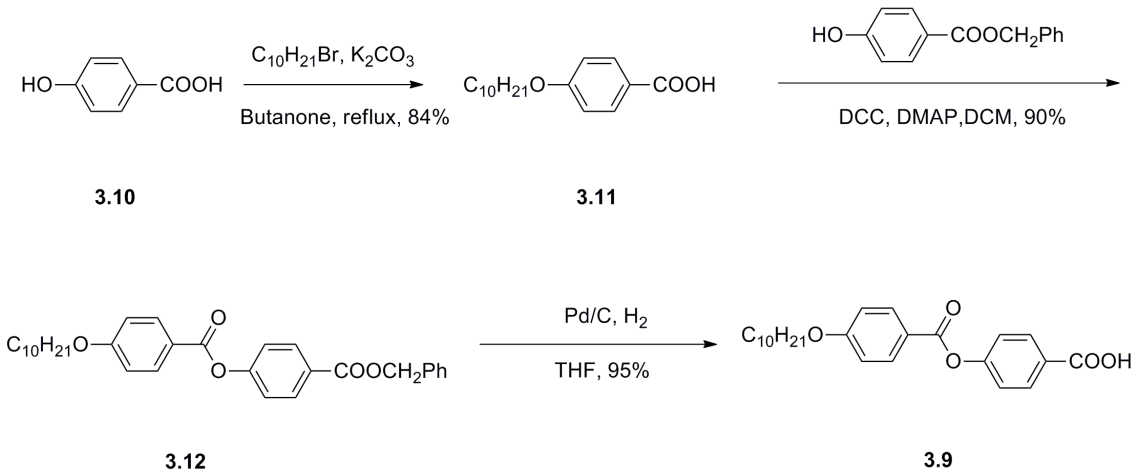

3.10 **3.11**

3.12 **3.9**

Figure 3.8 Preparation of benzoic acid component **3.9**.

3.2.3 Preparation of *p*-hydroxyphenyl nitronyl nitroxide

Preparation of *p*-hydroxyphenyl nitronyl nitroxide was carried out following the literature procedure.[103] 2,3-Dimethyl-2,3-dinitrobutane was prepared from 2-nitropropane. Zinc powder was used to reduce nitrobutane to obtain 2,3-bis(hydroxyamino)-2,3-dimethylbutane. This product was then reacted with benzaldehyde to yield imidazolidine derivative **3.16**. Compound **3.16** was then oxidized with lead dioxide to form *p*-hydroxyphenyl nitronyl nitroxide (Figure 3.9).

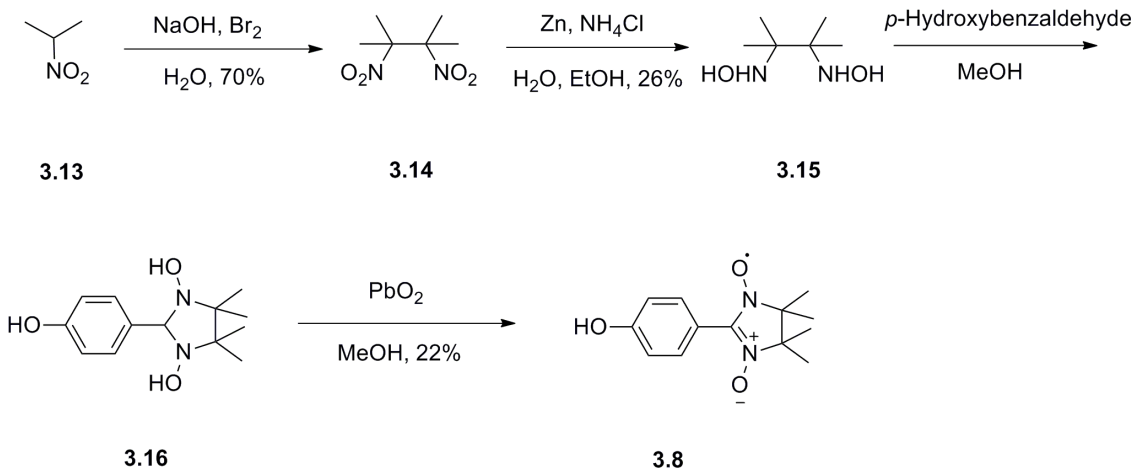

Figure 3.9 Preparation of *p*-hydrophenyl nitronyl nitroxide.

The EPR spectrum of nitronyl nitroxide **3.8** shows 5 peaks with a 1 : 2 : 3 : 2 : 1 ratio (Figure 3.10). The hyperfine constant of two nitrogens were obtained from simulation, a_{N1} = 7.53 G, a_{N2} = 7.53 G, which are similar to that of nitronyl nitroxide **3.2** (a_N= 7.5 G).

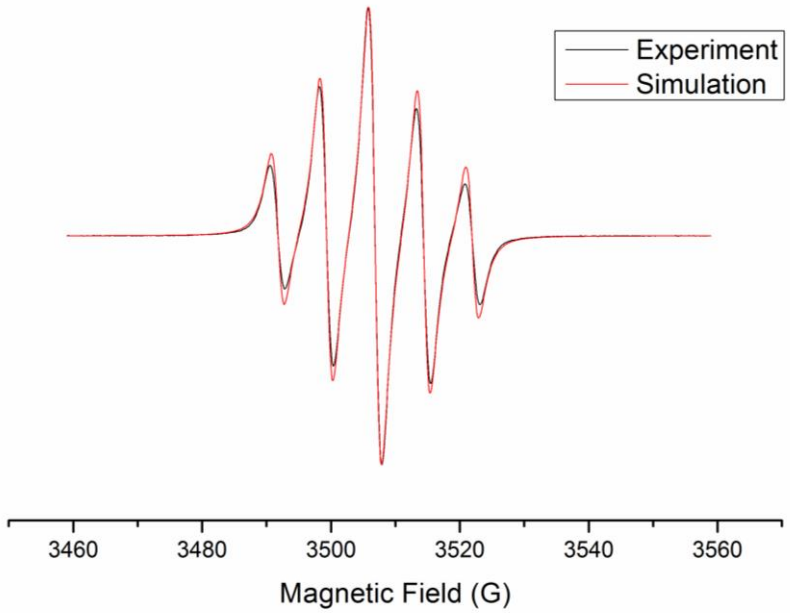

Figure 3.10 EPR spectra of *p*-hydroxyphenyl nitronyl nitroxide. Black line is experimental data, red one is simulation data, a_{N1}=7.53 G, a_{N2} = 7.53 G.

Preparation of *p*-hydroxyphenyl nitronyl nitroxide is not straightforward. The overall yield of the radical is very low (less than 5% from dinitro compound). Moreover, the reproducibility of this procedure is poor. The key step of the synthesis is the reduction of the dinitrobutane **3.14** to bis(hydroxylamine) **3.15**. Most of published literature on the preparation of nitronyl nitroxide radicals uses zinc powder to reduce dinitrobutane **3.14**.[103-106] We have optimised the procedure as follows. Zinc powder was added slowly (over 2 h) to an ethanol/water solution of the dinitro compound and ammonium chloride at the temperature lower than 12 °C. After the addition of zinc powder, the mixture was stirred at room temperature for 12 h. The solid was filtered off, and the solvent was removed under vacuum. Most of the reported yields of bis(hydroxylamine) **3.15** are higher than 50%. However, even with the optimised synthesis, we could never get a crude yield higher than 30%.

A. Caneschi and co-workers mentioned this reaction in a review about metal nitronyl nitroxide complexes. In their lab, the yield of compound **3.15** was never higher than 35%.[105] They believed that the bis(hydroxylamine) product is volatile, and is lost during the removal of solvent under reduced pressure. They suggested that only filtration should be involved in the

work up procedure, and the filtrate should be used directly in the next step to react with acetaldehyde. Sodium metaperiodate rather than lead dioxide was used in the final oxidation step, and a 64% yield of nitronyl nitroxide from dinitro compound was reported. However, in our reaction, the crude mixture of bis(hydroxylamine) reacted very slowly with *p*-hydroxybenzaldehyde (reaction time over 2 days). This synthesis, however, gave *p*-hydroxyphenyl imino nitroxide **3.17** rather than nitronyl nitroxide (Figure 3.11). Figure 3.12 shows the EPR spectrum of this radical. The spectrum has 7 peaks in a 1 : 1 : 2 : 1 : 2 : 1 : 1 ratio. The hyperfine constants were obtained from spectrum simulation, a_{N1} = 9.10 G, a_{N2} = 4.36 G. Figure 3.13 shows MS spectrum of this radical.

Imino nitroxides were prepared successfully by E. F. Ullman and co-workers in 1970.[107] Imino nitroxide could be obtained by treating nitronyl nitroxide with nitrous acid or heating nitronyl nitroxide with triphenylphosphine in benzene. However, they found that some nitronyl nitroxides may convert to a diamagnetic species which can be oxidised further to imino nitroxide at room temperature.[103] Possibly, in our reaction, nitronyl nitroxide was formed first, and then converted to imino nitroxide in the reaction system.

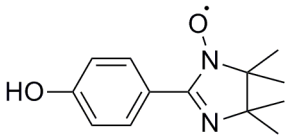

3.17

Figure 3.11 Structure of p-hydroxyphenyl imino nitroxide.[107]

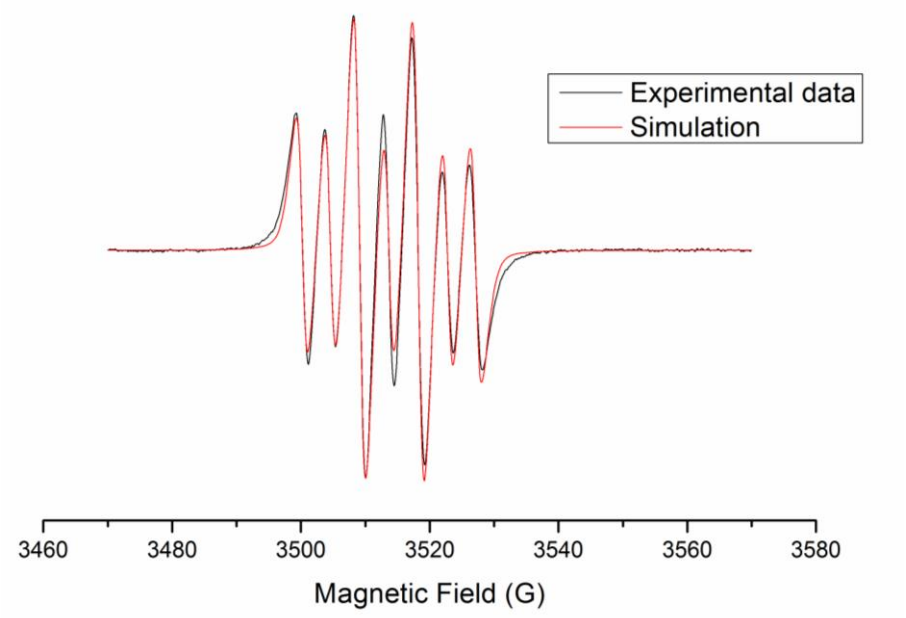

Figure 3.12 EPR spectrum of *p*-hydroxyphenyl imino nitroxide.

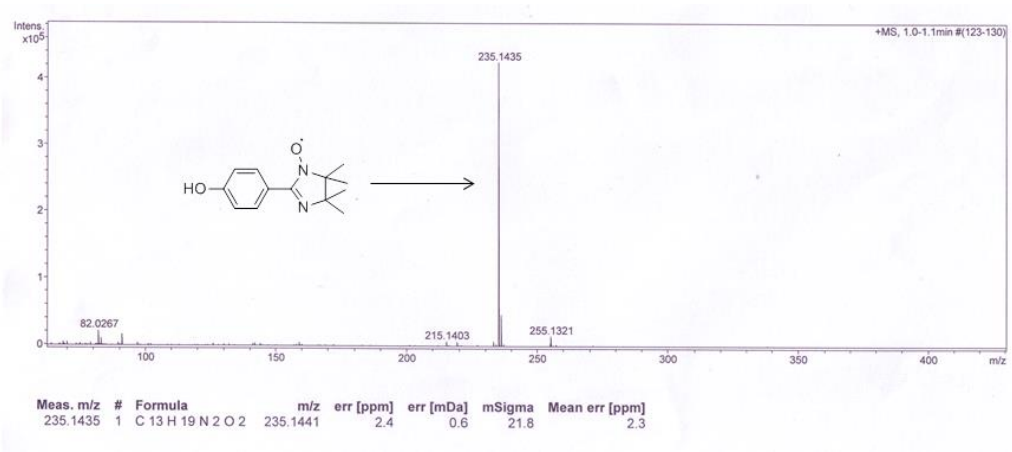

Figure 3.13 MS spetrum of *p*-hydroxyphenyl imino nitroxide.

A comprehensive study of the reduction of dinitrobutane **3.14** was carried out by C. Hirel and co-workers.[104] They found that the addition of acid to obtain bis(hydroxylamine) salt did not increase the yield of this reaction. They believe that the evaporation of the bis(hydroxylamine) is not the main reason for the low yield. They suggested that ethanol/water mixture should be replaced by THF/water mixture, because ethanol can be oxidised by the bis(hydroxylamine), and 8 equivalents of ammonium chloride are needed in the reaction. However, based on more than one hundred repeats of the synthesis, the reproducibility of this reaction was still poor. These authors also reported a modified procedure which can give a better reproducibility and

yield. Instead of adding zinc powder to the solution, aqueous ammonium chloride solution was added slowly (over 2 h) to the dinitro derivative and zinc powder in THF/water (1 : 1) mixture. They concluded that the poor reproducibility of the traditional procedure is caused by the poor control of addition of zinc powder. We have tried this procedure for our compound; it still resulted in low yield and poor reproducibility.

An alternative reducing reagent was used to prepare nitronyl nitroxide derivatives by G. Harada and co-workers.[108] Dinitro compound **3.14** was reduced by aluminium-amalgam in THF in a few minutes. Around 50% yield of bis(hydroxylamine) product was obtained. However, the crude yield was only around 10% in our hands. The reproducibility of this reaction was better than the reaction which uses zinc powder.

The other problem with the reduction of dinitro compound **3.14** is that the bis(hydroxylamine) product cannot be purified easily. Continuous extraction with DCM using Soxhlet apparatus was recommended by C. Hirel and co-workers.[104] However, it did not work well for us. Most published reports suggested that the crude product can be used directly to react with excess aldehyde. The purification was carried out at the final step when nitronyl nitroxide product was formed. In this chapter, the bis(hydroxylamine) compound was not isolated from the crude product mixture.

In summary, different methods have been used to prepare 2,3-bis(hydroxylamine)-2,3-dimethylbutane. The yields of all these methods are poor. The reproducibility of this reaction could be improved by using aluminium-amalgam to replace zinc powder as a reducing reagent.

The reaction between *p*-hydroxybenzaldehyde and bis(hydroxylamine) **3.15** is the other difficult step in the synthesis of *p*-hydroxyphenyl nitronyl nitroxide. The reaction between bis(hydroxylamine) **3.15** and aliphatic aldehyde is quick (several hours) with a high yield. However, bis(hydroxylamine) **3.15** reacted slowly with *p*-hydroxybenzaldehyde (reaction time more than 2 days). S.Shimono and co-workers found that the yield of this reaction decreased

when the electron donating group was introduced at the para position of benzaldehyde (Figure 3.14).[109] For R = H, the yield was 74% after the mixture was stirred at room temperature for 2 days. However, for R = OCH_3 the yield dropped to 27%, and 47% yield was obtained for R = OH. Very low yield (4%) of a similar reaction was also reported by S. Nakatsuji and co-workers for a reaction that was stirred at room temperature for 1 day (Figure 3.15).[102] Because we were using *p*-hydroxybenzaldehyde, the reaction took more than 2 days and the yield was poor.

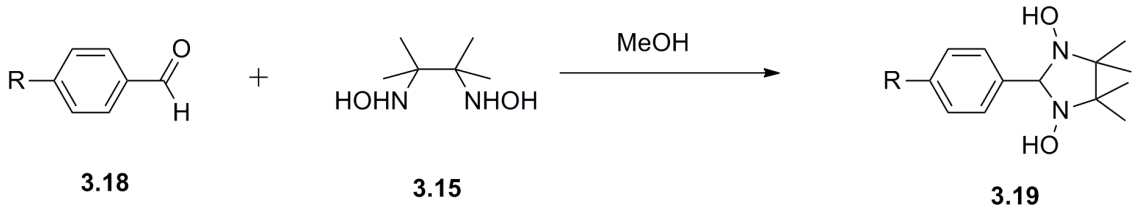

3.18 **3.15** **3.19**

Figure 3.14 The reaction between substituted benzaldehyde and bis(hydroxylamine) compound.[109]

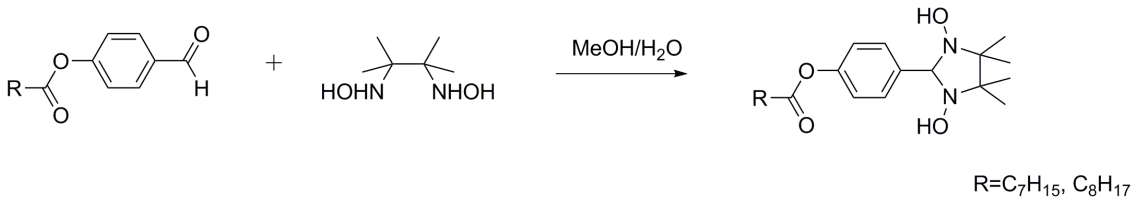

3.20 **3.15** **3.21**

Figure 3.15 The reaction between substituted benzaldehyde and bis(hydroxylamine) compound.[102]

3.2.4 Nitronyl nitroxide and imino nitroxide radicals

A set of nitronyl and imono nitroxide radicals was prepared by esterificaition of *p*-hydroxyphenyl nitronyl nitroxide and imino nitroxide with several substituted benzoic acid to yield **3.22**, **3.23**, **3.25** and **3.27**. Radical **3.22** was prepared by Steglich coupling reaction according to the scheme shown in Figure 3.16. Figure 3.17 shows the MS analysis of compound **3.22**. *p*-Hydroxyphenyl imino nitroxide was also used to react with carboxylic acid component **3.9** to obtain compound **3.23** (Figure 3.18 and 3.19). Two other benzoic acid components **3.24** and **3.26** were coupled with *p*-hydroxyphenyl nitronyl nitroxide to yield **3.25** and **3.27** (Figure

3.20). These two carboxylic acids were commonly used to prepare liquid crystals. Unfortunately, no mesophase was observed for all these four radicals **3.22**, **3.23**, **3.25** and **3.27**.

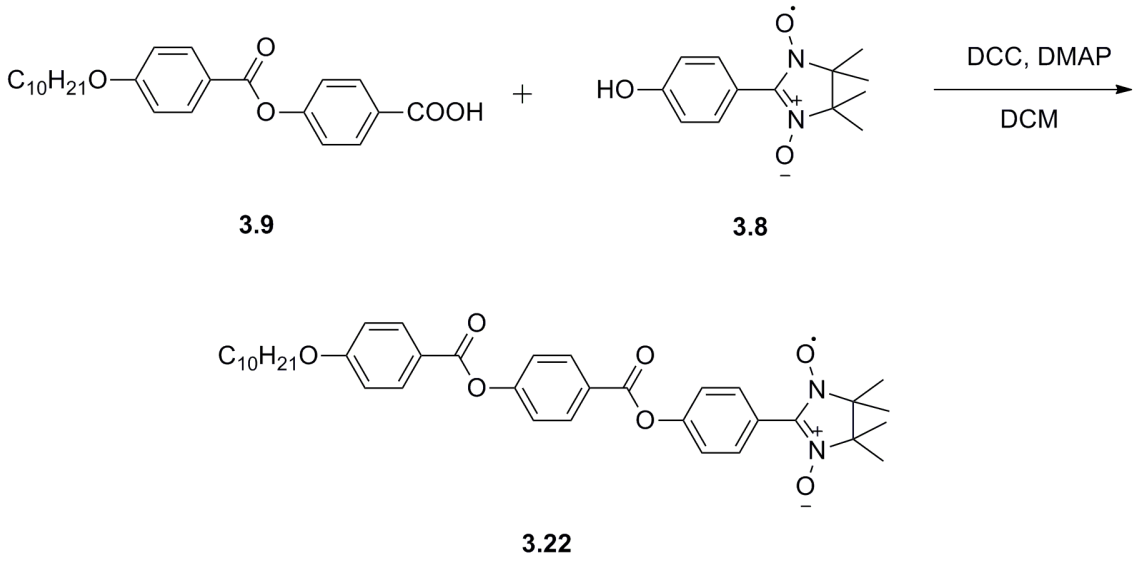

Figure 3.16 Preparation of radical **3.22**.

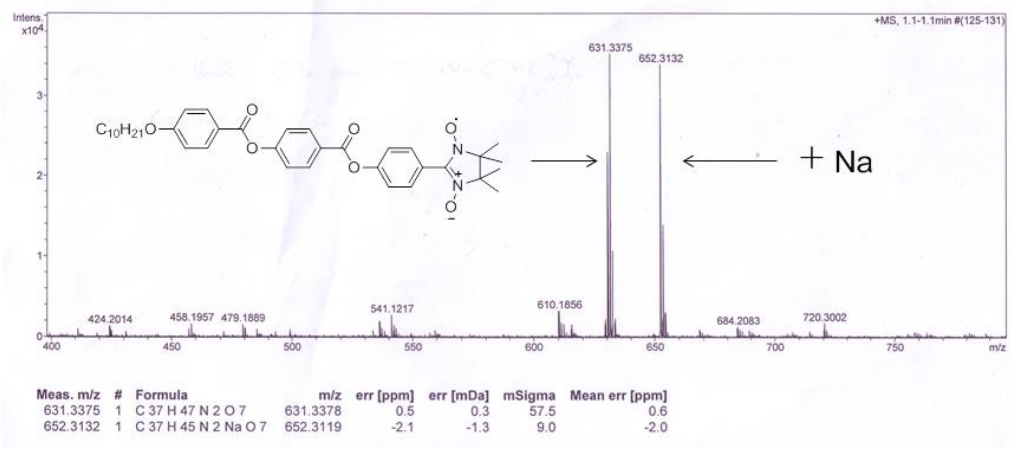

Figure 3.17 MS analysis of radical **3.22**.

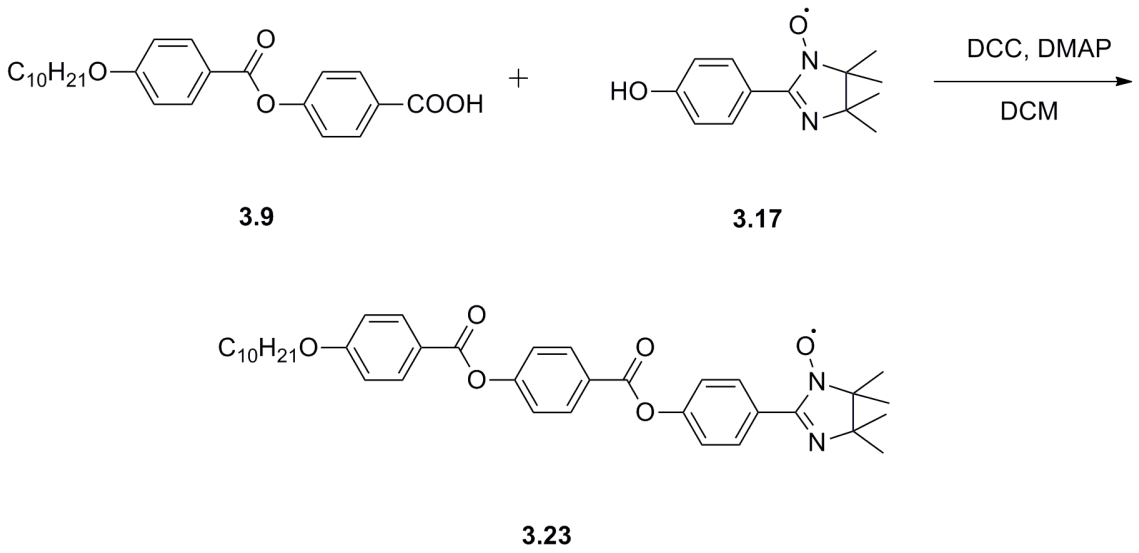

Figure 3.18 Preparation of radical **3.23**.

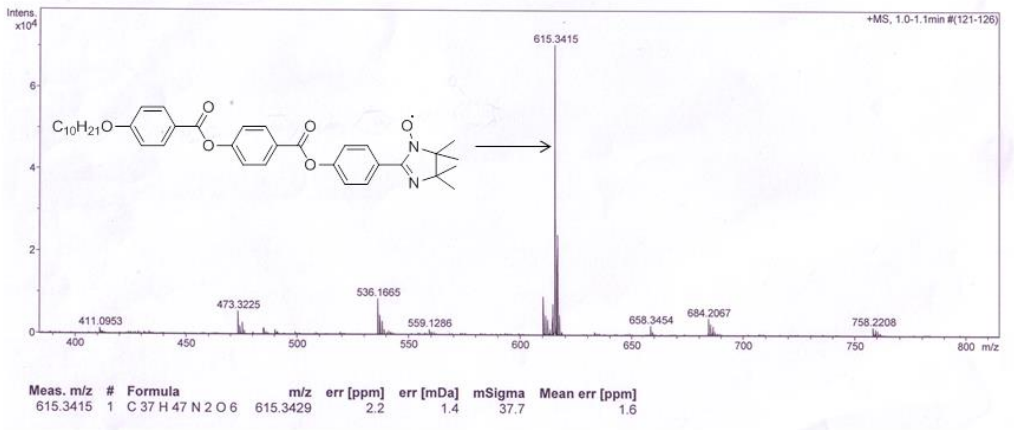

Figure 3.19 MS analysis of radical **3.23**.

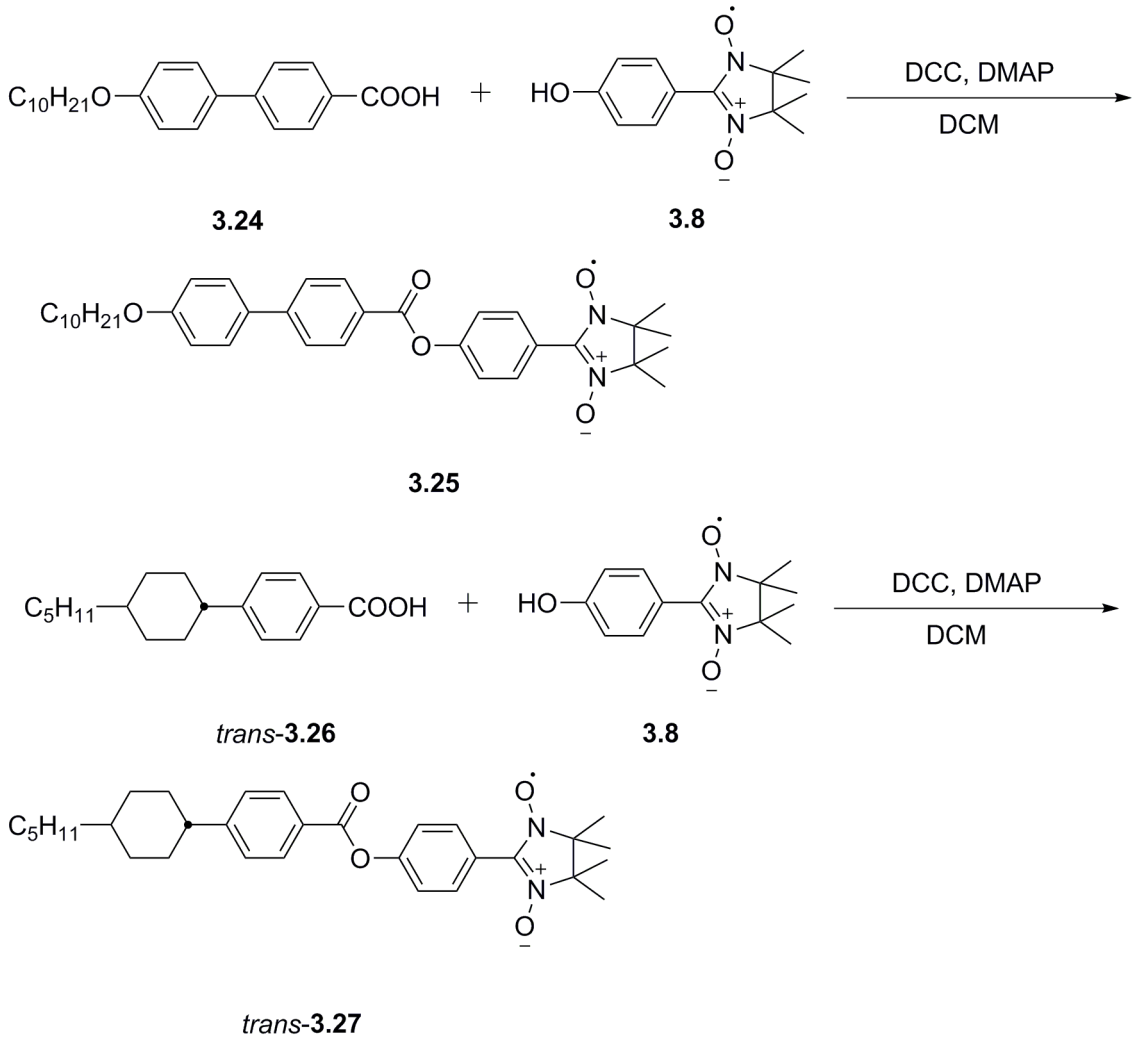

Figure 3.20 Reactions of two carboxylic acid components with nitronyl nitroxide.

Table 3.1 exhibits the thermal properties of **3.22**, **3.23**, **3.25** and **3.27**. Surprisingly, the melting point of radical **3.23** is much lower than **3.22**. Possibly the strong intermolecular ionic interactions of radical **3.22** result in the higher melting point. The decomposition of radicals **3.25** and **3.27** were observed around 130 °C before reaching to the melting point. As there are no linking groups between two ring structures of benzoic acid **3.24** and **3.26**, the melting points of radical **3.25** and **3.27** may higher than radical **3.23**.

Table 3.1 Thermal properties of radicals **3.22**, **3.23**, **3.25** and **3.27**.

Radicals	Thermal properties (°C)
3.22	Cr 122.3 IsoLiq
3.23	Cr 101.6 IsoLiq
3.25	Decomposed at 130
3.27	Decomposed at 130

The molecular structure of compound **3.6a** was reported by S. Nakatsuji and his co-workers.[102] The three rings in this compound are not coplanar. The dihedral angle between the imidazoline ring and the benzene ring is 25.3°, and the dihedral angle between two benzene rings connected by the ester group is 103.9°. This molecular structure may destroy the mesogenic stability.

Only a few papers report liquid crystal-like nitronyl nitroxide derivatives.[101,102] Mesophase was only observed by S. Greve and cowokers. Presumably, the steric demands of the nitronyl nitroxide end group of the rigid core, is detrimental to mesomorphic behaviour as it may preclude effective core-core interactions. Therefore, these radicals are not suitable for the preparation of liquid crystals.

3.3 Conclusions

New nitronyl nitroxide and imino nitroxide containing compounds **3.22**, **3.23**, **3.25** and **3.27** were prepared successfully by Steglich coupling of *p*-hydroxyphenyl nitronyl and imino nitroxide with several substituted benzoic acids. However, it was found that the preparation of *p*-hydroxyphenyl nitronyl nitroxide is not straightforward. The reduction of 2,3-nitro-2,3-dimethylbutane by zinc gave a poor yield of 26% and the reproducibility of this reaction was poor. Better reproducibility was obtained by using aluminium-amalgam. However, the yield did not improve. Although several different procedures for the preparation of

2,3-bis(hydroxylamino)2,3-dimethylbutane **3.15** were reported, the yield and reproducibility of all reductions were still poor. The reaction between *p*-hydroxybenzaldehdye and bis(hydroxylamine) **3.15** is slow and the yield is not good.

No liquid crystalline properties were observed for these radicals. The large dihedral angle between benzene and imidazoline rings and between the two benzene rings may hamper the formation of the mesophases.

Chapter 4 Mesogens Based on Blatter-type radical

4.1 Introduction

4.1.1 Blatter's radical

1,3-Diphenyl-1,2,4-benzotriazinyl radical was first prepared by H. M. Blatter and H. Lukaszewski in 1968. The stability of the radical is remarkable, better than the stability of the EPR calibration standard 2,2-diphenyl-1-picrylhydrazyl (DPPH) (Figure 4.1).[64]

4.1: R=H
4.1': R=CH_3

4.2

Figure 4.1 Structures of 1,3-diphenyl-1,2,4-benzotriazinyl radicals and DPPH **4.2**.

Blatter's radical was prepared by two different synthetic routes, starting from *N*'-phenyl-*N*-phenyliminobenzamidine and benzoyl 2,2-bis-(*p*-tolyl)-hydrazide (Figure 4.2). The second route was used to confirm the structure of the radical (Figure 4.3).

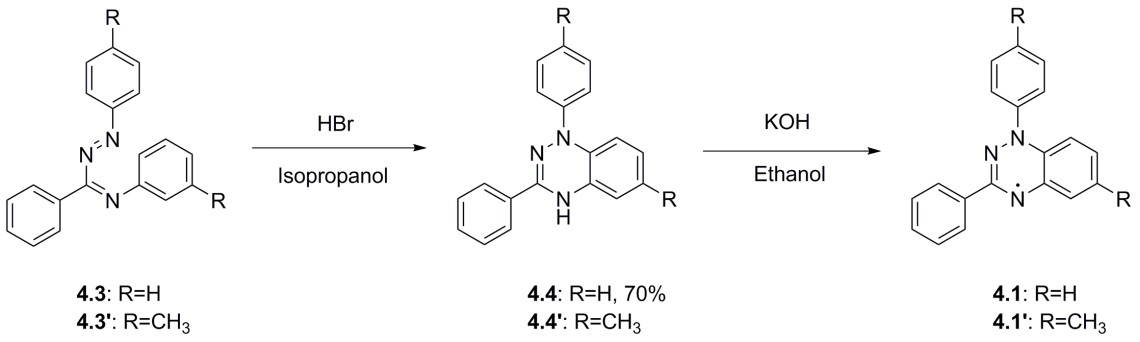

Figure 4.2 Radical prepared from *N'*-phenyl-*N*-phenyliminobenzamidine; yields of other compounds were not reported.[64]

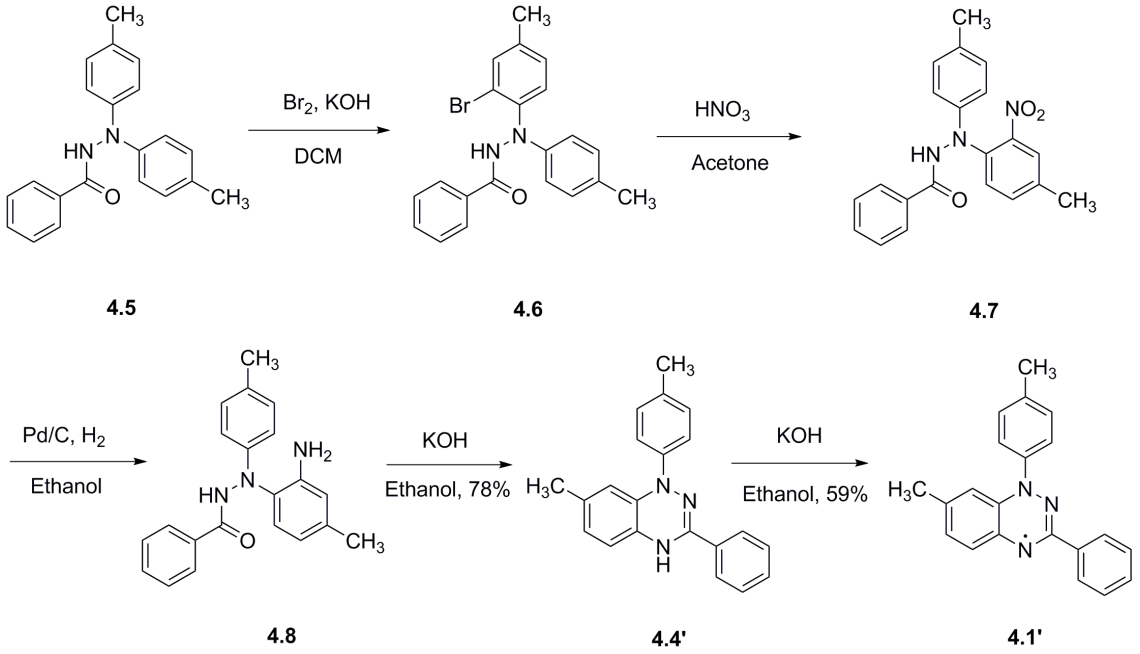

Figure 4.3 Radical prepared from benzoic 2,2-bis-(*p*-tolyl)-hydrazide; yields of **4.6** and **4.7** were not reported.[64]

However, the authors did not investigate any properties of these radicals. Surprisingly, these outstanding stable radicals did not attract too much attention. Only a few papers about these radicals were published during the 1960s to 1970s, maybe because it is not easy to prepare and functionalize them.[110-114]

A new one step procedure was reported by R. Huisgen and J. Wulff which simplifies the synthesis of these radicals (Figure 4.4).[111] Figure 4.5 shows an EPR spectrum of radical **4.14**. In

order to increase the yield of this reaction, the mild oxidant chloranil was added. However, the addition of this oxidant led to a new side reaction. The by-product was assigned the structure of compound **4.15**, although no characterisation was presented (Figure 4.6).

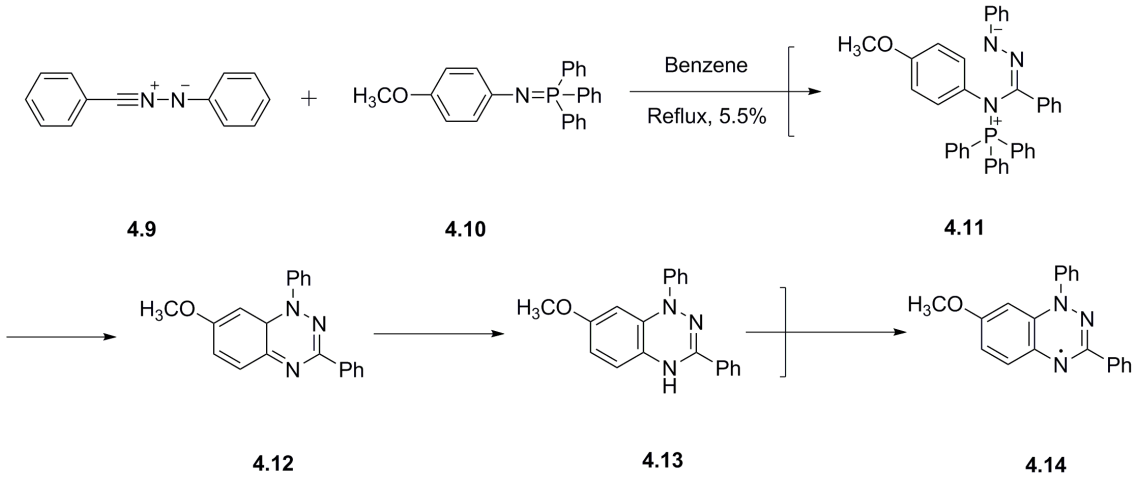

Figure 4.4 The new procedure reported by R. Huisgen and J. Wulff; compounds in the brackets are intermediates, not isolated.[111]

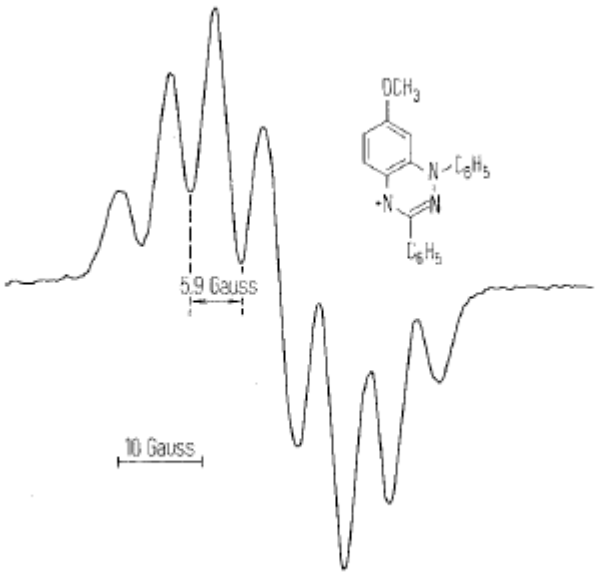

Figure 4.5 EPR spectrum of radical **4.14.**[111]

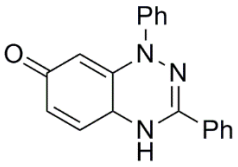

4.15

Figure 4.6 The proposed structure of the byproduct.

The Blatter-type radical was obtained accidentally by B.I. Buzykin and N. G. Gazetdinova when they investigated the reaction between 1,3-diphenylnitrilimine and benzaldehyde phenylhydrazone.[115] The cleavage of N-N bond (Figure 4.7) of hydrazidine compound **4.17** resulted in azoimine compound **4.3** which gave radical **4.1** upon refluxing in anisole for 20 min. In order to prove the structure of compound **4.4**, ascorbic acid was used to reduce radical **4.1**. However, the product converted back to the radical during the isolation.

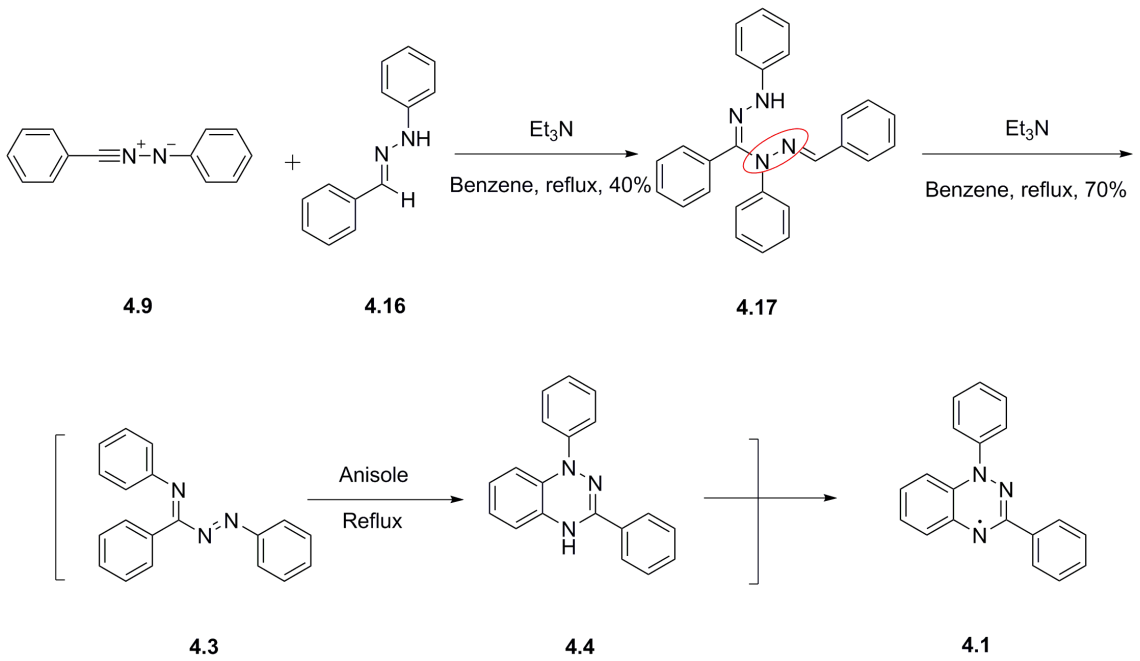

4.9 **4.16** **4.17**

4.3 **4.4** **4.1**

Figure 4.7 The formation of Blatter-type radical from hydrazidine, compound **4.3** and **4.4** were not isolated.[115]

In 1980, a comprehensive study of Blatter-type radicals was carried out by F. A. Neugebauer and I. Umminger.[116] A range of Blatter-type radicals was prepared (Figure 4.8).

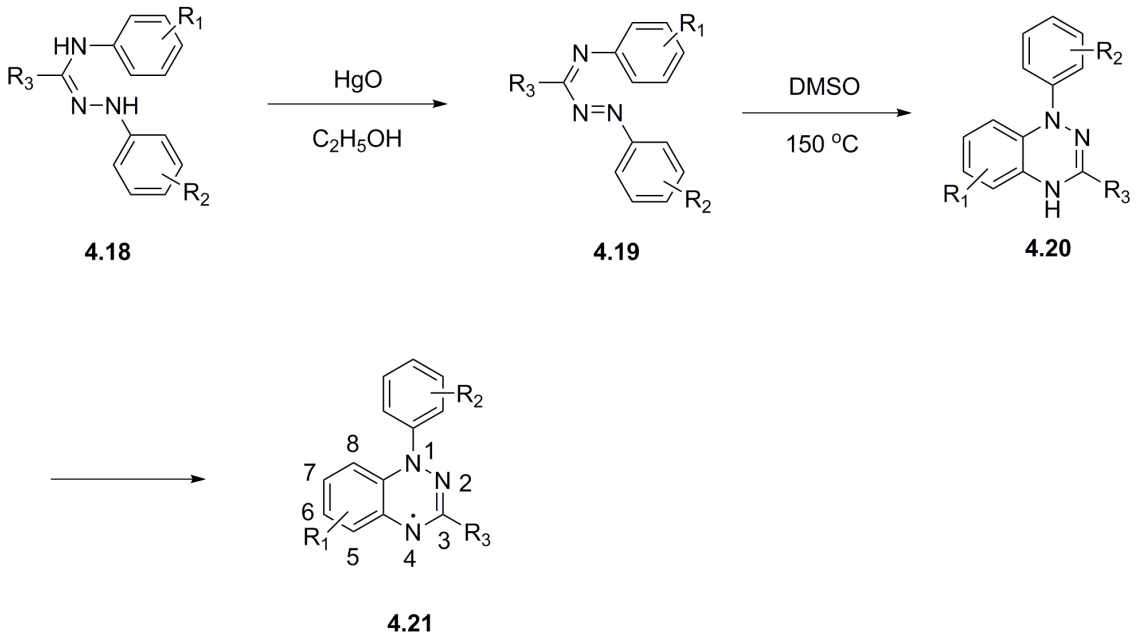

Figure 4.8 Preparation of Blatter-type radicals.[117]

They found that the methoxy group in C7 position of compound **4.21** (Figure 4.8) facilitates a side reaction. A purple dye was formed when the radical **4.14** was exposed to air (Figure 4.9). The structure of this dye was confirmed by NMR analysis as compound **4.15** proposed by R. Huisgen and J. Wulff in 1969.[111] For radical **4.1**, this decomposition product was found after 6 weeks of exposure to the air. C. P. Constantinides and co-workers found that the stability of Blatter-type radical was improved significantly by introducing a substituent in C7, especially trifluoromethyl group.[118] No oxidation product was found when compound **4.20a** ($R_1 = CF_3$) was treated with 10 equivalents of $KMnO_4$ in refluxing benzene for 2 days (Figure 4.10).

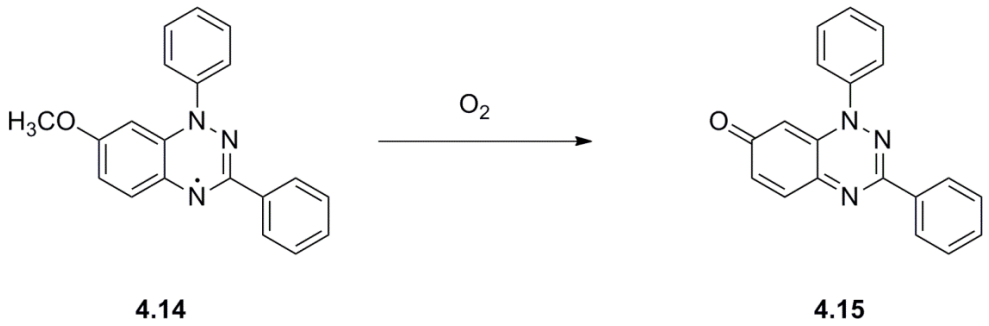

Figure 4.9 Decomposition of Blatter-type radical.[117]

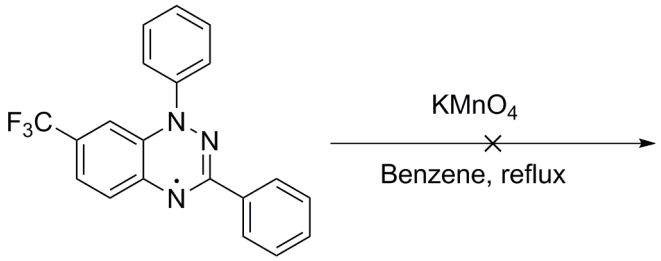

4.20a

Figure 4.10 Radical **4.20a** in benzene with 10 equivalents $KMnO_4$.

The EPR spectrum of radical **4.1** was collected by F. A. Neugebauer and I. Umminger (Figure 4.11). The hyperfine coupling constants of three nitrogen atoms are 7.4 G, 5.1 G and 5.1 G.

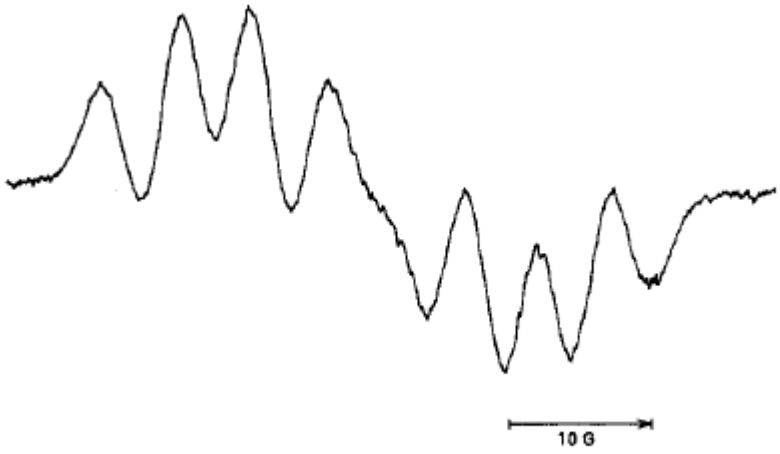

Figure 4.11 EPR spectrum of radical **4.1**.[116]

In order to assign the hyperfine coupling constants to each nitrogen nucleus, radical **4.22** was prepared (Figure 4.12). ^{15}N has a nuclear spin 1/2, while ^{14}N has a nuclear spin 1. The contribution of ^{15}N hyperfine can therefore be determined by simulation. The EPR spectrum of radical **4.22** is shown in Figure 4.13. The hyperfine coupling constants of three nitrogens are 10.35 G, 5.1 G and 5.1 G. By comparison with the nitrogen hyperfine constants of radical **4.1**, the largest hyperfine coupling was assigned to N_1 (Figure 4.8 compound **4.21**). The authors suggested that the large hyperfine of N_1 should be the result of a significant contribution of resonance structure of **4.1b** (Figure 4.14).

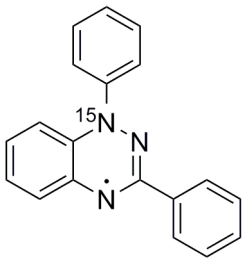

4.22

Figure 4.12 The structure of radical **4.22**.[116]

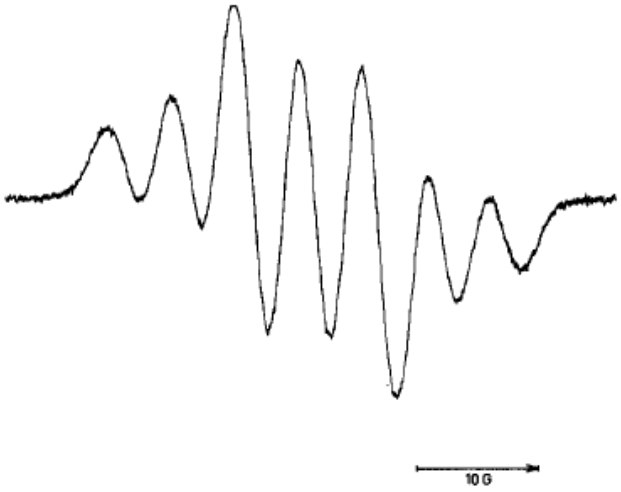

Figure 4.13 EPR spectrum of radical **4.22**.[116]

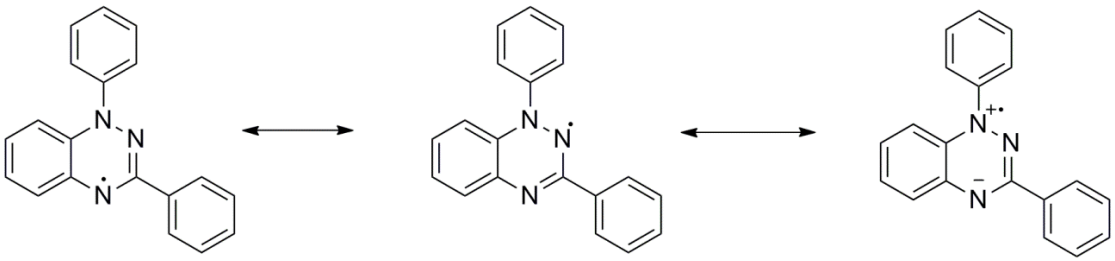

4.1 **4.1a** **4.1b**

Figure 4.14 Resonance structures of Blatter-type radical.[116]

The attempt to get X-Ray crystallographic data failed because single crystals could not be obtained.[116] The first report of the crystal structure of Blatter's radical appeared in 1994.[119] Crystals suitable for X-Ray analysis of radical compound **4.23** were obtained (Figure 4.15). The result of crystallographic analysis indicated that not all phenyl rings are in the same plane. The

torsion angle between 1-(4-chlorophenyl) ring plane and 1,2,4-benzotriazin-4-yl ring plane was found to be 56.9° due to repulsion between protons on these two rings. The bond length of N1-N2 (1.365 Å), N2-C3 (1.327 Å), and C3-N4 (1.315 Å) showed double bond character which proved the delocalised structure of this radical.

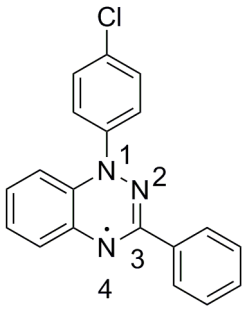

4.23

Figure 4.15 Radical compound **4.23**.[119]

During the last 5 years, a range of Blatter-type radicals was prepared by different methods.[118,120-125] The synthetic route presented by B. Yan and co-workers showed a relatively easy method to functionalise Blatter-type radical on all phenyl rings (Figure 4.16).[121] Various Blatter-type radical derivatives could be prepared by functionalization of the benzaldehyde, phenylhydrazine and aniline components.

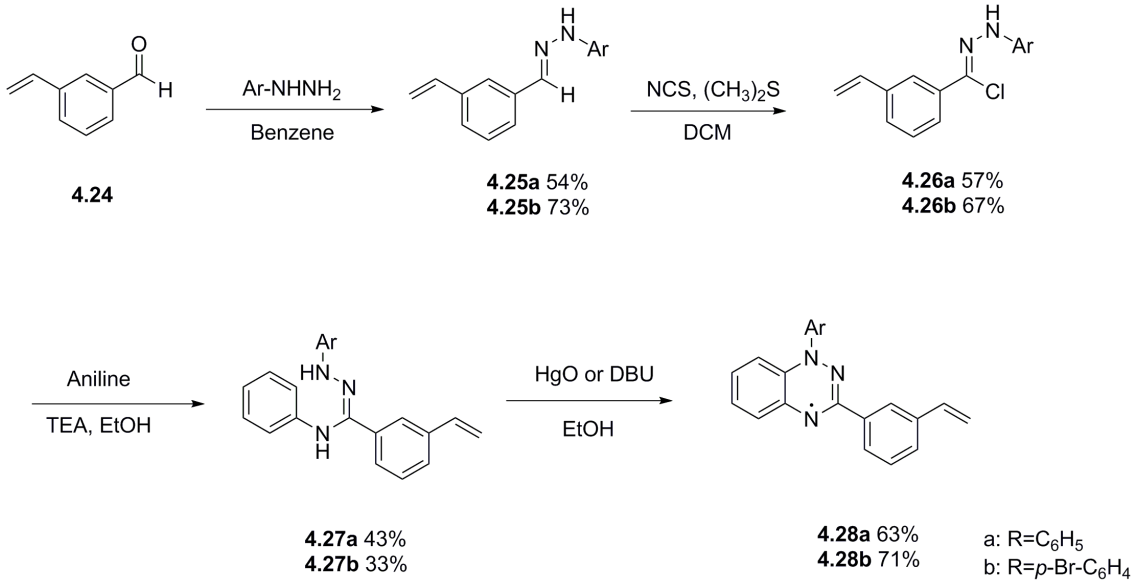

Figure 4.16 Preparation of Blatter-type radicals presented by B. Yan and co-workers.[121]

4.1.2 Aims

Blatter's radicals have a relatively flat, rigid structure and hence could be used to form the core of a discotic liquid crystal. However, they have never been used to prepare liquid crystals. Moreover, only a few organic paramagnetic discotic liquid crystals have been prepared successfully.[28,34,38] In this chapter we report the preparation of discotic liquid crystals based on Blatter's radical. The liquid crystalline properties of these mesogens are investigated by differential scanning calorimetry (DSC), optical microscopy. Magnetic properties are studied by EPR spectroscopy.

4.2 Preparation of Blatter-type mesogens

4.2.1 Design of target mesogen

Based on the synthetic method presented by B. Yan and co-workers, discotic liquid crystals based on Blatter's radical (Figure 4.16) can be obtained by functionalization of three components, benzaldehyde, phenylhydrazine and aniline. Based on the comprehensive study about discotic triphenylene mesogens, two flexible chains are needed to be introduced into each phenyl ring of this radical in order to achieve effective space filling around the core (Figure 4.17). To minimise the number of synthetic steps, these flexible chains should be alkoxyl chains.

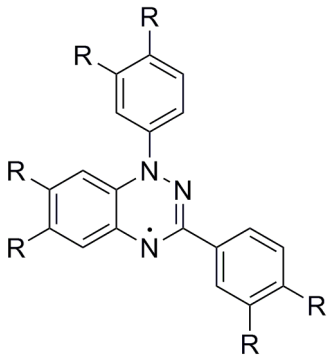

4.29

Figure 4.17 Structure of target compound.

Before functionalizing benzaldehyde, phenylhydrazine and aniline, we prepared a simple non-mesogenic analogue **4.30** in order to optimise the reaction conditions (Figure 4.18).

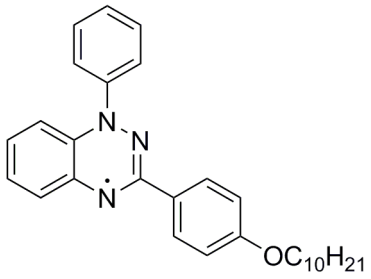

4.30

Figure 4.18 Structure of compound **4.30**.

4.2.2 Preparation of Blatter-type radical 4.30

Compound **4.30** was prepared by the method presented by B. Yan and co-workers (Figure 4.19). The hydrazone compound **4.33** was obtained from the reaction between phenylhydrazine and *p*-decyloxy benzaldehyde. The chlorination reaction of **4.33** was carried out with *N*-chlorosuccinimide (NCS). Then product **4.34** was reacted with aniline to yield compound **4.35** followed by the oxidation reaction with lead dioxide which resulted in radical product **4.30**. Some reaction conditions were modified to improve yields.

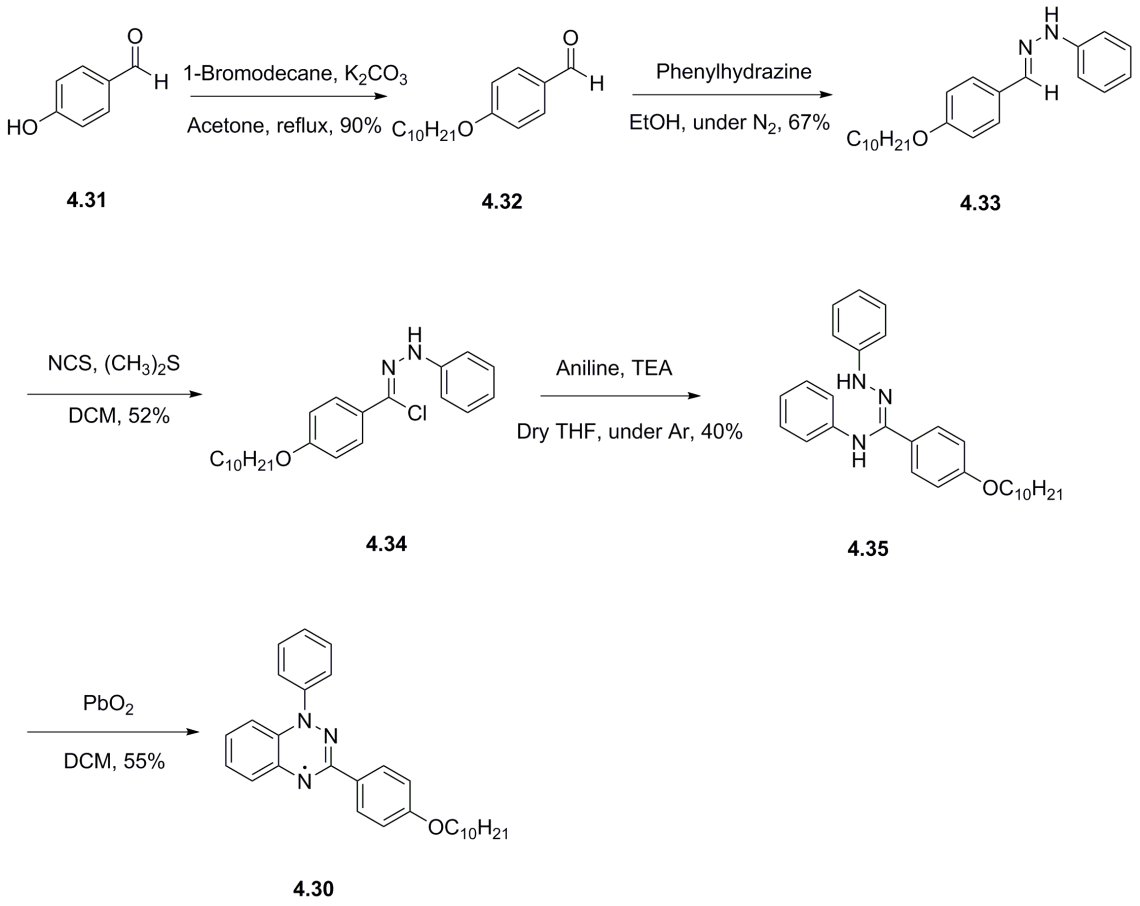

Figure 4.19 Preparation of compound **4.30**.

Preparation of hydrazone compound **4.33** was initially carried out in toluene rather than benzene on safety grounds. However, starting materials were recovered nearly quantitatively. Only several very weak new spots can be seen on the TLC plate. When the reaction was set up with ethanol as a solvent and 2 equivalents of phenylhydrazine under N_2 atmosphere, the aldehyde starting material was consumed in about 3 h, and the product was isolated by column chromatography in a 67% yield. Presumably, the protic solvent ethanol improves the reactivity of the ketone group.

The reported procedure for the preparation of amidrazone **4.35** did not work for our reaction. Many byproducts were observed on the TLC plate, the target compound could not be isolated from the crude product mixture. Compound **4.35** was formed by using dry THF as a solvent at room temperature under Ar atmosphere, using excess aniline. Compound **4.35** was isolated in a 40% yield.

Surprisingly, in the first batch of this reaction, radical **4.30** was obtained directly from compound **4.34**. We found that pure amidrazone **4.35** was stable in air for several days. However, it seems to be spontaneously oxidised under some unindentified conditions to yield Blatter's radical **4.30**.

The method reported in the literature for the oxidation of amidrazone **4.35** uses mercury oxide. However, mercury compounds are very toxic. Based on our experience of preparing similar stable radicals, amidrazone **4.35** should be oxidised by lead dioxide. Therefore, lead dioxide was used to replace the mercury oxide to oxidise amidrazone **4.35**. Radical **4.30** was obtained after purification. Figure 4.20 shows MS spectrum of radical 4.**30**. The nitrogen hyperfine coupling constants were obtained from the simulation of EPR spectrum, a_{N1} = 7.63 G, a_{N2}= 4.80 G, a_{N3} = 5.16 G which are similar to the reported results (Figure 4.21).[117,121,126]

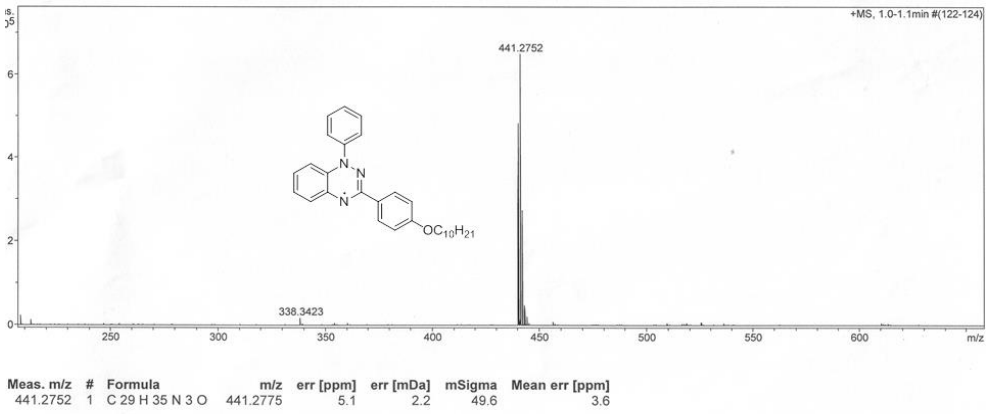

Meas. m/z	#	Formula	m/z	err [ppm]	err [mDa]	mSigma	Mean err [ppm]
441.2752	1	C 29 H 35 N 3 O	441.2775	5.1	2.2	49.6	3.6

Figure 4.20 MS analysis of radical compound **4.30**.

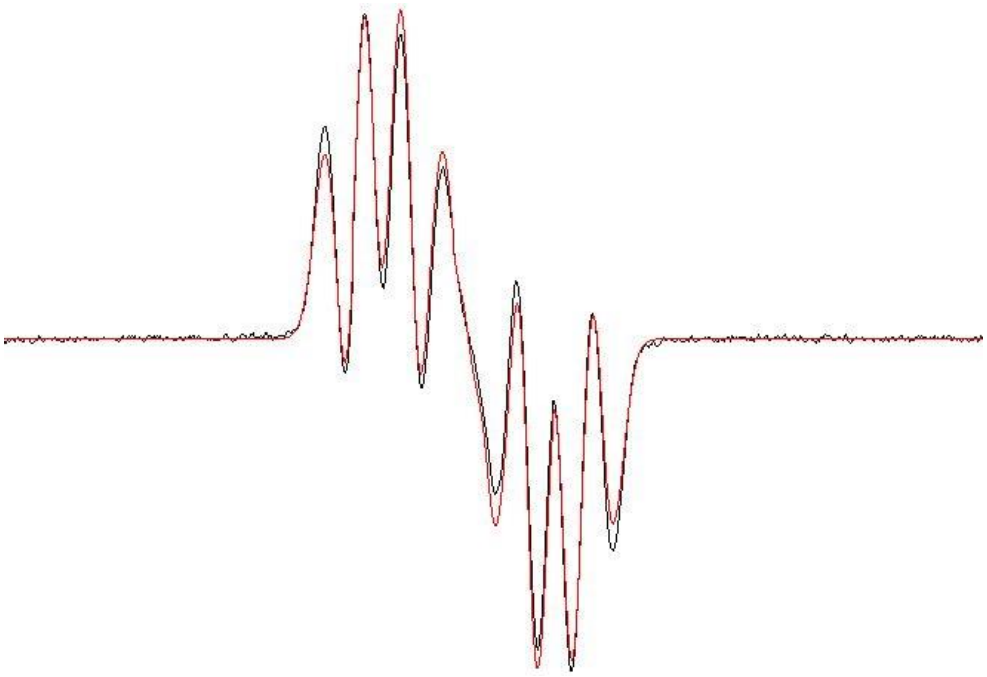

Figure 4.21 EPR spectra of radical **4.30**. Black line is experiment data, red one is simulation, a_{N1} = 7.63 G, a_{N2}= 4.80 G, a_{N3} = 5.16 G.

This radical is quite stable in air. No decomposition was observed after storing in air at room temperature for several days. Unsurprisingly, radical **4.30** did not show any liquid crystal properties.

The reaction conditions for the preparation of Blatter-type radical were optimised, and bench stable radical **4.30** was obtained. These results suggested that target compound **4.29** could be obtained and hopefully stable enough to be isolated, if substituted phenylhydrazine, benzaldehyde and aniline components can be prepared successfully.

4.2.3 Preparation of substituted phenylhydrazines

Before preparation of a suitable disubstituted phenylhydrazine compound, we want to confirm that a mono long alkoxyl chain substituted phenylhydrazine can be prepared successfully. Therefore, *p*-heptyl phenylhydrazine was prepared.

4.2.3.1 *p*-Heptyl phenylhydrazine

Usually, substituted phenylhydrazines are prepared by reducing the corresponding diazonium salts with tin(II) chloride in the presence of hydrochloric acid (Figure 4.22). Other agents can be used, such as sodium sulfite, zinc and nickel(II) chloride.[127,128]

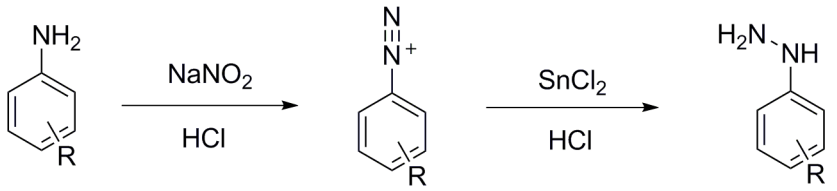

4.36 **4.37** **4.38**

Figure 4.22 Preparation of phenylhydrazines from corresponding diazonium salts.

p-Heptyl aniline is a commercially available aniline substituted with a long alkyl chain. *p*-Heptyl hydrazine was prepared successfully by reducing the corresponding diazonium salt with $SnCl_2$ as confirmed by MS analysis. NMR may not be an ideal way to distinguish the starting material aniline and product phenylhydrazine, since ^{1}H NMR. and ^{13}C NMR spectra of these two species are similar (normally the proton of NH or NH_2 group cannot be seen). Therefore, the most straightforward way to identify the product is MS spectroscopy. The peak with strong intensity at m/z = 190.1584 may be a fragment of *p*-heptyl phenylhydrazine following loss an NH_3 group (Figure 4.23). Because *p*-heptyl phenylhydrazine was prepared successfully, we reasoned that the presence of a long alkyl chain on the aromatic ring could not influence the stability of phenylhydrazine significantly.

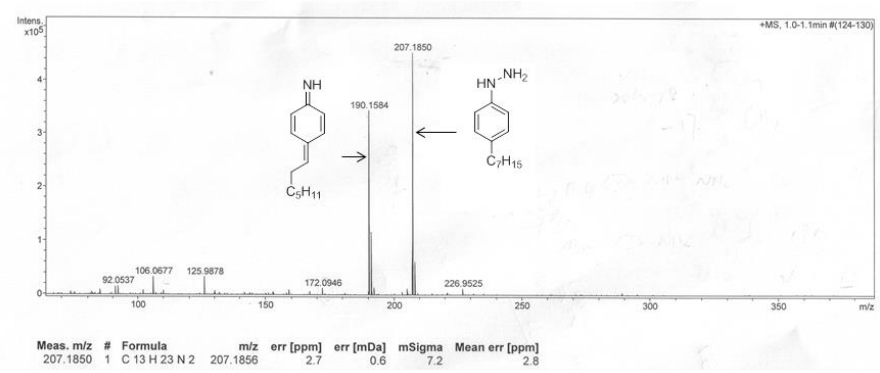

Figure 4.23 MS of *p*-heptyl phenylhydarzine.

4.2.3.2 3,4-Didecyloxy phenylhydrazine: reduction route

In 1926, W. H. Perkin and his co-workers prepared 3,4-dimethoxy phenylhydrazine by reducing the diazonium salt.[129] One further study of the preparation of 3,4-dimethoxy phenylhydrazine by the same method was reported in 1949.[130] We therefore believed that it would be possible to prepare 3,4-didecyloxy phenylhydrazine by this method (reduction of the diazonium salt). However, no 3,4-didecyloxy phenylhydrazine was formed. The formation of the parent diazonium salt was confirmed by MS analysis (Figure 4.24). The reduction of diazonium salt with $SnCl_2$ in the presence of concentrated HCl led to the formation of 3,4-didecyloxy aniline (m/z = 406.3668) and other byproducts (Figure 4.25).

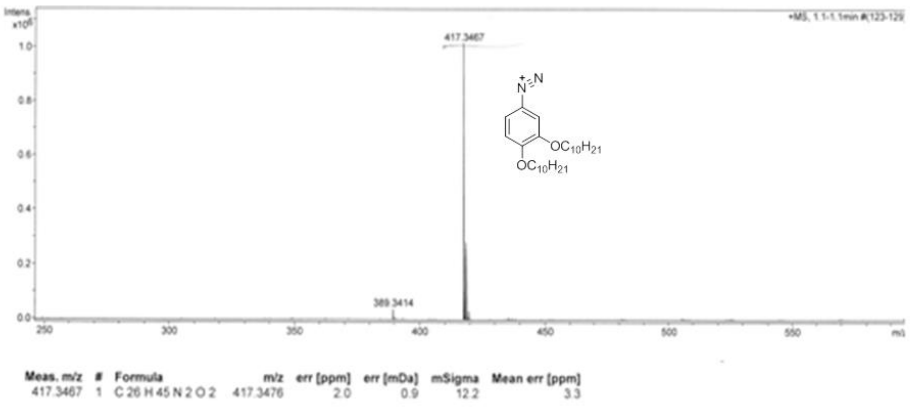

Figure 4.24 MS of diazonium salt prepared from 3,4-didecyloxy aniline.

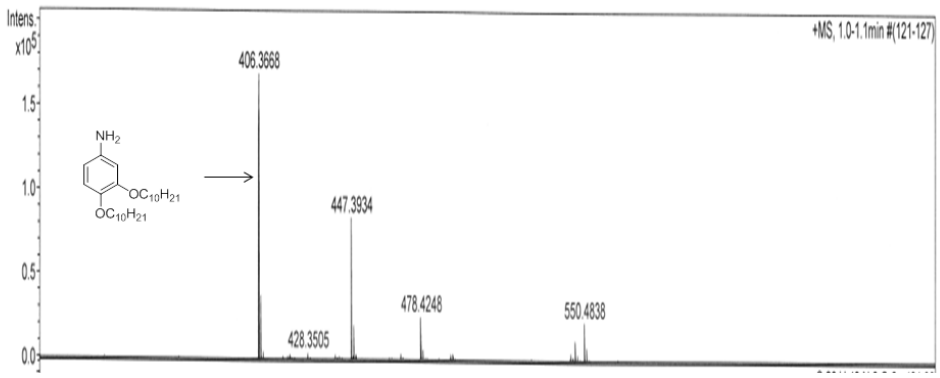

Figure 4.25 MS of a product obtained by reduction of diazonium salt.

Changing the reaction temperature and reducing reagents did not help (Table 4.1). It appears that the two electron donating groups on the phenyl ring make the hydrazine more susceptible to be over reduced to aniline. The corresponding phenylhydrazine cannot be obtained by this method. It is likely that the failure of this method is due to over-reduction which yields aniline. Therefore, we need prepare this hydrazine compound by a different method.

Table 4.1 Modification of aniline reducing reaction condition

Temperature	Reducing agent	Hydrazine product
Room temperature	$SnCl_2$	No
0 °C	$SnCl_2$	No
-15 °C	$SnCl_2$	No
-40 °C	$SnCl_2$	No
Room temperature	Na_2SO_3	No
0 °C	Na_2SO_3	No
Room temperature	Zn, $NiCl_2$	No
0 °C	Zn, $NiCl_2$	No

4.2.3.3 3,4-Didecyloxy phenylhydrazine: deprotection route

The other way to prepare substituted phenylhydrazines is deprotection of hydrazides **4.40** (Figure 4.26).[131-133] For different protecting groups, the deprotection reaction could be carried out under different conditions, such as acidic conditions (R'=*t*-Bu), reducing conditions (R'=CH_2CCl_3) and neutral conditions (R'=CH_2CH_2TMS). Removal of Boc group (R'=*t*-Bu) under acidic conditions is the most straightforward method.

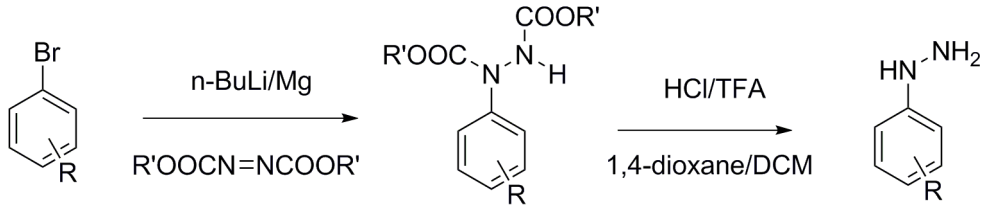

4.39 **4.40** **4.38**

Figure 4.26 Preparation of phenylhydrazines from hydrazides

Bromination reaction of 1,2-didecyloxybenzene **4.42** was carried out with *N*-bromosuccinimide (NBS) in THF. Then compound **4.43** was treated with *n*-BuLi in dry THF at -78 °C, followed by addition of di-tert-butyl azodicarboxylate (DTBAD) to obtain hydrazide **4.44**. The deprotection reaction of **4.44** was carried out with either HCl in 1,4-dioxane[131] or trifluoroacetic acid (TFA) in DCM[134] (Figure 4.27). However, MS analysis of reaction mixtures showed that products of these reactions were the corresponding aniline and other byproducts (Figure 4.28).

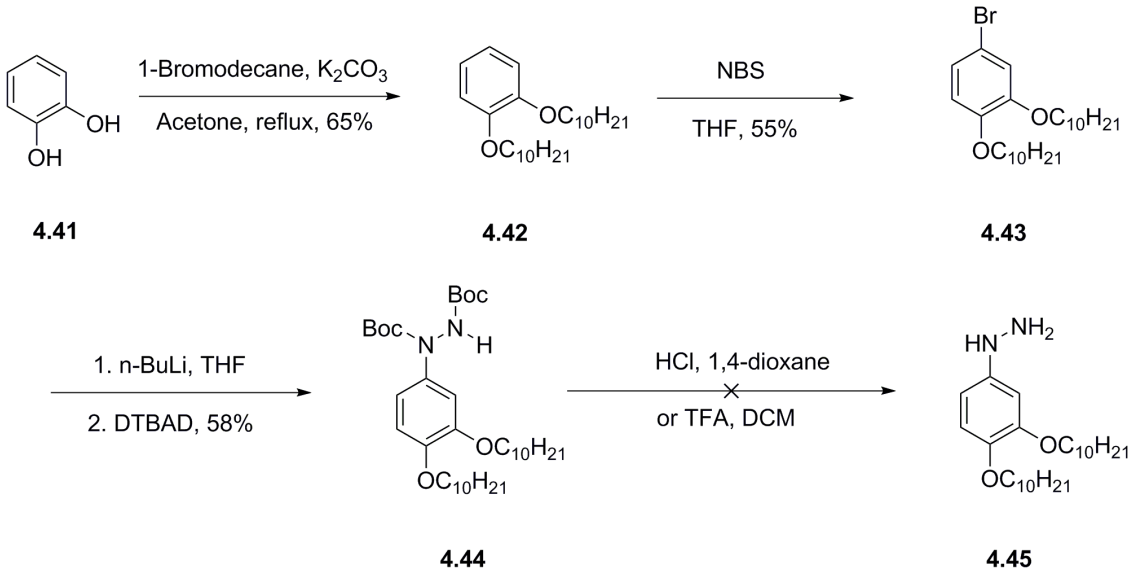

Figure 4.27 Preparation of hydrazine from 1,2-dihydroxybenzene.

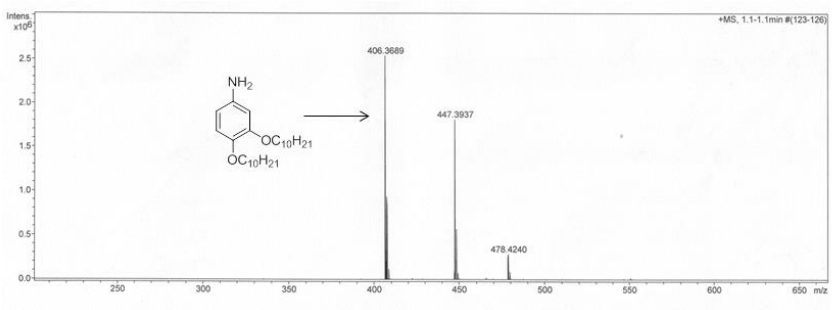

Figure 4.28 MS spectrum of reaction mixture of compound **4.45.**

An attempt to optimise the deprotection conditions was carried out. The reaction was set up at different temperatures with different acids (Table 4.2). However, no phenylhydrazine was obtained under these conditions.

Table 4.2 Modification of deprotection reaction condition

Temperature	Acid	Solvent
Reflux	HCl	1,4-dioxane
Ambient temperature	HCl	1,4-dioxane
0 °C	HCl	1,4-dioxane
Ambient temperature	TFA	DCM
0 °C	TFA	DCM

A new procedure for the preparation of electron-rich phenylhydrazines was recently reported by A. Jankowiak and co-workers (Figure 4.29).[135] They found that electron-rich phenylhydrazine derivatives, such as **4.45**, were not stable. The conventional deprotection conditions are not suitable for the preparation of these phenylhydrazines. The authors found that these phenylhydrazines can be obtained by the removal of Boc group with trifluoromethanesulfonic acid (TfOH) at -40 °C under Ar in 2 min. Longer reaction times lead to side reactions. Surprisingly, hydrochloric salts of these compounds cannot be obtained due to their poor stability.

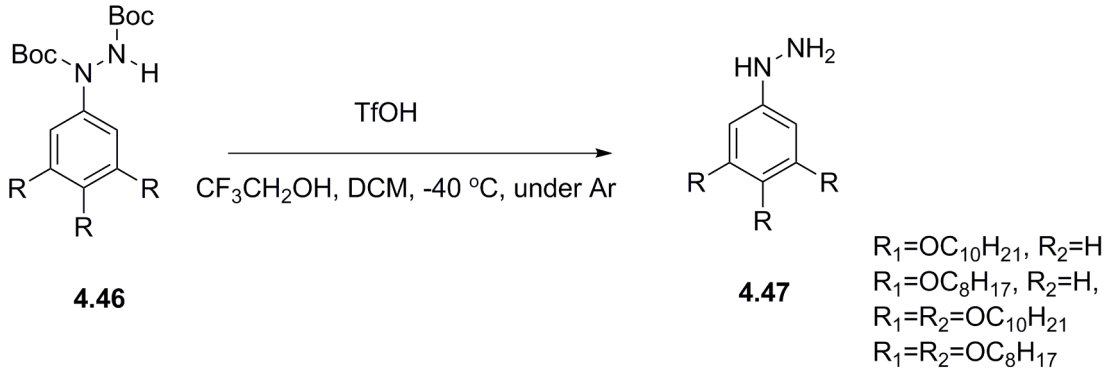

4.46 **4.47**

Figure 4.29 Deprotection reaction with TfOH.[135]

However, the preparation of our phenylhydrazine **4.45** by this method failed. MS analysis of the reaction mixture after 1.5 min did not show the peak of hydrazine **4.45** (Figure 4.30). The intense peaks with m/z = 465 and 521 may correspond to the compounds presented in Figure 4.30. These results suggested that the deprotection reaction did not go to completion. However, when the reaction time was increased by 15 s, the peaks corresponding to incomplete deprotection disappeared but no phenylhydrazine was detected by MS analysis (Figure 4.31).

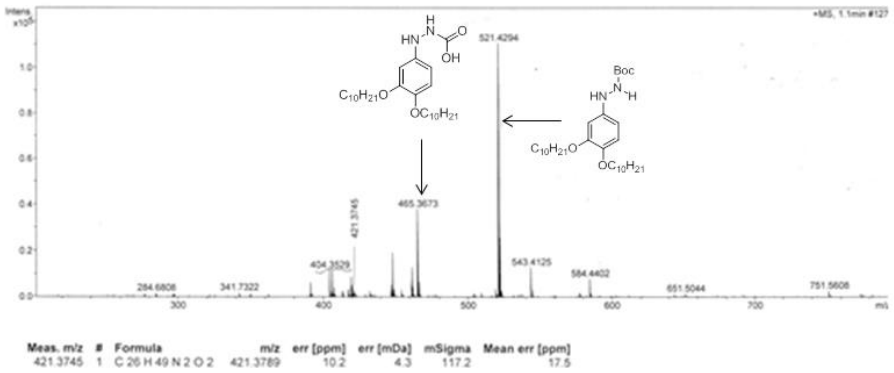

Figure 4.30 MS analysis of deprotection reaction mixture after 1.5 min.

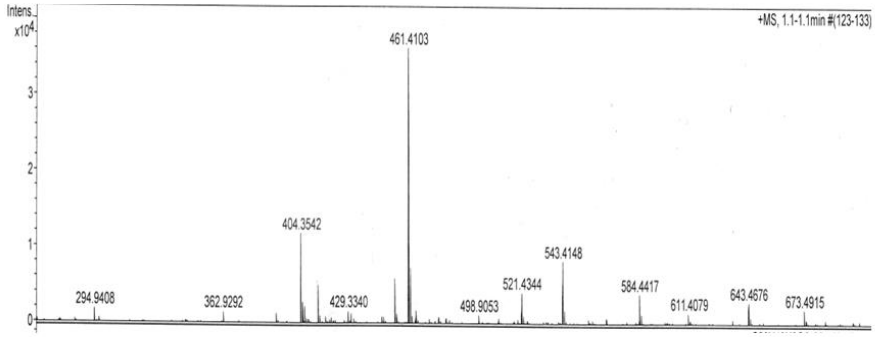

Figure 4.31 MS analysis of deprotection reaction mixture after 105 s.

The mechanism of the deprotection of aryl hydrazides shows that the product hydrazine can react with t-butyl cation to form other byproducts (Figure 4.32).[135] A. Jankowiak and co-workers suggested that for less reactive hydrazines, $k_1 << k_2$, and the deprotection reaction can be carried out using HCl or TFA in conventional solvents; however, for dialkoxyphenylhydrazines $k_1>>k_2$, and t-butyl cation scavengers are needed. In the preparation of hydrazine **4.45**, 2,2,2-trifluoroethanol was added as a t-butyl cation scavenger. We argued that the amount of 2,2,2-trifluoroethanol added might be insufficient to prevent the reaction between the t-butyl cation and hydrazine **4.45**.

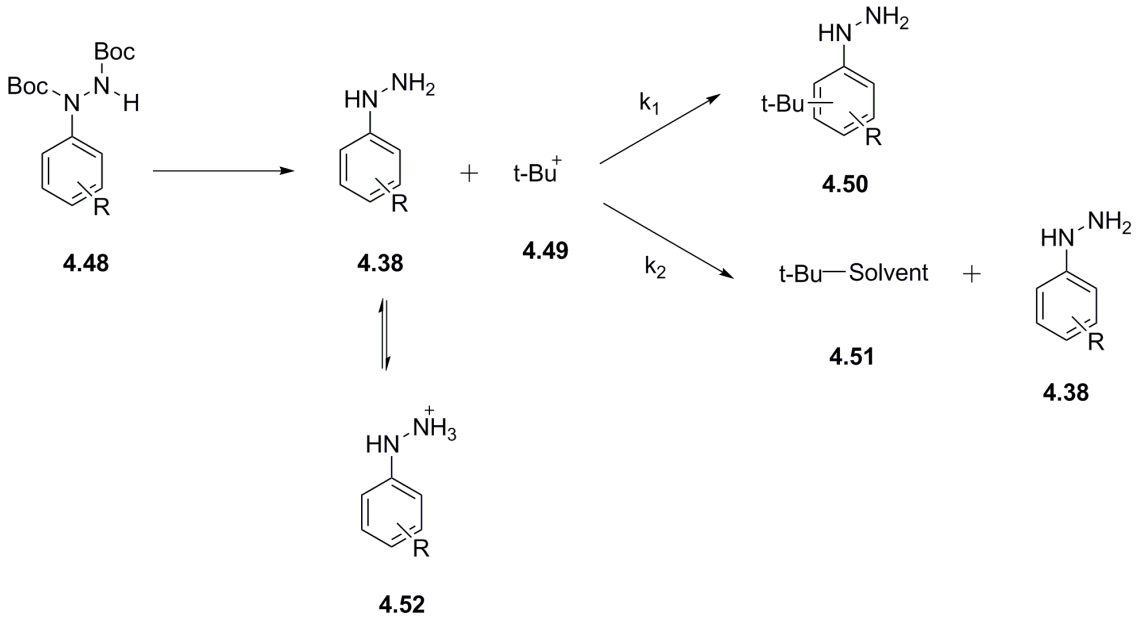

Figure 4.32 Mechanism for the deprotection of arylhydrazides.[135]

In order to test this hypothesis, the amount of 2,2,2-trifluoroethanol was tripled. Hydrazine **4.45** was detected in the reaction mixture (Figure 4.33). However, the peak with m/z = 406.3665 showed that aniline was still formed with this method. Massive amount of impurities was detected by TLC. Because of the huge amount of impurities and poor stability of hydrazine **4.45**, the isolation of pure phenylhydrazine is challenging. Moreover, reproducibility of the synthesis of compound **4.45** was poor, different batch-dependent impurities were detected by TLC.

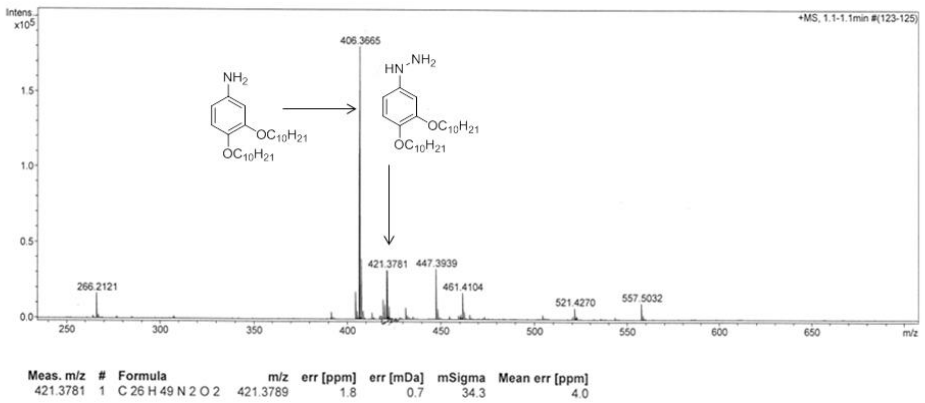

Figure 4.33 MS analysis of reaction mixture with excess trifluoroethanol.

4.2.3.4 3,4-Didecylphenylhydrazine

We also tried to prepare 3,4-didecylphenylhydrazine **4.57** by a similar procedure (Figure 4.34). We reasoned that the stability of the hydrazine with alkyl substituents may be higher than that of the hydrazine with more electron-donating alkoxy groups. 1,2-Didecylbenzene **4.54** was prepared by Tamao-Kumada coupling. Bromination of didecylbenzene was carried out with Br_2 in DCM. n-BuLi was then added to the dry THF solution of compound **4.55** at -78 °C under N_2. DTBAD was added to the mixture after 1 h to form hydrazide **4.56**. Trifluoromethanesulfonic acid in trifluoroethanol and DCM was used to remove the Boc group. However, no hydrazine **4.57** was detected by MS analysis (Figure 4.34). These results suggested that electron rich phenylhydrazine derivatives cannot be easily prepared.

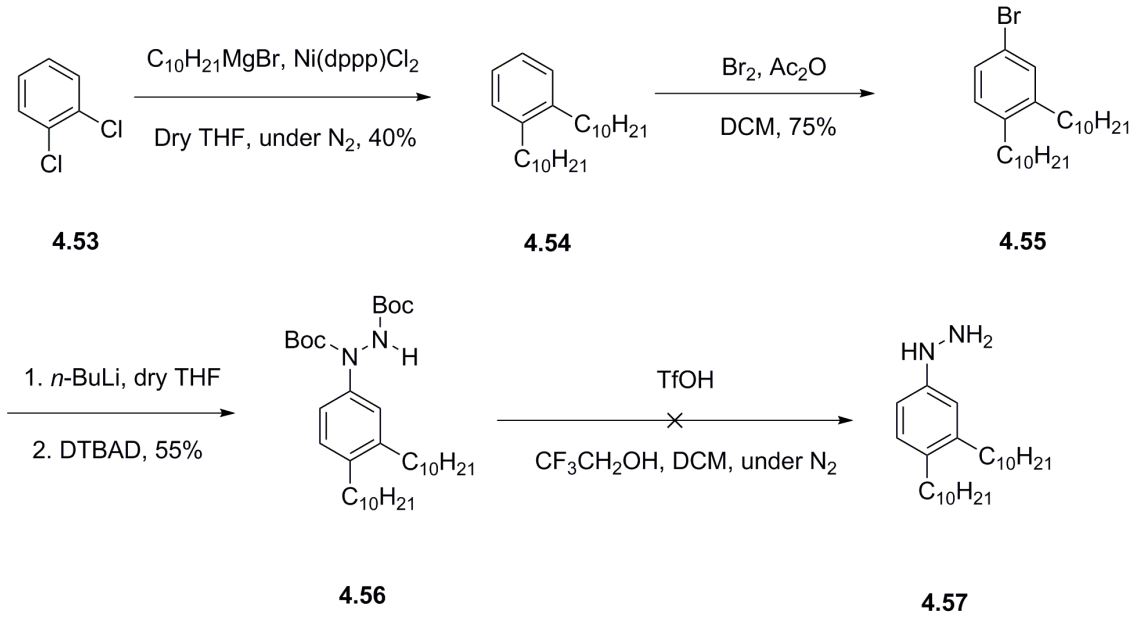

Figure 4.34 Preparation of 3,4-didecylphenylhydrazine.

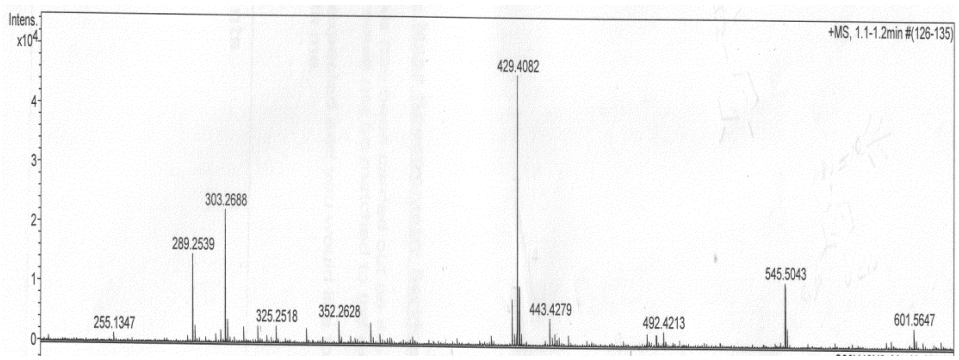

Figure 4.35 MS analysis of the reaction mixture of compound **4.57**.

In summary, 3,4-disubstituted phenylhydrazines cannot prepared by any methods attempted in this work because of the poor stability of these compounds. Based on our experience, the reduction of the corresponding diazonium salt is difficult to control; over-reduced product (aniline) was always obtained. Deprotection of hydrazides seems to be a potentially better way to prepare these electron-rich phenylhydrazines, although poor yield and poor reproducibility were observed in our experiments.

4.2.3.5 *p*-Decyloxyphenylhydrazine

Because *p*-heptylphenylhydrazine was prepared successfully, we reasoned that other mono-substituted phenylhydrazines, such as 4-decyloxyphenylhydrazine, can also be prepared. The attempt to prepare 4-decyloxyphenylhydrazine was carried out by the two synthetic approaches (reduction of the corresponding diazonium salt and deprotection of the hydrazide) (Figure 4.36). For the deprotection reaction, hydrazide **4.64** was treated with either HCl in 1,4-dioxane or TfOH in 2,2,2-trifluoroethanol.

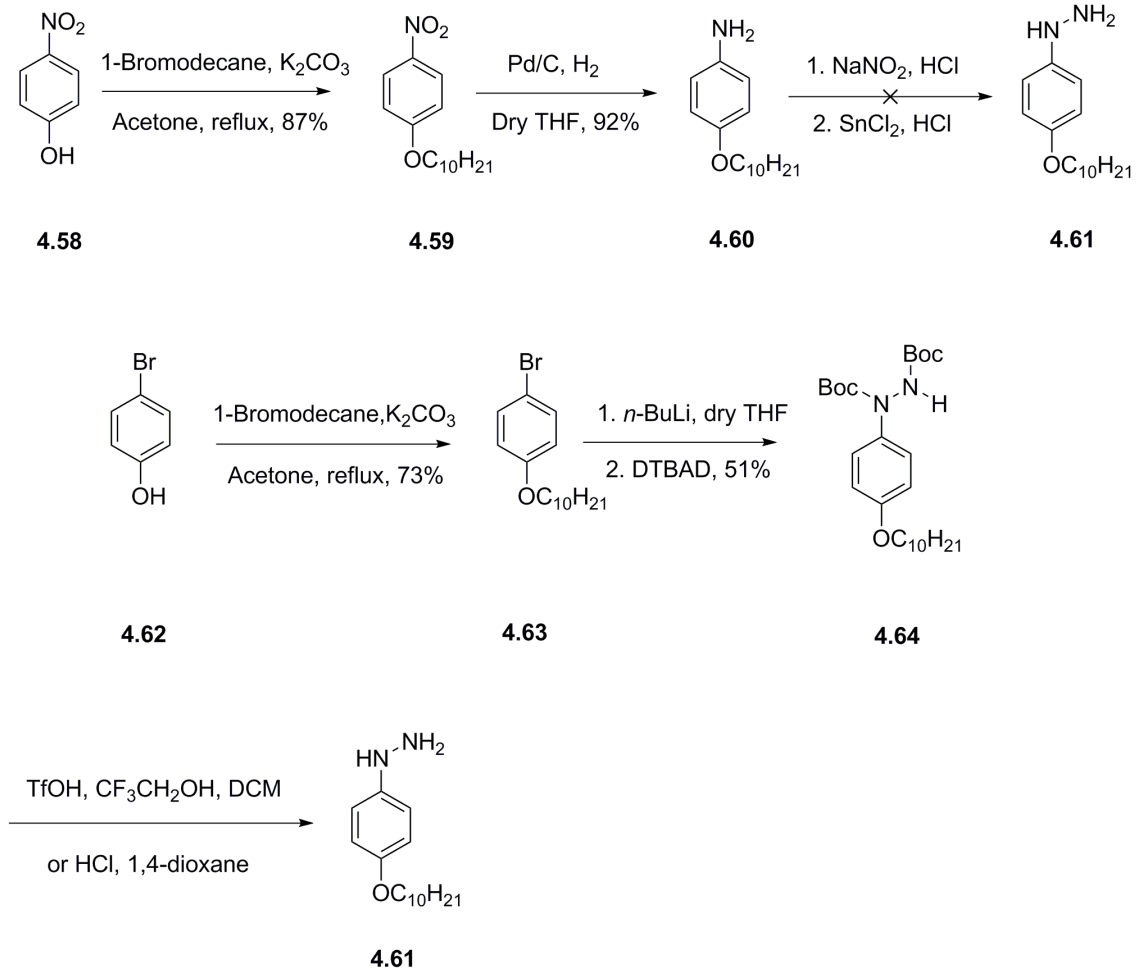

Figure 4.36 Preparation of 4-decyloxyphenylhydrazine, hydrazine **4.61** could not be isolated.

Unfortunately, MS analysis showed that the product of reduction of the diazonium salt is aniline rather than phenylhydrazine (Figure 4.37). The formation of corresponding diazonium salt was confirmed by MS spectrum. This result suggested that the preparation of alkoxyl substituted phenylhydrazine is not as straightforward as that of alkyl substituted phenylhydrazine, and results in over-reduction.

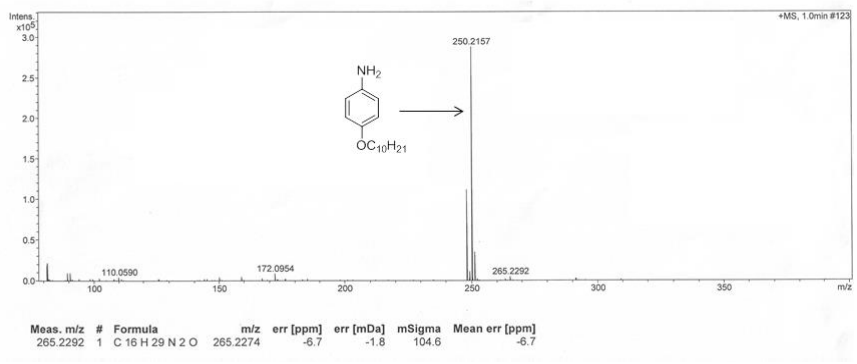

Figure 4.37 MS analysis of reaction mixture of 4-decyloxyaniline reduction.

For the deprotection pathway, MS analysis of the deprotection product of hydrazide **4.64** showed the peak of hydrazine **4.61** with very low intensity. No aniline was detected by MS analysis. The peak with strong intensity on the MS spectrum may be a fragment of 4-decyloxyphenylhydrazine formed by losing an NH_3 group which was also observed for 4-heptylphenylhydrazine (Figure 4.23). It is therefore possible that the preparation of 4-decyloxyphenylhydrazine was successful. However, pure compound **4.61** could not be isolated from the complex mixture containing a large number of byproducts.

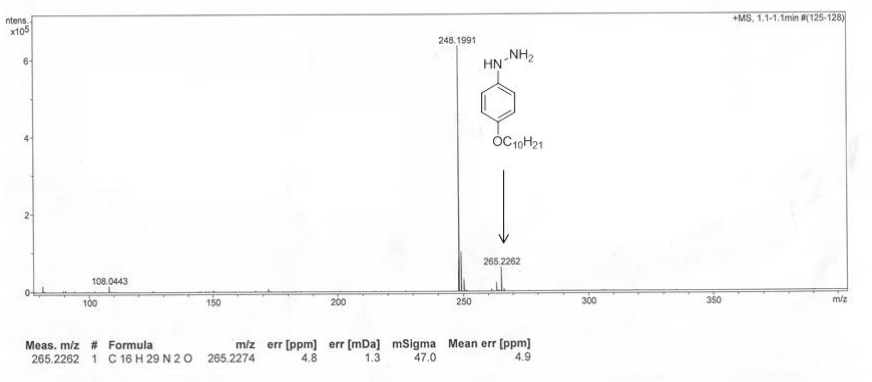

Figure 4.38 MS analysis of deprotection reaction mixture.

4.2.3.6 Decyloxy-4-hydrazinylbenzoate

To summarise, the preparation of electron-rich phenylhydrazines was not successful. The stability of phenylhydrazine derivatives with an electron withdrawing group on the aromatic

ring should be better than that of phenylhydrazine derivatives with electron donating groups. To test this hypothesis, compound **4.66** was prepared by Fisher esterification in the presence of concentrated H_2SO_4 (Figure 4.39). No decomposition of this hydrazinylbenzoate was observed after several weeks of storage in air at room temperature.

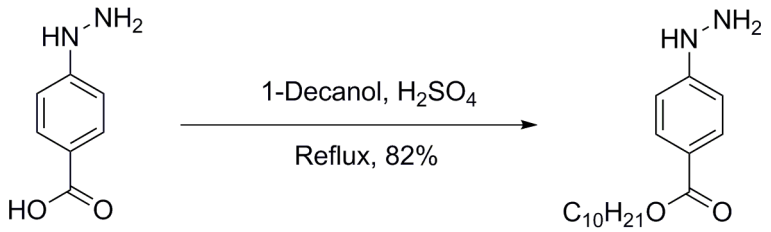

4.65 **4.66**

Figure 4.39 Preparation of decyloxy-4-hydrazinylbenzoate.

We therefore decided to use the ester functionality to attach an alkyl chain to the hydrazine component of the Blatter's type mesogen. The structure of the target compound was hence modified to compound **4.67,** which still has 6 flexible chains in total (Figure 4.39). Generally, the nature of the discotic mesophase is not changed by introducing dissymmetric side chains. However, the melting point and clearing point may decrease a lot which is not a problem for our target compound.

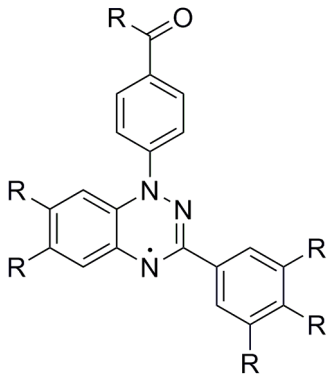

4.67 R=$OC_{10}H_{21}$

Figure 4.40 Structures of new target compound **4.67**.

The synthesis of this new target compound requires preparation of trisubstituted benzaldehyde and disubstituted aniline derivatives which is discussed in the next sections.

4.2.4 Preparation of 3,4,5-tridecyloxybenzaldehyde

Many reported procedures for the preparation of 3,4,5-tridecyloxybenzaldhyde start from 3,4,5-trihydroxybenzaldehyde.[136-140] However, this commercially available compounds is quite expensive (£79 for 100 mg, Sigma-Aldrich UK). The most straightforward method to prepare 3,4,5-trihydroxybenzaldehyde is demethylation of 3,4,5-trimethoxybenzaldehyde (Figure 4.41). However, the work up of this reaction mixture is complex and time consuming. Moreover the isolated yield is poor (less than 1%).

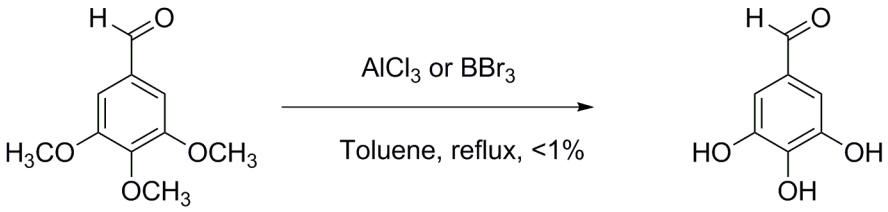

4.68 **4.69**

Figure 4.41 Preparation of 3,4,5-trihydroxybenzaldehyde.

Therefore, we prepared 3,4,5-tridecyloxybenzaldehyde by a different route, starting from ethyl-3,4,5-trihydroxybenzoate (Figure 4.42).[141] Ethyl-3,4,5-tridecyloxybenzoate was prepared from ethyl-3,4,5-trihydroxybenzoate and then reduced by $LiAlH_4$ in dry diethyl ether to form 3,4,5-tridecyloxybenzyl alcohol. 3,4,5-Tridecyloxybenzaldehyde was obtained by oxidizing benzyl alcohol **4.72** with 2,3-dichloro-5,6-dicyano-*p*-benzoquinone(DDQ) in dry 1,4-dioxane. The products of each step were isolated in good yields (more than 75%).

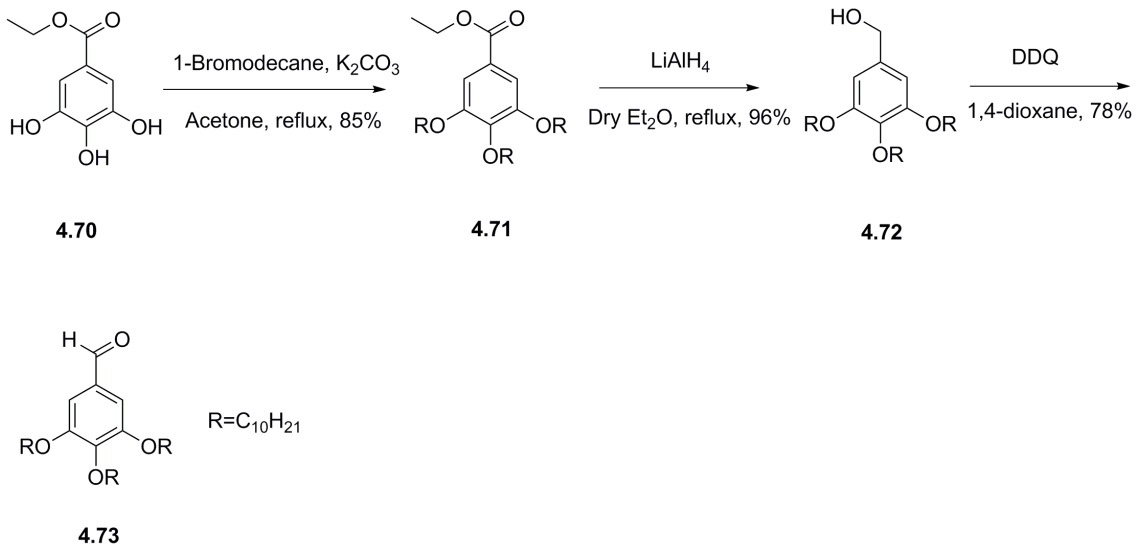

Figure 4.42 Preparation of 3,4,5-tridecyloxybenzaldehyde from ethyl-3,4,5-trihydroxybenzoate.

4.2.5 Aniline derivatives

Substituted anilines were prepared from hydroxyl benzene derivatives by following a literature procedure (Figure 4.43).[142] Decyloxybenzenes were prepared from hydroxybenzenes. DCM solution of sodium nitrite and nitric acid were added to decyloxybenzenes to form nitrobenzene derivatives. Reduction of nitrobenzene derivatives to give the desired aniline was carried out with hydrogen using Pd/C catalyst.

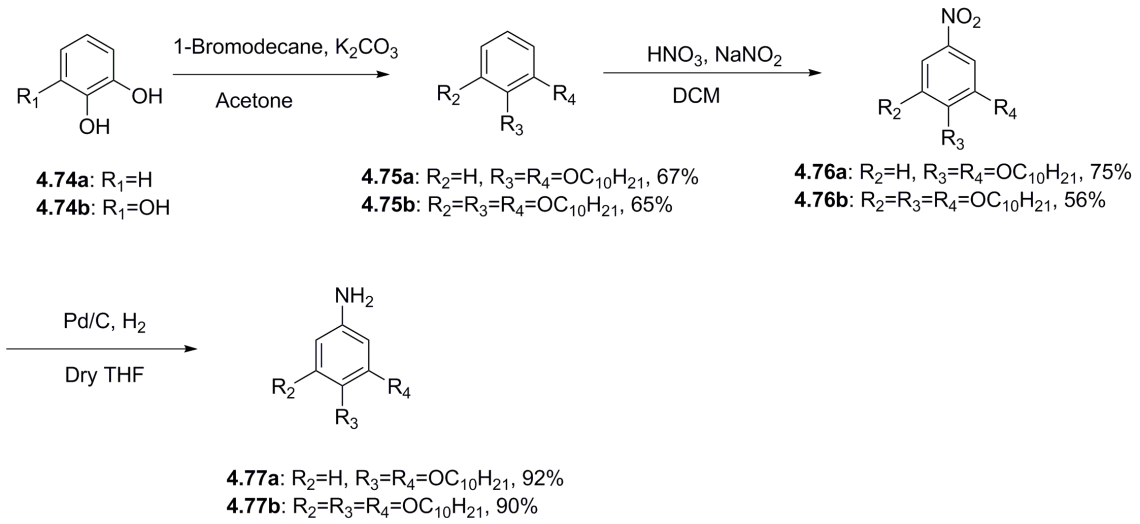

Figure 4.43 Preparation of aniline derivatives.

4.2.6 Preparation of 6 chains Blatter-type radical 4.67

Benzohydrazonoyl chloride compound **4.79** was prepared by the same procedure as for compound **4.34** (Figure 4.44). Hydrazone **4.78** was obtained from the reaction between benzaldehyde **4.73** and hydrazine **4.66**. The chlorination reaction of **4.78** was carried out with NCS.

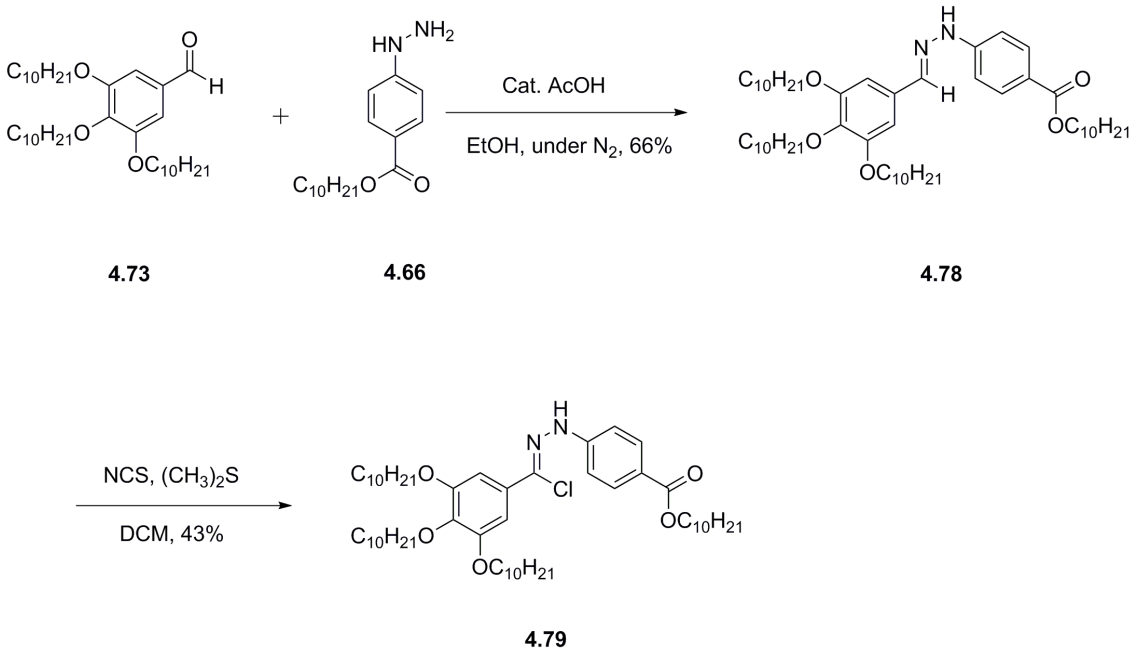

4.73 **4.66** **4.78**

4.79

Figure 4.44 Preparation of benzohydrazonoyl chloride **4.79**.

The formation of compound **4.78** was confirmed by ^{1}H NMR and ^{13}C NMR. However, no product could be detected by MS (ESI) spectrum (Figure 4.45). The peak of compound **4.78** could only be observed in an MS spectrum by using matrix-assisted laser desorption ionization (MALDI, Figure 4.46). Possibly because the molecular weight of compound **4.78** is relatively large (M_w 849), electrospray ionisation is inefficient. Then the chlorination reaction was carried out with NCS in DCM. The yield of benzohydrazonyl chloride **4.79** was poor (43%).

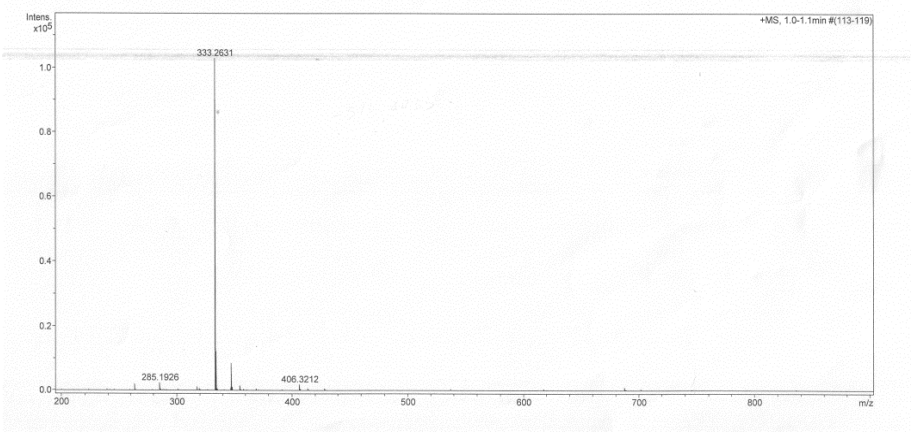

Figure 4.45 MS (ESI) spectrum of compound **4.78**.

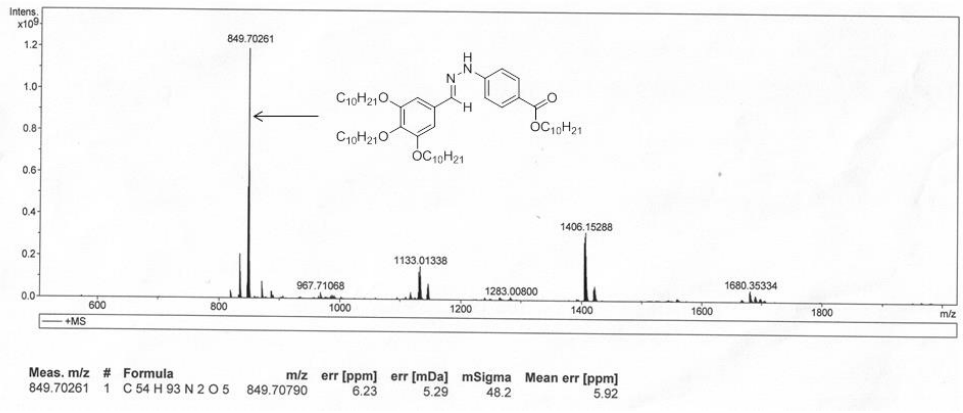

Figure 4.46 MS analysis (MALDI) spectrum of compound **4.78**.

Surprisingly, an EPR signal was observed in the reaction mixture of benzohydrazonoyl chloride **4.79** and aniline derivative **4.77a** after stirring overnight under N_2 atmosphere. Simulation of the spectrum was consistent with a Blatter-type radical. Nitrogen hyperfine coupling constants are a_{N1} = 6.94 G, a_{N2}= 4.80 G, a_{N3} = 4.32 G (Figure 4.47 and 4.48). These results suggested that radical was spontaneously formed in the reaction mixture. MS spectrum of the reaction mixture suggested the radical was Blatter-type radical compound **4.66** (Figure 4.49).

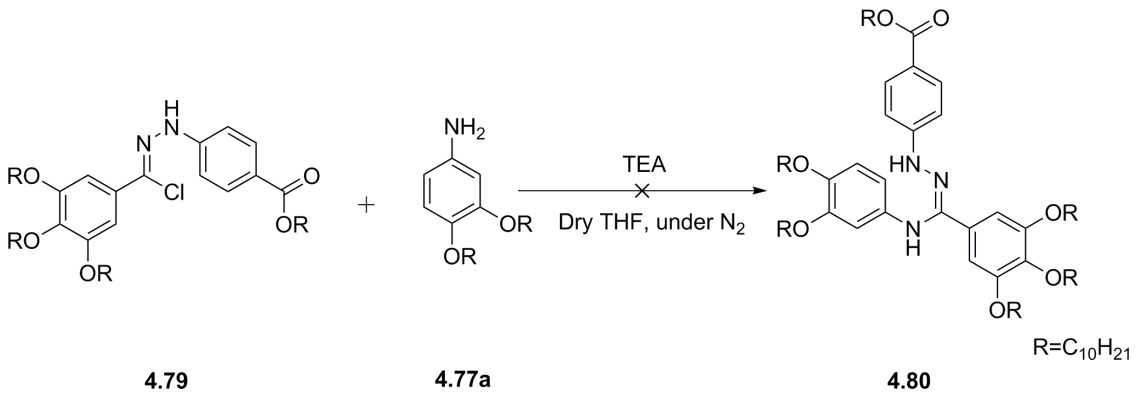

Figure 4.47 Preparation of benzohydrazonamide **4.80** was not successful.

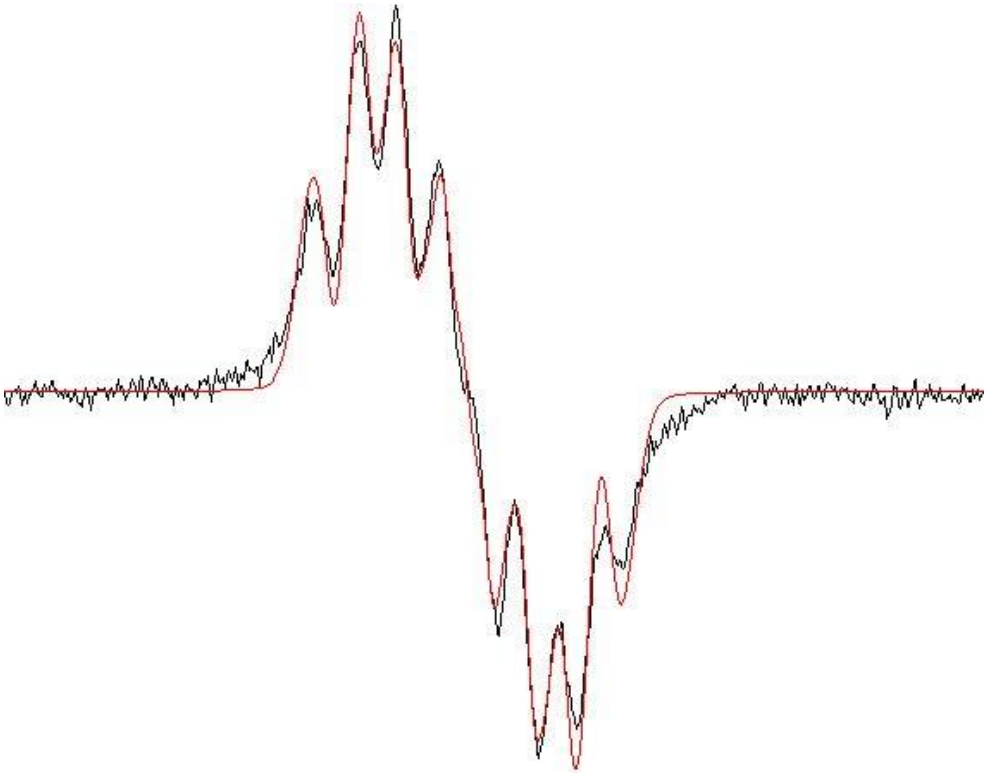

Figure 4.48 EPR spectrum of the reaction mixture. The black line is experimental data, the red line is simulation, a_{N1} = 6.94 G, a_{N2} = 4.80 G, a_{N3} = 4.32 G.

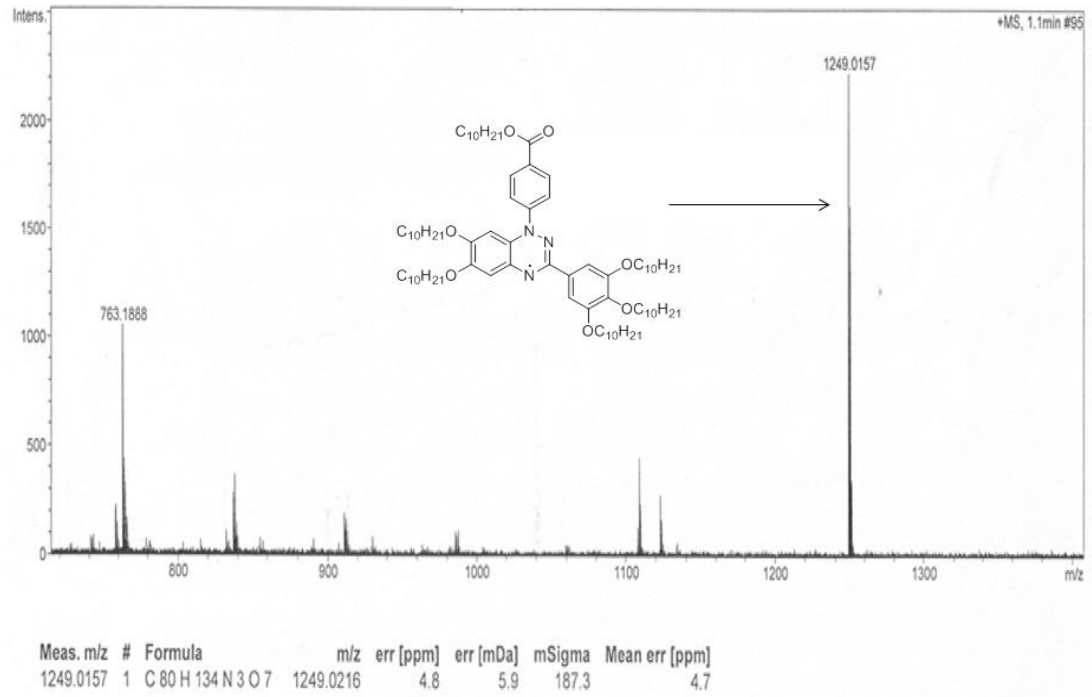

Figure 4. 49 MS spectrum of reaction mixture.

During the preparation of Blatter's radical **4.30,** we found that benzohydrazonamides (such as

compound **4.35**) are not stable under some conditions. As benzohydrazonamide **4.80** has four extra electron donating group on the phenyl rings as compared to **4.35**, it may be more prone to oxidation. Several new batches of this reaction were set up. In every batch, EPR signals were detected with crude reaction mixtures.

The oxidation of benzohydrazonamide **4.80** could have taken place during work up of crude reaction mixtures. In order to test this hypothesis, small scale reaction was set up in a Schlenk tube which can be directly loaded in EPR cavity. The formation of radical was monitored by EPR spectroscopy. Surprisingly, EPR signal was observed after the reaction mixture was left at room temperature under nitrogen overnight (Figure 4.50). The intensity of EPR signal increased over time during the following two days. These results suggest that the oxidation of benzohydrazonamide **4.80** occurs even in the absence of air.

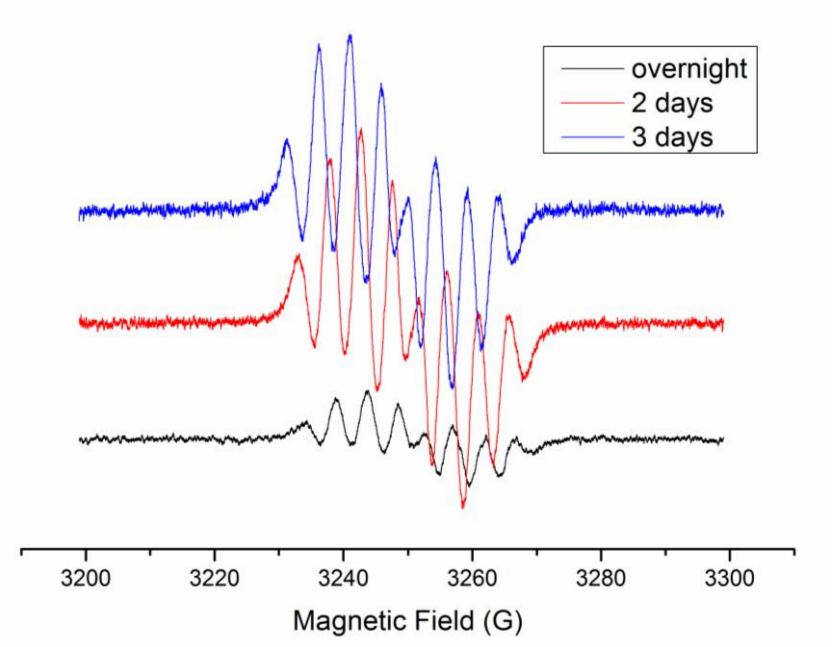

Figure 4.50 EPR spectra of the reaction mixture.

A mechanism of formation of Blatter's radicals from benzohydrazonamides, presented by A. T. Gubaidullin (Figure 4.51),[143] requires an oxidising reagent. For these reactions, excess of relatively strong oxidising reagents, such as mercury(II) oxide and silver(I) oxide is usually used.[117,144] A new catalytic oxidation of benzohydrazonamides was reported by P. A. Koutentis and co-workers in 2010 (Figure 4.52).[145] As the aerobic oxidation of alcohols can be catalysed

by Pd/C, they believed that oxidation of benzohydrazonamides in an atmosphere of air can also be catalysed by Pd/C.[146,147] Moreover, these catalytic oxidations were influenced by the pH. Therefore, DBU was added to adjust the pH. However, spontaneous transformation of benzohydrazonamide to Blatter's radical was not reported.

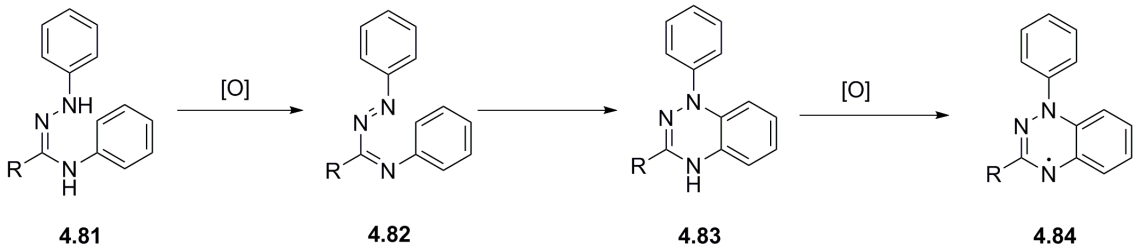

Figure 4.51 The mechanism of oxidation of benzohydrazonamide.[143]

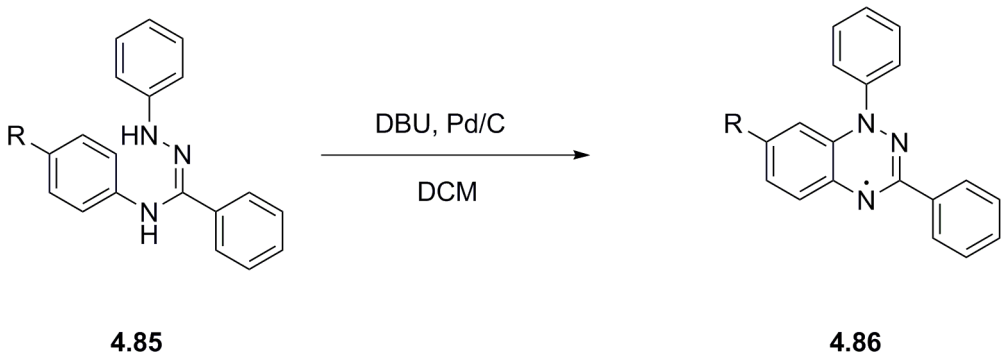

Figure 4.52 New catalytic oxidation of benzohydrazonamides.[145]

Possibly, the radical **4.67** formed from benzohydrazonamides **4.80** through a self-oxidising route. Imine compounds can be reduced by some mild reducing agents to get amines, such as sodium cyanoborohydride[148] and Hantzsch dihydropyridine.[149] It suggests that imines can potentially to be oxidising reagent. For our reaction, possibly, one molecule of benzohydrazonamide acts as oxidising reagent to reduce the other benzohydrazonamide molecule (Figure 4.53). The cyclization product **4.89** was oxidised by benzohydrazonamide again to give the radical product **4.67**.

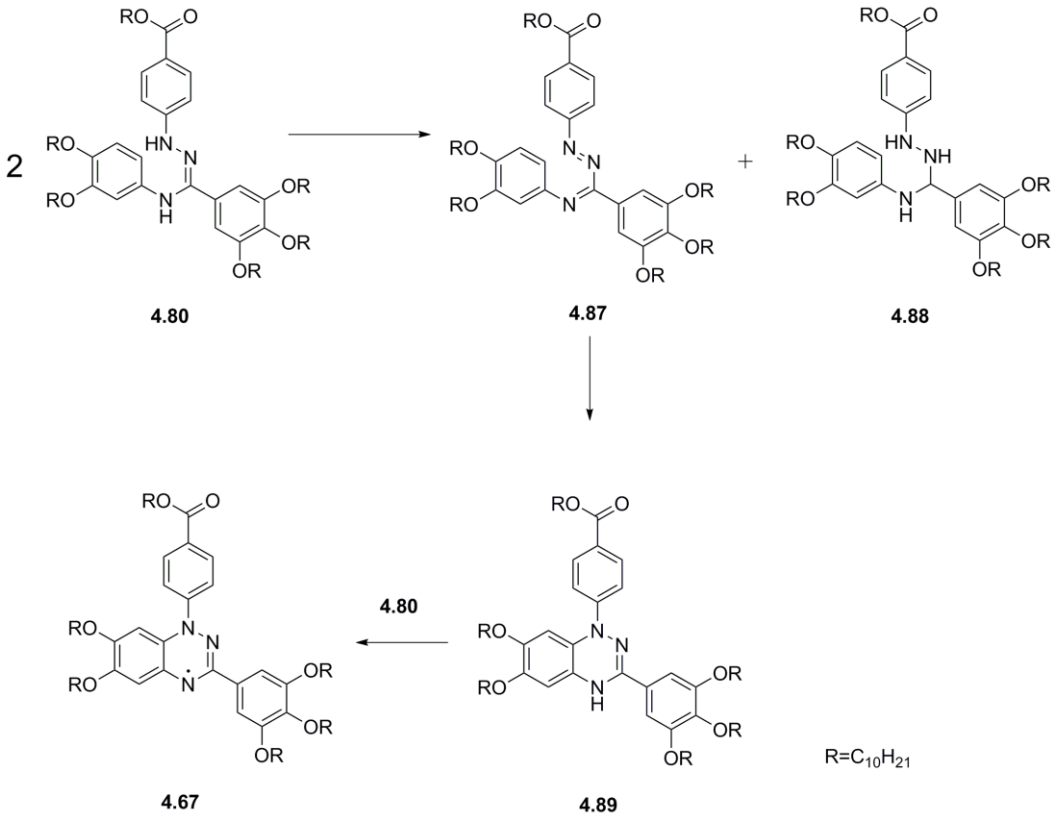

Figure 4.53 Proposed self-oxidising route of benzohydrazonamide.

4.2.7 Optimisation of reaction conditions

4.2.7.1 Addition of oxidising reagents

We found that benzohydrazonamide **4.80** cannot be isolated and Blatter's radical was formed in poor yield directly in the reaction mixture. We need to optimise the reaction condition to get Blatter's radical in a high yield and reduce the reaction time. We attempted to add an oxidising reagent in order to accelerate the formation of the radical. However, no EPR signal was detected after lead dioxide or silver(I) oxide were added to the reaction mixture. This suggested that Blatter-type radical **4.67** is not stable in the presence of strong oxidising reagents.

We also tried to add mild oxidising reagents to the reaction mixture, such as copper(I) iodide, copper(II) oxide and 2,5-di-t-butyl quinone. The reaction between benzohydrazonoyl chloride **4.79** and didecyloxyaniline without any oxidising reagent under N_2 atmosphere was set up as a control experiment. Reaction progress was monitored by EPR.

For the reaction with copper(I) iodide, a very weak EPR signal was detected after 5 min. The intensity of EPR signal increased slowly over time (Figure 4.54). Compared to the control experiment, the EPR signal was very weak after the reaction mixture was stirred overnight (Figure 4.55). These results suggested that this radical may not be stable in the presence of copper(I) iodide.

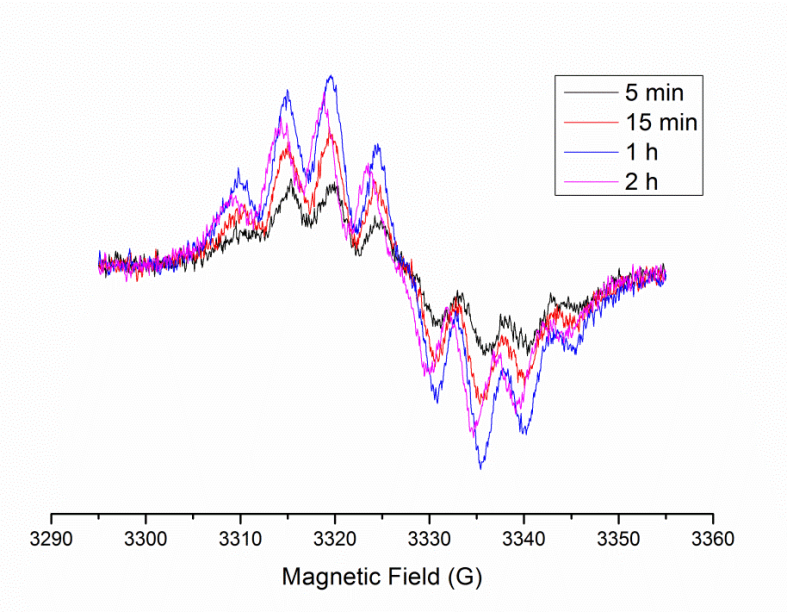

Figure 4.54 EPR spectra of copper(I) reaction system

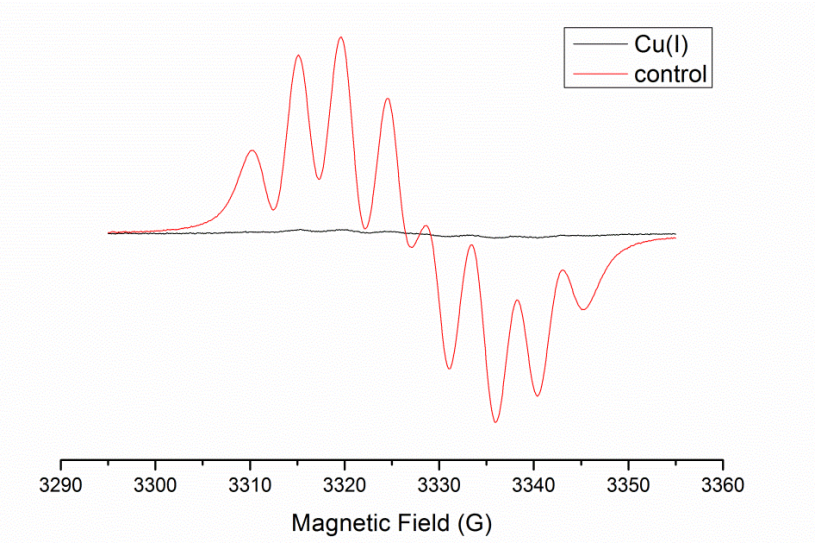

Figure 4.55 EPR spectra of control experiment and copper(I) system after the mixture was stirred overnight.

For the mixture with copper(II) oxide, a strong EPR signal was detected after 5 min (Figure 4.56). However, the intensity of EPR signal decreased rapidly over time, and after 2 h no EPR signal was observed. These results suggested that copper(II) oxide may accelerate the formation of radical compound, but the radical was not stable in this reaction mixture.

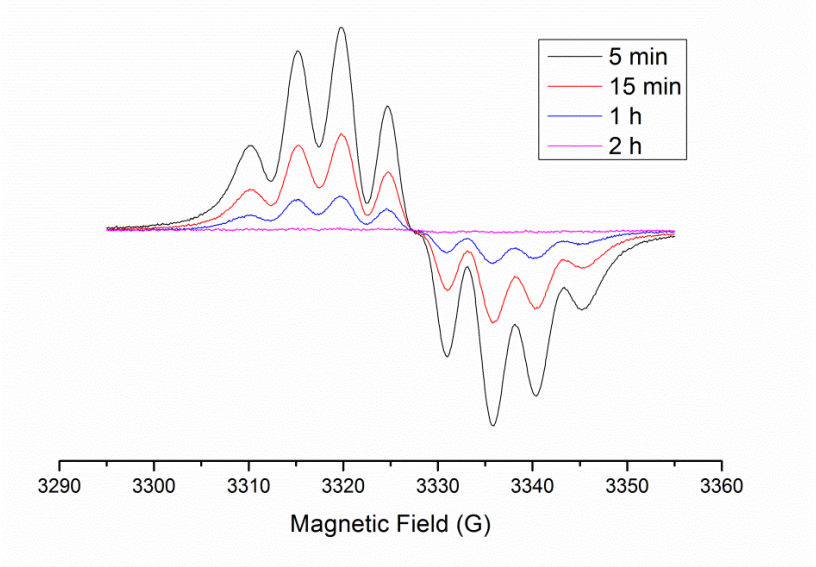

Figure 4.56 EPR spectra of copper(II) reaction system.

For the mixture with 2,5-di-t-butyl quinone, the radical formation seems to be slower than in the control experiment (Figure 4.57). This suggested that 2,5-di-t-butyl quinone cannot

accelerate the radical formation.

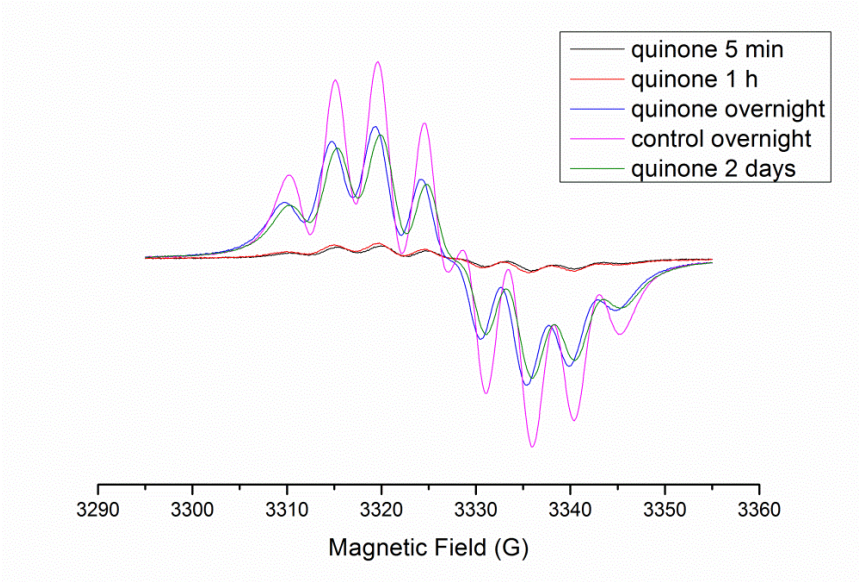

Figure 4.57 EPR spectra of quinone system and control experiment.

In summary, a range of oxidising reagents were added to the reaction mixture, however, most of the oxidising reagents could not improve the yield. It seems that copper(II) oxide can accelerate the formation of radical significantly, but the radical is not stable in presence of this oxidising reagent.

4.2.7.2 Catalytic oxidation route

We have also tried the new catalytic oxidation method using DBU and Pd/C catalyst presented by P. A. Koutentis and co-workers.[145] In our reaction, benzohydrazonamide cannot be isolated; DBU and Pd/C were thus added to the reaction mixture when the starting material benzohydrazonoyl chloride **4.79** was consumed (monitored by TLC). Unfortunately, decomposition of the target radical in the mixture was observed. After a 2 h reaction, no radical was detected in the reaction mixture. Moreover, the crude product mixture was less stable on silica column; only a tiny amount (less than 1%) of the target radical was isolated after column chromatography. Five alkoxyl chains on the aromatic rings may increase the electron density

significantly; the stability of this radical is not as good as other Blatter's radicals. It can be oxidised easier.[126]

Attempts to improve the yield of target radical by adding oxidising reagents failed. Then we resorted back to the spontaneous oxidation. We found that EPR signal of benzohydrazonyl chloride **4.79** and substituted aniline **4.77a** reaction mixture in dry THF under N_2 did not change significantly (neither increase nor drop) after 2 days (Figure 4.50). It suggested that the radical is relatively stable under this condition and no other oxidising reagents are needed for our reaction.

Unfortunately, purification of this radical is challenging because of the presence of numerous by-products and poor stability of the radical on the silica column. Addition of triethylamine to the eluent did not improve the stability of the radical on the column. The attempt to recrystallize this radical from acetonitrile failed, because the solubility of reaction mixture did not increase significantly with temperature. We have also attempted recrystallization from DMF. However, byproducts precipitated out with the target radical. Moreover, decomposition of the radical may occur at high temperatures required for recrystallization from DMF. The radical showed good solubility in most other organic solvents; no alternative solvents for recrystallization were identified. The attempt to separate the target radical from by-products by gel permeation chromatography (GPC) also failed; presumably, by-products and the target radical have similar molecular weights.

The optimal purification procedure included column chromatography to remove some byproducts followed by several recrystallizations from a DCM/acetonitrile mixture. This yielded pure radical **4.67** (29%). Figure 4.58 shows the MS spectrum of the radical after purification.

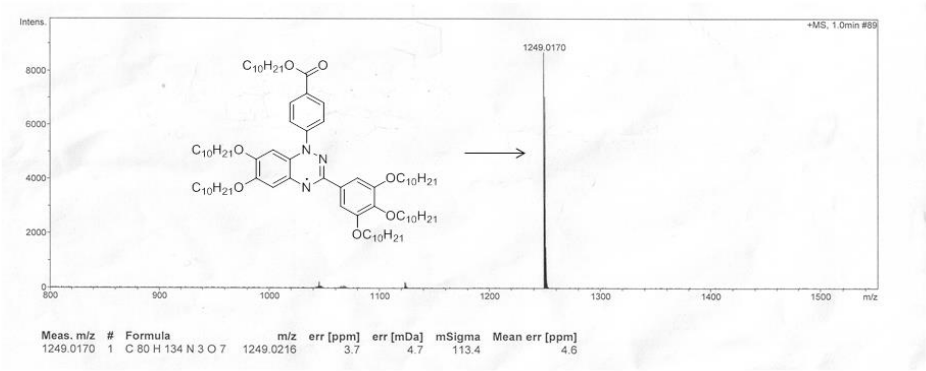

Figure 4.58 MS spectrum of radical **4.67** after purification.

4.2.8 Regiochemistry of 6 chains Blatter-type radical.

The cyclization of benzohydrazonamide **4.80** could potentially yield two isomeric structures (Figure 4.59). In order to confirm the regioselectivity of this reaction, dideuterium substituted aniline **4.90** was prepared (Figure 4.60). The benzohydrazonamide formed from this compound can cyclise to give to Blatter-type radicals which are no longer isomeric and can be distinguished by MS analysis (Figure 4.60).

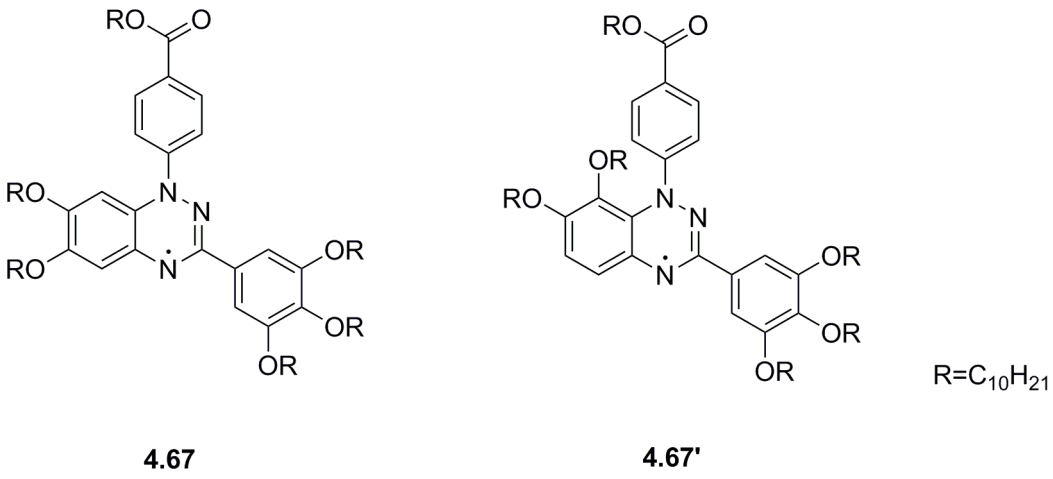

Figure 4.59 Two possible structures of the 6 chains radical.

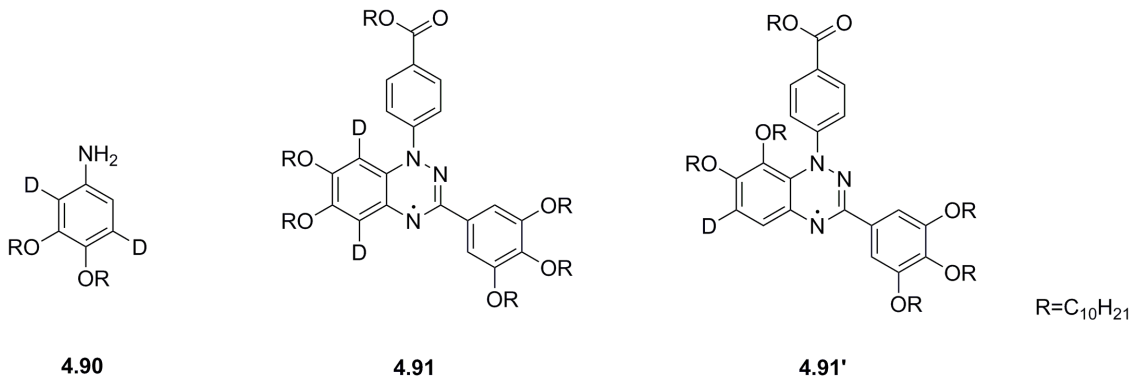

4.90 **4.91** **4.91'**

Figure 4.60 Structures of dideuterium aniline and two possible radical products.

In order to confirm the structure of Blatter's radical **4.67**, dideuteriated aniline was prepared. Mono-deuteriated 1,2-dimethoxybenzene was prepared in a 95% yield by T. Matsumoto and co-workers in 1991.[150] Di-deuteriated aniline **4.90** was prepared by the same method (Figure 4.61). In order to increase the deuterium incorporation, reaction of 1,2-didecyloxy aniline was carried out several times.

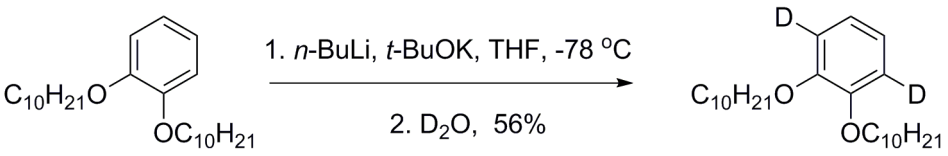

4.92 **4.93**

Figure 4.61 Preparation of deuterium dimethoxybenzene.[150]

After carrying out the deuterium exchange of 1,2-didecyloxybenzene for 7 times, 3,6-dideuterium-1,2-didecyloxybenzene **4.93** was prepared successfully as confirmed by NMR and MS analysis (Figure 4.62).

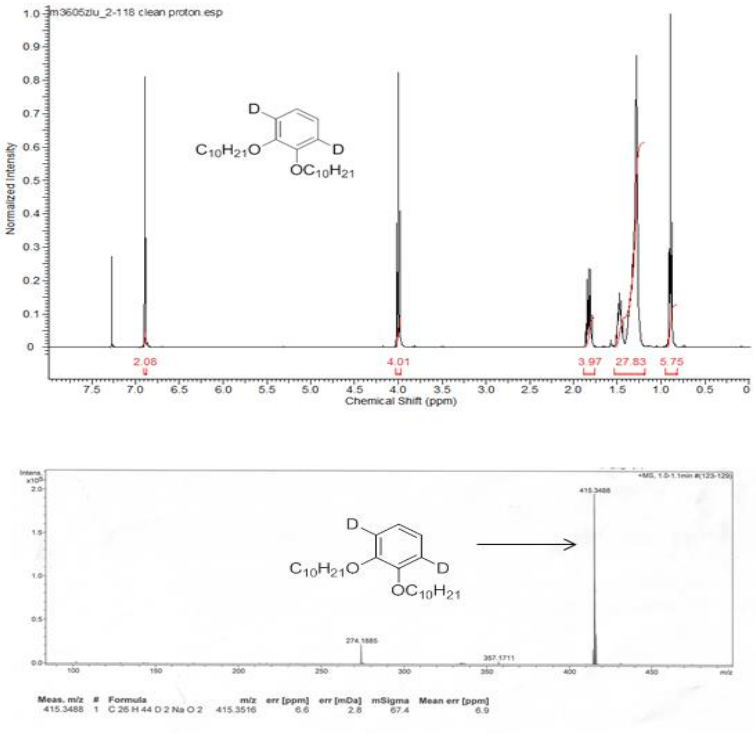

Figure 4.62 NMR and MS analysis of 3,6-dideuterium-1,2-didecyloxybenzene **4.93**.

2,5-Dideuterium-3,4-didecyloxy aniline was prepared by the same method as unlabelled didecyloxy aniline. DCM solution of sodium nitrite and nitric acid were added to 2,5-dideuterium-3,4-didecyloxybenzene to form 2,5-dideuterium-3,4-didecyloxy nitrobenzene. Reduction of nitrobenzene derivatives to give the desired aniline **4.90** was carried out with hydrogen using Pd/C catalyst. Then the reaction between benzohydrazonoyl chloride **4.79** and aniline **4.90** was set up (Figure 4.63).

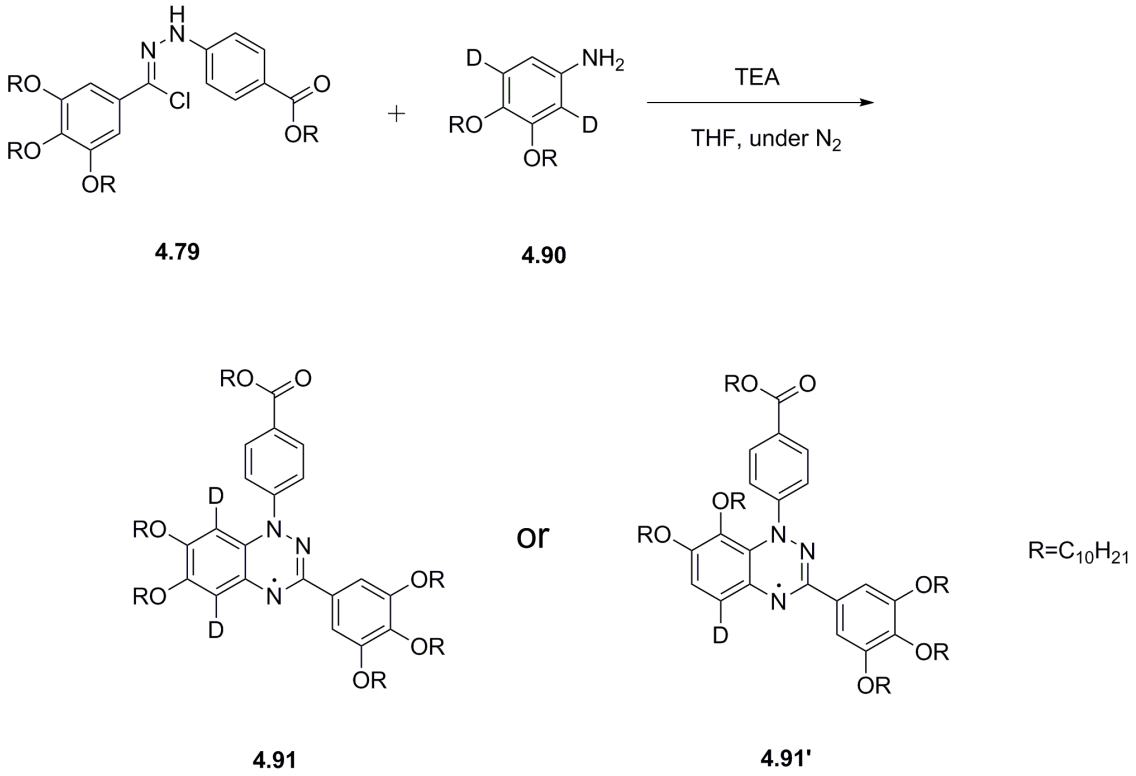

4.79 **4.90** **4.91** **4.91'**

Figure 4.63 The reaction between benzohydrazonyl chloride **4.79** and aniline **4.90**.

Figure 4.64 shows an MS spectrum of the isolated product. By comparing these results with the MS spectrum of unlabelled product (Figure 4.58), peak for mono-deuterium labelled radical was not observed on MS spectrum. Therefore, we conclude that the labelled product is dideuterium labelled radical **4.91**. The regioselectivity may arise from the small steric hindrance of radical **4.91**. This confirms the structure of unlabelled Blatter-type radical as **4.67** rather than **4.67'**.

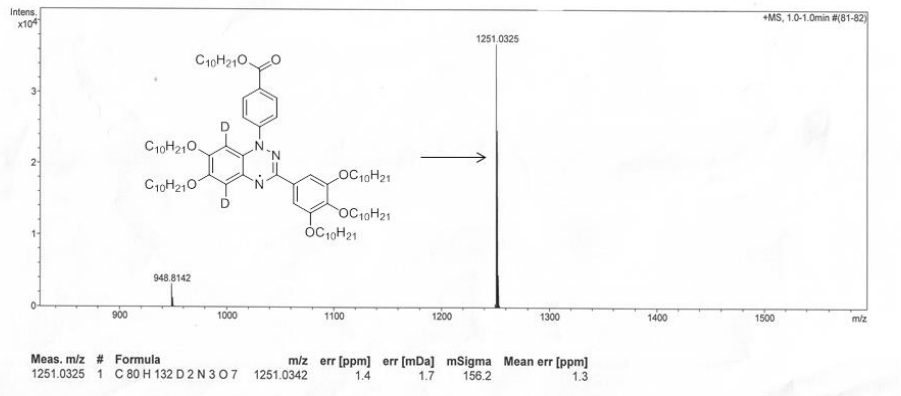

Figure 4.64 MS analysis of deuterium-labelled radical.

4.2.9 Preparation of 7 chains Blatter-type radical

Seven chains Blatter-type radical **4.87** was prepared successfully by the same procedure as for 6-chain radical **4.66** (Figure 4.65). Figure 4.66 and 4.67 show the EPR spectrum and the MS spectrum of the radical. Nitrogen hyperfine coupling constants were obtained from the simulation of EPR spectrum, a_{N1} = 6.80 G, a_{N2} = 4.51 G, a_{N3} = 4.61 G.

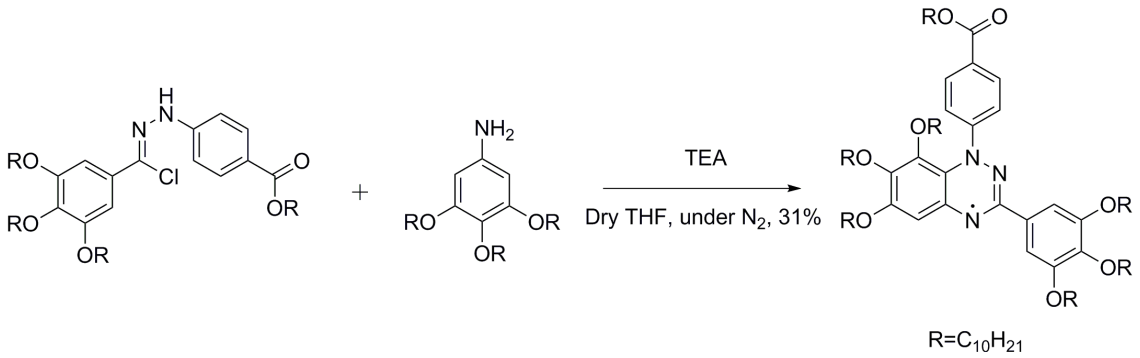

4.79 **4.77b** **4.94**

Figure 4.65 Preparation of 7 chains Blatter-type radical.

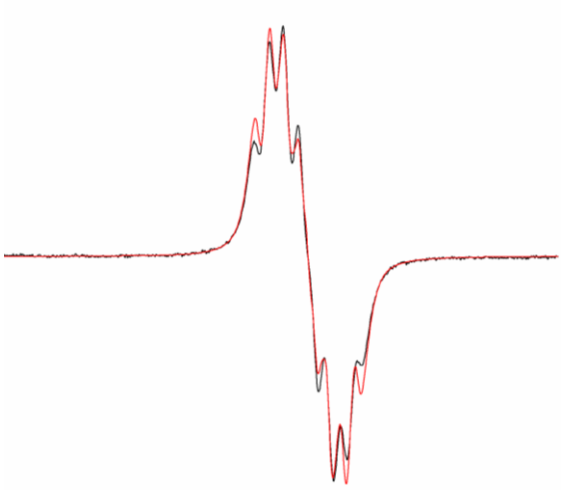

Figure 4.66 EPR spectrum of 7 chains radical. Black one is experimental data; red one is simulation spectrum, a_{N1} = 6.80 G, a_{N2} = 4.51 G, a_{N3} = 4.61 G.

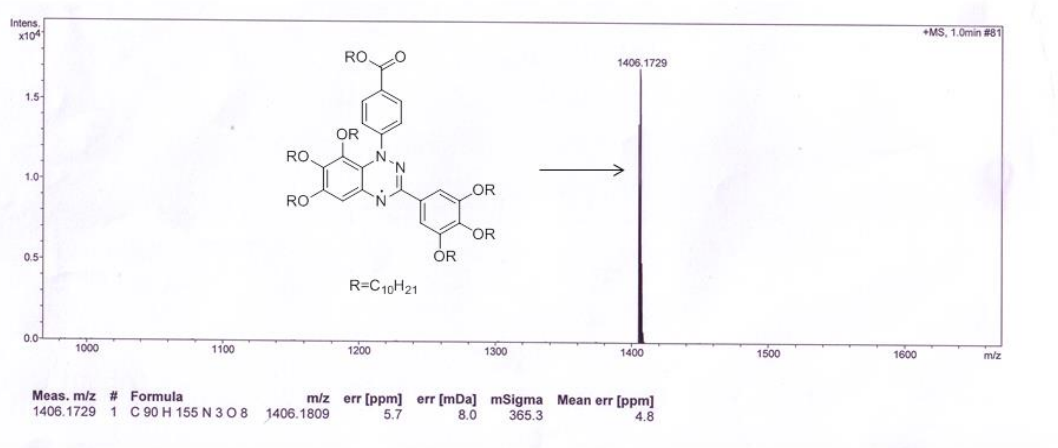

Figure 4.67 MS analysis of 7 chains radical.

4.2.10 Stability of new Blatter-type radicals

Radicals **4.67** and **4.94** are relatively stable in the presence of air at room temperature, no significant decomposition was observed after the radical was exposed in the air for 2 days. It was found that these two radicals are much more stable under inert atmosphere when heated. When the radical **4.67** was heated to 160 °C in presence of air, no EPR signal was detected. It suggested that radical was destroyed immediately at this temperature. However, under N_2 atmosphere, about 15% decay of EPR signal was observed after 5 min (Figure 4.68). Similar phenomenon was observed with radical **4.94**. These results suggested that the thermal stability of these radicals is much better under inert atmosphere.

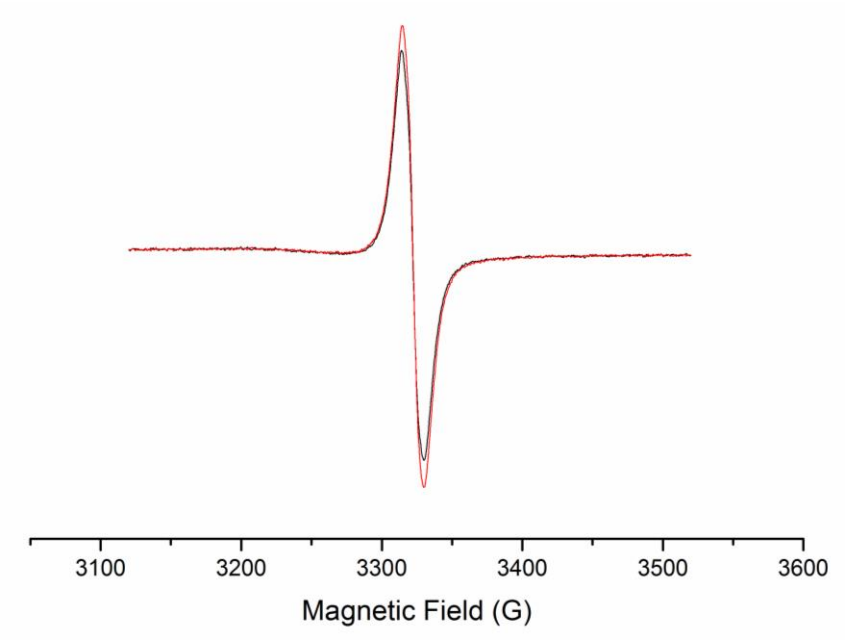

Figure 4.68 EPR spectra of radical **4.67** at 160 °C under N_2 atmosphere; red line is spectrum recorded immediately when the temperature reached to 160 °C; black one is spectrum recorded after 5 min.

4.3 Liquid crystal properties of Mesogens 4.67 and 4.94

4.3.1 Phase transition behaviour.

The phase transition temperatures of radicals **4.67** and **4.94** were studied by DSC and polarized optical microscopy. Two peaks were observed for both of these two radicals during the heating and cooling process (Figure 4.69 and 4.70). Radical **4.67** underwent a phase transition from isotropic to a columnar phase at 82.7 °C, and then columnar to crystal phase transition at -25.4 °C. For radical **4.94**, isotropic to columnar phase transition was observed at 57.3 °C and crystallization was observed at -31.0 °C (Table 4.3).

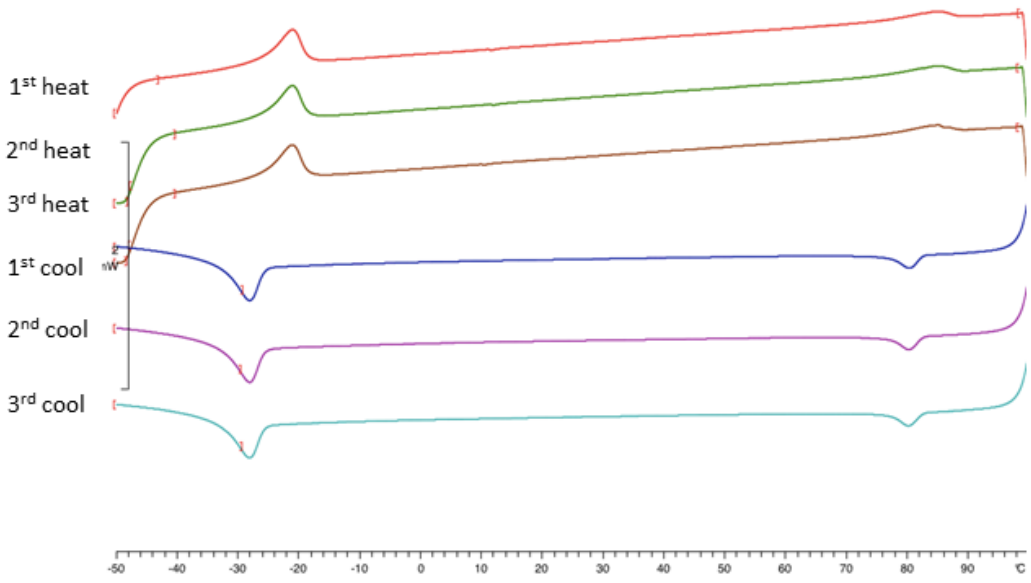

Figure 4.69 DSC trace for 6 chains radical **4.67**.

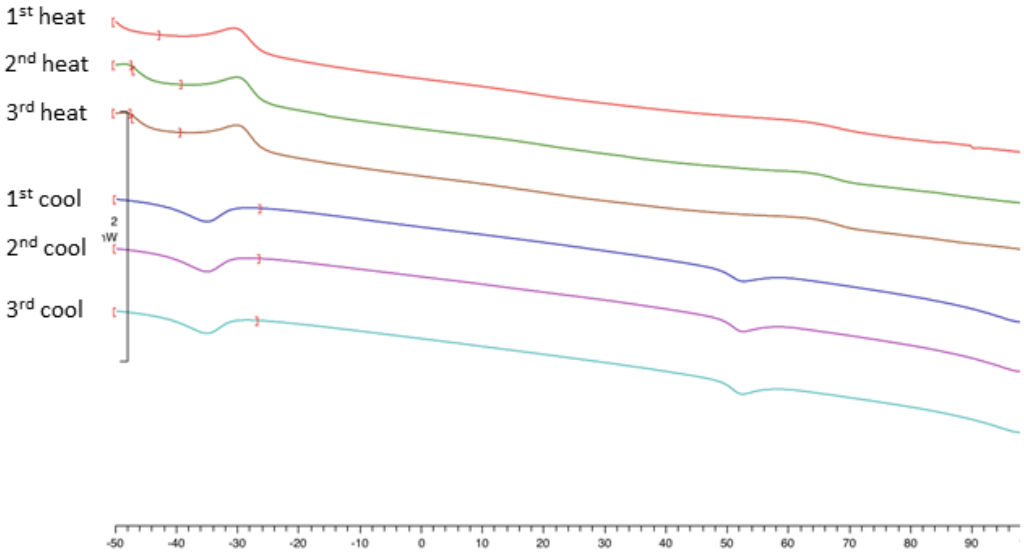

Figure 4. 70 DSC trace for 7 chains radical **4.94**.

Table 4.3 Transition temperatures (in the 2nd heating cycle) for radicals **4.67** and **4.94**.

Radical	Melting point		Clearing point	
	T / °C	ΔH / (J g^{-1})	T / °C	ΔH / (J g^{-1})
4.67	-25.4	9.62	82.7	2.69
4.94	-31.0	6.97	57.3	1.97

In both cases, it is clear that the transition temperatures are perfectly reproducible for several heating and cooling cycles, showing that no apparent decomposition takes place after this treatment. The isotropisation temperature for **4.94** shows a very small supercooling (Figure 4.70).

Mesogen **4.67** was cooled slowly (1 °C/min) from the isotropic liquid (85 °C) to 78.8 °C and observed by polarized optical microscopy. The texture of liquid crystal phase grew very slowly. However, after mesogen **4.67** was annealed at this temperature for several hours, a typical texture of a columnar phase was observed (Figure 4.71). Several straight lines were observed in some 'tiles' of the texture, a characteristic feature of the columnar phase.[151,152] For mesogen **4.94**, similar texture was observed at 50 °C, when the mesogen was cooled from 60 °C at the rate 1 °C/min and then annealed at 50 °C for several hours (Figure 4.72).

Based on symmetry arguments, the disc space filling in **4.94** is effective, despite the fact that each aromatic ring carries a different number of alkyl chains. Therefore, packing of **4.94** in columns results from core-core interactions; the columns are further arranged in a lattice to achieve the columnar mesophase. Without clear X-Ray analysis it is difficult to infer the symmetry of the columnar phase.

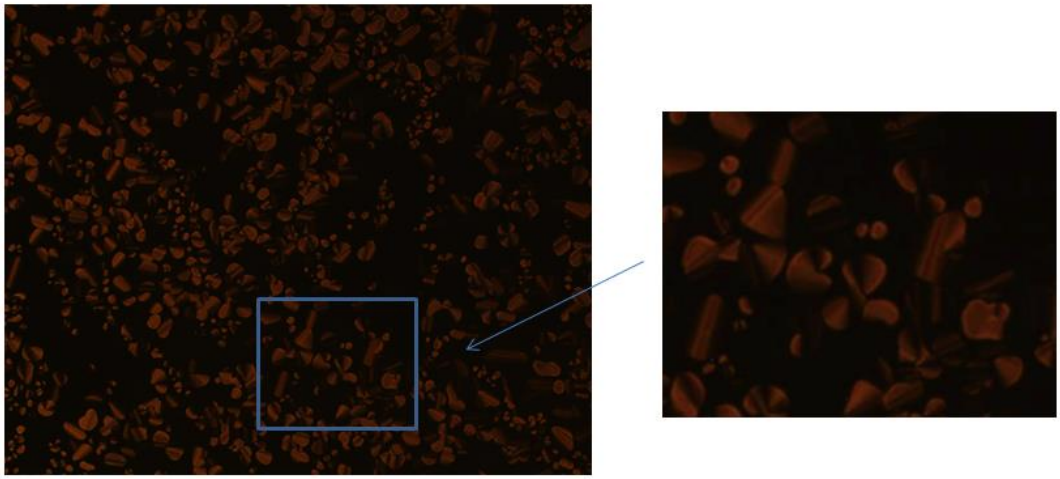

Figure 4.71 Optical polarised micrographs of radical **4.67** at 78.8 °C.

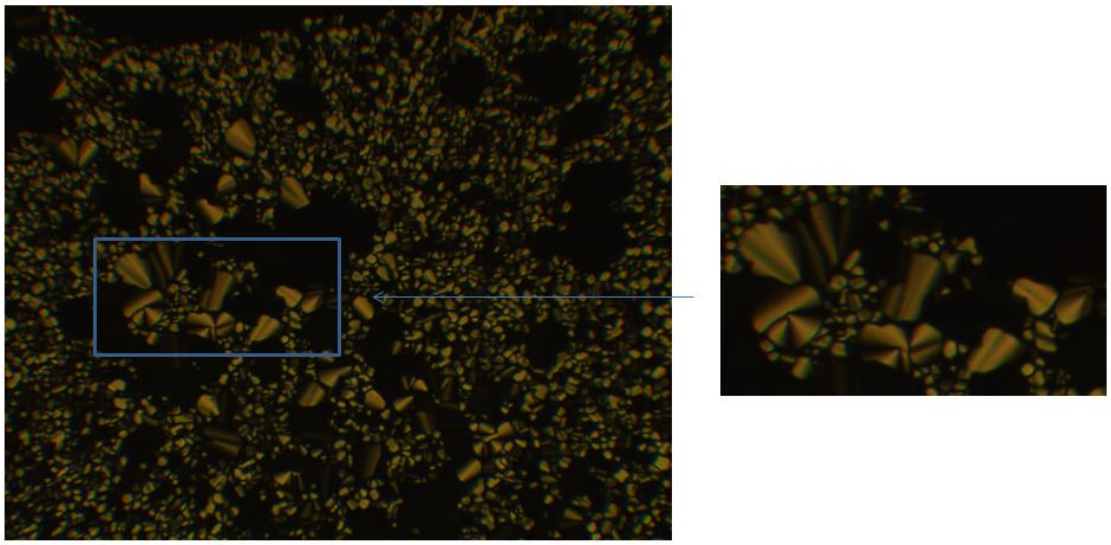

Figure 4.72 Optical polarised micrographs of radical **4.94** at 50 °C.

Comparison of the isotropisation temperatures of **4.67** and **4.94** shows that the mesophase stability of **4.67** is considerately higher than that of **4.94** (82.7 °C and 57.3 °C respectively). Similarly, the enthalpy of the isotropisation transition is higher for **4.67** than for **4.94**. Furthermore, the range of the mesophase for the hexa-substituted radical is considerately larger than the mesophase range for the hepta-substituted radical (108.1 °C and 88.3 °C respectively). Additionally, the melting point of **4.94** (with seven chains) is lower than that of **4.67** (with six chains), suggesting that it is easier to melt the alkyl chains in the radical **4.94** than in the radical **4.67**.

Qualitatively, these facts point to the conclusion that increasing the number of chains in the core decreases the melting point (which is beneficial for radical stability), but decreases the isotropisation temperature , because it causes a reduction in the molecular symmetry, the seventh chain precluding effective packing of the disks. Therefore a reduction of mesophase range and mesophase stability is observed.

4.3.2 Photoconductivity Measurements

The potential to be used as a one-dimensional (1D) conductor is a fascinating application of discotic LCs. The aromatic rings stacked in columns can act as the conducting core, and the flexible chains around the aromatic rings are insulating. Charges can hop from one aromatic ring to another and therefore, the conductivity along the columns is much higher than that perpendicular to the columns (Figure 4.73). Hence, efficient π-stacking is considered as an important factor to obtain this conducting property.[153] Therefore, triphenylene derivatives have been extensively investigated. The breakthrough in this field was achieved by D. Adam and co-workers in 1994 with 2,3,6,7,10,11-hexahexylthiotriphenylene (HHTT, Figure 4.74).[154] A charge carrier mobility of 0.1 $cm^2 V^{-1} s^{-1}$ in a columnar phase was obtained in time-of-flight (ToF) measurement. This was the highest charge carrier mobility value achieved by organic photoinduced systems at that time. Since radicals **4.67** and **4.94** have a relatively large core, it was anticipated that these two radicals might be photoconductive. In order to test this hypothesis, ToF measurements of these two radicals were carried out.

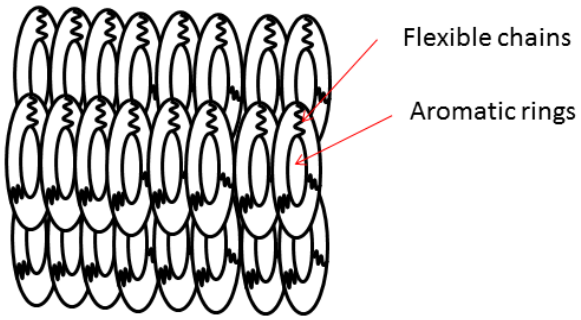

Figure 4.73 Schematic representation of discotic liquid crystals.

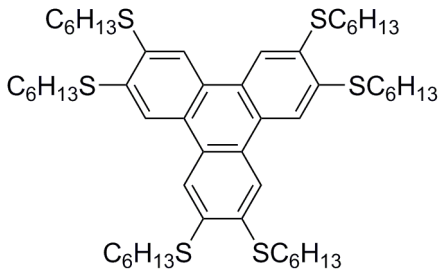

4.95

Figure 4.74 The structure of HHTT.

4.3.2.1 Introduction to Time-of-Flight measurement of photoconductivity

ToF is the most commonly used technique to study the charge transport properties of discotic LCs. Discotic LCs are homeotropically aligned in an indium tin oxide (ITO) coated sandwich conductive cell. Charge carriers are produced by laser light irradiation. Electrical field is applied between the two surfaces of the cell to induce a drift of the charges. Then the charge will move across the cell inducing a transient current which can be detected (Figure 4.75). The charge carrier mobility, μ, is obtained from the time that these charges take to transfer between two electrodes (equation 4.1); here v is drift velocity, E is applied electrical field, d is the thickness of cell, V is applied voltage and t is transit time.

$$\mu = v/E = d^2/Vt \qquad (4.1)$$

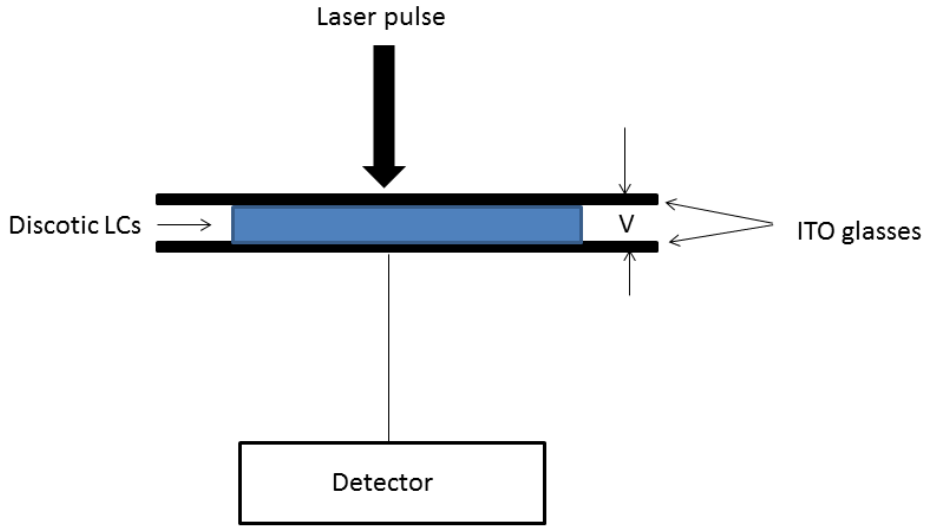

Figure 4. 75 Schematic representation of a ToF experimental set up.

For ToF measurement, a homeotropic alignment of discotic LC molecules has to be achieved. In the case of homeotropic alignment, the columns are arranged along the direction perpendicular to the surface of the cell (Figure 4.76). This alignment of LCs can be confirmed by polarised optical microscopy. For a homeotropic alignment of liquid crystals, only dark background can be observed in Col_h phase by polarized optical microscopy, while a dendritic texture with branches derived from the main axis at 90° in Col_r phase (Figure 4.77) is observed. The charge mobility is difficult to detect with unaligned samples. Therefore, in order to test the charge mobility of mesogens **4.67** and **4.94**, they must be homeotropically aligned.

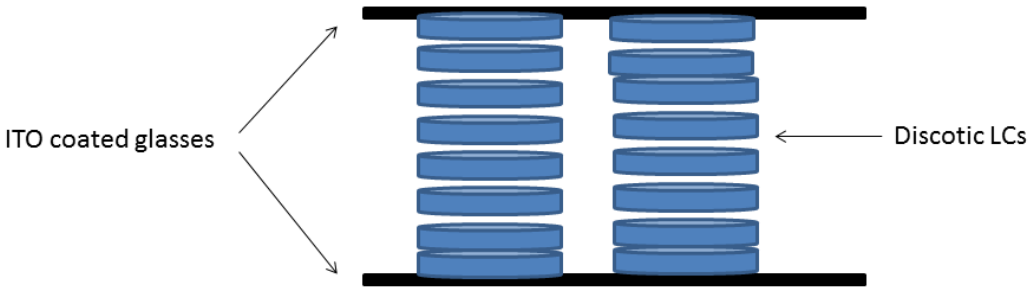

Figure 4.76 Schematic representation of homeotropic alignment.

Figure 4.77 Dendritic texture of Col_r phase.[3]

4.3.2.2 Alignment of radicals 4.67 and 4.94

Homeotropic alignment of discotic LCs can often be obtained by slowly cooling the samples from the isotropic phase.[155] However, textures of non-aligned discotic LCs were observed by polarized optical microscopy with both radicals **4.67** and **4.94** when the samples were slowly cooled (0.1 °C/min) from isotropic phase (Figure 4.78). Surprisingly, a dendritic texture was observed with radical **4.67** when the sample was cooled from 86 °C to 60 °C at the rate of 1 °C/min followed by slow cooling to 30 °C at the rate of 0.1 °C/min (Figure 4.79). The branches deviate from the main axis at 90°; thereby it suggesting that radical **4.67** forms the rectangular columnar phase. This dendritic texture originated from the homeotropic alignment of molecules in Col_r phase. However, the mosaic texture was still observed in some areas (for example, in the middle of the photomicrograph shown in Figure 4.79). This observation indicates that mesogen **4.67** was not completely homeotropically aligned. For mesogen **4.94**, no homeotropic alignment was obtained. These results suggest that these two mesogens are difficult to align using conventional methodologies.

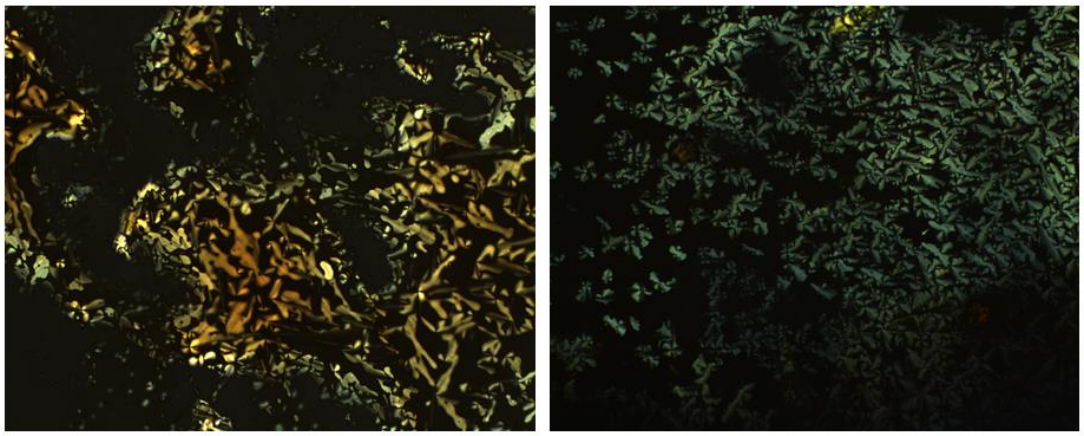

a b

Figure 4.78 Optical polarised micrographs of radicals **4.67** and **4.94**; a) radical **4.67** at 60 °C cooled from 85 °C b) radical **4.94** at 40 °C cooled from 60 °C.

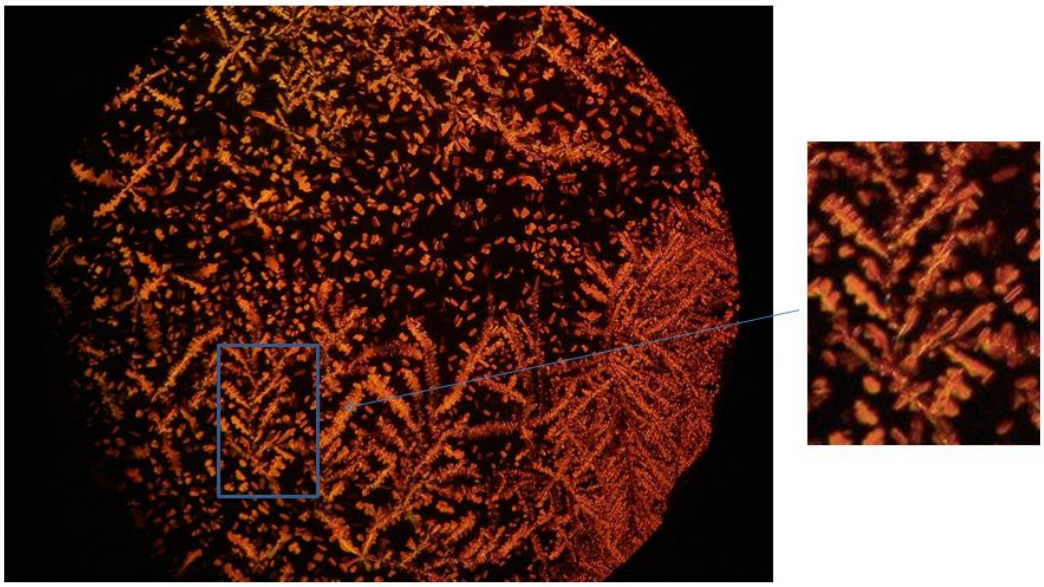

Figure 4.79 Dendritic texture of radical **4.67** at 30 °C.

A recent literature report quoted a value of 1.52×10^{-3} cm^2 V^{-1} s^{-1} for charge carrier mobility of unaligned mesogen **1.47** (R=SC_8H_{17}, Figure 4.80).[38] Encouraged by this result, the charge carrier mobilities of mesogens **4.67** and **4.94** with partial or non- aligned samples were measured using the TOF technique.

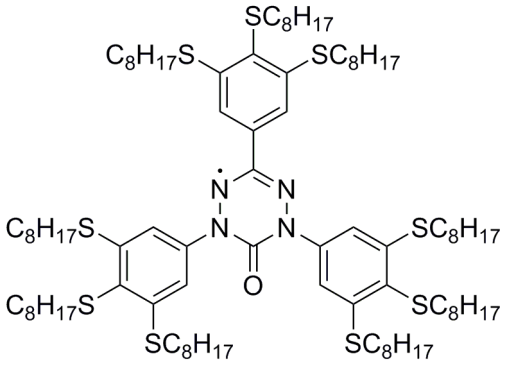

1.47

Figure 4.80 Structure of photoconductive mesogen **1.47**.[38]

The signal of a reported photoconductive mesogen 2,3,6,7,10,11-hexakishexyloxytriphenylene (HAT6) in ToF measurement was observed. However, no signals were observed for these two mesogens in columnar phase in the ToF measurements with the same experimental set up. The failure of this experiment could be due to incomplete homeotropic alignment of these two mesogens or insufficient signal strength in ToF measurement. The other possibility is that these two mesogens are not photoconductive.

4.4 EPR Investigation

4.4.1 Mesogens 4.67 and 4.94

EPR spectroscopy is a useful technique for studying the magnetic properties of PMLCs, asmicroscopic information about arrangement of molecules in different phases can be obtained by investigating the EPR spectra. EPR spectra of mesogen **4.67** were recorded at various temperatures on heating (220 K to 360 K at 10 °C intervals) and on cooling.

As g factor is anisotropic, a change in molecular orientation results in a change of g value

(chapter 1). Therefore, a change in molecular orientation in liquid crystals phase within a magnetic field can be determined from the g value.

A small change of g value (around 0.0006) was reported for discotic mesogen **1.37** during the isotropic to columnar phase transition due to the molecules in columnar phase tend to align along the direction of the $2p_z$ orbital of the unsaturated carbon centre parallel to the applied field.[34] However, for rod-like mesogen **1.14c**, a significant drop (0.0013) of g value was observed upon the crystal to liquid crystal phase (nematic phase) transition. Therefore molecules in the liquid crystal phase tend to align with the direction of the N-O axis perpendicular to the applied field (chapter 1).[12] Moreover, a striking increase in intensity was observed during the crystal to liquid crystal phase transition of mesogen **1.14c**. As intensity of EPR is proportional to the magnetic susceptibility, it suggested that the magnetic susceptibility increased significantly during the crystal to liquid crystal phase transition which means strong spin-spin interactions (magneto-LC effect, chapter 1) were introduced by the applied field. A large increase of magnetic susceptibility was also observed by SQUID magnetometry.[9,35]

However, for mesogen **4.67**, only a slight change of g value (around 0.0002) was observed during the heating process from crystal to Col phase and further to isotropic phase (Figure 4.81). During the cooling process from isotropic to liquid crystal phase, again, only a small difference in g factor was observed. These results suggested that the molecular alignment in columnar phase of mesogen **4.67** is poor in the applied field, possibly due to the high viscosity of this discotic mesogen.

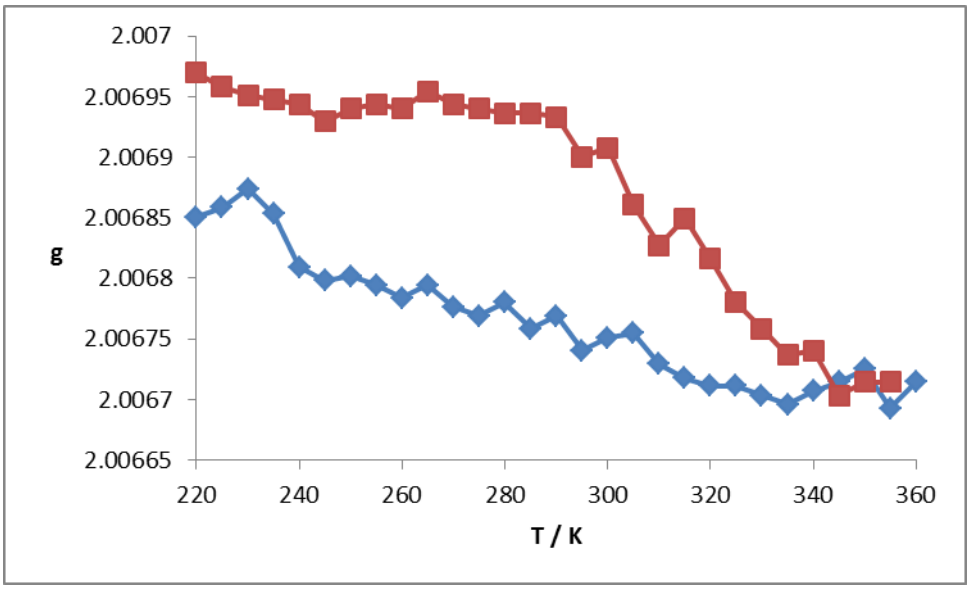

Figure 4.81 Plot of g factor vs T of mesogen **4.67**. Blue line represents heating process; red line represents cooling process.

As the intensity of the EPR signal is proportional to the magnetic susceptibility, the intermolecular magnetic interactions in the columnar phase of mesogen **4.67** could be studied by EPR spectroscopy as well. Compared to SQUID magnetometry, EPR spectroscopy is a better technique for investigation of the magnetic susceptibility of organic PMLCs because 1) the contribution of diamagnetic components can be ignored; 2) precise data is obtained even at high temperature.

As shown in Figure 4.82, the intensity of EPR spectra decreased slowly with increasing temperature from 220 K to 360 K, which suggested that the magnetic susceptibility decreased with increasing temperature. This is because the spin coupling energy is much small compared to the thermal energy at high temperature. No significant change in intensity was observed around the phase transition temperature. This suggests that the magneto-LC effect does not exist in the columnar phase of mesogen **4.67**, possibly due to the poor alignment of this mesogen in the applied field.

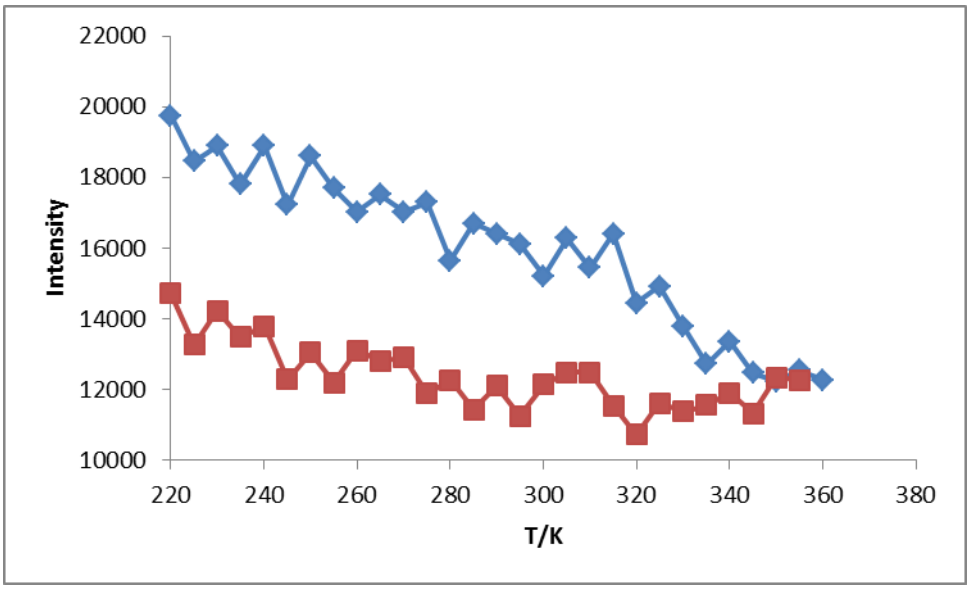

Figure 4.82 Plot of intensity vs T of mesogen **4.67**. Blue line represents heating process; red line represents cooling process.

The intermolecular magnetic interactions have two contributors, spin-spin dipolar interaction and spin-spin exchange interaction. The information on these two interactions can be obtained from the linewidth of EPR spectra.[156] Therefore, the linewidth of EPR spectra was investigated. It increased with increasing temperature from 320 K to 360 K as shown in Figure 4.83. Spin-spin dipolar interactions are related to the distance between spins and their relative orientation. The intermolecular distance in liquid crystal phase does not change significantly with increased temperature. Only slight change in g value suggested that molecular alignment in liquid crystal did not occur. Therefore the contribution of spin-spin dipolar interaction is small. The stronger exchange interactions at high temperature reduce the life time of spin state which results in broader EPR spectra. The increased linewidth at high temperature thus probably arises from the contribution of spin exchange interactions. Only slight change in the linewidth was observed below 320 K. This suggests that the spin-lattice and spin-spin relaxation times are temperature-independent. A similar phenomenon was observed for discotic mesogen **1.37.** The authors suggested that this stabilization of relaxation times may come from the formation of columnar phase.[34]

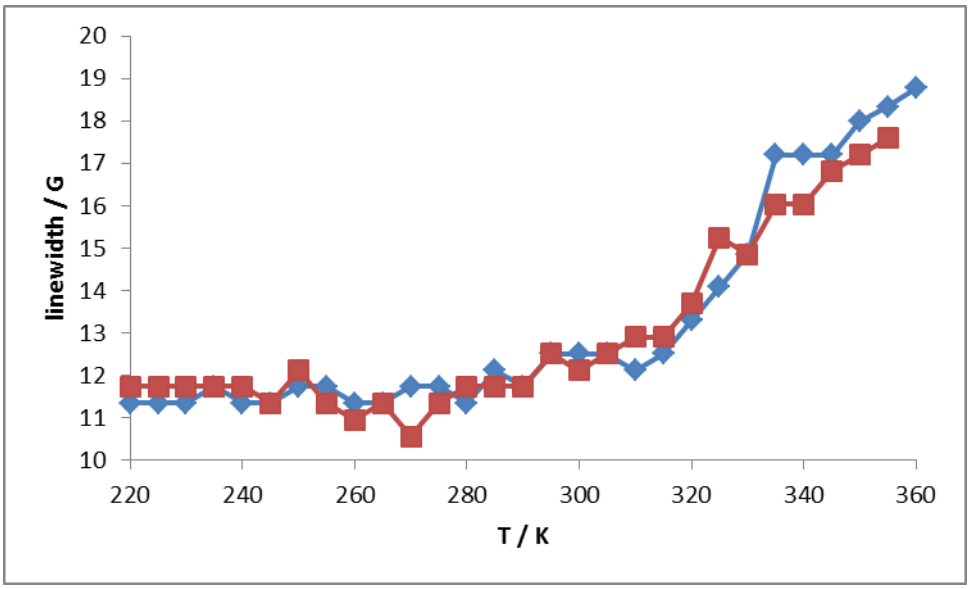

Figure 4.83 Plot of linewidth vs T of mesogen **4.67**. Blue line represents heating process; red line represents cooling process.

EPR spectra of mesogen **4.94** were recorded at various temperatures. Similar results were obtained (Figure 4.84, 4.85 and 4.86).

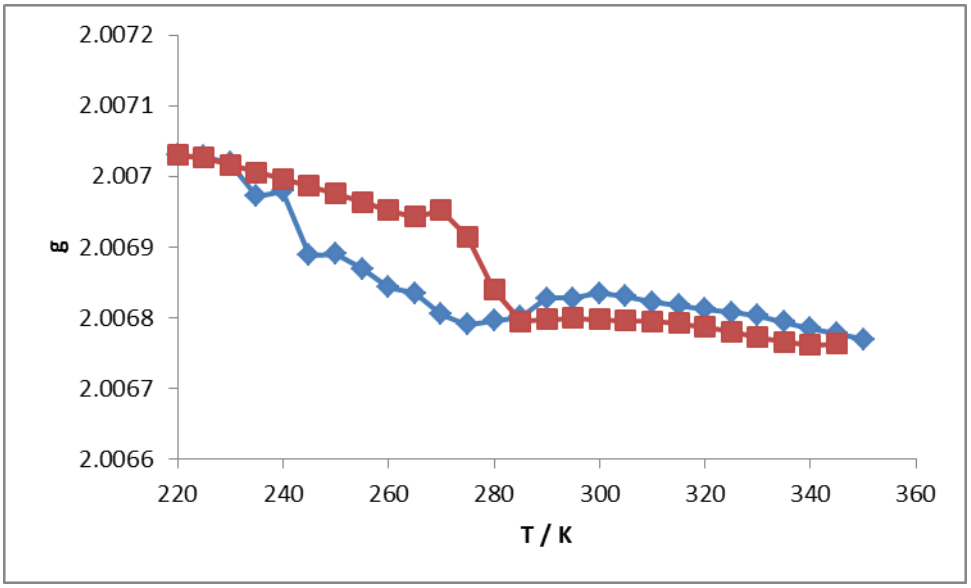

Figure 4.84 Plot of g factor vs T of mesogen **4.94**. Blue line represents heating process; red line represents cooling process.

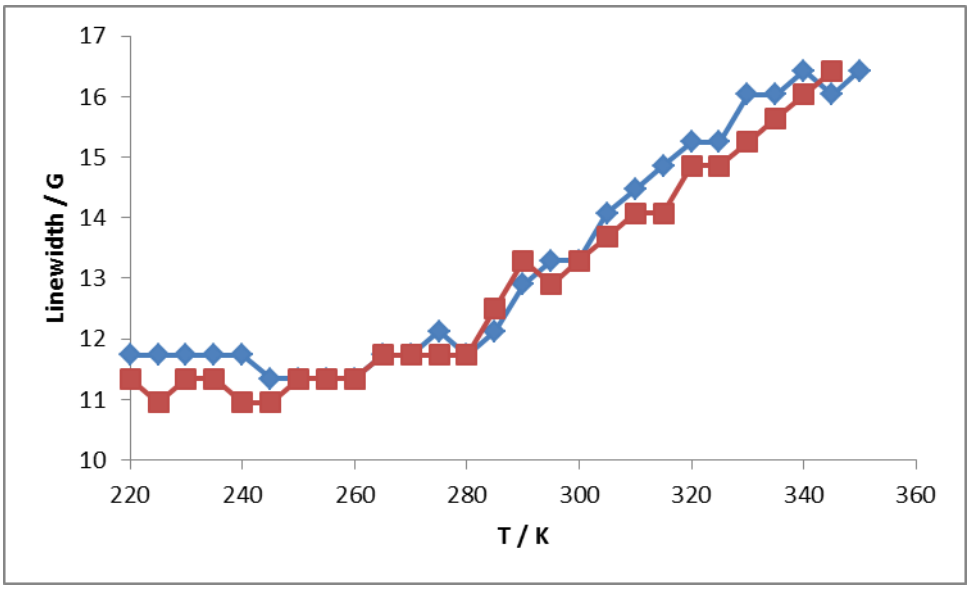

Figure 4.85 Plot of linewidth vs T of mesogen **4.94**. Blue line represents heating process; red line represents cooling process.

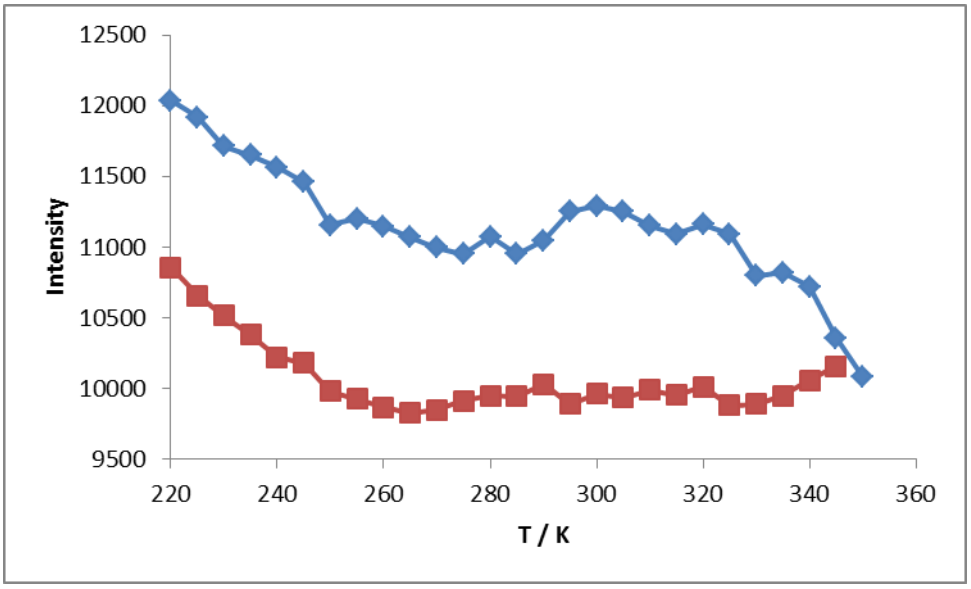

Figure 4.86 Plot of intensity vs T of mesogen **4.94**. Blue line represents heating process; red line represents cooling process.

During the EPR investigation of mesogen **4.67** and **4.94**, additional peaks were observed in the EPR spectra at low temperature (Figure 4.87). These peaks could arise from the formation of spin-triplet dimers. For a spin triplet species (S = 1), three spin states (m_s = -1, 0, +1) are not degenerate in the absence of a magnetic field, due to the dipolar-dipolar interaction and spin-orbital coupling. This is called zero field splitting. Therefore, the two allowed EPR transitions do not occur at the same magnetic field (Figure 4.88).

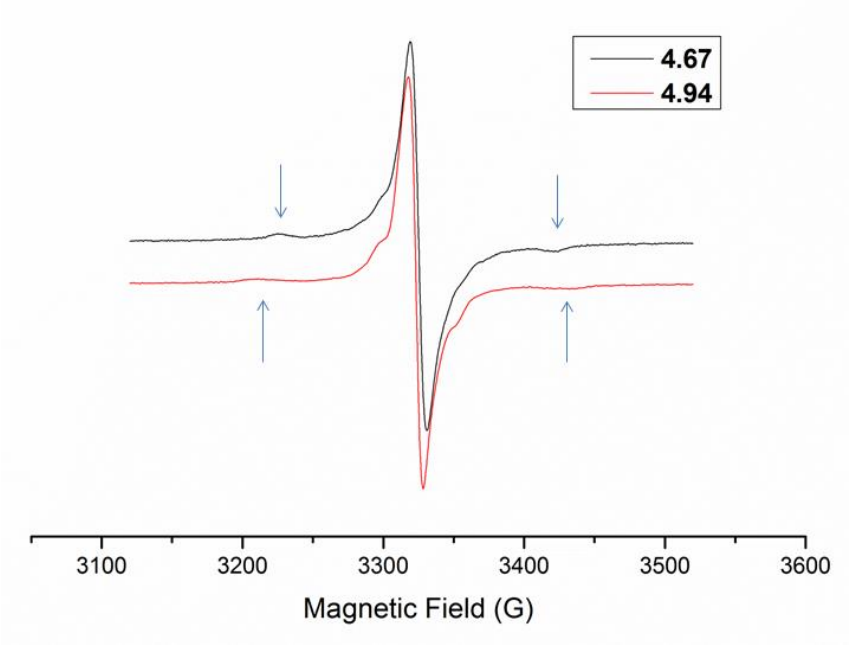

Figure 4.87 EPR spectra of mesogen **4.67** and **4.94** at 240 K. Triplet resonance lines are marked by arrows.

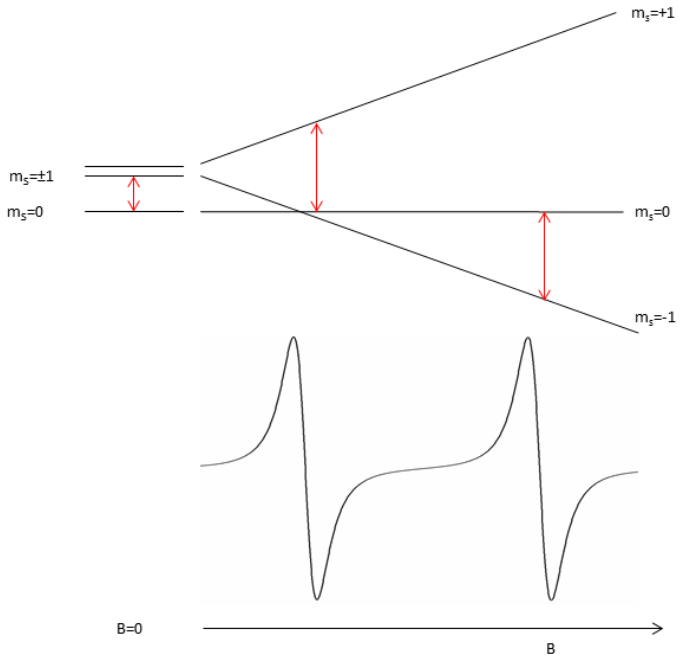

Figure 4.88 Schematic representation of zero field splitting.

Spin-triplet dimerization of a Blatter-type radical was observed with radical **4.96** by C. Constantinides and co-workers (Figure 4.89).[157] Based on a comprehensive study of a series of Blatter-type radicals, they found that Blatter-type radicals tend to form π-slipped stacked

columns, as shown in Figure 4.90.[121,157-160] They suggested that the small interplanar distance results in the dimerization of radical **4.96** (radicals II and III in Figure 4.90). Triplet resonance in EPR spectrum was observed with radical **4.96** at low temperature (Figure 4.91). It was also found that the intermolecular interactions of Blatter-type radicals strongly depend on the molecular packing. A slight change in molecular structure could result in different molecular conformations, leading to the observation of different molecular interactions.

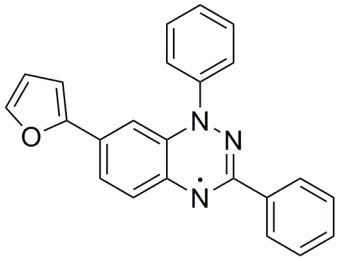

4.96

Figure 4.89 Structure of Blatter-type radical **4.96**.[157]

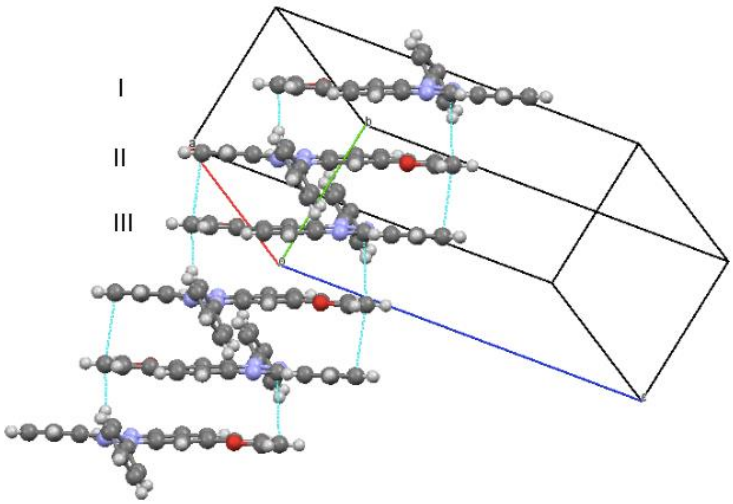

Figure 4.90 Schematic representation of solid-state packing of radical **4.96**.[157]

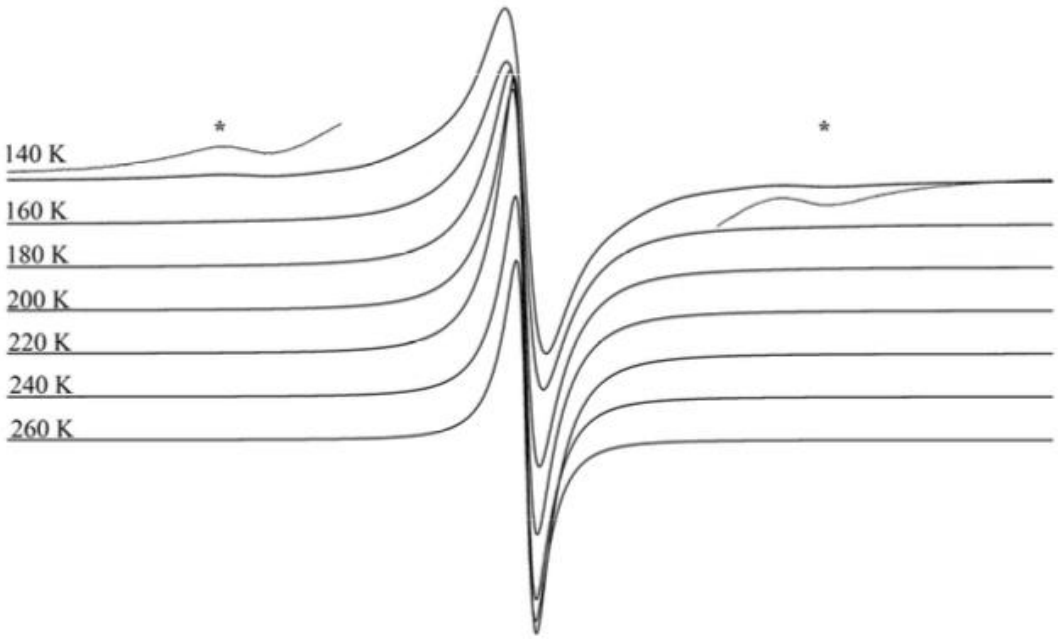

Figure 4.91 EPR spectra of radical 4.96, triplet resonance lines are marked by an asterisk.[157]

During the EPR investigation of mesogens **4.67** and **4.94**, it was found that EPR results are strongly influenced by impurities in these mesogens, affecting the reproducibility of EPR results. Figure 4.92 is HPLC chromatogram of mesogen **4.67**. The strong peak at 22.845 min corresponds to mesogen **4.67** as shown by LC-MS. However, there is a small shoulder, presumably of an impurity that cannot be separated or identified due to low intensity.

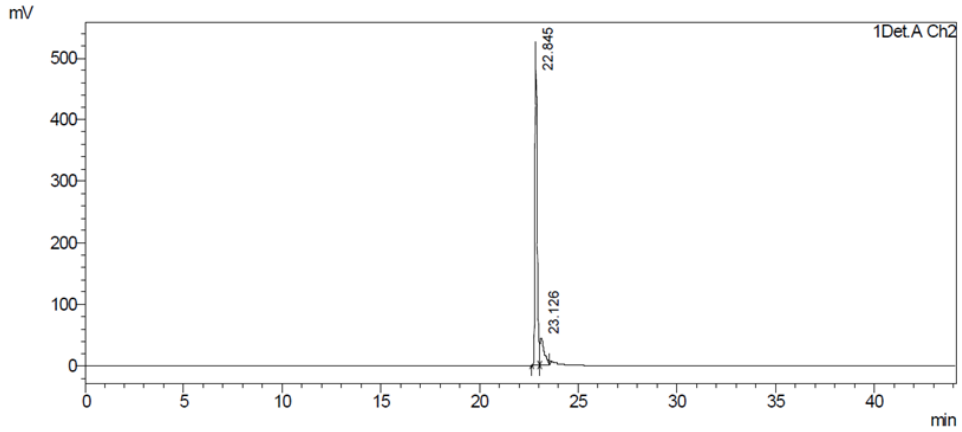

Figure 4.92 HPLC spectrum of mesogen **4.67**.

In summary, an EPR study of mesogens **4.67** and **4.94** was carried out at variable temperatures. The molecular orientations of mesogen **4.67** and **4.94** did not change during the phase transition. In these two mesogens, spin-triplet dimerization and weak anitiferromagnetic interactions were observed. For EPR investigation of these mesogens, samples with high purity must be used to collect the precise and reproducible data.

4.4.2 Radicals in Discotic LC Host

Rod-shaped EPR spin probes have been used to study the rod-like liquid crystals, especially nCBs. However, the EPR studies of spin probes in discotic LCs are very rare, as the conventional spin probe molecules are incompatible with discotic mesogens. To be a suitable spin probe for investigating discotic LCs, the spin probe itself should resemble the host molecules as closely as possible which can minimize the influence of the phase formation of the host. The other requirement is that the spin probe should be orientationally rigid. Free rotation of spin probe can average out the anisotropic effect, therefore EPR spectra will not change significantly during the phase transition, and then not much information can be obtained.

The first EPR investigation of discotic LC system was reported by H. Gopee and co-workers using spin probe **4.97**.[161] The EPR study of this probe in discotic LC hexakis(*n*-hexyloxy) triphenylene (HAT6) was carried out (Figure 4.93). EPR spectra of spin probe **4.97** in HAT6 showed strong sensitivity to the liquid crystal phase formation and molecular oriental dynamics. Therefore, the authors suggested that EPR spectroscopy is a powerful tool to study discotic liquid crystals with spin probes.

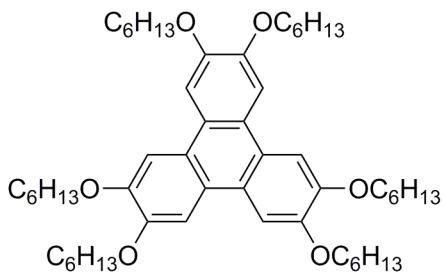

HAT6

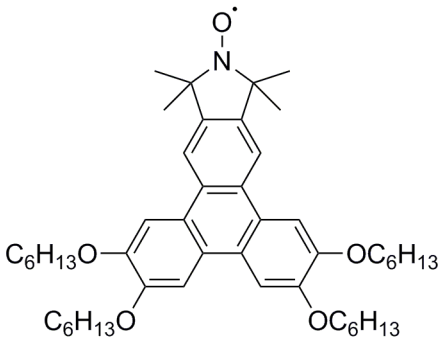

4.97

Figure 4.93 Structures of HAT6 and spin probe **4.97**.[161]

Encouraged by Gopee and co-workers' results, we used radical **4.67** as a spin probe in a discotic LC host **4.98** (Figure 4.94). LC host **4.98** was chosen because it has relatively low clearing point and relatively large temperature range of liquid crystal phase. A *ca.* 0.03 w/w% mixture of radical **4.67** in LC **4.98** was prepared. Surprisingly, only very weak EPR signal was observed. However, a significantly increase intensity (around 30 times) of the EPR spectrum was observed when 20 µl DCM was added to this mixture (Figure 4.95). As discussed above, dimerization of mesogen **4.67** was observed in neat mesogens, and the intermolecular interactions strongly depend on the molecular packing.[157-159,162] Possibly, in the liquid crystal host **4.98**, molecular packing of mesogen **4.64** changed, and then spin-singlet dimerization occurred which reduced the EPR signal significantly.

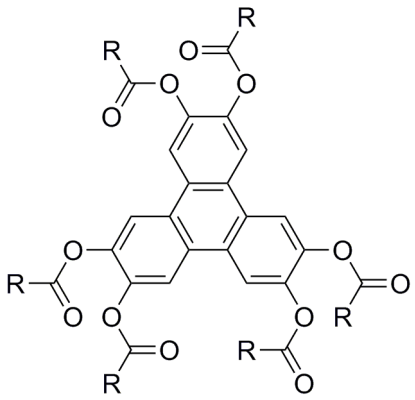

$R=C_{13}H_{27}$

Cr $\xrightarrow{57.7^{o}C}$ Col_h $\xrightarrow{97.4^{o}C}$ Iso

4.98

Figure 4.94 The structure of LC host **4.98**.

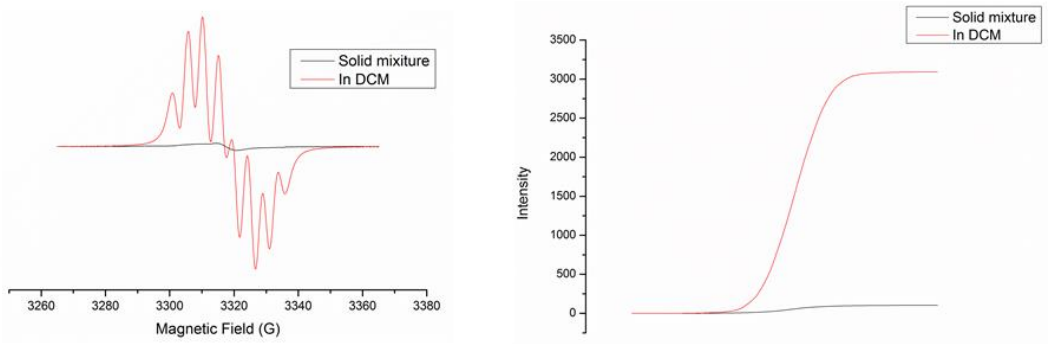

a b

Figure 4.95 a) EPR spectra of radical **4.67** in LC **4.98** , b) double integration of spectra.

A control experiment was carried out with *N*,*N*-diphenyl-*N*'-picrylhydrazyl (DPPH) radical in LC host **4.98**. DPPH is a stable radical, and dimerization of DPPH is observed. However, no significant difference of intensity of the EPR spectrum was observed after 20 µl DCM was added to the solid mixture (Figure 4.96). Another stable radical, TEMPO, was also doped in LC **4.98**. Again, the dimerization of TEMPO is rare. There was almost no change in intensity of EPR spectra observed after 20 µl DCM was added to the solid mixture (Figure 4.97). These results

suggested that spin-singlet dimerization of mesogen **4.67** may occur in LC host **4.98**.

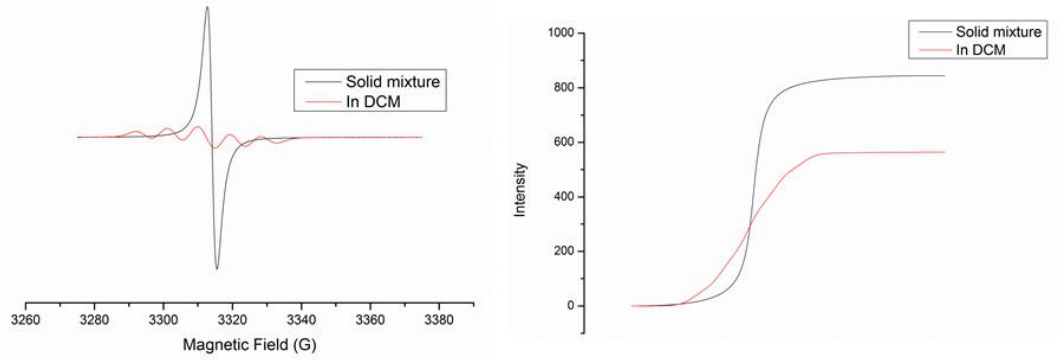

a b

Figure 4.96 a) EPR spectra of DPPH in LC host **4.98** solid mixture and in DCM solution, b) double integration of spectra.

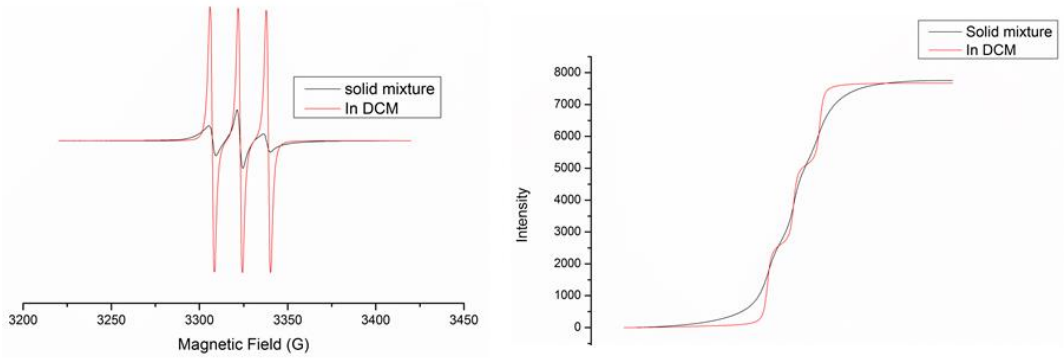

a b

Figure 4.97 a) EPR spectra of Tempo in LC host **4.98** solid mixture and in DCM solution, b) double integration of spectra.

Mesogen **4.94** was doped into LC host **4.98** as well. Similar phenomenon was observed with that of mesogen **4.67** in **4.98**. Again, possibly spin-singlet dimerization of mesogen **4.94** occurred in the LC host **4.98**.

4.5 Conclusion

Two new mesogenic Blatter-type radicals **4.67** and **4.94** were prepared successfully. Both these mesogens exhibit a columnar phase over a large temperature range. The procedure for the preparation of these Blatter-type radicals was optimised. However, it was found that the preparation of electron rich phenylhydrazine derivatives is challenging. Over-reduced products (anilines) were always obtained by reduction the corresponding diazonium salts. Deprotection of the corresponding hydrazides with trifluoroacetic acid seems to be a promising method. The stability of these electron-rich hydrazine derivatives is poor and isolation of pure hydrazine products is difficult. Moreover, the benzohydrazonamides are not stable under certain conditions. Oxidation of these compounds was observed both in the presence of air and under inert atmosphere.

Variable temperature EPR investigation of these two mesogens suggested that the molecular alignment of these two mesogens in the applied magnetic field is poor. No magneto-LC effect was observed with these two mesogens. Spin-triplet dimerization of these two mesogens was observed. However, in LC host **4.98**, spin-singlet dimerization was observed. Different types of dimerization may arise from the different molecular packing of these mesogens.

Compared to mesogen **4.67**, **4.94** has lower melting and clearing points, possibly due to the seventh chain precluded effective packing of the disks. No charge carrier mobility was observed by TOF measurement, possibly because these two mesogens are not photoconductive.

Chapter 5 From Nitron to Blatter-type Radical

5.1 Introduction

Carbenes play an important role in both inorganic and organic chemistry, for instance as ligands for transition metal ions. In 1968, two metal complexes **5.1** and **5.2** were prepared in Germany (Figure 5.1). These complexes with *N*-heterocyclic carbenes (NHCs) as ligands were quite unusual at that time and therefore attracted attention.[163,164]

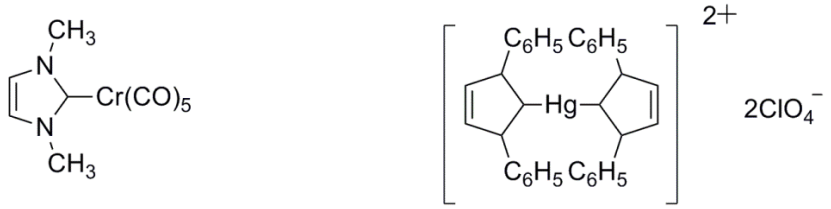

5.1 **5.2**

Figure 5.1 The structure of *N*-heterocyclic carbene metal complexes.[163,164]

The properties of NHCs could not be easily investigated until the first thermodynamically and kinetically stable *N*-heterocyclic carbene **5.4** was isolated and characterised by Arduengo in 1991 (Figure 5.2).[165] The deprotonation of the azolium chloride with strong base NaH produced stable carbene **5.4** with 96% yield.

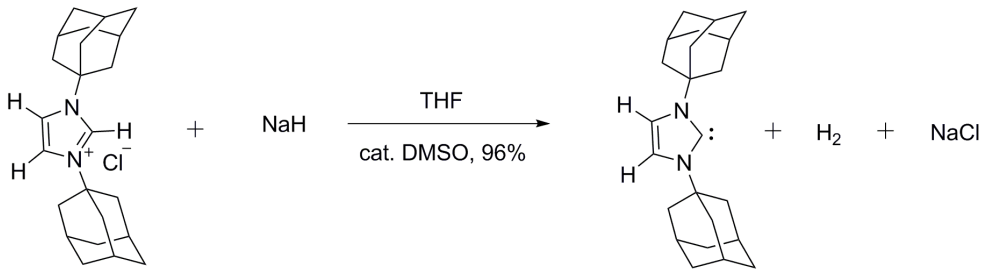

5.3 **5.4**

Figure 5.2 Preparation of N-heterocyclic carbene **5.4**.[165]

Only a limited number of NHCs are commercially available at a fairly high cost. However, a relatively cheap compound 1,4-diphenyl-3-phenylimino-1,2-dihydro-1,2,4-triazolium hydroxide (Nitron) exhibits reactivity compatible with the NHC-type tautomer **5.5'** rather than the conventional structure **5.5** (Figure 5.3).[166]

5.5 **5.5'**

Figure 5.3 Lewis structures of Nitron tautomers **5.5** and **5.5'**.[166]

For instance, the reaction between Nitron and sulfur gave compound **5.6** which is a typical reaction of nucleophilic carbenens. And the metal complex **5.7** prepared from Nitron also demonstrates the electron donor properties of the carbene type tautomer (Figure 5.4).

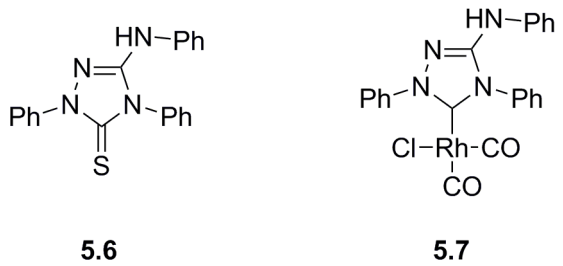

5.6 **5.7**

Figure 5.4 Structures of compound **5.5** and **5.6**.[166]

The O'Donoghue group at Durham University conducted a comprehensive study of

proton-deuterium exchange reaction in a series of triazolium ions including compound **5.5'** (Figure 5.4).[167] In their deuterium exchange studies (Figure 5.5), the colour of solutions of Nitron in deuterated acetonitrile changed from orange to brown over a 24 hour period. Red residue was obtained when the solvent was removed. Black crystals precipitated out when ethanol was added to the red residue.

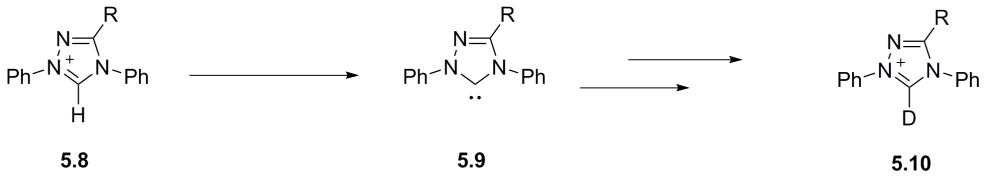

Figure 5.5 Proton-deuterium exchange reaction of triazolium ions.

Surprisingly, ^{1}H NMR spectra of the black crystals showed only broad peaks and low signal/noise ratio in several solvents, which suggested that this material is paramagnetic. EPR and X-Ray crystallographic analysis of the black crystal made it possible to assign the structure of this material to 1,2,4-benzotriazinyl radical **5.11** which is similar to the Blatter radical **4.1** prepared in 1968 (Figure 5.6, 5.7 and 5.8).[64] Radical **5.11** is stable in air for several months at room temperature. This reaction therefore provides a new one step reaction to prepare a Blatter-type radical from Nitron. Moreover, compound **5.11** is the first Blatter-type radical with an amido substituent.

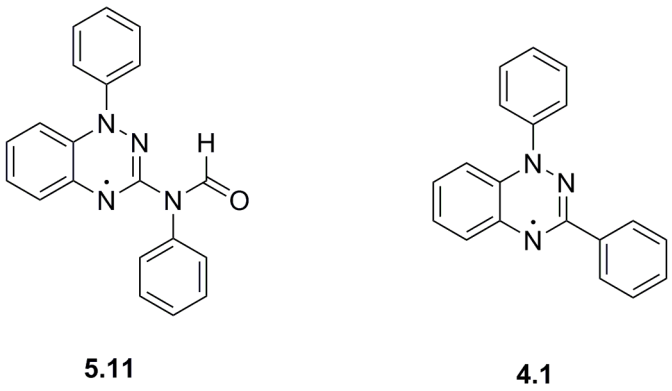

Figure 5.6 The structure of radicals **5.11** and **4.1**.

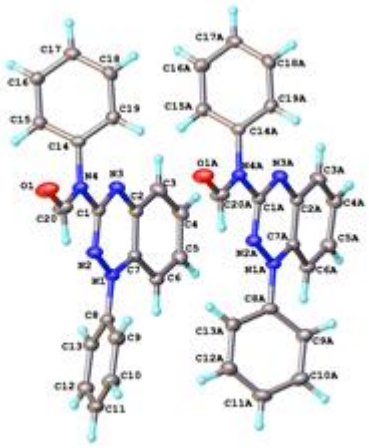

Figure 5.7 X-Ray crystallographic structure of radical **5.11**.

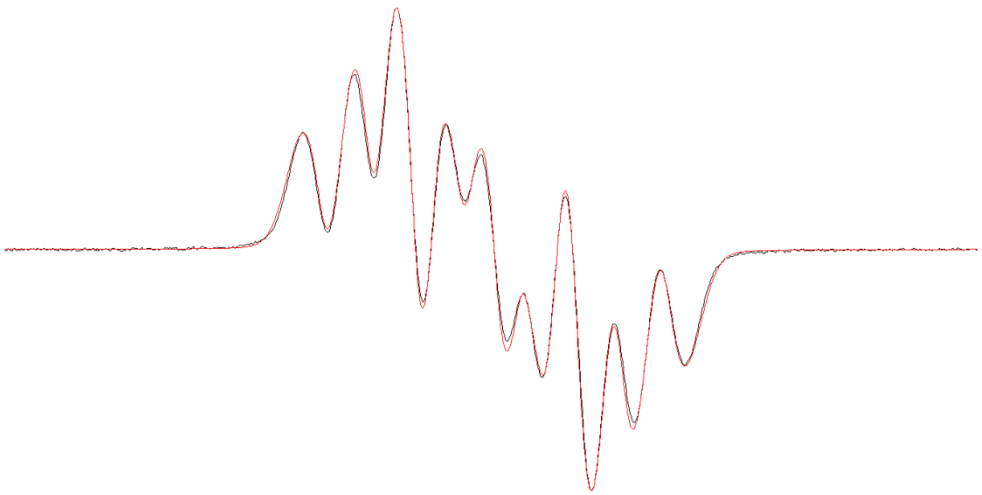

Figure 5.8 EPR spectra of radical **5.11**. The black line is experimental result; the red line is a simulation with a_{N1}= 8.19 G, a_{N2}= 4.75 G, a_{N3}= 4.78 G.

The first publication on Nitron preparation appeared back in 1905.[168] However, the reported yield was very low. Fortunately, a new publication which came out in 2006, optimised the reaction conditions to give ca. 80% yield for each step (Figure 5.9).[169] Thiourea is desulfurized with Pb_3O_4. The crude product was used directly in next step to react with phenylhydrazine. Then aminoguanidine was reacted with formaldehyde to obtain 1,2,4-triazole **5.15**, followed by oxidation with sodium nitrite. The low yield in the original preparation was attributed to the tautomerisation of intermediate aminoguanidine **5.14** to give **5.17**, although no

characterisation of **5.17** was reported (Figure 5.10).

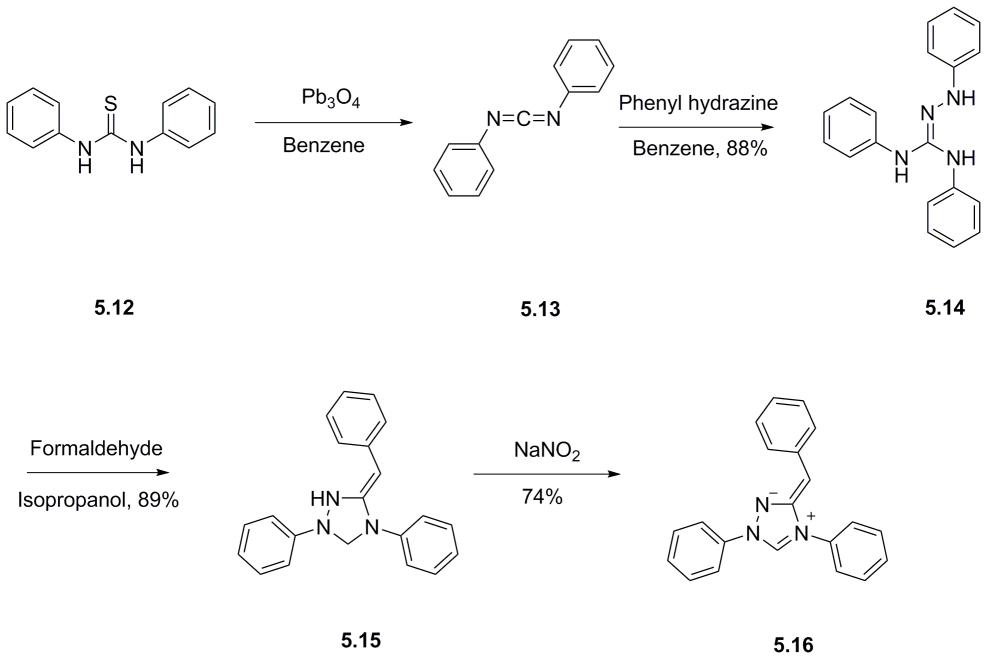

Figure 5.9 Preparation of Nitron from diphenyl thiourea.[169]

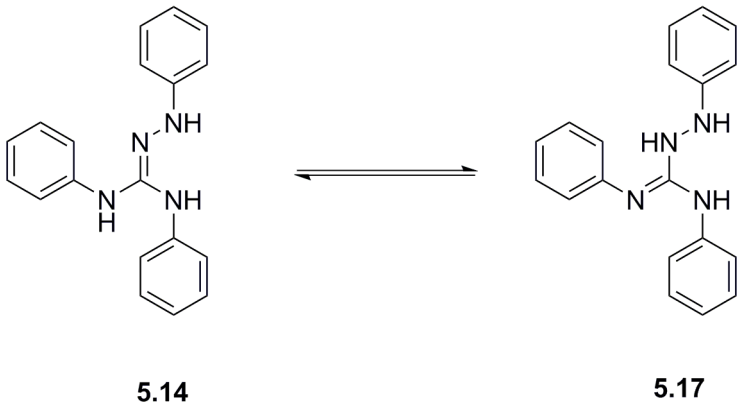

Figure 5.10 The tautomer **5.17** of aminoguanidine compound **5.14**.[169]

Because of our experience in the preparation of Blatter-type radicals and magnetic properties study in our group, it was decided to explore this new radical formation in collaboration with the O'Donoghue group. The new procedure for preparing Nitron made it possible to prepare a series of Nitron derivatives with reasonable yield.

5.2 Preparation of Nitron Derivatives.

To test the scope of the new method of Nitron preparation, it was decided to investigate formation of Nitron derivatives with different substituents on the aromatic rings and the methylene group. The functionalization of the Nitron involves thiourea, aldehyde and hydrazine components of this reaction.

5.2.1 Functionalization of the Aldehyde Component

A range of aromatic and aliphatic aldehydes were reacted with aminoguanidine **5.14** to prepare Nitron derivatives (Figure 5.11). Surprisingly, no product was obtained from aromatic aldehydes, such as benzaldehyde. At the same time, the reaction with aliphatic aldehydes **5.23** and **5.24** worked well.

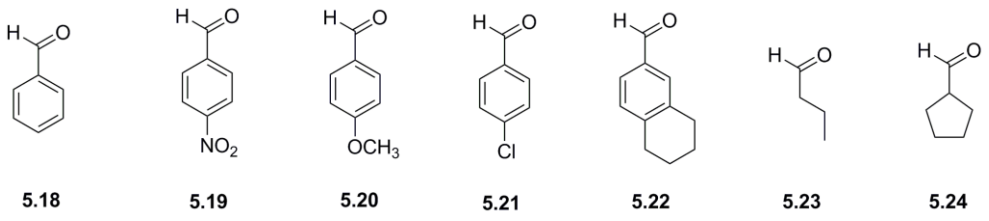

5.18 **5.19** **5.20** **5.21** **5.22** **5.23** **5.24**

Figure 5.11 Aldehydes utilized to prepare Nitron derivatives.

The first step in the preparation of Nitron involves addition of aminoguanidine **5.14** and aldehyde in isopropanol and stirring the mixture at 58 °C. The colour of the mixture is reported to change from red to light yellow, and light yellow solid precipitates out after 0.5 h. For aldehydes **5.23** and **5.24**, the colour of the mixture changed to yellow. However, no precipitate was found in the reaction system with aldehyde **5.24**. Fortunately, the product **5.26** can be purified by column chromatography. Only small amount of byproducts could not be removed from the product **5.26** (Figure 5.12).

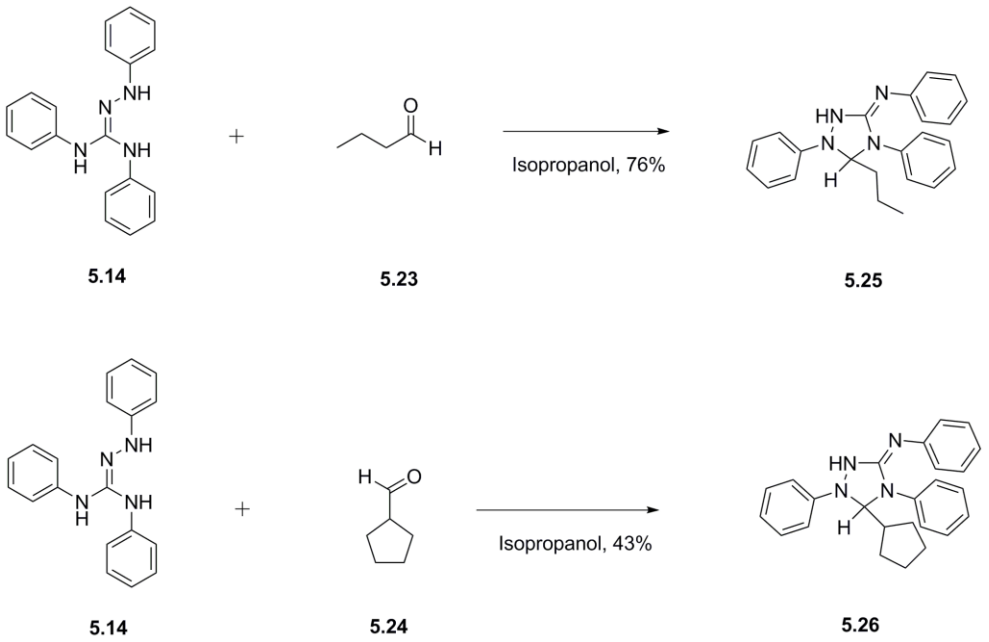

5.14 5.23 5.25

5.14 5.24 5.26

Figure 5.12 Preparation of compounds **5.25** and **5.26**.

The CH group of products **5.25** and **5.26** gives a diagnostic ^{1}H NMR peak at δ = 5.32 and 5.27 ppm, respectively (Figure 5.13 and 5.14).

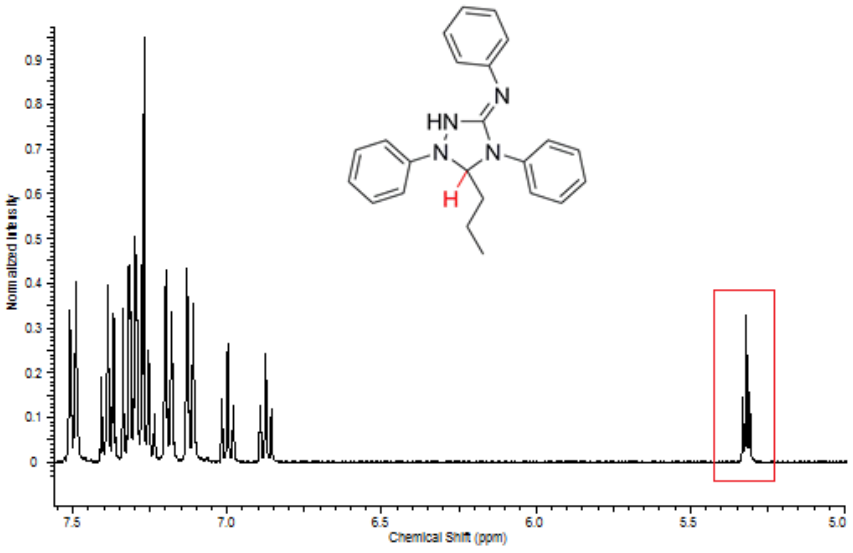

Figure 5.13 A fragment of ^{1}H NMR spectrum of compound **5.25**; the triplet at 5.32 ppm is the diagnostic peak of CH group.

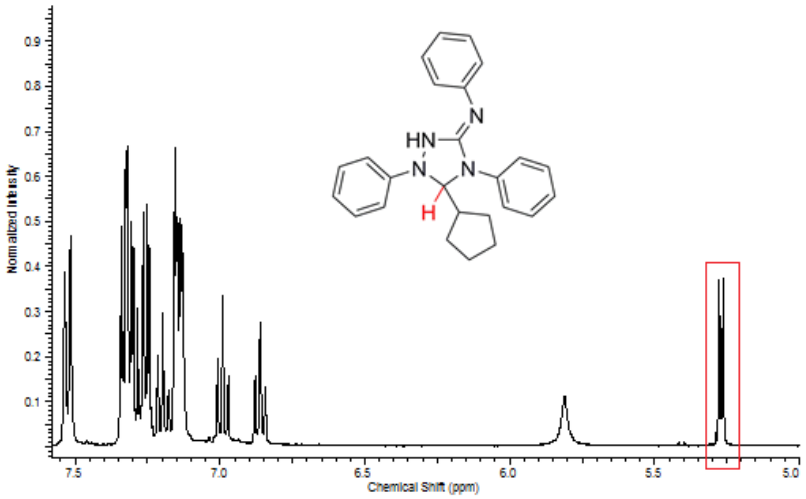

Figure 5.14 A fragment of ^{1}H NMR spectrum of compound **5.26**, doublet at 5.27 ppm is the peak of the CH group.

However, for all aromatic aldehydes, the colour of the reaction mixture did not change. ^{1}H NMR spectra of crude reaction mixtures did not show the diagnostic peak around 5-6 ppm. MS analysis of crude reaction mixtures did not show the peak for the expected product. No pure compounds could be isolated from a complex mixture containing a large number of different products. It seems likely that the conjugation of the aromatic ring with the carbonyl group prevents the reaction of aromatic aldehydes with aminoguanidine **5.14**.

A catalytic amount of acid was added to reaction mixture in an attempt to increase the reactivity of the carbonyl group, following literature examples of a reaction between aldehydes and substituted phenyl hydrazine.[170-172] Unfortunately, no products were isolated from these reactions and the ^{1}H NMR spectra of crude products did not show the diagnostic peak of the CH group. The MS spectra also showed no peak of the expected product in the crude mixture. In an attempt to deprotonate the aminoguanidine and thus increase its nucleophilicity, several different bases, such as sodium hydroxide, triethyl amine or n-butyl lithium were also added to this reaction mixture. However, no product was obtained as confirmed by ^{1}H NMR and MS spectra of the crude reaction mixtures.

Two further aldehydes **5.27** and **5.28** were reacted with aminoguanidine **5.14** (Figure 5.15). However the target product was not obtained. This can possibly be explained by the steric effect of the large substituents bonded to the carbonyl group. Because of the time constraints, no more work on this problem was carried out.

5.27 **5.28**

Figure 5.15 Aldehydes used to react with aminoguanidine **5.14**.

In summary, only two new Nitron derivatives **5.29** and **5.30** were prepared with different aldehydes (Figure 5.16).

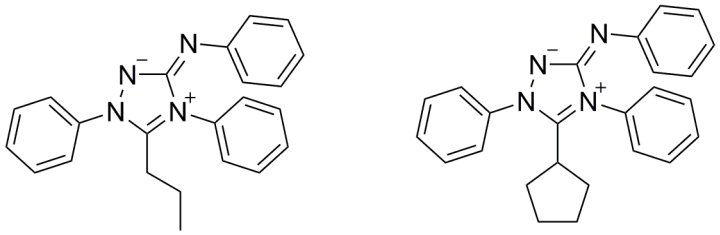

5.29 **5.30**

Figure 5.16 The structure of two new Nitron derivatives.

5.2.2 Functionalization of the Hydrazine Component

A range of hydrazines was used to react with carbodiimide **5.13** to prepare different aminoguanidines (Figure 5.17). However, the expected product was not formed.

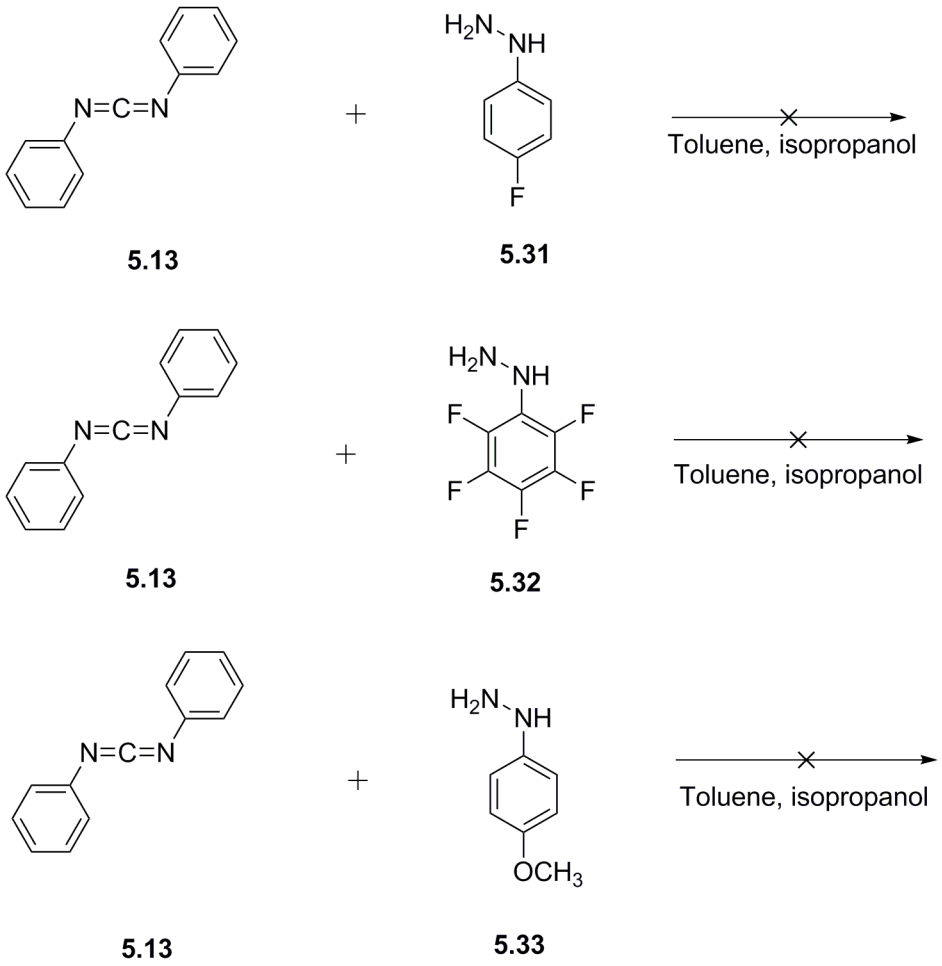

Figure 5.17 Hydrazines used in a reaction with carbondiimide **5.13**.

Surprisingly, Busch reported in 1906 the reaction between *p*-bromophenylhydrazine and diphenyl carbodiimide.[173] The difference between the reported reaction conditions and our procedure is the temperature and solvent. In an attempt to facilitate the reaction between the hydrazines and carbodiimide, we reproduced Bush's conditions, with one exception: benzene, used in the original study, was replaced in our work with toluene on safety grounds. However, the expected product was not formed in a reaction procedure with compounds **5.31** and **5.33**. Presumably, the reactivity of phenylhydrazines is strongly influenced by the substituent in the aromatic ring.

Aminoguanidine derivatives have attracted much attention, since some of them can be used as inhibitors of dopamine β-oxidase and antihypertensives.[174] In principle, the addition of amine, aniline or hydrazine to carbodiimide should be straightforward. However, except for some

primary amines and unsubstituted aniline, most other less reactive amines, anilines, and hydrazines hardly react with carbodiimdes.[175]

Hartke and Radau's work showed that tetrafluoroboric acid is a catalyst for the reaction between carbodiimides and amines or hydrazines (Figure 5.18). However, the hydrazine adducts obtained with this catalyst tautomerised to form compounds such as compound **5.17** (Figure 5.10) rather than the aminoguanidine required in our work.[176]

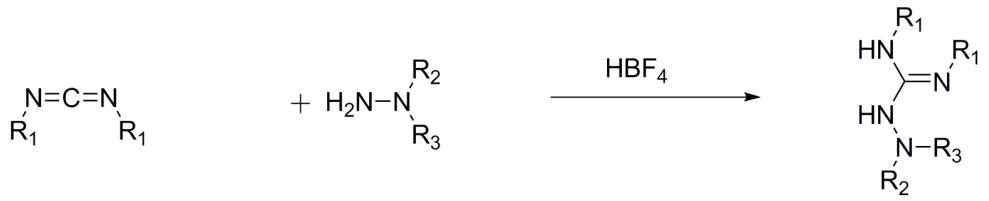

5.34 **5.35** **5.36**

Figure 5.18 Preparation of an aminoguanidine tautomer catalysed by HBF_4.[176]

Recently, several metal complex catalysts were used to facilitate the addition of amines to carbodiimides, such as titanium, lithium and aluminum complexes (Figure 5.19).[175,177-185]

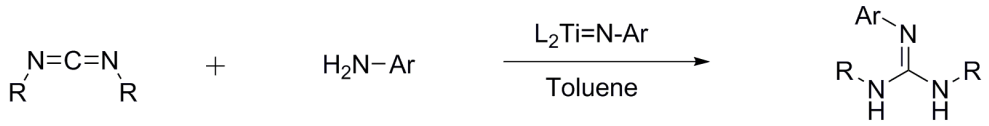

5.37 **5.38** **5.39**

Figure 5.19 Reaction of carbodiimides and anilines catalysed by a titanium complex.[175]

Only a few papers focussed on the reaction between phenylhydrazines and carbodiimides.[173,176,186] A new procedure was presented by Schweizer and his co-workers in 2013 (Figure 5.20).[186] Titanium complex (Figure 5.21) was used to catalyse the hydrazination of the carbodiimide. The special titanium catalyst cannot be prepared easily, so this procedure is not good for our case.

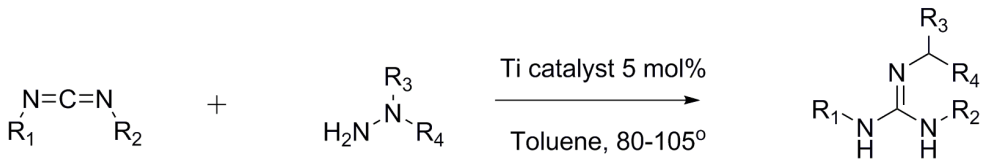

5.40 **5.41** **5.42**

Figure 5.20 New procedure to prepare aminoguanidine.[186]

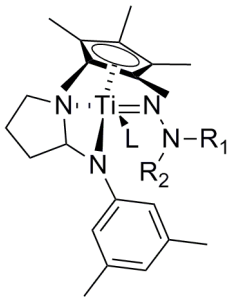

Figure 5.21 The structure of titanium catalyst.[186]

Unfortunately, no new Nitron derivatives with functionalised phenylhydrazines were prepared. Because of the time constraints, no more work has been carried out in this field.

5.2.3 Functionalization of the Thiourea Component

Different carbodiimides can be prepared from various thioureas. Two commercially available thioureas have been used to prepare carbodiimides. Then two new Nitron derivatives were prepared successfully by following the similar procedure described in section 5.1 (Figure 5.10). Figure 5.22 shows the preparation of these two new Nitron derivatives **5.47a** and **5.47b**.

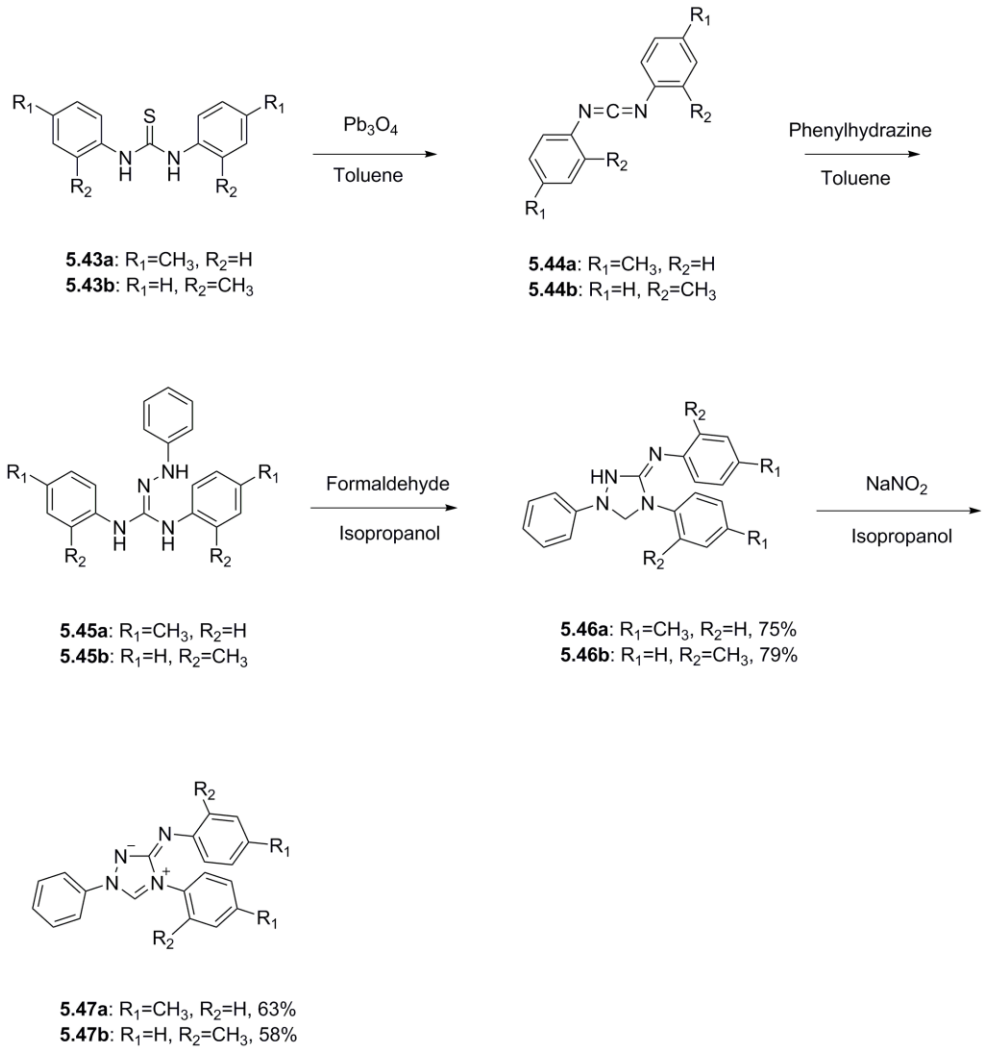

5.43a: R_1=CH_3, R_2=H
5.43b: R_1=H, R_2=CH_3

5.44a: R_1=CH_3, R_2=H
5.44b: R_1=H, R_2=CH_3

5.45a: R_1=CH_3, R_2=H
5.45b: R_1=H, R_2=CH_3

5.46a: R_1=CH_3, R_2=H, 75%
5.46b: R_1=H, R_2=CH_3, 79%

5.47a: R_1=CH_3, R_2=H, 63%
5.47b: R_1=H, R_2=CH_3, 58%

Figure 5.22 Preparation of two new Nitron derivatives.

Compounds **5.47a** and **5.47b** are not as stable as compound **5.29** and **5.30**. Good quality ^{1}H NMR spectrum of **5.47a** can only be obtained immediately after the compound was collected. The ^{1}H NMR spectrum of compound **5.47b** showed broad peaks indicative of the presence of paramagnetic compounds (Figure 5.23). EPR spectrum of compound **5.47b** in toluene showed that the paramagnetic species is the Blatter-type radical (Figure 5.24).

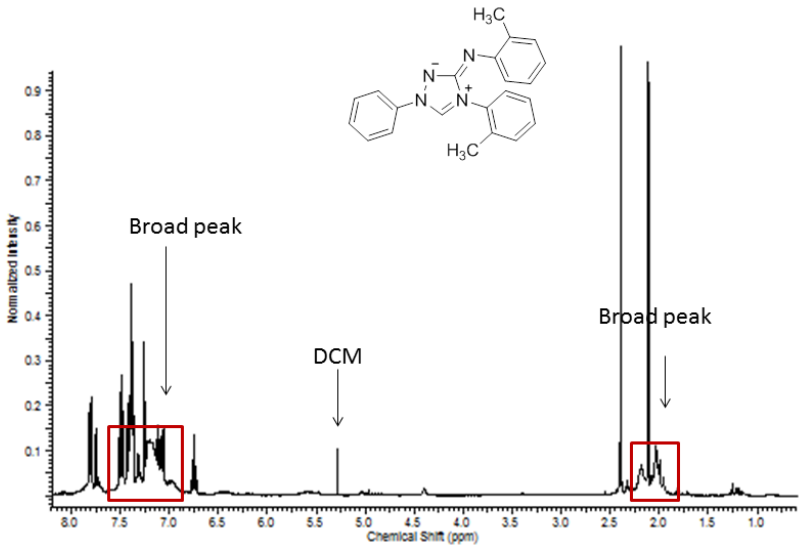

Figure 5.23 ^{1}H NMR spectrum of compound **5.47b**.

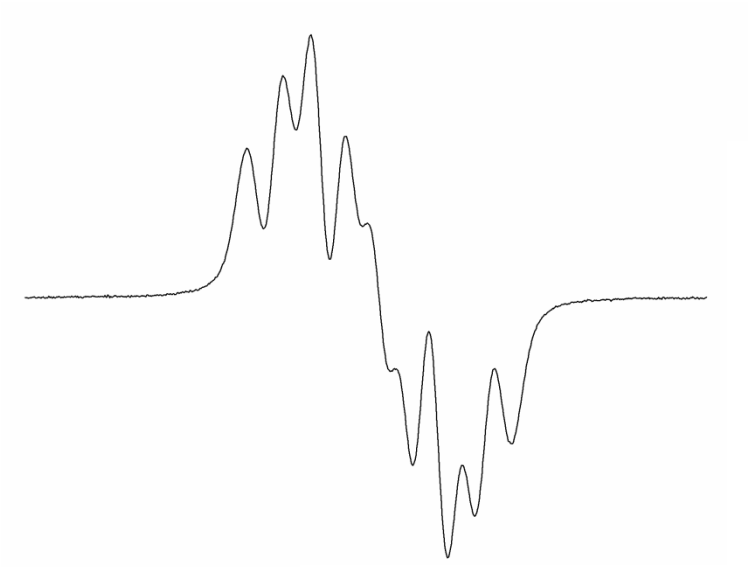

Figure 5.24 EPR spectrum of compound **5.47b** in toluene.

Nitron **5.47a** also slowly reacts with air to form a radical product. The colour of the Nitron changed from yellow to red after 3 days of storage in air and an EPR spectrum revealed formation of a radical.

In summary, two new Nitron derivatives **5.47a** and **5.47b** were prepared from substituted

thioureas. The stability of these two Nitron derivatives is not very good. Both of them can react with air slowly to form a radical product.

5.3 Mechanistic Investigation

Conversion of the Nitron to a Blatter-type radical is an unexpected reaction presumably involving ring-opening followed by cyclisation. The mechanism of this transformation is not clear. The work in O'Donoghue group observed that the addition of aqueous KOH (0.5 M) solution to a solution of Nitron (30 mM) in acetonitrile resulted in the precipitation of red crystals. X-ray crystallographic analysis showed the formation of compound **5.51** likely the result of attack of hydroxide ion to the carbonyl group of compound **5.48** (Figure 5.25 and 5.26). The formation of Blatter-type radical **5.11** may thus involve the same intermediate compound **5.49** followed by oxidation reactions (Figure 5.25).

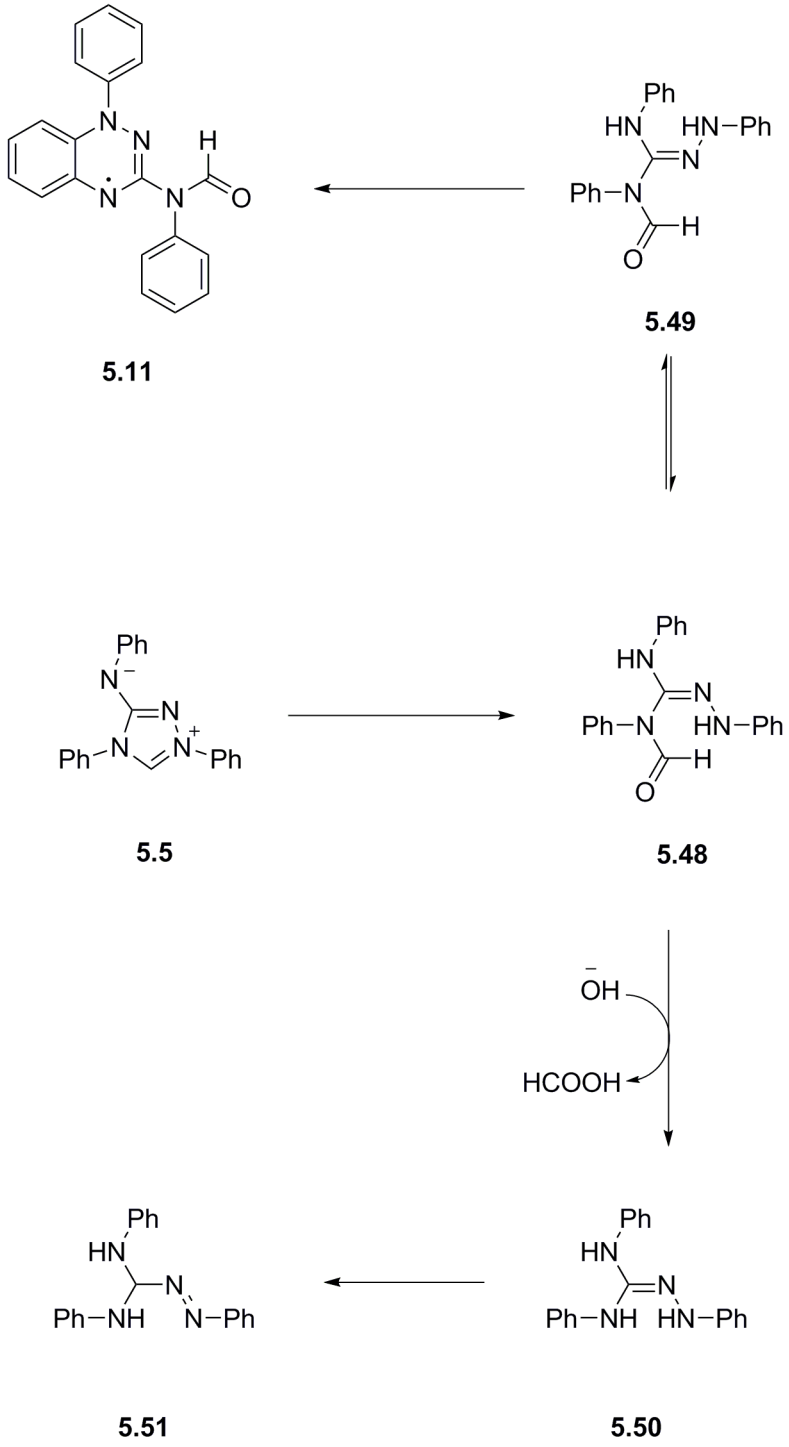

Figure 5.25 Possible mechanism for the formation of compound **5.5** and **5.51**.

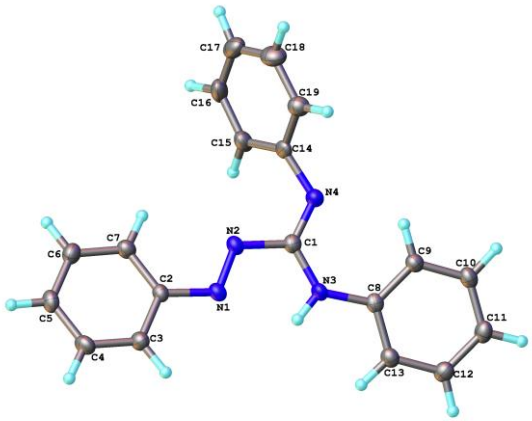

Figure 5.26 X-Ray crystallographic structure of compound **5.37**.

The formation of compound **5.48** may be the result of the hydrolysis of Nitron **5.5**. Because Nitron **5.29** shows better stability than that of Nitron **5.5**, it is a better choice for mechanism investigation.

When substituted Nitron **5.29** was dissolved in dry CH_3CN and stirred under oxygen atmosphere, no EPR signal can be detected after 3 days. However, when Nitron **5.29** was stirred in 2% aqueous CH_3CN for 3 days under oxygen, a weak EPR signal was detected (Figure 5.27). These results suggest that small amount of water facilitates the formation of the Blatter-type radical.

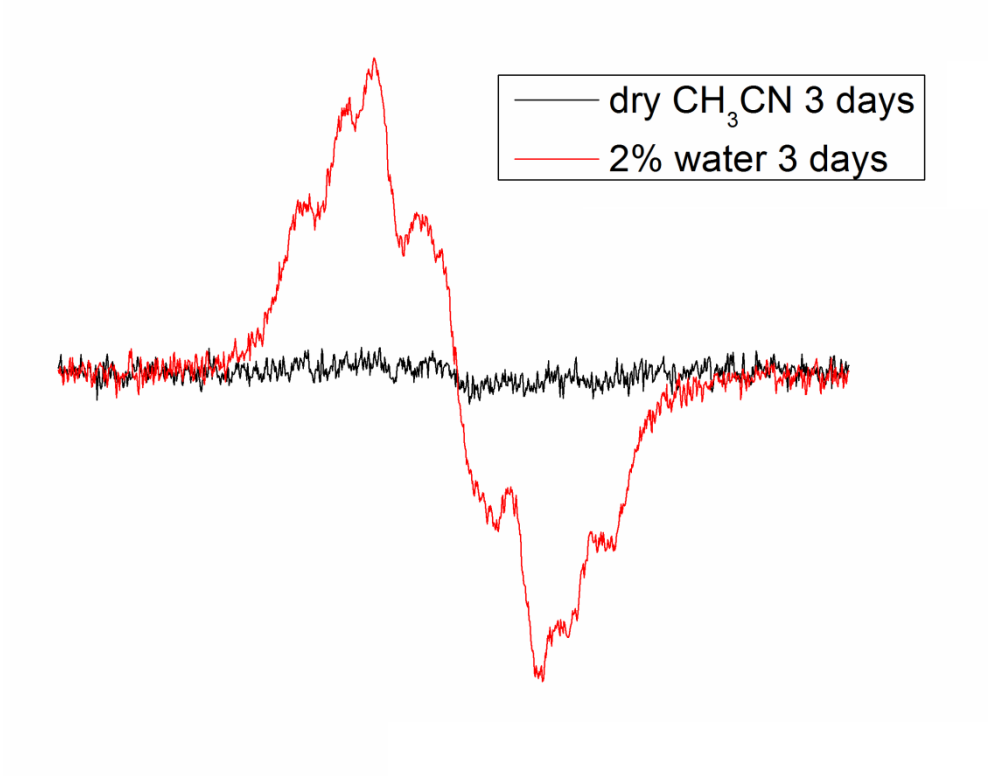

Figure 5.27 EPR spectra of Nitron in dry CH_3CN and CH_3CN with 2% water.

The conversion of Nitron to Blatter's radical may be photoactivated. In order to test this hypothesis, the solution of Nitron **5.29** in dry CH_3CN under oxygen atmosphere was exposed to UV irradiation (100 W Hg lamp) for 4 h, no signal was obtained by EPR. This suggests that in the absence of water, radical formation was not facilitated by UV irradiation. Presumably, Blatter's radical is formed via hydrolysis of Nitron.

The formation of compound **5.51** during Nitron conversion to Blatter's radical **5.11** indicates the competition of the hydrolysis and oxidation in the second step of the reaction. The addition of oxidising reagents may facilitate the oxidation reaction to form the radical product. To test this hypothesis, different oxidizing reagents, silver(I) oxide and lead dioxide were added to the reaction mixture. The reaction process was monitored by EPR. Radical formation was detected in both of these two mixtures when they were stirred overnight. However, no radical was detected by EPR when no oxidising reagent was added to the mixture. It suggests that radical formation was accelerated by oxidising reagents.

Moreover, after 3 days, the reaction mixture contained silver(I) oxide showed much stronger EPR signal than that of the reaction mixture contained lead dioxide (Figure 5.28). It suggests that radical is more stable in the presence of silver(I) oxide than that of in the presence of lead dioxide.

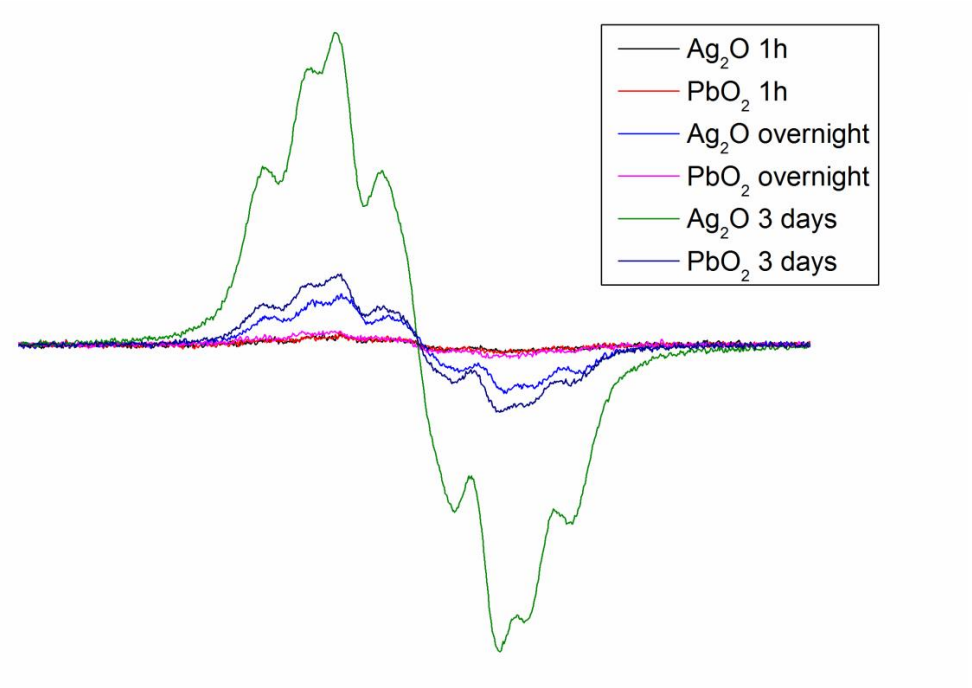

Figure 5.28 EPR spectra of Nitron **5.29** in the presence of different oxidizing reagents.

Based on these results, we believe that the formation of intermediate compound **5.48** is the result of the hydrolysis of Nitron compound. A competition of hydrolysis and oxidation is involved in the second step (Figure 5.25).

5.4 From Nitron to Blatter-type radical

The work of the O'Donoghue group showed that Nitron **5.5** forms radical **5.11** when stirred at room temperature in HPLC grade acetonitrile for 24 h. However, subjecting Nitron derivatives **5.29** and **5.30** to the same reaction conditions over 48 h did not lead to formation of radicals as detected by EPR spectroscopy. Only a very weak and noisy EPR signal was obtained after 60 h. The stability of these two Nitron compounds is thus much higher than that of compound **5.5**.

New reaction condition had to be developed.

Increasing the reaction temperature to 70 °C overnight led to the conversion of the nitron to the radical. The attempts to purify the radical, however, failed, because the byproducts could not be separated by column chromatography or recrystallization. The yield of this reaction was poor.

Other solvents such as methanol and DMSO were tried in an attempt to improve the rate, yield, and selectivity of radical formation from these two Nitron compounds. Unfortunately, no positive results were obtained: the yield of the radicals did not increase and purification of the radicals by column chromatography failed. Moreover, DMSO was difficult to remove under mild conditions.

The formation of radical was accelerated in the presence of oxidising reagents. However, at room temperature, the conversion of Nitron **5.29** to the radical in the presence of Ag_2O or PbO_2 is still very slow and the yield is very low (<10%) even after the mixture was stirred for 3 days (Figure 5.29).

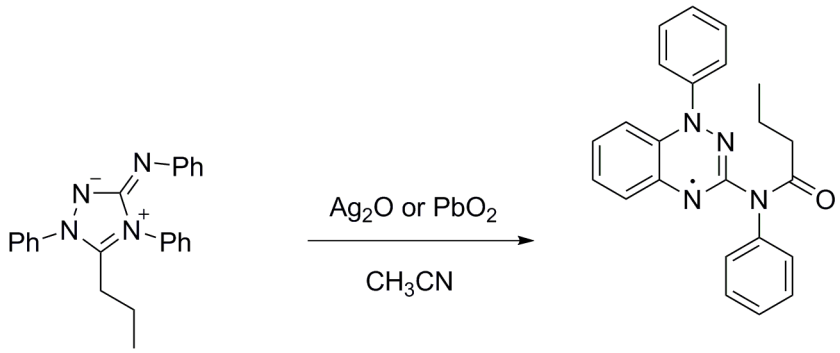

5.29 **5.52**

Figure 5.29 Preparation of radical **5.52** from Nitron **5.29** with oxidizing reagent.

Much stronger EPR signal was obtained after the mixture was stirred at 50 °C (Figure 5.30) overnight. The conversion of Nitron to the radical was about 5 times higher than that at room temperature over 3 days.

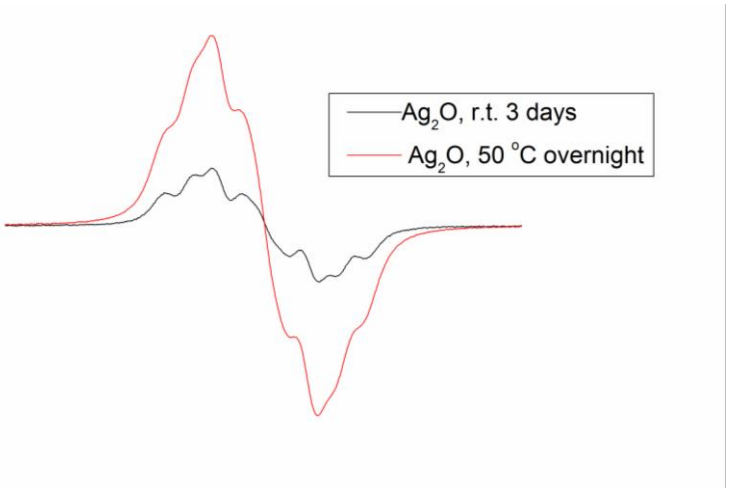

Figure 5.30 EPR spectra of Nitorn **5.29** reaction mixture at different temperatures.

However, the reaction mixture cannot be separated by column chromatography, and byproducts cannot be removed from radical **5.52**. Recrystallization did not remove all impurities, either (Figure 5.31).

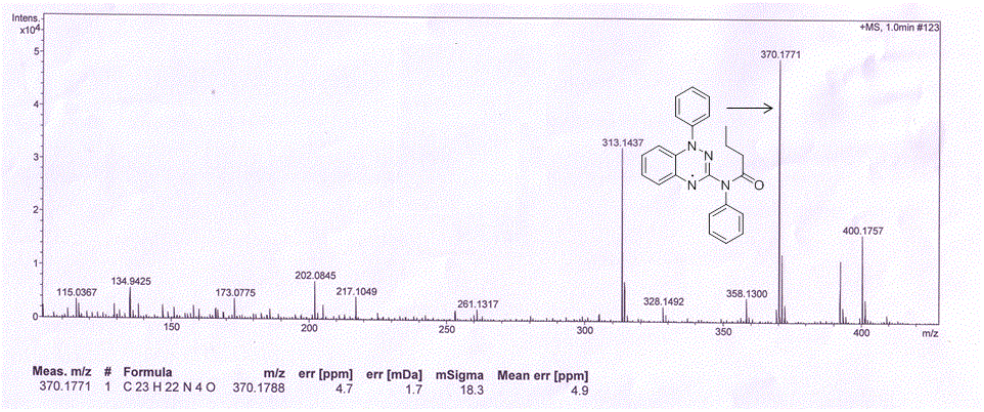

Figure 5.31 MS of sample of radical **5.52** after purification by column chromatography.

Because we believe hydrolysis is the first step of this Blatter-type radical formation, the addition of base should facilitate the reaction. Different amounts (1%, 2%, 5%, 10%, 20%, 50% v/v) of aqueous potassium hydroxide (0.5 M) in CH_3CN were used as a solvent for this reaction. Addition of a 5% KOH solution in CH_3CN was found to give the best conversion to radical and least amount of impurities. The radical could be purified by column chromatography to give a pure product according to TLC. MS analysis of the product also showed only small peaks of

byproducts (Figure 5.32).

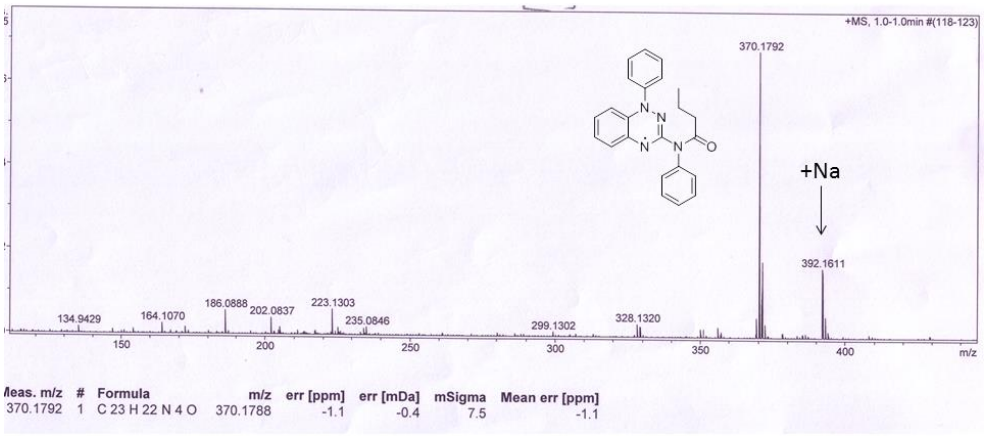

Figure 5.32 MS of sample collected from the system with KOH.

Buffer solutions were also used instead of the KOH solution. Reactions in pH = 9.2 and 12 phosphate buffer solutions were monitored by EPR. These reactions were very slow and conversion of Nitron to radical was very low (<10% after 24 h).

In summary, optimum reaction conditions were found to be stirring Nitrons in CH_3CN with aqueous 5% KOH (0.5 M) solution in presence of Ag_2O at room temperature overnight. For Nitrons **5.30**, **5.47a** and **5.47b**, corresponding radical products could be obtained with these conditions (Figure 5.33).

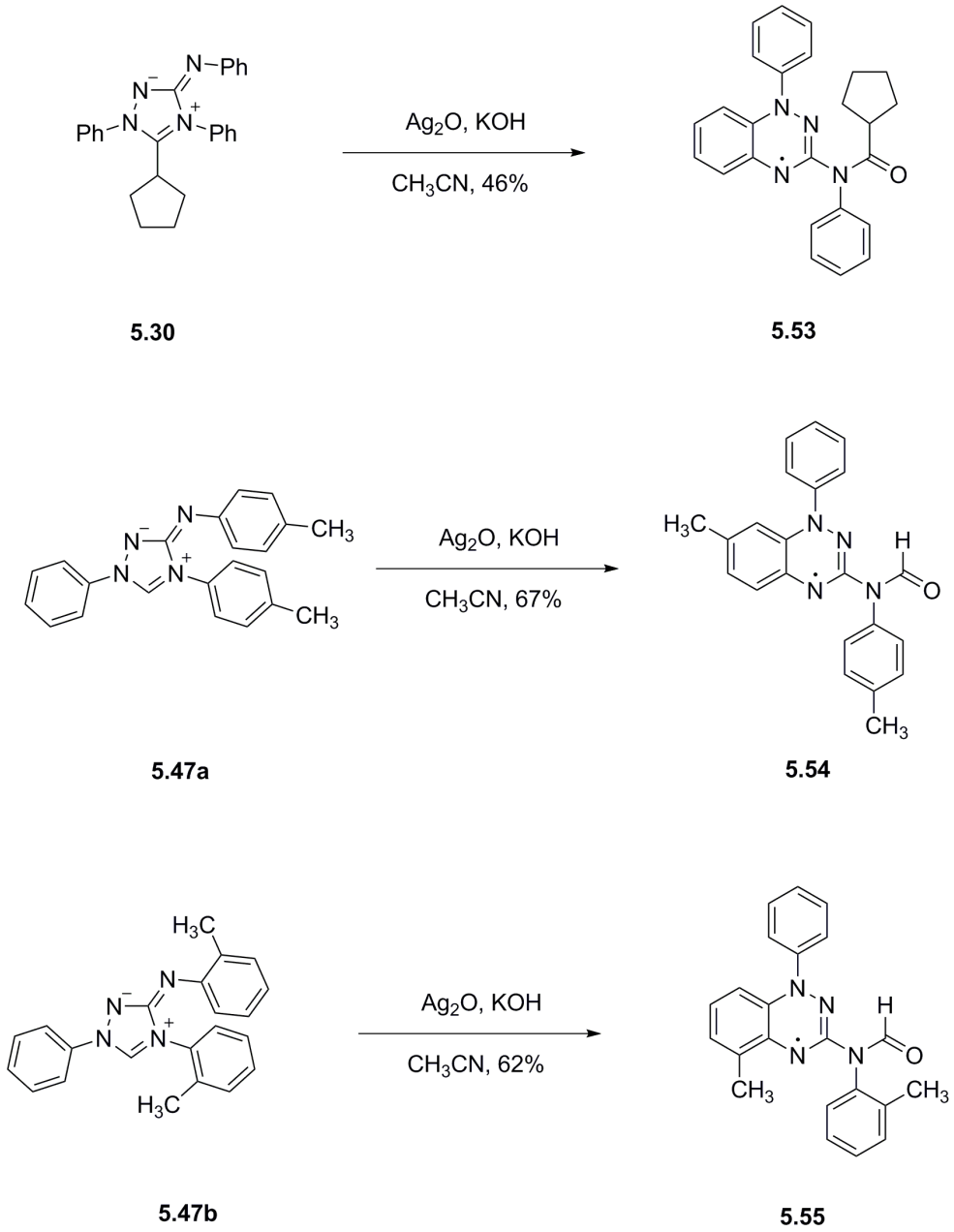

Figure 5.33 Preparations of Blatter-type radical **5.53**, **5.54** and **5.55**.

5.5 Conclusions

The synthetic scope of the new procedure for Nitron preparation was determined. A range of new Nitron derivatives was obtained by this procedure with good yield. Unfortunately, it is not compatible with substituents on some aromatic rings. Preparation of aminoguanidines with substituted phenylhydrazines is not straightforward. The conjugation of the aromatic ring with

the carbonyl group prevents the reaction between aminoguanidine and aromatic aldehydes.

Preparation of Blatter-type radical from Nitron was achieved with different Nitron derivatives. The reaction is accelerated by the addition of base, increasing the temperature and oxidising reagents. However, for less stable Nitron derivatives, the addition of oxidising reagents leads to side reactions. The conversion yield could be increased by increasing the temperature to 50 °C. However, more byproducts were obtained and radical products could not be isolated from byproducts. Addition of suitable amount (5%) of KOH can improve the yield. Moreover, pure radicals can be isolated from the reaction mixture in a relatively good yield.

The mechanistic investigation of this reaction confirmed that the conversion of Nitron into Blatter-type radical proceeds via hydrolysis followed by oxidation.

Chapter 6 Conclusions and Future Work

A set of new stable radicals were prepared successfully and characterized by Mass Spectrometry, EPR spectroscopy and elemental analysis. It was found that the preparation of these mesomorphic organic radicals was difficult due to complex molecular design and working with reactive radicals.

Radical **2.19** was prepared using click chemistry. However, the yield of this radical obtained through click reaction is poor, possibly due to the steric hindrance of the TEMPO-azide. EPR studies of radical **2.19** in different LC hosts suggested that it is not a suitable spin probe for these rod-like hosts. Two components of EPR spectra were observed in the solution of radical **2.19** in liquid crystal matrices possibly due to the existence of two orientations of this radical in liquid crystals. As radical **2.19** is bent-shaped, possibly it is a suitable spin probe for bent-core liquid crystals. This can be confirmed by EPR study of radical **2.19** in bent-core liquid crystal host.

Nitronyl and imino nitroxide containing compounds **3.22**, **3.23**, **3.25** and **3.27** did not exhibit any liquid crystalline properties. The large dihedral angle between benzene and imidazoline rings and between the two benzene rings is detrimental to mesomorphic behaviour of these radicals. It was also found that the preparation of *p*-hydroxyphenyl nitronyl nitroxide is not straightforward, due to the poor reproducibility and yield.

Two new discotic mesogens **4.67** and **4.94** were prepared successfully. A columnar phase was observed with mesogens **4.67** and **4.94**. The dendritic texture with branches derived from the main axis at 90° was observed by **4.67**, this suggested that it forms a columnar rectangular phase. However, the symmetry of the mesophase formed by **4.94** was not confirmed. As different columnar phases show different X-ray diffraction patterns, the mesophase formed by **4.94** can be confirmed by X-ray diffraction. It would be good to confirm the mesophase of **4.67**

by x-ray diffraction as well. During the preparation of mesogens **4.67** and **4.94**, it was found that electron-rich phenylhydrazine derivatives were difficult to prepare due to the poor stability of these compounds. As phenylhydrazine derivatives are important intermediates in the synthesis of heterocycles,[135,187] it would be useful to optimise the reaction conditions for the preparation of these electron-rich phenylhydrazine derivatives. The deprotection pathway seems to be a promising method. The optimization of reaction conditions may involve changing acid, solvent and temperature.

It was also found that benzohydrazonamide intermediates are not stable. Oxidation of these compounds occurred both in the presence of air and under inert atmosphere. Mesogens **4.67** and **4.94** are formed through a unusual self-oxidising route. It would be interesting to establish the mechanism of this reaction. This could possibly be achieved by isolating and characterising byproducts of the reaction.

EPR investigation suggested that the molecular alignment of mesogens **4.67** and **4.94** is poor in the applied magnetic field. No magneto-LC effect was observed with these mesogens. It would be good to study the magnetic susceptibility of these mesogens by SQUID magnetometry to confirm the results obtained by EPR study. Spin-triplet and spin-singlet dimerization of these mesogens were observed under different conditions.

It was also found that the introducing of the seventh chain in mesogen **4.67** decreased the melting point and isotropisation temperature, possibly due to this additional chain precluding effective packing of the disks. Unfortunately, these two mesogens did not show photoconductive properties.

Blatter-type radicals with amido substituent could be prepared from Nitron derivatives. However, it is difficult to introduce substituents on some aromatic rings. The mechanism investigation suggested that conversion of Nitron into Blatter-type radical proceeds via hydrolysis followed by oxidation.

Charpter 7 Experimental

7.1 General Procedures

All chemicals were purchased from Sigma-Aldrich, Fluka, Acros or other companies. These commercially available chemicals were utilized directly unless stated otherwise. 4-[2-(4-decyloxyphenyl)-1-ethenyl]pyridine, 4-[2-(3,4-didecyloxyphenyl) -1-ethenyl]pyridine, 4-[2-(3,4,5-tridodeloxyphenyl)-1-ethenyl]pyridine and 2,3,6,7,10,11-hexa-*n*-tridecyloxy triphenylene were kindly provided by the liquid crystal group, the University of York.

TLC

TLC silica gel 60 F_{254} aluminium sheets are bought from Merck Millipore.

Silica gel for column chromatography

Silica gel with pore size 60 Å 220-440 mesh particle size was bought from Fluka Analytical.

NMR spectra were recorded at 25 °C on JEOL 400 or ECS 400. Chemical shifts are reported in parts per million, and are described as position (δ), multiplicity (s=singlet, d=doublet, t=triplet, q=quartet, m=multiplet, br=broad), coupling constant (J in Hz).

EPR spectra were recorded at different temperature on Bruker EMX_{micro} and ESP300E X-band CW-EPR spectrometers.

UV-Vis spectra were recorded on U-3000 Spectrophotometer from HITACHI.

Infrared spectra were recorded on IRPrestige 21 from SHIMADZU.

Mass spectra were recorded on Bruker micro-TOF machine. All mass spectra were recorded by using ESI, with the exception of specific examples.

DSC data were collected on DSC822E from METTLER TOLEDO.

Microscope images were collected on Axioskop 40 from Carl Zeiss Ltd.

Elemental analyses were carried out on CE-440 Exeter Analytical Inc. C, H, N, S machine at the University of York.

High-performance liquid chromatography was performed on a Shimadzu Prominence modular HPLC system comprising a LC-20A liquid chromatograph, a DGU-20A5 and DGU-20B degasser, a SIL-20A autosampler, a CBM-20A communication bus, a CTO-20A column oven, and a SPO-20A dual wavelength UV-vis detector operating in this instance at 270⁄370 nm. The column used was an Alltech C18 bonded reverse-phase silica column with a 5 µm pore size, an internal diameter of 10 mm and a length of 250 mm.

7.2 Sample Preparing for EPR.

Most samples were recorded as solutions. For the radicals mentioned in this thesis, a concentration of 10^{-6} M is detectable. In order to get good spectra, 10^{-4} M to 10^{-3} M solutions were utilized to characterise radicals in our work. Samples for EPR measurements were typically loaded into a Pasteur pipette flame sealed at the bottom. When polar solvents were used, samples were loaded in small capillaries with diameter 1.3mm flame sealed at the bottom.

Some samples had to be degassed before EPR spectra were recorded to eliminate the broadening effect of oxygen. For these samples, the solutions in a Pasteur pipette with a rubber stopper on the top were frozen with liquid nitrogen. Then the Pasteur pipette was attached to a Schlenk line to remove the dissolved oxygen under vacuum. After 10 min, the Pasteur pipette was filled with nitrogen. This procedure was repeated 3 times to remove all the oxygen.

7.3 Experimental procedures from chapter 2

7.3.1 4-Decyloxybenzoic acid 2.21

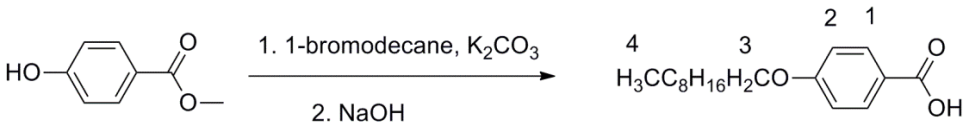

Figure 7.1 Preparation of 4-decyloxybenzoic acid **2.21**.

Preparation of 4-decyloxybenzoic acid was carried out following literature procedure.[188] Methyl-4-hydroxybenzoate (5 g, 33 mmol) and 1-bromodecane (8 g, 36 mmol) were dissolved in butanone (60 ml). To this solution, potassium carbonate (24.88 g, 180 mmol) was added. Then the mixture was refluxed under nitrogen atmosphere overnight. Then the solid was removed by filtration and solvent was removed under reduced pressure. The resulting white solid (9 g) was added to ethanol (100 ml). To this mixture, potassium hydroxide (2.1 g) in water (100 ml) was added. Then the mixture was refluxed for 2 h. After the mixture was cooled down, concentrated HCl was added to the mixture until pH 1. The precipitate was collected and recrystallization from ethanol gave white solid. Yield: 74%.

^{1}H-NMR (400 MHz; $CDCl_3$): δ 8.04 (d, J = 9 Hz, 2H, H^1), 6.94 (d, J = 9 Hz, 2H, H^2), 4.01 (t, J = 6 Hz,

2H, H^3), 1.78-1.71 (m, 2H, OCH_2CH_2), 1.51-1.23 (m, 14H, CH_2), 0.87 (t, J = 7 Hz, 3H, CH_3).

MS (ESI): m/z 279.1960 ($[M+H]^+$, 100%)

Spectroscopic data consistent with those reported in the literature.[188]

7.3.2 4-(Trimethylsilylethynyl)phenol 2.24

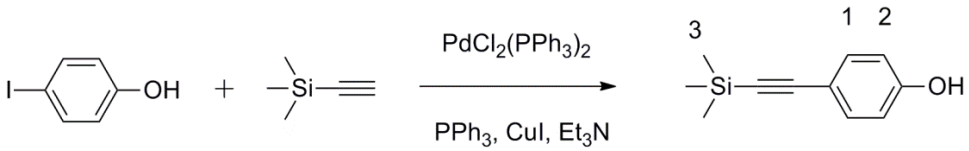

Figure 7.2 Preparation of 4-(trimethylsilylethynyl)phenol **2.24**.

Preparation of 4-(trimethylsilylethynyl)phenol was carried out following literature procedure.[80] 4-Iodophenol (3.3 g, 15.15 mmol), bis(triphenylphosphine) palladium dichloride (0.21 g, 0.30 mmol), copper(I) iodide (0.23 g, 1.21 mmol) and triphenylphosphine (0.32 g, 1.21 mmol) were added to dry triethylamine (25 ml) under nitrogen atmosphere. Then (trimethylsilyl)acetylene (3.2 ml, 22.73 mmol) was added to the mixture at 0 °C. The resulting mixture was stirred at room temperature under nitrogen overnight. Then solvent was removed under reduced pressure, the residue was purified by column chromatography to get brown oil (petroleum ether : ethyl acetate = 4 : 1, R_f = 0.3). Yield: 81%.

^{1}H-NMR (400 MHz; $CDCl_3$): δ 7.33 (d, J = 9 Hz, 2H, H^1), 6.68 (d, J = 9 Hz, 2H, H^2), 0.22 (s, 9H, H^3).

MS (ESI): m/z 191.0892 ($[M+H]^+$, 100%)

Spectroscopic data consistent with those reported in the literature.[80]

7.3.3 4-(Trimethylsilylethynyl)phenyl 4-decyloxybenzate 2.25

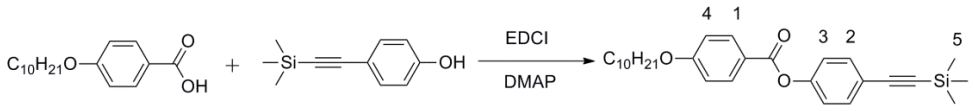

Figure 7.3 Preparation of 4-(trimethylsilylethynyl)phenyl 4-decyloxybenzate **2.25**.

Preparation of 4-(trimethylsilylethynyl)phenol 4-decyloxybenzate was carried out following literature procedure.[80] A solution of *N*-(3-dimethylaminopropyl)-*N'*-ethylcarbodiimide (EDCI, 552 mg, 3.56 mmol) in DCM (5 ml) was added dropwise to a solution of 4-(trimethylsilyl ethynyl) phenol (980 mg, 5.15 mmol), 4-(decyloxy)benzoic acid (790 mg, 2.84 mmol), 4-(dimethylamino)pyridine (DMAP, 48.9 mg, 0.4 mmol) in DCM at 0 °C. After EDCI solution was added completely, the mixture was allowed to warm to room temperature and stirred overnight. Then solvent was removed under reduced pressure, the residue was purified by column chromatography to get white solid. (petroleum ehter : ethyl acetate = 30 : 1, R_f = 0.3). Yield: 44%.

^{1}H-NMR (400 MHz; $CDCl_3$): δ 8.11 (d, J = 9 Hz, 2H, H^1), 7.51 (d, J = 9 Hz, 2H, H^2), 7.15 (d, J = 9 Hz, 2H, H^3), 6.96 (d, J = 9 Hz, 2H, H^4), 4.02 (t, J = 6 Hz, 2H, OCH_2), 1.78-1.71 (m, 2H, OCH_2CH_2), 1.51-1.23 (m, 14H, CH_2), 0.87 (t, J = 7 Hz, 3H, CH_3), 0.22 (S, 9H, H^5).

MS (ESI): m/z 451 ($[M+H]^+$, 100%)

Spectroscopic data consistent with those reported in the literature.[80]

7.3.4 4-Ethynylphenyl-4-decyloxybenzate 2.18

Figure 7.4 Preparation of 4-ethynylphenyl-4-decyloxybenzate **2.18**.

Preparation of 4-ethynyl-4-decyloxybenzate was carried out following literature procedure.[80] Tetrabutylammonium fluoride (TBAF, 374 mg, 1.4mmol) was added to the solution of 4-(trimethylsilyl ethynyl)phenyl-4-decyloxybenzate (430 mg, 0.96 mmol) in THF (10 ml), the mixture was stirred at room temperature overnight. The solvent was removed under reduced pressure; and then the residue was dissolved in DCM (20 ml) and washed with $NaHCO_3$ (3%) and water, the organic layer was collected and dried with $MgSO_4$. Then solvent was removed under reduced pressure, the residue was purified by column chromatography to get white solid (petroleum ether : ethyl acetate = 30 : 1, R_f = 0.3). Yield: 64%.

^{1}H-NMR (400 MHz; $CDCl_3$): δ 8.14 (d, J = 9 Hz, 2H, H^1), 7.56 (d, J = 9 Hz, 2H, H^2), 7.19 (d, J = 9 Hz, 2H, H^3), 6.98 (d, J = 9 Hz, 2H, H^4), 4.04 (t, J = 7 Hz, 2H, OCH_2) 3.08 (s, 1H, H^5), 1.78-1.71 (m, 2H, OCH_2CH_2), 1.51-1.23 (m, 14H, CH_2), 0.87 (t, J = 7 Hz, 3H, CH_3).

MS (ESI): m/z 379.2273 ($[M+H]^+$, 100%)

Spectroscopic data consistent with those reported in the literature.[80]

7.3.5 4-Methanesulfonyl-2,2,6,6-tetramethyl-1-piperidinyloxy radical 2.28

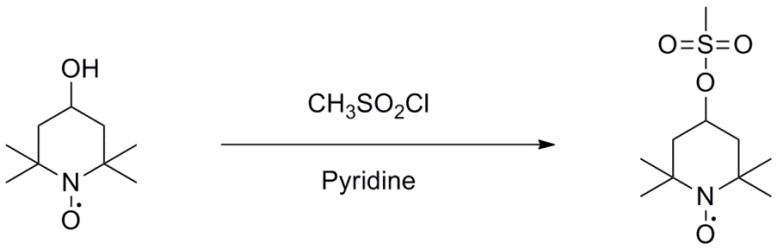

Figure 7.5 Preparation of 4-methanesulfonyl-2,2,6,6-tetramethyl-1-piperidinyloxy radical **2.28**.

Preparation of 4-methanesulfonyl-2,2,6,6-tetramethyl-1-piperidinyloxy radical was carried out following literature procedure.[81] To a solution of 4-hydroxy-2,2,6,6-tetramethylpiperidine 1-oxyl (4-hydroxy-TEMPO, 8.65 g, 50 mmol) in dry pyridine (35 ml), methane sulfonyl chloride (8 ml, 100 mmol) was added dropwise at 0 °C. Then the mixture was allowed to warm to room

temperature and stirred for 4 h. Then saturated $NaHCO_3$ aqueous solution (100 ml) was added to the mixture at 0 °C. After that, the mixture was extracted with chloroform (3 × 100 ml). The organic layers were combined together and washed with saturated $NaHCO_3$ aqueous solution (2 × 50 ml), water (2 × 50 ml), and then dried with Na_2SO_4. Then the solvent was removed under reduced pressure. Recrystallization from ethanol gave light red solid. Yield: 95%.

MS (ESI): m/z 251.1186 ($[M+H]^+$, 100%), 273.1004 ($[M+Na]^+$)

EPR: a_N= 15.46 G.

Spectroscopic data consistent with those reported in the literature.[81]

7.3.6 4-Azido-2,2,6,6-tetramethyl-1-piperidinyloxy radical 2.13

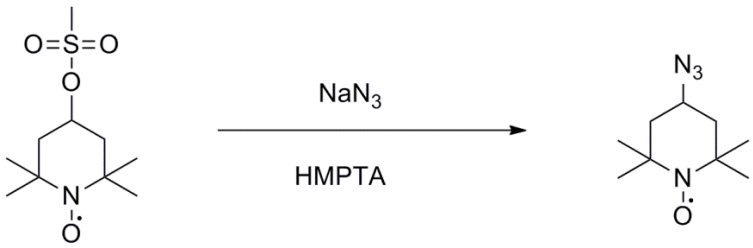

Figure 7.6 Preparation of 4-azido-2,2,6,6-tetramethyl-1-piperidinyloxy radical **2.13**.

Preparation of 4-azido-2,2,6,6-tetramethyl-1-piperidinyloxy radical was carried out following literature procedure.[81] Sodium azide (7.8 g, 120 mmol) was added to a solution of 4-methanesulfonyl-2,2,6,6-tetramethyl-1-piperidinyloxy radical (5 g, 20 mmol) in hexamethylphosphoric triamide (HMPTA, 25 ml). The mixture was stirred at 80 °C for 90 min. After the mixture was cooled to room temperature, water (100 ml) was added to the mixture; and then the mixture was extracted with ether (5 × 100 ml). The organic layers were combined together and dried with $CaCl_2$. The solvent was removed under reduced pressure. Recrystallization from hexane twice gave red needle shaped solid. Yield: 85%.

MS (ESI): m/z 198.1482 ($[M+H]^+$, 100%), 220.1303 ($[M+H]^+$)

EPR: a_N= 15.53 G.

Spectroscopic data consistent with those reported in the literature.[81]

7.3.7 Radical 2.19

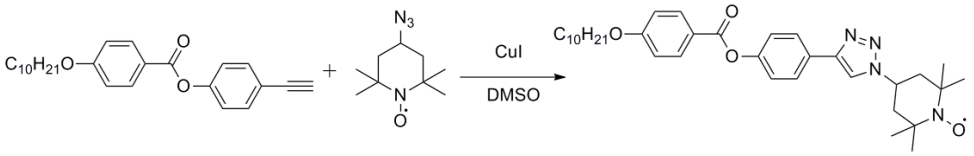

Figure 7.7 Preparation of radical **2.19**.

4-Ethynylphenyl-4-decyloxybenzate (70.2 mg, 0.19 mmol) and 4-amino-2,2,6,6 -tetramethyl-1-piperidinyloxy radical (36.6 mg, 0.19 mmol) were dissolved in dimethyl sulfoxide (DMSO, 20 ml). To this solution, copper(I) iodide (14.1 mg, 0.07 mmol) was added. Then the mixture was stirred at 40 °C for 4 days. Then the solid was removed by filtration and solvent was removed under reduced pressure The residue was purified by column chromatography to give light yellow solid (petroleum ether : ethyl acetate = 5 : 2, R_f = 0.3). Yield: 39%.

MS (ESI): m/z 576.3669 ($[M+H]^+$, 100%)

EPR: a_N= 14.07 G.

Analysis for $C_{34}H_{47}N_4O_4$. Calcd (%): C 70.93 H 8.23 N 9.73; found: C 70.96 H 8.05 N 9.45.

7.3.8 1-Azidocyclohexane 2.29

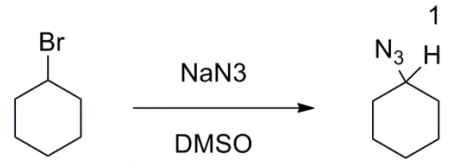

Figure 7.8 Preparation of 1-azidocyclohexane **2.29**.

Preparation of 1-azidocyclohexane was carried out following literature procedure.[189] To a solution of sodium azide (2.21 g, 34mmol) in DMSO (68 ml), cyclohexyl bromide (5 g, 31 mmol) was added. The mixture was stirred at 75 °C for 4 h. Then the mixture was quenched with water (150 ml) and extracted with ether (3 × 30 ml). The organic layers were combined together, washed with water (2 × 50 ml), dried with $MgSO_4$. The solvent was removed under reduced pressure to give yellow oil. Yield: 66%.

^{1}H-NMR (400 MHz; $CDCl_3$): δ 3.26 (m, 1H, H^1), 1.24-1.35 (m, 10H, CH_2).

MS (ESI): m/z 126.1031 ($[M+H]^+$, 100%)

Spectroscopic data consistent with those reported in the literature.[189]

7.3.9 Triazole derivative 2.30

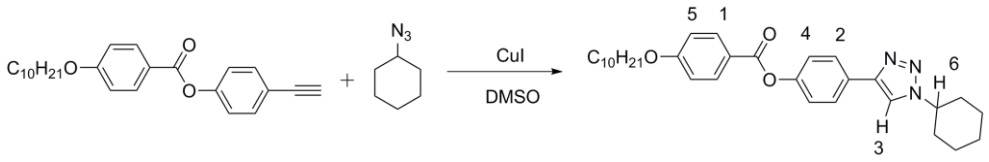

Figure 7.9 Preparation of triazole derivative **2.30**.

Preparation of triazole derivative **2.30** was carried out following literature procedure.[80] 4-Ethynylphenyl-4-decyloxybenzate (50 mg, 0.13 mmol), CuI (2.5 mg, 0.0132 mmol) and Et_3N

(2.3 µl) were added to a solvent mixture of ethanol (5 ml) and water (5 ml). Then cyclohexane azide (16.54 mg, 0.13 mmol) was added to the mixture dropwise. The mixture was refluxed for 48 h. The undissolved solid was removed by filtration, and solvent was removed under reduced pressure. Recrystallization from hexane gave yellow solid. Yield: 69%.

^{1}H-NMR (400 MHz; $CDCl_3$): δ 8.08 (d, J = 9 Hz, 2H, H^1), 7.81 (d, J = 9 Hz, 2H, H^2), 7.69 (s, 1H, H^3), 7.19 (d, J = 9 Hz, 2H, H^4), 6.98 (d, J = 9 Hz, 2H, H^5), 4.43 (m, 1H, H^6), 3.97 (t, J = 7 Hz, 2H, OCH_2), 1.75-1.71 (m, 2H, OCH_2CH_2), 1.53-1.21 (m, 24H, CH_2), 0.87 (t, J = 7 Hz, 3H, CH_3).

MS (ESI): m/z 504.3226 ($[M+H]^+$, 100%)

Spectroscopic data consistent with those reported in the literature.[80]

7.4 Experimental procedures from chapter 3

7.4.1 2,3-Dimethyl-2,3-nitrobutane 3.14

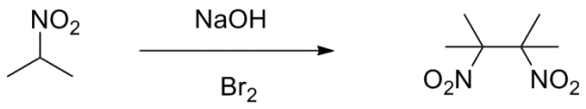

Figure 7.10 Preparation of 2,3-dimethyl-2,3-dinitrobutane **3.14**.

Preparation of 2,3-dimethyl-2,3-dinitrobutane was carried out following literature procedure.[190] To a solution of 2-nitropropane (69 g, 0.78 mol) and NaOH (31.2 g, 0.78 mol) in 130 ml water, Br_2 (20 ml, 0.4 mol) was added dropwise., after that, ethanol (256 ml) was added to this mixture. And the mixture was stirred at 84 °C for 3 h. Then reaction mixture was cooled to room temperature and quenched with water (400 ml). The precipitate was collected by filtration and dried in the vacuum oven (60 °C, 18 mbar). Yield: 70%.

^{1}H-NMR (400 MHz; $CDCl_3$): δ 1.72 (s, 12H).

MS (ESI): m/z 177.0875 ([M+H]$^+$, 100%)

Spectroscopic data consistent with those reported in the literature.[190]

7.4.2 2,3-Bis(hydroxyamino)-2,3-nitrobutane 3.15

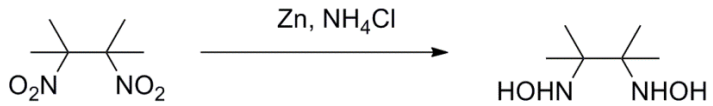

Figure 7.11 Preparation of 2,3-bis(hydroxyamino)-2,3-nitrobutane **3.15**.

Preparation of 2,3-dimethyl-2,3-dinitrobutane was carried out following literature procedures.[109,190]

Reduction with Zinc: To a solution of 2,3-dimethyl-2,3-dinitrobutane (17.6 g, 0.1 mol) in THF (300 ml), NH_4Cl (43 g, 0.8 mol) in 150 ml water was added. Then the mixture was cooled to 10 °C. Zinc power (27 g, 0.4 mol) was added by portions over 2 h, while the temperature was kept below 12 °C. After all zinc power had been added, the mixture was stirred at 10 °C for 3 h. Then the mixture was filtered, and the solid was washed with THF (4 × 50 mL). Then solvent was removed under reduced pressure to obtain white waxy solid. This white waxy solid can be used without purification for the preparation of nitronyl and imino nitroxide.

Sodium carbonate (30 g), sodium chloride (20 g), H_2O (20 ml) and anhydrous sodium sulphate (20 g) were added to the waxy solid. The resulting mixture was extracted in a Soxlet apparatus overnight with DCM. Then solvent was removed to get white solid. Yield: 26%.

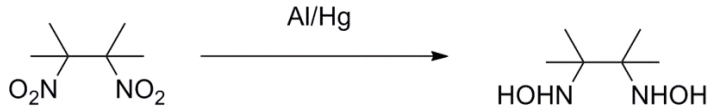

Figure 7.12 Preparation of 2,3-bis(hydroxyamino)-2,3-nitrobutane **3.15**.

Reduction with aluminium amalgam: Aluminum foil (77 mg, 2.8 mmol) was added to a 3% aqueous $HgCl_2$ (67.88 mg, 0.25 mmol). The mixture was stirred at room temperature for 2 min. Then the liquid was removed by a pipette and the residual solid was washed with water and THF three times each. After that, THF (4 ml) and water (0.4 ml) and a solution of 2,3-dimethyl-2,3-dinitrobutane in THF (4 ml) were added to the solid at 0 °C, and the mixture was stirred at 0 °C for 20 min. The solid was removed by filtration, and solvent was removed to get white solid. Yield: 13%.

^{1}H-NMR (400 MHz; D_2O): δ 1.25 (s, 12H).

^{13}C-NMR (400 MHz; D_2O): δ 63.7 (C-C), 19.4 (CH_3)

MS (ESI): m/z 149.1290 ($[M+H]^+$, 100%)

Spectroscopic data consistent with those reported in the literature.[190]

7.4.3 *p*-Hydroxyphenyl nitronyl nitroxide 3.8

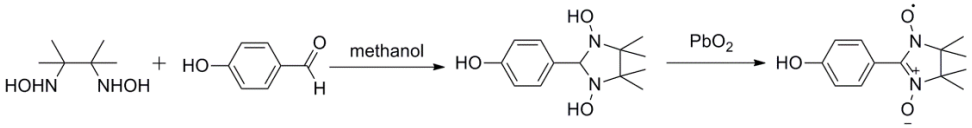

Figure 7.13 Preparation of *p*-hydroxyphenyl nitronyl nitroxide **3.8**.

Preparation of *p*-hydroxyphenyl nitronyl nitroxide was carried out following literature procedure.[190] 2,3-Bis(hydroxyamino)-2,3-dimethylbutane (500 mg, 3.37 mmol) and 4-hydorxybenzaldehyde (412 mg, 3.37 mmol) were dissolved in methanol (20 ml) and the mixture was stirred at room temperature overnight. The mixture was then filtered, and the solvent was removed under reduced pressure to get light yellow solid. This solid was dissolved in methanol (20 ml), lead dioxide (500 mg) was added to this mixture. Then the mixture was

stirred at room temperature for 3 h. The undissolved solid was removed by filtration, and solvent was removed under reduced pressure. The residue was purified by column chromatography (petroleum ether : ethyl acetate = 2 : 1, R_f = 0.3).

MS (ESI): m/z 250.1311 ($[M+H]^+$, 100%)

EPR: a_{N1}= 7.53 G, a_{N2}= 7.53 G.

7.4.4 *p*-Hydroxyphenyl imino nitroxide 3.17

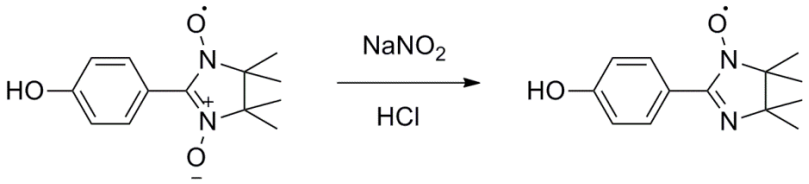

Figure 7.14 Preparation of *p*-Hydroxyphenyl imino nitroxide **3.17**.

Preparation of *p*-hydroxyphenyl imino nitroxide was carried out following literature procedure.[191] *p*-Hydroxyphenyl nitronyl nitroxide (69 mg, 0.3 mmol) and sodium nitrite (138 mg, 2 mmol) were dissolved in methanol (10 ml). Concentrated HCl (0.2 ml) was added to this solution. Then the mixture was stirred at room temperature for 1 h. Saturated aqueous $NaHCO_3$ solution was added to the solution. Then the mixture was extracted with DCM (3 × 20 ml), the organic layers were combined together, dried with Na_2SO_4. Solvent was removed under reduced pressure, and the residue was purified by column chromatography ($CHCl_3$: CH_3OH = 20 : 1, R_f = 0.3). Yield: 58%.

MS (ESI): m/z 235.1439 ($[M+H]^+$, 100%)

EPR: a_{N1}= 9.10 G, a_{N2}= 4.36 G.

7.4.5 Benzyl 4-[[4-(decyloxy)benzoyl]oxy]benzoate 3.12

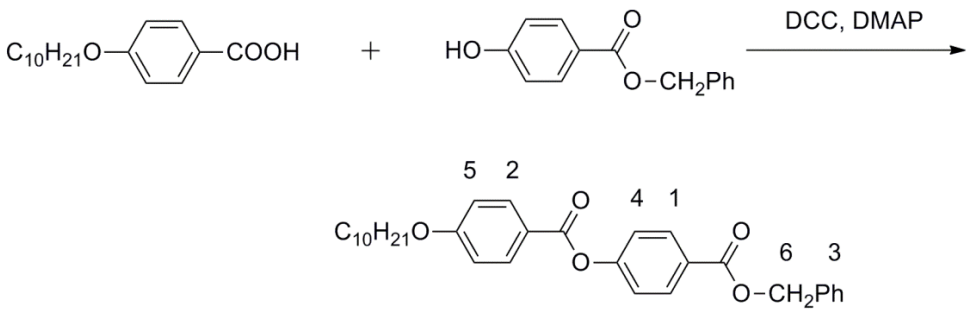

Figure 7.15 Preparation of benzyl 4-[[4-(decyloxyl)benzoyl]oxy]benzoate **3.12**.

Preparation of benzyl 4-[[4-(decyloxyl)benzoyl]oxy]benzoate was carried out following literature procedure.[4] A solution of DCC (2.5 g, 12 mmol) in DCM (50 ml) was added dropwise to a solution of benzyl 4-hydroxybenzoate (2.3 g, 10 mmol), 4-(decyloxy)benzoic acid (3.4 g, 12 mmol), DMAP (160 mg, 1.3 mmol) in DCM at 0 °C. After DCC was added completely, the mixture was allowed to warm to room temperature and stirred overnight. Then solvent was removed under reduced pressure, the residue was purified by column chromatography to get white solid (petroleum ether : ethyl acetate = 20 : 1, R_f = 0.3). Yield: 90%.

^{1}H-NMR (400 MHz; $CDCl_3$): δ 8.16 (d, J = 9 Hz, 2H, H^1), 8.14 (d, J = 9 Hz, 2H, H^2), 7.47-7.38 (m, 5H, H^3), 7.30 (d, J = 9 Hz, 2H, H^4), 6.98 (d, J = 9 Hz, 2H, H^5), 5.38 (s, 2H, H^6), 4.05 (t, J = 7 Hz, 2H, OCH_2), 1.75-1.71 (m, 2H, OCH_2CH_2), 1.51-1.21 (m, 14H, CH_2), 0.87 (t, J = 7 Hz, 3H, CH_3).

MS (ESI): m/z 489.2641 ($[M+H]^+$, 100%)

Spectroscopic data consistent with those reported in the literature.[4]

7.4.6 4-[[4-(Decyloxy)benzoyl]oxy]benzoic acid 3.9

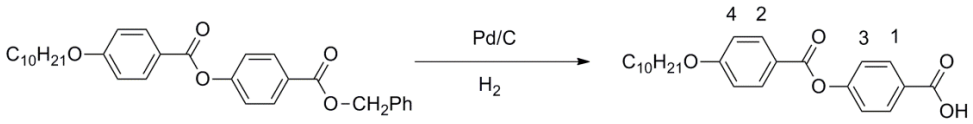

Figure 7.16 Preparation of 4-[[4-(decyloxy)benzoyl]oxy]benzoic acid.

Preparation of 4-[[4-(decyloxy)benzoyl]oxy]benzoic acid was carried out following literature procedure.[4] To a solution of benzyl 4-[[4-(decyloxyl)benzoyl]oxy]benzoate (2.1 g, 4.27 mmol) in dry THF (50 ml), palladium on carbon (10 wt.% 200 mg) was added. The mixture was stirred at room temperature under H_2 atmosphere overnight. Then the solid was filtered and solvent was removed under reduced pressure. The residue was purified by column chromatography to get white solid (petroleum ether : ethyl acetate = 2 : 1, R_f = 0.4). Yield: 95%.

^{1}H-NMR (400 MHz; $CDCl_3$): δ 8.20 (d, J = 9 Hz, 2H, H^1), 8.15 (d, J = 9 Hz, 2H, H^2), 7.34 (d, J = 9 Hz, 2H, H^3), 6.99 (d, J = 9 Hz, 2H, H^4), 4.05 (t, J = 7 Hz, 2H, OCH_2), 1.75-1.71 (m, 2H, OCH_2CH_2), 1.51-1.21 (m, 14H, CH_2), 0.87 (t, J = 7 Hz, 3H, CH_3).

MS (ESI): m/z 399.2171 ($[M+H]^+$, 100%)

Spectroscopic data consistent with those reported in the literature.[4]

7.4.7 Nitronyl nitroxide containing compound 3.22

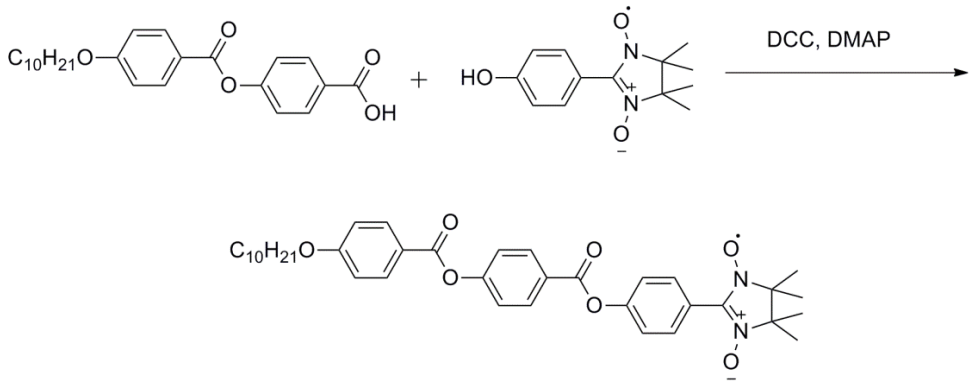

Figure 7.17 Preparation of nitronyl nitroxide containing compound **3.22**.

A solution of DCC (40 mg, 0.2 mmol) in DCM (5 ml) was added dropwise to a solution of 4-[[4-(decyloxy)benzoyl]oxy]benzoic acid (76 mg, 0.2 mmol), nitronyl nitroxide (40 mg, 0.2 mmol), DMAP (3 mg, 0.03 mmol) in DCM at 0 °C. After DCC was added completely, the mixture was allowed to warm to room temperature and stirred overnight. Then solvent was removed under reduced pressure, the residue was purified by column chromatography to get blue solid. (petroleum ether : ethyl acetate = 5 : 1, R_f = 0.3). Yield: 32%.

MS (ESI): m/z 631.3375 ($[M+H]^+$, 100%)

EPR: a_{N1}= 7.42 G, a_{N2}= 7.42 G.

7.4.8 Imino nitroxide containing compound 3.23

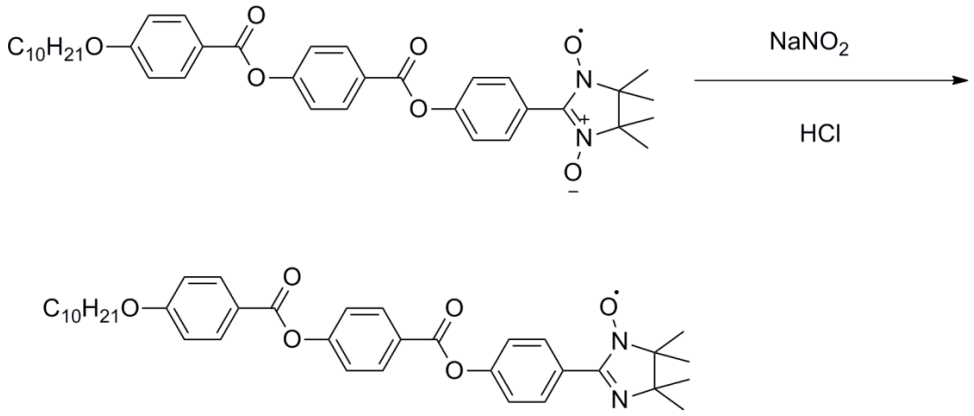

Figure 7.18 Preparation of imino nitroxide containing mesogen **3.23**.

Compound **3.22** (10 mg, 0.01 mmol) and sodium nitrite (11 mg, 0.1 mmol) were dissolved in methanol (10 ml). Concentrated HCl (0.1 ml) was added to this solution. Then the mixture was stirred at room temperature for 1 h. Saturated aqueous $NaHCO_3$ solution was added to the solution. Then the mixture was extracted with DCM (3 × 20 ml), the organic layers were combined together, dried with Na_2SO_4. Solvent was removed under reduced pressure, and the residue was purified by column chromatography to get yellow solid ($CHCl_3$: CH_3OH = 20 : 1, R_f = 0.3). Yield: 50%.

MS (ESI): m/z 615.3415 ($[M+H]^+$, 100%)

EPR: a_{N1}= 9.01 G, a_{N2}= 4.43 G.

7.5 Experimental procedures from chapter 4

7.5.1 Benzaldehyde derivatives

7.5.1.1 4-Decyloxybenzaldehyde 4.32

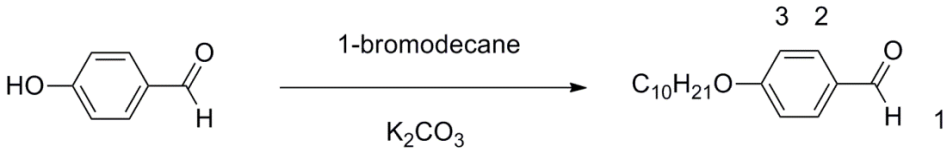

Figure 7.19 Preparation of 4-decyloxybenzaldehyde **4.32**.

Preparation of 4-decyloxybenzaldehyde was carried out following literature procedure.[192] To a solution of 4-hydroxybenzaldehyde (5 g, 41 mmol) and 1-bromodecane (10 g, 45 mmol) in butanone (100 ml), potassium carbonate (28.3 g, 205 mmol) was added. The mixture was refluxed overnight. Then the mixture was filtered, solvent was removed under reduced pressure. The residue was purified by column chromatography to get white solid (petroleum ether : DCM = 1: 1, R_f = 0.3). Yield: 90%.

^{1}H-NMR (400 MHz; $CDCl_3$): δ 9.80 (s, 1H, H^1), 7.75 (d, J = 9 Hz, 2H, H^2), 6.91 (d, J = 9 Hz, 2H, H^3), 3.95 (t, J = 7 Hz, 2H, OCH_2), 1.75-1.71 (m, 2H, OCH_2CH_2), 1.50-1.21 (m, 14H, CH_2), 0.87 (t, J = 7 Hz, 3H, CH_3).

MS (ESI): m/z 263.2011 ($[M+H]^+$, 100%)

Spectroscopic data consistent with those reported in the literature.[192]

7.5.1.2 3,4-Didecyloxybenzaldehyde

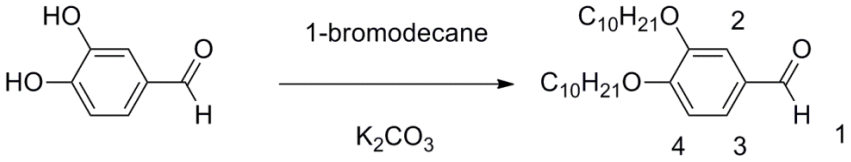

Figure 7.20 Preparation of 3,4-didecyloxybenzaldehyde.

Preparation of 3,4-didecyloxybenzaldehyde was carried out following literature procedure.[193] To a solution of 4-hydroxybenzaldehyde (10 g, 72 mmol) and 1-bromodecane (18 g, 80 mmol) in butanone (200 ml), potassium carbonate (50 g, 362 mmol) was added. The mixture was refluxed overnight. Then the mixture was filtered, the solvent was removed under reduced pressure. Recrystallization from ethanol gave white solid. Yield: 91%.

^{1}H-NMR (400 MHz; $CDCl_3$): δ 9.84 (s, 1H, H^1), 7.42-7.40 (m, 2H, H^2, H^3), 6.96 (d, J = 8 Hz, 1H, H^4), 4.10-4.04 (m, 4H, OCH_2), 1.89-1.82 (m, 4H, OCH_2CH_2), 1.59-1.21 (m, 28H, CH_2), 0.87 (t, J = 7 Hz, 6H, CH_3).

MS (ESI): m/z 419.3525 ($[M+H]^+$, 100%)

Spectroscopic data consistent with those reported in the literature.[193]

7.5.1.3 3,4,5-Trihydroxybenzaldehyde 4.69

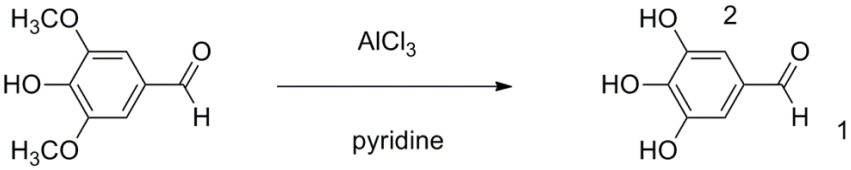

Figure 7.21 Preparation of 3,4,5-trihydroxybenzaldehyde **4.69**.

Preparation of 3,4,5-trihydroxybenzaldehyde was carried out following literature procedure.[194]

Syringaldehyde (2.2 g, 12 mmol) was added to toluene (30 ml) at room temperature, and then the mixture was cooled to 0 °C. To this mixture, aluminium chloride (11.9 g, 91 mmol) was added by portions. Then the mixture was heated to 55 °C, and pyridine (14.3 g, 181 mmol) was added to the mixture slowly. Then the mixture was refluxed overnight. After that, the mixture was cooled to 50 °C and concentrated HCl was added slowly to the mixture. And the mixture was cooled to room temperature and extracted with ethyl acetate (5 × 100 ml), organic layers were combined together, washed with water and dried with $MgSO_4$. Then the solvent was removed under reduced pressure to get black crystal. The black crystal was added to 100 ml acetone. Undissolved solid was removed by filtration and solvent was removed under reduced pressure to get white solid. Yield: 1%.

^{1}H-NMR (400 MHz; CD_3OD): δ 9.62 (s, 1H, H^1), 6.93 (s, 1H, H^2).

MS (ESI): m/z 155.0339 ($[M+H]^+$, 100%)

Spectroscopic data consistent with those reported in the literature.[194]

7.5.1.4 Ethyl-3,4,5-tridecyloxybenzoate 4.71

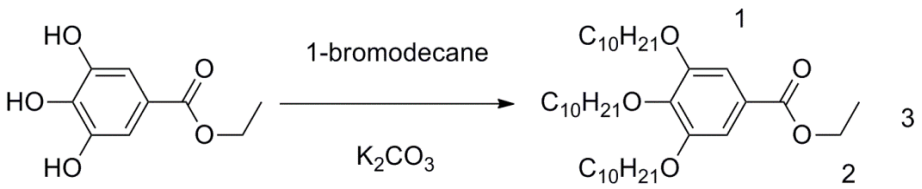

Figure 7.22 Preparation of ethyl-3,4,5-tridecyloxybenzoate **4.71**.

Preparation of ethyl-3,4,5-tridecyloxybenzoate was carried out following literature procedure.[195] To a solution of ethyl 3,4,5-trihydroxybenzoate (10 g, 51 mmol) and 1-bromodecane (37 g, 167 mmol) in acetone (200 ml), potassium carbonate (28 g, 200 mmol) was added. The mixture was refluxed for 4 days. Then the mixture was filtered, and solvent was removed under reduced pressure. The distillation yielded white solid (bp 254 °C, 0.8 tor). Yield:

85%.

^{1}H-NMR (400 MHz; $CDCl_3$): δ 7.26 (s, 2H, H^1), 4.35 (q, J = 7 Hz, 2H, H^2), 4.01 (t, J = 7 Hz, 4H, OCH_2), 3.96 (t, J = 7 Hz, 2H, OCH_2), 1.80-1.70 (m, 6H, OCH_2CH_2), 1.50-1.20 (m, 42H, CH_2), 1.38 (t, J = 7 Hz, 3H, H^3), 0.87 (t, J = 7 Hz, 9H, CH_3)

MS (ESI): m/z 641.5096 ($[M+Na]^+$, 100%)

Spectroscopic data consistent with those reported in the literature.[195]

7.5.1.5 3,4,5-Tridecyloxybenzyl alcohol 4.72

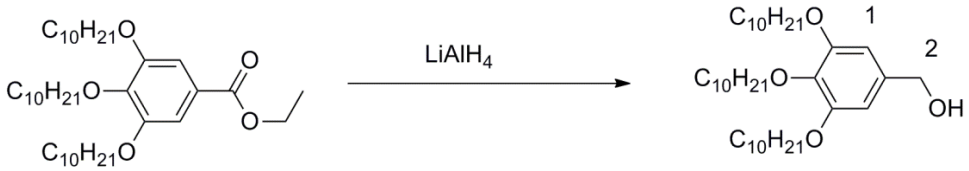

Figure 7.23 Preparation of 3,4,5-tridecyloxybenzyl alcohol **4.72**.

Preparation of ethyl-3,4,5-tridecyloxybenzyl alcohol was carried out following literature procedure.[195] Ethyl-3,4,5-tridecyloxybenzoate (1 g, 1.87 mmol) was dissolved in dry diethyl ether (20 ml). $LiAlH_4$ (40 mg, 0.93 mmol) was added slowly to the solution under nitrogen atmosphere. Then the mixture was refluxed for 1 h. 2M HCl aqueous solution was added to the mixture at 0 °C to remove excess $LiAlH_4$. Then the mixture was extracted with DCM (3 × 50 ml). The organic layers were combined together, dried with $MgSO_4$. The solvent was removed under reduced pressure to give white solid. Yield: 96%.

^{1}H-NMR (400 MHz; $CDCl_3$): δ 6.56 (s, 2H, H^1), 4.60 (s, 2H, H^2), 3.98 (t, J = 7 Hz, 4H, OCH_2), 3.93 (t, J = 7 Hz, 2H, OCH_2), 1.82-1.69 (m, 6H, OCH_2CH_2), 1.51-1.20 (m, 42H, CH_2), 0.87 (t, J = 7 Hz, 9H, CH_3)

MS (ESI): m/z 577.5181 ([M+H]$^+$, 100%)

Spectroscopic data consistent with those reported in the literature.[195]

7.5.1.6 3,4,5-Tridecyloxybenzaldehyde 4.73

Figure 7.24 Preparation of 3,4,5-tridecyloxybenzaldehyde **4.73**.

Preparation of ethyl-3,4,5-tridecyloxybenzaldehyde was carried out following literature procedure.[195] To a solution of 3,4,5-Tridecyloxybenzyl alcohol (1 g, 1.73 mmol) in dry 1,4-dioxane (30 ml), 2,3-dichloro-5,6-dicyano-p-benzoquinone (DDQ) (0.51 g, 2.25 mmol) was added under nitrogen atmosphere. The mixture was stirred at room temperature overnight. Then the mixture was filtered, the solvent was removed under reduced pressure. The residue was purified by column chromatography to get white solid (petroleum ether : ethyl acetate = 49 : 1, R_f = 0.4). Yield: 78%.

^{1}H-NMR (400 MHz; $CDCl_3$): δ 9.84 (s, 1H, H^1), 7.09 (s, 2H, H^2), 4.06 (t, J = 7 Hz, 4H, OCH_2), 4.03 (t, J = 7 Hz, 2H, OCH_2), 1.86-1.71 (m, 6H, OCH_2CH_2), 1.51-1.20 (m, 42H, CH_2), 0.87 (t, J = 7 Hz, 9H, CH_3)

MS (ESI): m/z 575.5061 ([M+H]$^+$, 100%)

Spectroscopic data consistent with those reported in the literature.[195]

7.5.2 Phenylhydrazine derivatives

7.5.2.1 4-Heptyl phenylhydrazine

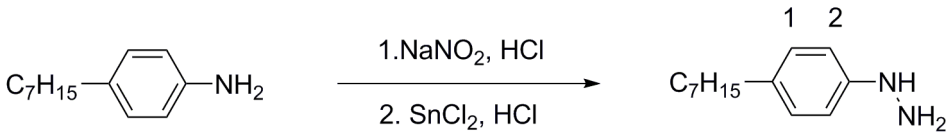

Figure 7.25 Preparation of 4-heptyl phenylhydrazine.

Concentrated HCl (8 ml) was added to 4-heptyl aniline (500 mg, 2.6 mmol) to get the hydrochloride salt. A solution of $NaNO_2$ (180 mg, 2.6 mmol) in water (5 ml) was added to the salt at -10 °C. Then the mixture was stirred at 0 °C for 0.5 h. The mixture was added to $SnCl_2$ (1.98 g, 10.4 mmol) in concentrated HCl (5 ml) by portions at -10 °C. Then the mixture was stirred at room temperature for 1 h. After that, the mixture was filtered; the solid was washed with ethyl (3 × 20 ml). Recrystallization from ethanol gave white solid. Yield: 64%.

^{1}H-NMR (400 MHz; DMSO-d_6): δ 7.06 (d, J = 8 Hz, 2H, H^1), 6.90 (d, J = 8 Hz, 2H, H^2), 2.48 (t, J = 7 Hz, 2H, CH_2), 1.47 (m, 2H, CH_2CH_2), 0.98-1.24 (m, 8H, CH_2), 0.83 (t, J = 7 Hz, 3H, CH_3)

MS (ESI): m/z 207.1850 ($[M+H]^+$, 100%)

7.5.2.2 1,2-Didecyloxybenzene 4.42

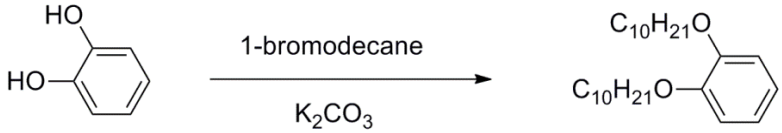

Figure 7.26 Preparation of 1,2-didecyloxybenzene **4.42**.

Preparation of 1,2-didecyloxybenzene was carried out following literature procedure.[142] Potassium carbonate (188.4 g, 1.36 mmol) was added to a solution of pyrocatechol (30 g, 0.27 mol) and 1-bromodecane (132.7 g, 0.58 mol) in butanone (400 ml). The mixture was refluxed for 3 days. Then the mixture was filtered, the solvent was removed under reduced pressure. Recrystallization from ethanol gave white solid. Yield: 67%.

^{1}H-NMR (400 MHz; $CDCl_3$): δ 6.88-6.89 (m, 4H, aromatic protons), 3.98 (t, J = 7 Hz, 4H, OCH_2), 1.84-1.77 (m, 4H, OCH_2CH_2), 1.49-1.23 (m, 28H, CH_2), 0.87 (t, J = 7 Hz, 6H, CH_3)

MS (ESI): m/z 391.3576 ($[M+H]^+$, 100%)

Spectroscopic data consistent with those reported in the literature.[142]

7.5.2.3 3,4-Didecyloxy nitrobenzene

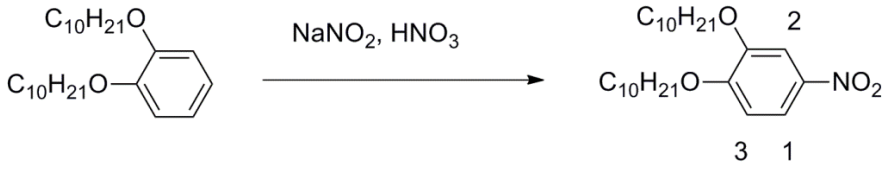

Figure 7.27 Preparation of 3,4-didecyloxy nitrobenzene.

Preparation of 3,4-didecyloxy nitrobenzene was carried out following literature procedure.[142] To a solution of 1,2-didecyloxybenzene (1 g, 2.56 mmol) in DCM (20 ml), sodium nitrite (24.7 mg, 0.36 mmol) was added at 0 °C. To this ice-cooled suspension, a solution of concentrated HNO_3 (484 mg, 7.68 mmol) in DCM (10 ml) was added slowly. Then the mixture was stirred at room temperature for 2 h. After that, the mixture was poured into water (100 ml), and then extracted with DCM (3 × 50 ml). Organic layers were combined together, and washed with 5% aqueous $NaHCO_3$, water and brine, then dried by Na_2SO_4. The solvent was removed under reduced pressure, and recrystallization from ethanol gave light yellow solid. Yield: 75%.

^{1}H-NMR (400 MHz; $CDCl_3$): δ 7.88 (dd, J = 9, 2 Hz, 1H, H^1), 7.73 (d, J = 2 Hz, 1H, H^2), 6.88 (d, J = 9 Hz, 1H, H^3), 4.08 (t, J = 7 Hz, 2H, OCH_2), 4.06 (t, J = 7 Hz, 2H, OCH_2), 1.89-1.81 (m, 4H, OCH_2CH_2), 1.51-1.21 (m, 28H, CH_2), 0.87 (t, J = 7 Hz, 6H, CH_3)

MS (ESI): m/z 436.3427 ($[M+H]^+$, 100%)

Spectroscopic data consistent with those reported in the literature.[142]

7.5.2.4 3,4-Didecyloxy aniline

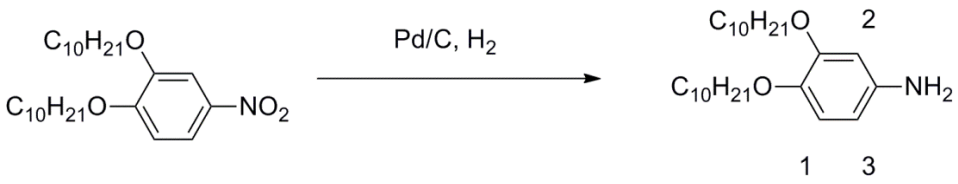

Figure 7.28 Preparation of 3,4-didecyloxy aniline.

Preparation of 3,4-ddecyloxy aniline was carried out following literature procedure.[142] To a solution of 3,4-didecyloxy nitrobenzene (1 g, 2.3 mmol) in dry THF (30 ml), palladium on carbon (10 wt. % 100 mg) was added under N_2 atmosphere. The mixture was stirred at room temperature under hydrogen atmosphere overnight. Then the mixture was filtered, the solvent was removed under reduced pressure. Then the residue was purified by column chromatography (petroleum ether : ethyl acetate = 3 : 1, R_f = 0.4) to get white solid. Yield: 92%.

^{1}H-NMR (400 MHz; $CDCl_3$): δ 6.74 (d, J = 8 Hz, 1H, H^1), 6.31 (d, J = 2 Hz, 1H, H^2), 6.21 (dd, J = 9,2 Hz, 1H, H^3), 3.93 (t, J = 7 Hz, 2H, OCH_2), 3.89 (t, J = 7 Hz, 2H, OCH_2), 1.83-1.70 (m, 4H, OCH_2CH_2), 1.48-1.21 (m, 28H, CH_2), 0.87 (t, J = 7 Hz, 6H, CH_3)

MS (ESI): m/z 406.3685 ($[M+H]^+$, 100%)

Spectroscopic data consistent with those reported in the literature.[142]

7.5.2.5 3,4-Didecyloxy bromobenzene 4.43

Figure 7.29 Preparation of 3,4-didecyloxy bromobenzene **4.43**.

Preparation of 3,4-ddecyloxy bromobenzene was carried out following literature procedure.[196] 1,2-Didecyloxy benzene (3 g, 7.7 mmol) and *N*-bromosuccinimide (NBS, 1.44 g, 8.1 mol) was dissolved in THF (30 ml). The mixture was stirred at room temperature overnight. Then the solvent was removed under reduced pressure, the residue was purified by column chromatography (petroleum ether : DCM = 5 : 1, R_f = 0.3). Yield : 55 %.

^{1}H-NMR (400 MHz; $CDCl_3$): δ 6.98-7.0 (m, 2H, H^1, H^2), 6.74 (d, J = 9 Hz, 1H, H^3), 3.96 (t, J = 7 Hz, 2H, OCH_2), 3.95 (t, J = 7 Hz, 2H, OCH_2), 1.84-1.75 (m, 4H, OCH_2CH_2), 1.49-1.24 (m, 28H, CH_2), 0.88 (t, J = 7 Hz, 6H, CH_3)

MS (ESI): m/z 469.2689 ($[M+H]^+$, 100%).

Spectroscopic data consistent with those reported in the literature.[196]

7.5.2.6 1,2-Bis(tert-butoxycarbonyl)-1-(3,4-didecyloxyphenyl)- hydrazine 4.44

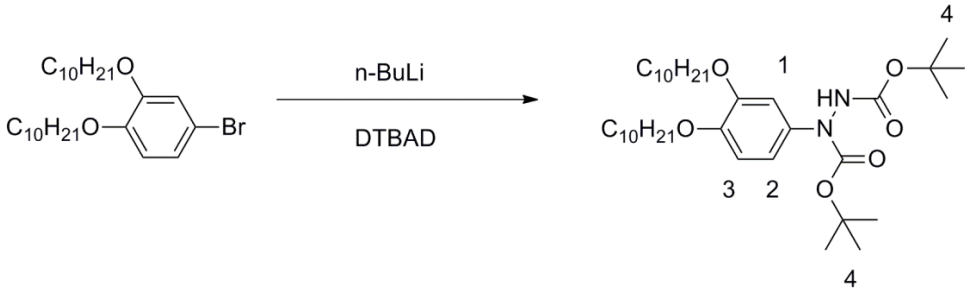

Figure 7.30 Preparation of 1,2-bis(tert-butoxycarbonyl)-1-(3,4-didecyloxyphenyl)- hydrazine **4.44**.

Preparation of 1,2-bis(tert-butoxycarbonyl)-1-(3,4-didecyloxyphenyl)-hydrazine was carried out following literature procedure.[135] To a solution of 3,4-didecyloxy bromobenzene (2 g, 4.24 mmol) in dry THF (150 ml), n-BuLi (2.5 M in hexane, 5.12 mmol) was added under N_2 at -78 °C. The mixture was stirred at -78 °C for 1.5 h. Then a solution of di-tert-butyl azodicarboxylate (DTBAD, 1.18 g, 5.12 mmol) in dry THF was added dropwise. The mixture was stirred at -78 °C for 0.5 h, then 1 h at room temperature. Then the mixture was quenched with 5% HCl. The mixture was extracted with ether, and the organic layers were combined together, dried by Na_2SO_4. The solvent was removed under reduced pressure, and the residue was purified by column chromatography (petroleum ether : DCM = 1 : 1, then pure DCM) to give white solid. Yield: 58%.

^{1}H-NMR (400 MHz; $CDCl_3$): δ 6.72-7.0 (m, 3H, H^1, H^2, H^3), 3.97 (t, J = 7 Hz, 2H, OCH_2), 3.96 (t, J = 7 Hz, 2H, OCH_2), 1.83-1.74 (m, 4H, OCH_2CH_2), 1.49 (S, 18H, H^4), 1.49-1.24 (m, 28H, CH_2), 0.88 (t, J = 7 Hz, 6H, CH_3)

MS (ESI): m/z 643.4638 ($[M+Na]^+$, 100%)

Spectroscopic data consistent with those reported in the literature.[197]

7.5.2.7 3,4-didecyloxyphenylhydrazine 4.45

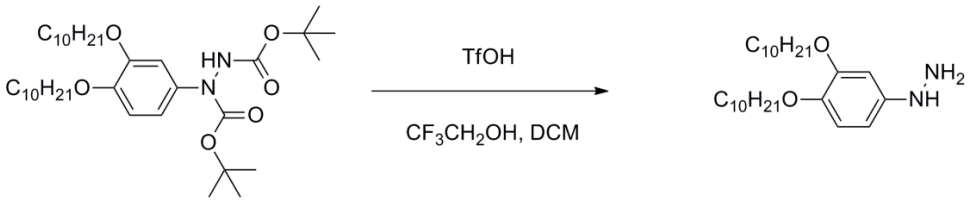

Figure 7.31 Preparation of 3,4-didecyloxyphenylhydrazine **4.45**.

Preparation of 3,4-didecyloxyphenylhydrazine was carried out following literature procedure.[135] A solution of 1,2-bis(tert-butoxycarbonyl)-1-(3,4-didecyloxyphenyl)- hydrazine (500 mg, 0.8 mmol) in a mixture of DCM (3 ml) and 2,2,2-trifluoroethanol (4 ml) was rapidly added to a solution of trifluoromethanesulfonic acid (TfOH, 604 mg, 4 mmol) in CF_3CH_2OH (1 ml) at -40 °C under argon. The mixture was stirred for 1.5 min, and DCM (5 ml) and saturated $NaHCO_3$ (10 ml) were added. The mixture was extracted with DCM (3 × 20 ml). The organic layers were combined together and dried with Na_2SO_4. Then the solvent was removed under reduced pressure. The product cannot be isolated due to the poor stability.

MS (ESI): m/z 421.3783 ($[M+H]^+$)

7.5.2.8 1,2-Didecylbenzene 4.54

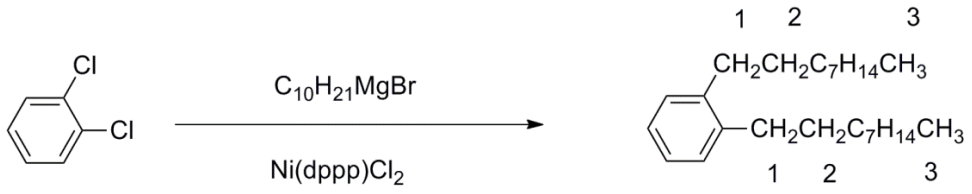

Figure 7.32 Preparation of 1,2-didecylbenzene **4.54**.

Preparation of 1,2-didecylbenzene was carried out following literature procedure.[135] Magnesium turning (1.58 g, 65 mmol) was added to dry THF (5 ml) under nitrogen. To this

mixture, a solution of 1-bromodecane (12 g, 54 mmol) in dry THF (50 ml) was added slowly. Then the mixture was refluxed for 3 h under nitrogen. 1,2-Dichlorobenzene (2 g, 6.8 mmol) and [1,3-bis(diphenylphosphino)propane] dichloronickel ($Ni(dppp)Cl_2$, 74 mg, 0.07 mmol) were added to this mixture. Then the mixture was refluxed overnight. After that, the mixture was filtered, and the solvent was removed under reduced pressure. The residue was purified by column chromatography (hexane, R_f = 0.5) to get colorless oil. Yield: 40%.

^{1}H-NMR (400 MHz; $CDCl_3$): δ 7.11-7.2 (m, 4H, aromatic protons), 2.56-2.62 (m, 4H, H^1), 1.53-1.64 (m, 4H, H^2), 1.41-1.22 (m, 28H, CH_2), 0.88 (t, J = 7 Hz, 6H, H^3)

MS (ESI): m/z 359.3678 ($[M+H]^+$, 100%)

Spectroscopic data consistent with those reported in the literature.[197]

7.5.2.9 1-Bromo-3,4-didecylbenzene 4.55

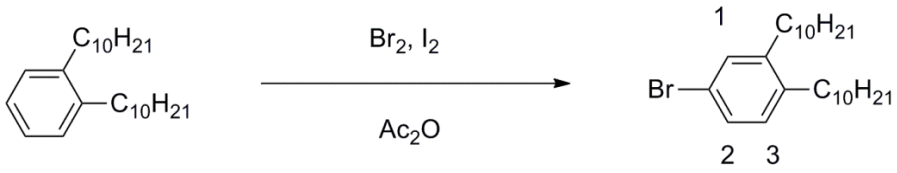

Figure 7.33 Preparation of 1-bromo-3,4-didecylbenzene **4.55**.

Preparation of 1-bromo-3,4-didecylbenzene was carried out following literature procedure.[135] To a solution of 1,2-didecylbenzene (0.9 g, 2.5 mmol) in a mixture of acetic anhydride (3 ml) and DCM (3 ml), Br_2 (0.3 ml, 5 mmol) and catalytic amount of I_2 were added. The mixture was stirred at room temperature overnight. The mixture was poured into water (30 ml); and then extracted with hexane (3 × 20 ml). The organic layers were combined together and dried by Na_2SO_4. The solvent was removed under reduced pressure, the residue was purified by column chromatography (hexane, R_f = 0.5). Yield: 75%.

^{1}H-NMR (400 MHz; $CDCl_3$): δ 7.39 (d, J = 2 Hz, 1H, H^1), 7.22 (dd, J= 8, 2 Hz, 1H, H^2), 7.0 (d, J = 8 Hz, 1H, H^3), 2.51-2.56 (m, 4H,CH_2), 1.59-1.49 (m, 4H, CH_2CH_2), 1.38-1.22 (m, 28H, CH_2), 0.88 (t, J = 7 Hz, 6H, CH_3)

MS (ESI): m/z 437.2783 ([M+H]$^+$, 100%)

Spectroscopic data consistent with those reported in the literature.[197]

7.5.2.10 1,2-Bis(tert-butoxycarbonyl)-1-(3,4-didecylphenyl)- hydrazine 4.56

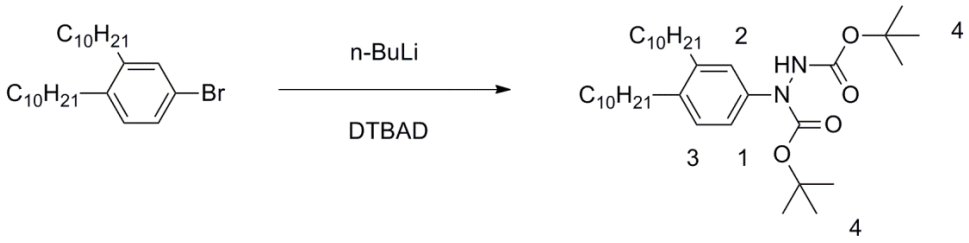

Figure 7.34 Preparation of 6.3.3.2.6 1,2-bis(tert-butoxycarbonyl)-1-(3,4-didecyloxyphenyl)-hydrazine **4.56**.

Preparation of 1,2-bis(tert-butoxycarbonyl)-1-(3,4- didecyloxyphenyl)-hydrazine was carried out following literature procedure.[135] To a solution of 3,4-didecyl bromobenzene (0.9 g, 2.1 mmol) in dry THF (150 ml), n-BuLi (2.5 M in hexane, 4.1 mmol) was added under N_2 at -78 °C. The mixture was stirred at -78 °C for 1.5 h. Then a solution of DTBAD (0.6 g, 2.5 mmol) in dry THF was added dropwise. The mixture was stirred at -78 °C for 0.5 h, then 1 h at room temperature. Then the mixture was quenched with 5% HCl. The mixture was extracted with ether, and the organic layers were combined together, dried by Na_2SO_4. The solvent was removed under reduced pressure, and the residue was purified by column chromatography (petroleum ether : DCM = 1 : 1, R_f = 0.1, then pure DCM R_f = 0.4) to give white solid. Yield: 55%.

^{1}H-NMR (400 MHz; $CDCl_3$): δ 7.21 (dd, J = 8, 2 Hz, 1H, H^1), 7.04-7.08(m, 2H, H^2, H^3), 2.50-2.56 (m, 4H, CH_2) 1.48-1.60 (m, 4H, CH_2CH_2), 1.50 (S, 18H, H^4), 1.39-1.21 (m, 28H, CH_2), 0.88 (t, J = 7 Hz, 6H, CH_3)

MS (ESI): m/z 589.4944 ([M+H]$^+$, 100%)

Spectroscopic data consistent with those reported in the literature.[197]

7.5.2.11 4-Decyloxy nitrobenzene 4.59

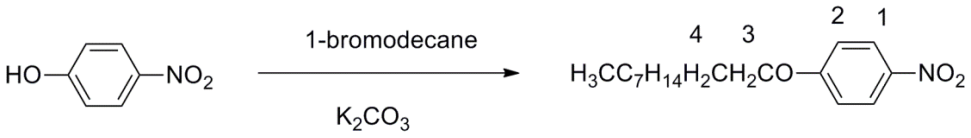

Figure 7.35 Preparation of 4-decyloxy nitrobenzene **4.59**.

Preparation of 4-decyloxy nitrobenzene was carried out following literature procedure.[142] To a solution of 4-hydroxy nitrobenzene (5 g, 36 mmol) and 1-bromodecane (9.5 g, 43 mmol) in butanone (150 ml), potassium carbonate (24.8 g, 180 mmol) was added. Then the mixture was refluxed overnight. After that, undissolved solid was removed by filtration. The solvent was removed under reduced pressure. Recrystallization from ethanol gave white solid. Yield: 87%.

^{1}H-NMR (400 MHz; $CDCl_3$): δ 8.20 (d, J = 9 Hz, 2H, H^1), 6.94(d, 2H, H^2), 4.04 (t, J = 7 Hz, 2H, H^3) 1.78-1.85 (m, 2H, H^4), 1.40-1.29 (m, 14H, CH_2), 0.88 (t, J = 7 Hz, 3H, CH_3)

MS (ESI): m/z 280.1913 ([M+H]$^+$, 100%)

Spectroscopic data consistent with those reported in the literature.[142]

7.5.2.12 4-Decyloxy aniline 4.60

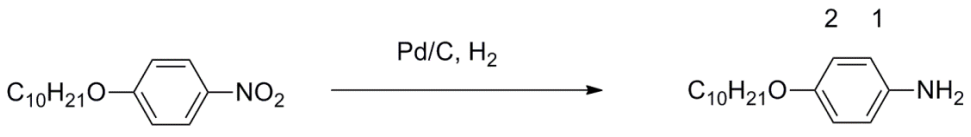

Figure 7.36 Preparation of 4-decyloxy aniline **4.60**.

Preparation of 4-decyloxy aniline was carried out following literature procedure.[142] To a solution of 4-decyloxy nitrobenzene (1 g, 3.6 mmol) in dry THF (20 ml), palladium on carbon (10 wt. % 100 mg) was added. Then the mixture was stirred overnight at room temperature under hydrogen atmosphere. The mixture was filtered. The solvent was removed under reduced pressure. The residue was purified by column chromatography to get white solid (petroleum ether : ethyl acetate = 5 : 1, R_f = 0.5). Yield: 92%.

^{1}H-NMR (400 MHz; $CDCl_3$): δ 6.73 (d, J = 9 Hz, 2H, H^1), 6.67(d, J = 9 Hz, 2H, H^2), 3.88 (t, J = 7 Hz, 2H, OCH_2) 1.70-1.77 (m, 2H, OCH_2CH_2), 1.46-1.21 (m, 14H, CH_2), 0.88 (t, J = 7 Hz, 3H, CH_3)

MS (ESI): m/z 250.2170 ($[M+H]^+$, 100%)

Spectroscopic data consistent with those reported in the literature.[142]

7.5.2.13 1-Bromo-4-decyloxybenzene 4.63

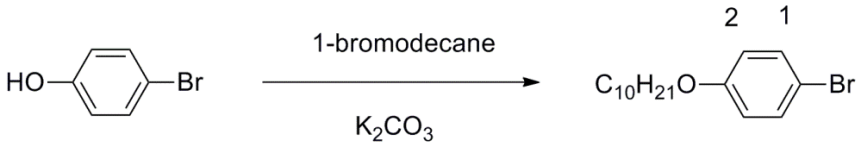

Figure 7.37 Preparation of 1-bromo-4-decyloxybenzene **4.63**.

To a solution of 4-bromopheno (10 g, 58.2 mmol) and 1-bromodecane (14.2 g, 64 mmol) in butanone, potassium carbonate (22.13 g, 160 mmol) was added. The mixture was reflux for 3 days, and then undissolved solid was removed by filtration. The solvent was removed under reduced pressure. Recrystallization from ethanol gave white solid. Yield: 73%.

^{1}H-NMR (400 MHz; $CDCl_3$): δ 7.36 (d, J = 9 Hz, 2H, H^1), 6.78(d, J = 9 Hz, 2H, H^2), 3.91 (t, J = 7 Hz, 2H, OCH_2) 1.72-1.79 (m, 2H, OCH_2CH_2), 1.47-1.20 (m, 14H, CH_2), 0.88 (t, J = 7 Hz, 3H, CH_3)

MS (ESI): m/z 313.1167 ($[M+H]^+$, 100%)

7.5.2.14 1,2-Bis(tert-butoxycarbonyl)-1-(4-decylphenyl)hydrazine 4.64

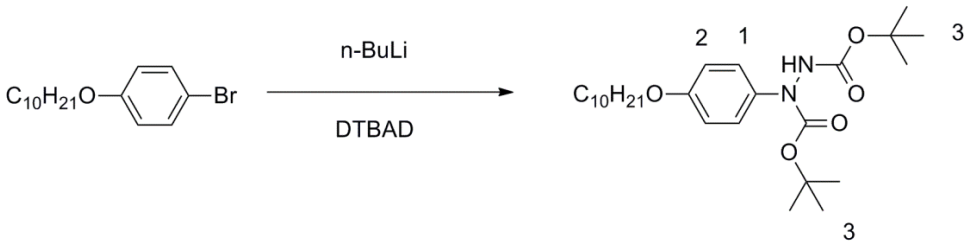

Figure 7.38 Preparation of 1,2-bis(tert-butoxycarbonyl)-1-(4-decylphenyl)hydrazine **4.64**.

To a solution of 4-decyl bromobenzene (1.8 g, 5.8 mmol) in dry THF (200 ml), n-BuLi (2.5 M in hexane, 11.6 mmol) was added under N_2 at -78 °C. The mixture was stirred at -78 °C for 1.5 h. Then a solution of DTBAD (1.6 g, 7 mmol) in dry THF was added dropwise. The mixture was stirred at -78 °C for 0.5 h, then 1 h at room temperature. Then the mixture was quenched with 5% HCl. The mixture was extracted with ether (3 × 50 ml), and the organic layers were combined together, dried by Na_2SO_4. The solvent was removed under reduced pressure, and the residue was purified by column chromatography (petroleum ether : DCM = 1 : 1, then pure DCM) to give white solid. Yield: 51%.

^{1}H-NMR (400 MHz; $CDCl_3$): δ 7.24-7.35 (b, 2H, H^1), 6.82(d, J = 8 Hz, 2H, H^2), 3.92 (t, 2H, OCH_2) 1.72-1.79 (m, 2H, OCH_2CH_2), 1.47 (S, 18H, H^3), 1.54-1.24 (m, 14H, CH_2), 0.88 (t, J = 7 Hz, 3H, CH_3)

MS (ESI): m/z 465.3319 ($[M+H]^+$, 100%)

7.5.2.15 4-Decyloxy phenylhydrazine 4.61

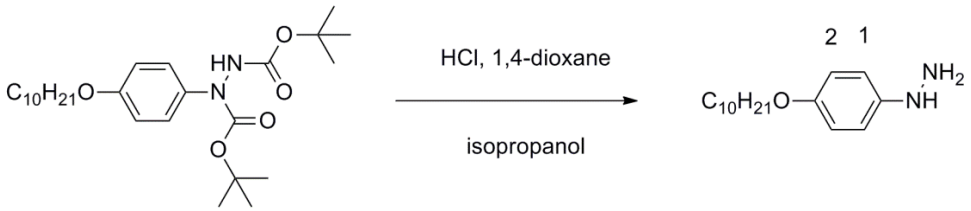

Figure 7.39 Preparation of 4-decyloxy phenylhydrazine **4.61**.

To a solution fo 1,2-bis(tert-butoxycarbonyl)-1-(4-decylphenyl)hydrazine (200 mg, 0.43 mmol) in isopropanol (5 ml), a solution of concentrated HCl (20 ml) in 1,4-dixoane (5 ml) was added. Then the mixture was refluxed for 1 h. After that, the mixture was cooled to room temperature. Ether (60 ml) was added to the mixture. The precipitate was collected by filtration, washed with ether (3 × 5 ml), dried in a vacuum oven to get white solid. The pure product cannot be isolated due to large amount of impurities.

MS (ESI): m/z 265.2267 ($[M+H]^+$)

7.5.2.16 Decyloxy-4-hydrazinylbenzoate 4.66.

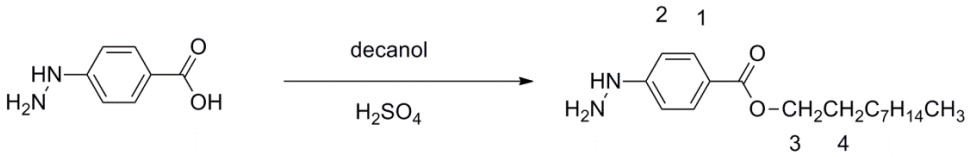

Figure 7.40 Preparation of decyloxy-4-hydrazinylbenzoate **4.66**.

4-Benzoic acid hydrazine (5 g, 33 mmol) was added to decanol (50 ml). To this mixture, concentrated H_2SO_4 (2.5 g) was added. Then the mixture was refluxed overnight. The precipitate was collected, washed with ether (3 × 20 ml). Then the solid was dissolved in triethylamine (30 ml). Diethyl ether (30 ml) was added, then the mixture was washed with

water (3 × 20 ml), dried by $MgSO_4$. The solvent was removed under reduced pressure, the residue was purified by column chromatography (petroleum ether : ethyl acetate = 1 : 1) to give a white solid. Yield: 82%.

^{1}H-NMR (400 MHz; $CDCl_3$): δ 7.92 (d, J = 9 Hz, 2H, H^1), 6.79 (d, 2H, H^2), 4.26 (t, J = 7 Hz, 2H, H^3) 1.68-1.75 (m, 2H, OCH_2CH_2), 1.40-1.03 (m, 14H, CH_2), 0.88 (t, J = 7 Hz, 3H, CH_3).

^{13}C-NMR (400 MHz; $CDCl_3$): δ 166.7, 154.5, 131.3, 120.6, 110.6, 64.6, 31.9, 29.5, 29.3,28.8, 26.0, 22.7, 14.1.

MS (ESI): m/z 293.2217 ($[M+H]^+$, 100%)

7.5.3 1-Phenyl-2-(4-decyloxybenzyl)hydrazine 4.33

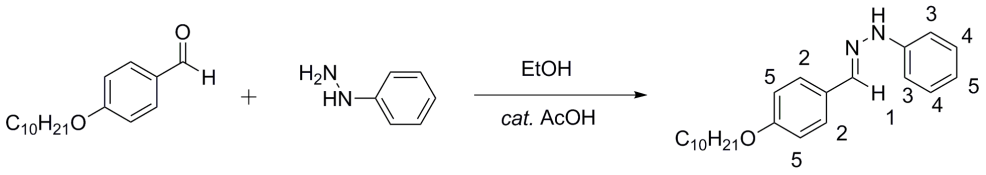

Figure 7.41 Preparation of 1-phenyl-2-(4-decyloxybenzyl)hydrazine **4.33**.

To a solution of 4-decyloxybenzaldehyde (123 mg, 0.47 mmol) in ethanol (20 ml), phenylhydrazine (56 mg, 0.51 mmol) and catalytic amount of AcOH were added under nitrogen atmosphere. Then the mixture was stirred at room temperature for 3 h. Then the solvent was removed, recrystallization from ethanol gave white solid. Yield: 67%.

^{1}H-NMR (400 MHz; $CDCl_3$): δ 7.59 (s, 1H, H^1), 7.51(d, J = 8 Hz, 2H, H^2), 7.18-7.21 (m, 2H, H^3) 7.02 (d, J = 8 Hz, 2H, H^4), 6.79-6.83 (m, 3H, H^5), 3.89 (t, J = 7 Hz, 2H, OCH_2), 1.68-1.74 (m, 2H, OCH_2CH_2), 1.48-1.18 (m, 14H, CH_2), 0.81 (t, J = 7 Hz, 3H, CH_3)

MS (ESI): m/z 353.2593 ([M+H]$^+$, 100%)

7.5.4 *N*-Phenyl-4-decyloxybenzohydrazonoyl chloride 4.34

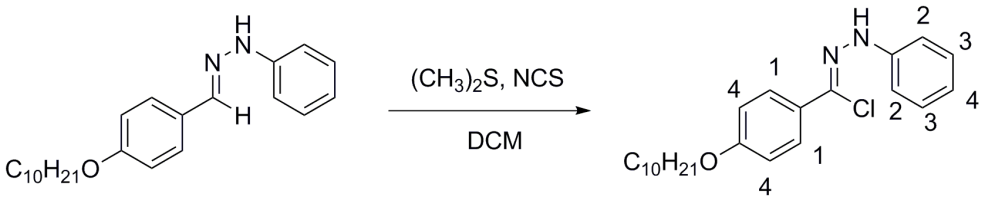

Figure 7.42 Preparation of *N*-phenyl-4-decyloxybenzohydrazonoyl chloride **4.34**.

To a solution of NCS (0.6 g, 4.3 mmol) in DCM (50 ml), dimethyl sulfide (0.5 g, 8.5 mmol) was added at 0 °C, and then the reaction mixture was cooled to -78 °C. To this reaction mixture, a solution of 1-phenyl-2-(4-decyloxybenzyl)hydrazine (1 g, 2.8 mmol) in DCM was added and the mixture was stirred for 1 h. Then the mixture was allowed to warm to room temperature and stirred for 2 h, then quenched with water, extracted with DCM (3 × 50 ml). The organic layers were combined together, washed with brine, and dried with $MgSO_4$. The solvent was removed under reduced pressure, and recrystallization from hexane gave light yellow solid. Yield: 52%.

^{1}H-NMR (400 MHz; $CDCl_3$): δ 7.76 (d, J = 8 Hz, 2H, H^1), 7.19-7.25 (m, 2H, H^2) 7.08 (d, J = 8 Hz, 2H, H^3), 6.81-6.87 (m, 3H, H^4), 3.92 (t, J = 7 Hz, 2H, OCH_2), 1.69-1.75 (m, 2H, OCH_2CH_2), 1.48-1.18 (m, 14H, CH_2), 0.81 (t, J = 7 Hz, 3H, CH_3)

MS (ESI): m/z 387.2203 ([M+H]$^+$, 100%).

7.5.5 *N*, *N'*-diphenyl-4-decyloxybenzohydrazonamide 4.35

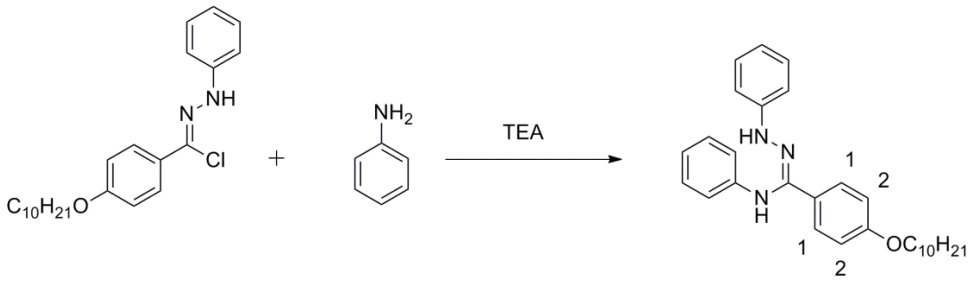

Figure 7.43 Preparation of *N*, *N'*-dihenyl-4-decyloxybenzohydrazonamide **4.35**.

To a solution of *N*-phenyl-4-decyloxybenzohydrazonoyl chloride (118 mg, 0.3 mmol) in dry THF (10 ml), a solution of aniline (34 mg, 0.4 mmol) and TEA (0.2 ml) in dry THF (5 ml) was added. The reaction mixture was stirred at room temperature overnight under nitrogen atmosphere. Then the reaction mixture was poured into water (50 ml), extracted with DCM (3 × 50 ml). The organic layers were combined together, washed with brine, and dried with $MgSO_4$. The residue was purified by column chromatography to get pale yellow solid (petroleum ether : ethyl acetate = 20 : 1, R_f = 0.3). Yield: 40%.

^{1}H-NMR (400 MHz; $CDCl_3$): δ 7.76 (d, J = 8 Hz, 2H, H^1), 7.21-7.28 (m, 5H, aromatic protons) 7.08-7.12 (m, 2H, aromatic protons), 6.84-6.93 (m, 4H, aromatic protons), 6.72 (d, J = 8 Hz, 2H, H^2), 3.96 (t, J = 7 Hz, 2H, OCH_2), 1.74-1.81 (m, 2H, OCH_2CH_2), 1.48-1.22 (m, 14H, CH_2), 0.88 (t, J = 7 Hz, 3H, CH_3)

MS (ESI): m/z 444.3015 ($[M+H]^+$, 100%)

7.5.6 1-Phenyl-3-(4-decyloxyphenyl)-1,2,3-benzotriazin-4-yl 4.30

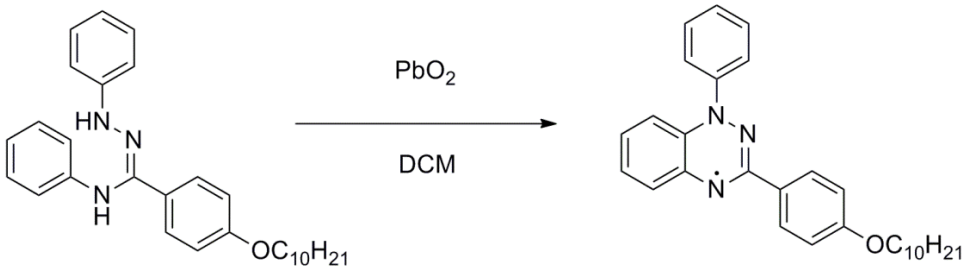

Figure 7.44 Preparation of 1-Phenyl-3-(4-decyloxyphenyl)-1,2,3-benzotriazin-4-yl **4.30**.

To a solution of *N*, *N'*-dihenyl-4-decyloxybenzohydrazonamide (100 mg, 0.2 mmol) in DCM (10 ml), lead dioxide (100 mg) was added. The mixture was stirred at room temperature for 3 h. Then the undissolved solid was removed by filtration, the solvent was removed under reduced pressure. The residue was purified by column chromatography (petroleum ether : ethyl acetate = 18 : 1, R_f = 0.3). Yield: 55%.

MS (ESI): m/z 441.2752 ($[M+H]^+$, 100%)

EPR: a_{N1} = 7.63 G, a_{N2} = 4.80 G, a_{N3} = 5.16 G.

7.5.7 *N*-phenyl-*N'*-(*p*-heptylphenyl)-4-decyloxybenzo- hydrazonamide

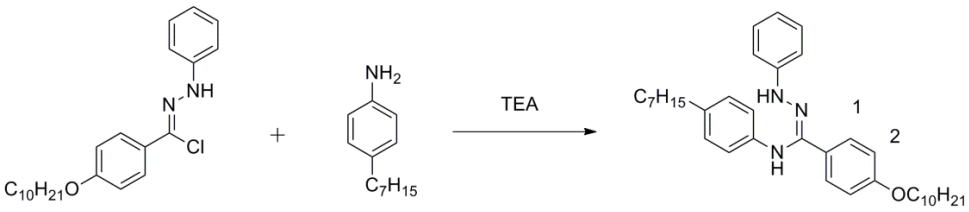

Figure 7.45 Preparation of *N*-phenyl-*N'*-(*p*-heptylphenyl)-4-decyloxybenzo hydrazonamide

To a solution of *N*-phenyl-4-decyloxybenzohydrazonoyl chloride (50 mg, 0.13 mmol) in dry THF

(10 ml), a solution of 4-heptyl aniline (123.6 mg, 0.65 mmol) and TEA (0.5 ml) in dry THF (5 ml) was added. The reaction mixture was stirred at room temperature overnight under nitrogen atmosphere. Then the reaction mixture was poured into water (50 ml), extracted with DCM (3 × 20 ml). Then organic layers were combined together, washed with brine, dried with $MgSO_4$. The solvent was removed under reduced pressure, the residue was purified by column chromatography to get pale yellow solid (petroleum ether : ethyl acetate = 15 : 1, R_f = 0.3). Yield: 38%.

^{1}H-NMR (400 MHz; $CDCl_3$): δ 7.64 (d, J = 8 Hz, 2H, H^1), 7.23-7.28 (m, 2H, aromatic protons) 7.03-7.10 (m, 4H, aromatic protons), 6.83-6.98(m, 3H, aromatic protons), 6.64 (d, J = 8 Hz, 2H, H^2), 3.96 (t, J = 7 Hz, 2H, OCH_2), 1.74-1.81 (m, 2H, OCH_2CH_2), 1.62-1.20 (m, 26H, CH_2), 0.85-0.90 (m, 6H, CH_3)

MS (ESI): m/z 542.4106 ($[M+H]^+$, 100%)

7.5.8 1-Phenyl-3-(4-decyloxyphenyl)-7-heptyl-1,2,3- benzotriazin-4-yl

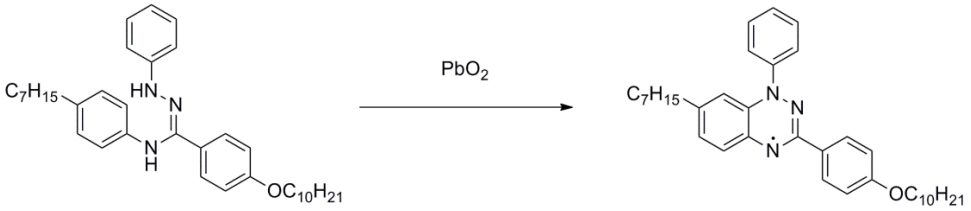

Figure 7.46 Preparation of 1-Phenyl-3-(4-decyloxyphenyl)-7-heptyl-1,2,3- benzotriazin-4-yl.

To a solution of *N*-phenyl-*N'*-(*p*-heptylphenyl)-4-decyloxybenzo hydrazonamide (30 mg, 0.06 mmol) in DCM (10 ml), lead dioxide (100 mg) was added. The mixture was stirred at room temperature for 3 h. Then the undissolved solid was removed by filtration, the solvent was removed under reduced pressure. The residue was purified by column chromatography (petroleum ether : ethyl acetate = 18 : 1, R_f = 0.3). Yield: 45%.

MS (ESI): m/z 539.3875 ([M+H]$^+$, 100%)

EPR: a_{N1} = 7.81 G, a_{N2} = 4.74 G, a_{N3} = 5.24 G.

7.5.9 *N-p*-Decyloxybenzoate-*N'*-(3,4,5-tridecyloxybenzyl) hydrazine 4.78

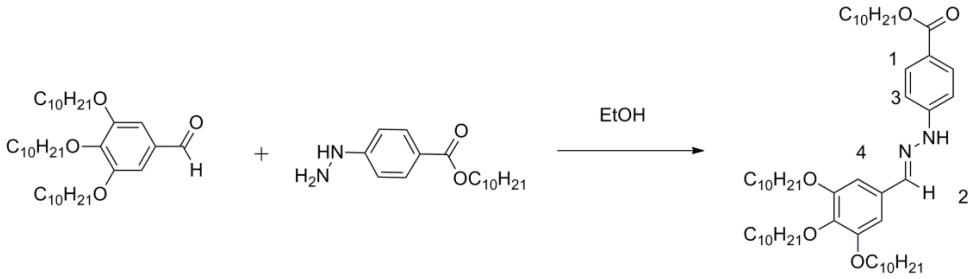

Figure 7.47 Preparation of *N-p*-decyloxybenzoate-*N'*-(3,4,5-tridecyloxybenzyl) hydrazine **4.78**.

To a solution of 3,4,5-tridecyloxybenzaldehyde (500 mg, 0.87 mmol) and decyloxy-4-hydrazinylbenzoate (509 mg, 1.74 mmol) in ethanol (40 ml), catalytic amount of AcOH were added under nitrogen atmosphere. Then the mixture was stirred at room temperature for 3 h under nitrogen. Then the solvent was removed, the residue was purified by column chromatography to give white solid (petroleum ether : ethyl acetate = 9 : 1, R_f = 0.4). Yield: 66%.

^{1}H-NMR (400 MHz; $CDCl_3$): δ 7.98 (d, J = 8 Hz, 2H, H^1), 7.62 (s, 1H, H^2), , 7.10 (d, 2H, J = 8 Hz, H^3) 6.86 (s, 2H, H^4), 4.27 (t, J = 7 Hz, 2H, OCH_2), 4.03 (t, J = 7 Hz, 4H, OCH_2), 4.00 (t, J = 7 Hz, 2H, OCH_2), 1.71-1.86 (m, 8H, OCH_2CH_2), 1.54-1.20 (m, 56H, CH_2), 0.88 (t, J = 7 Hz, 12H, CH_3)

^{13}C-NMR (400 MHz; CDCl3): δ 166.7, 153.4, 148.1, 139.5, 131.4, 129.7, 121.4, 111.7, 104.9, 73.5, 69.1, 64.6, 32.0, 30.4, 29.8,29.8, 29.7, 29.7, 29.5, 29.4, 29.4, 28.9, 26.2, 26.2, 26.1, 22.8, 14.2

MS (MALDI): m/z 849.7026 ([M+H]$^+$, 100%)

7.5.10 *N*-(*p*-Decyloxybenzoate)-3,4,5-tridecyloxybenzohydrazonoyl chloride 4.79

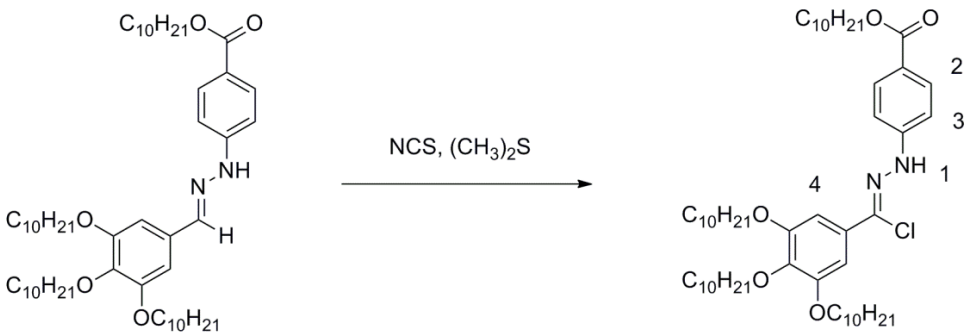

Figure 7.48 Preparation of *N*-(*p*-Decyloxybenzoate)-3,4,5-tridecyloxybenzohydrazonoyl chloride **4.79**.

To a solution of NCS (63 mg, 0.47 mmol) in DCM (50 ml), dimethyl sulfide (59 mg, 0.94 mmol) was added at 0 °C, and then the reaction mixture was cooled to -78 °C. To this reaction mixture, a solution of *N*-*p*-decyloxybenzoate-*N'*-(3,4,5- tridecyloxybenzyl)hydrazine (200 mg, 0.23 mmol) was added and the mixture was stirred for 1 h. Then the mixture was allowed to warm to room temperature and stirred for 2 h. Then the mixture was quenched with water, extracted with DCM (3 × 20 ml). The organic layers were combined together, washed with brine and dried with $MgSO_4$. The solvent was removed under reduced pressure, and the residue was purified by column chromatography (petroleum ether : ethyl acetate = 3 : 1). Yield: 43%.

^{1}H-NMR (400 MHz; $CDCl_3$): δ 8.21 (s, 1H, H^1), 8.02 (d, J = 8 Hz, 2H, H^2), 7.16 (d, 2H, J = 8 Hz, H^3) 7.14 (s, 2H, H^4), 4.29 (t, J = 7 Hz, 2H, OCH_2), 4.05 (t, J = 7 Hz, 4H, OCH_2), 4.00 (t, J = 7 Hz, 2H, OCH_2), 1.72-1.87 (m, 8H, OCH_2CH_2), 1.54-1.20 (m, 56H, CH_2), 0.88 (t, J = 7 Hz, 12H, CH_3)

^{13}C-NMR (400 MHz; CDCl3): δ 167.0, 153.4, 147.2, 140.4, 131.7, 129.1, 127.2, 123.0, 112.7, 105.7, 73.5, 69.2, 64.7, 31.7, 30.0, 29.5,29.4, 29.3, 29.2, 29.1, 29.0, , 28.5, 25.8, 25.8, 22.4, 22.4, 13.8

MS (MALDI): m/z 883.6670 ([M+H]$^+$, 100%)

7.5.11

1-(*p*-Decyloxybenzoate)-3-(3,4,5-tridecyloxyphenyl)-6,7-didecyloxyl-1,2,3-benzotriazin-4-yl 4.67.

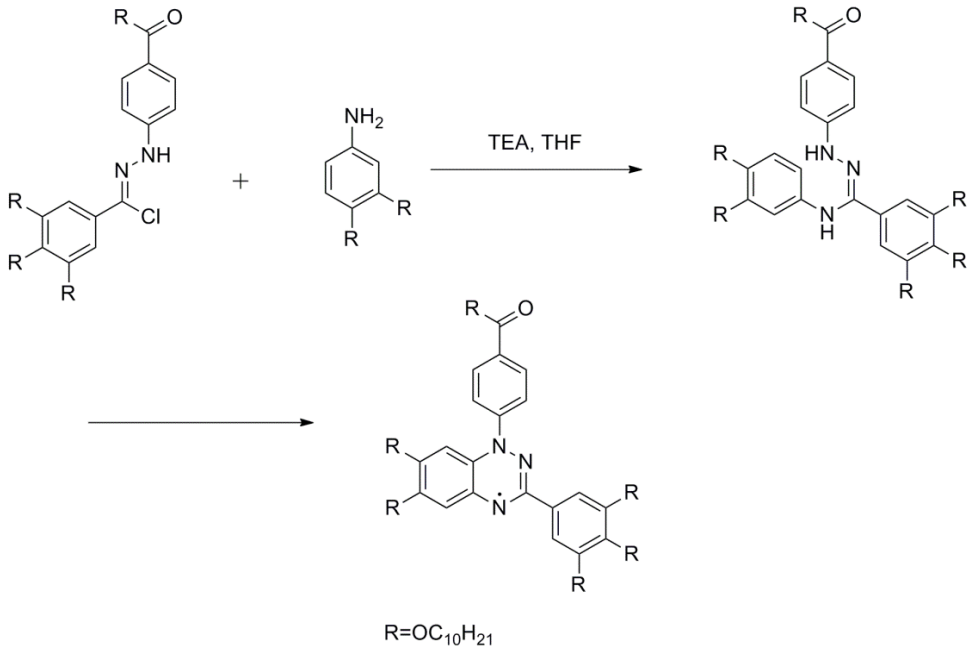

Figure 7.49 Preparation of 1-(p-Decyloxybenzoate)-3-(3,4,5-tridecyloxyphenyl)-6,7-didecyloxyl-1,2,3-benzotriazin-4-yl **4.67**.

To a solution of benzohydrazonoyl chloride **4.79** (100 mg, 0.11 mmol) in dry THF (10 ml), a solution of 3,4-dedecyloxy aniline (92.3 mg, 0.23 mmol) and TEA (0.5 ml) in dry THF (5 ml) was added. The reaction mixture was stirred at room temperature for 2 days under nitrogen atmosphere. Then the reaction mixture was poured into water (15 ml), extracted with DCM (3 × 20 ml). The organic layers were combined together, washed with brine, dried with $MgSO_4$. The residue was purified by column chromatography to get brown solid (petroleum ether : ethyl acetate = 15 : 1, R_f = 0.6). Yield: 29%.

MS (ESI): m/z 1249.0170 ([M]$^+$, 100%)

EPR: a_{N1}= 6.94 G, a_{N1}= 4.80 G a_{N1}= 4.32 G

Analysis for $C_{80}H_{134}N_3O_8$. Calcd (%): C 76.87 H 10.81 N 3.36; found: C 77.23 H 11.01 N 2.96.

7.5.12 Preparation of 3,4,5-tridecyloxy aniline.

7.5.12.1 1,2,3-Tridecyloxy benzene 4.75b

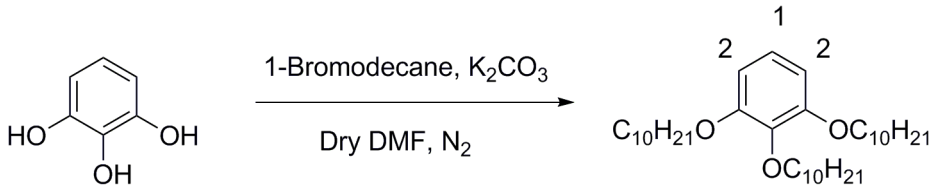

Figure 7.50 Preparation of 1,2,3-tridecyloxy benzene **4.75b**.

Preparation of 4-decyloxy aniline was carried out following literature procedure.[142] To a solution of 1,2,3-benzenetriol (2 g, 15.9 mmol) and 1-bromodecane (11.52 g, 52.3 mmol) in dry DMF (100 ml), potassium carbonate (8.8 g, 63.4 mmol) was added under nitrogen atmosphere. Then the mixture was stirred overnight at 80 °C under nitrogen. Then the mixture was filtered, the solvent was removed under reduced pressure, the residue was purified by column chromatography (petroleum ether : ethyl acetate = 25 : 1, R_f = 0.4). Yield : 65%.

^{1}H-NMR (400 MHz; $CDCl_3$): δ 6.92 (t, J = 8 Hz, 1H, H^1), 6.55 (d, J = 8 Hz, 2H, H^2), 3.97 (t, J = 7 Hz, 4H, OCH_2), 3.95 (t, J = 7 Hz, 2H, OCH_2), 1.71-1.83 (m, 6H, OCH_2CH_2), 1.50-1.20 (m, 42H, CH_2), 0.88 (t, J = 7 Hz, 9H, CH_3)

MS (ESI): m/z 547.5071 ([M+H]$^+$, 100%)

Spectroscopic data consistent with those reported in the literature.[142]

7.5.12.2 3,4,5-Tridecyloxy nitrobenzene 4.76b

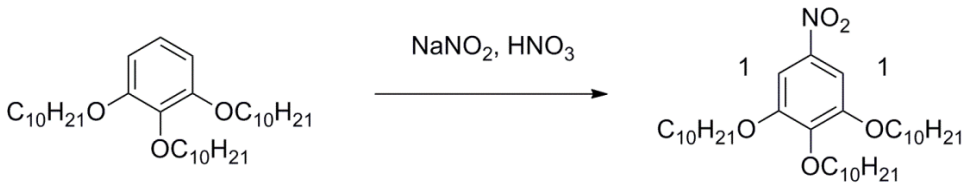

Figure 7.51 Preparation of 3,4,5-tridecyloxy nitrobenzene **4.76b**.

Preparation of 4-decyloxy aniline was carried out following literature procedure.[142] To a solution of 1,2,3-tridecyloxybenzene (4.29 g, 7.8 mmol) in DCM (50 ml), sodium nitrite (75.8 mg, 1.1 mmol) was added at 0 °C. To this ice-cooled suspension, a solution of concentrated HNO_3 (1.1 ml, 23.5 mmol) in DCM (10 ml) was added slowly. Then the mixture was stirred at room temperature for 2 h. After that, the mixture was poured into water (100 ml), and then extracted with DCM (3 × 50 ml). The organic layers were combined together, and washed with 5% aqueous $NaHCO_3$, water and brine, then dried by Na_2SO_4. The solvent was removed under reduced pressure, and the residue was purified by column chromatography to give light yellow solid (petroleum ether : DCM = 1 : 1, R_f = 0.4). Yield: 56%.

^{1}H-NMR (400 MHz; $CDCl_3$): δ 7.48 (s, 2H, H^1), 4.06 (t, J = 7 Hz, 2H, OCH_2), 4.03 (t, J = 7 Hz, 4H, OCH_2), 1.87-1.70 (m, 6H, OCH_2CH_2), 1.52-1.21 (m, 42H, CH_2), 0.88 (t, J = 7 Hz, 9H, CH_3)

MS (ESI): m/z 614.4749 ([M+Na]$^+$, 100%)

Spectroscopic data consistent with those reported in the literature.[142]

7.5.12.3 3,4,5-Tridecyloxy anline 4.77b.

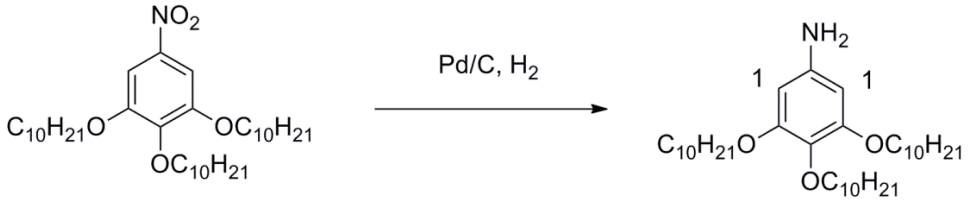

Figure 7.52 Preparation of 3,4,5-tridecyloxy aniline **4.77b**.

Preparation of 4-decyloxy aniline was carried out following literature procedure.[142] To a solution of 3,4,5-tridecyloxy nitrobenzene (460 mg, 0.78 mmol) in dry THF (20 ml), palladium on carbon (10 wt.% 40 mg) was added. Then the mixture was stirred overnight at room temperature under hydrogen atmosphere. The mixture was filtered. The solvent was removed under reduced pressure. The residue was purified by column chromatography to get white solid (petroleum ether : ethyl acetate = 4 : 1, R_f = 0.5). Yield: 90%.

^{1}H-NMR (400 MHz; $CDCl_3$): δ 5.92 (s, 2H, H^1), 3.91(t, J = 7 Hz, 4H, OCH_2), 3.84 (t, J = 7 Hz, 2H, OCH_2) 1.64-1.80 (m, 6H, OCH_2CH_2), 1.48-1.21 (m, 42H, CH_2), 0.88 (t, J = 7 Hz, 9H, CH_3)

MS (ESI): m/z 562.5175 ($[M+H]^+$, 100%)

Spectroscopic data consistent with those reported in the literature.[142]

7.5.13

1-(*p*-Decyloxybenzoate)-3-(3,4,5-tridecyloxyphenyl)-6,7,8-tridecyloxyl-1,2,3-benzotriazin-4-yl 4.94.

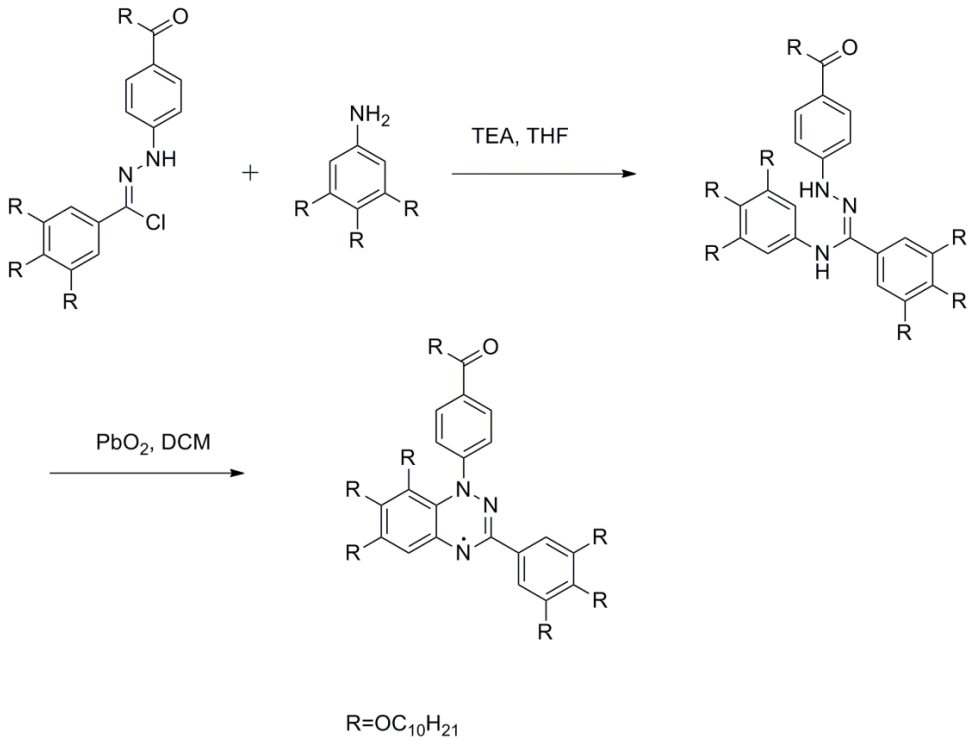

Figure 7.53 Preparation of 1-(p-Decyloxybenzoate)-3-(3,4,5-tridecyloxyphenyl)-6,7,8-tridecyloxyl-1,2,3-benzotriazin-4-yl **4.94**.

To a solution of benzohydrazonoyl chloride **4.79** (100 mg, 0.11 mmol) in dry THF (10 ml), a solution of 3,4,5-tridecyloxy aniline (129 mg, 0.23 mmol) and TEA (0.5 ml) in dry THF (5 ml) was added. The reaction mixture was stirred at room temperature for 2 days under nitrogen atmosphere. Then the reaction mixture was poured into water (15 ml), extracted with DCM (3 × 20 ml). The organic layers were combined together, and washed with brine, dried with $MgSO_4$. The residue was purified by column chromatography to get brown solid (petroleum ether : ethyl acetate = 20 : 1, R_f = 0.4). Yield: 31%.

MS (ESI): m/z 1406.1729 ($[M+H]^+$, 100%)

EPR: a_{N1}= 6.80 G, a_{N1}= 4.51 G a_{N1}= 4.61 G

Analysis for $C_{90}H_{154}N_3O_8$. Calcd (%): C 76.87 H 11.04 N 2.99; found: C 77.15 H 12.27 N 2.43.

7.5.14 2,5-Dideuterium-3,4-didecyloxy aniline 4.90.

7.5.14.1 3,6-dideuterium-1,2-didecyloxy benzene

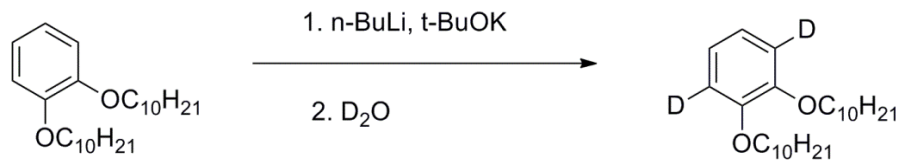

Figure 7.54 Preparation of 3,6-dideuterium-1,2-didecyloxy benzene.

To a suspension of t-BuOK (1.15 g, 10.24 mmol) in dry THF (20 ml) n-BuLi (2.5 M in hexane, 4.1 ml, 10.23 mmol) followed by 1,2-didecyloxy benzene (2 g, 5.12 mmol) in dry THF (400 ml) was added at -78 °C under nitrogen atmosphere. The mixture was stirred for 1 h. Then D_2O (5 ml) was added to the mixture at 0 °C. The mixture was stirred for 30 min. Then, pH 7 phosphate buffer was added. The mixture was extracted with DCM (3 × 50 ml). The organic layers were combined together, dried with $MgSO_4$. The solvent was removed under reduced pressure. The residue was used directly without further purification. After carrying out this deuterium exchange for 7 times, the crude product was purified by column chromatography (petroleum ether : ethyl acetate = 15 : 1, R_f = 0.5). Yield : 56%.

^{1}H-NMR (400 MHz; $CDCl_3$): δ 6.89 (s, 2H, aromatic protons), 3.99(t, J = 7 Hz, 4H, OCH_2), 1.77-1.84 (m, 4H, OCH_2CH_2), 1.50-1.21 (m, 28H, CH_2), 0.88 (t, J = 7 Hz, 6H, CH_3)

MS (ESI): m/z 415.3488 ($[M+Na]^+$, 100%)

7.5.14.2 2,5-Dideuterium-3,4-didecyloxy nitrobenzene

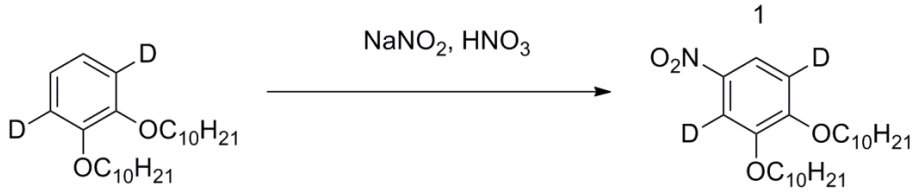

Figure 7.55 Preparation of 2,5-Dideuterium-3,4-didecyloxy nitrobenzene.

To a solution of 3,6-dideuterium-1,2-didecyloxy benzene (200 mg, 0.51 mmol) in DCM (50 ml), sodium nitrite (4.9 mg, 0.07 mmol) was added at 0 °C. To this ice-cooled suspension, a solution of concentrated HNO_3 (68 µl, 1.53 mmol) in DCM (10 ml) was added slowly. Then the mixture was stirred at room temperature for 2 h. After that, the mixture was poured into water (100 ml), and then extracted with DCM (3 × 50 ml). The organic layers were combined together, and washed with 5% aqueous $NaHCO_3$, water and brine, then dried by Na_2SO_4. The solvent was removed under reduced pressure, and the residue was purified by column chromatography to give light yellow solid (petroleum ether : DCM = 1 : 1, R_f = 0.4). Yield: 50 %.

^{1}H-NMR (400 MHz; $CDCl_3$): δ 7.88 (s, 1H, H^1), 4.08 (t, J = 7 Hz, 2H, OCH_2), 4.06 (t, J = 7 Hz, 2H, OCH_2), 1.81-1.89 (m, 4H, OCH_2CH_2), 1.51-1.22 (m, 28H, CH_2), 0.88 (t, J = 7 Hz, 6H, CH_3)

MS (ESI): m/z 460.3347 ($[M+Na]^+$, 100%)

7.5.14.3 2,5-Dideuterium-3,4-didecyloxy aniline 4.90

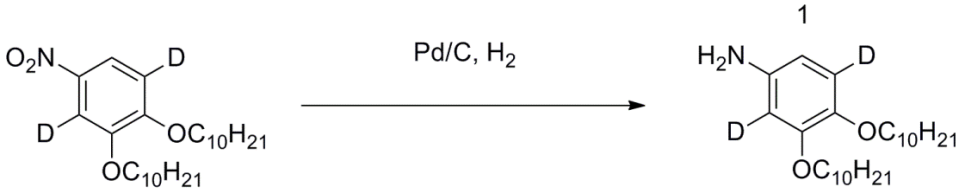

Figure 7.56 Preparation of 2,5-Dideuterium-3,4-didecyloxy aniline **4.90**.

To a solution of 2,5-dideuterium-3,4-didecyloxy nitrobenzene (100 mg, 0.23 mmol) in dry THF (20 ml), palladium on carbon (10 wt.% 20 mg) was added. Then the mixture was stirred overnight at room temperature under hydrogen atmosphere. The mixture was filtered. The solvent was removed under reduced pressure. The residue was purified by column chromatography to get white solid (petroleum ether : ethyl acetate = 4 : 1, R_f = 0.5). Yield: 90%.

^{1}H-NMR (400 MHz; $CDCl_3$): δ 6.21 (s, 1H, H^1), 3.93 (t, J = 7 Hz, 2H, OCH_2), 3.90 (t, J = 7 Hz, 2H, OCH_2), 1.71-1.83 (m, 4H, OCH_2CH_2), 1.48-1.25 (m, 28H, CH_2), 0.88 (t, J = 7 Hz, 6H, CH_3)

MS (ESI): m/z 408.3780 ($[M+H]^+$, 100%)

7.5.15 1-(*p*-Decyloxybenzoate)-3-(3,4,5-tridecyloxyphenyl)-5,8-dideuterium-6,7-didecyloxyl-1,2,3-benzotriazin-4-yl 4.91.

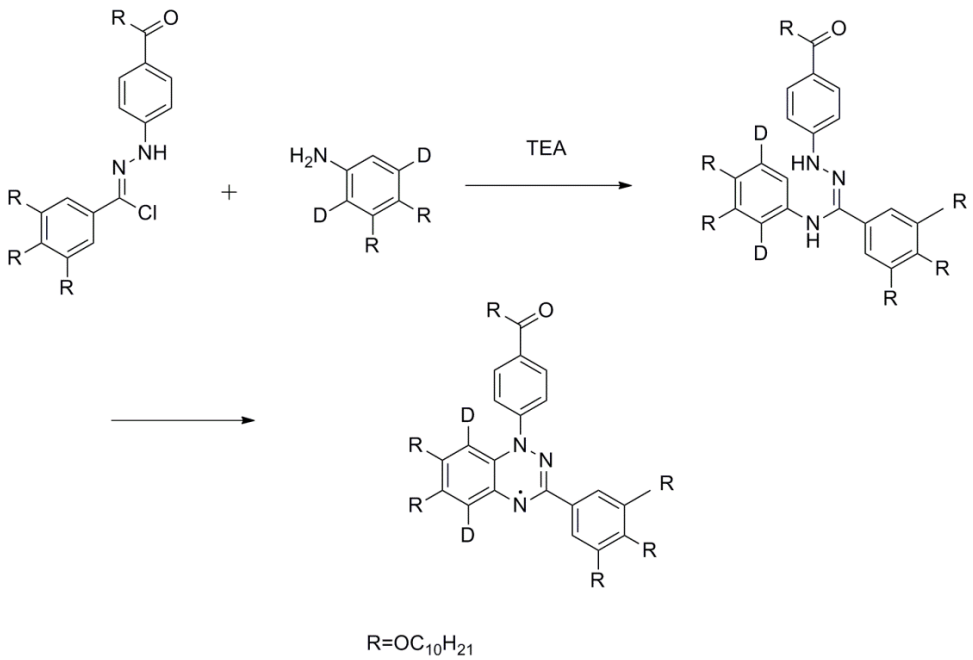

Figure 7.57 Preparation of 1-(*p*-Decyloxybenzoate)-3-(3,4,5-tridecyloxyphenyl)-5,8-dideuterium-6,7-didecyloxyl-1,2,3-benzotriazin-4-yl **4.91**.

To a solution of benzohydrazonoyl chloride **4.79** (50 mg, 0.06 mmol) in dry THF (10 ml), a solution of 2,5-dideuterium-3,4-didecyloxy aniline (47 mg, 0.12 mmol) and TEA (0.5 ml) in dry THF (5 ml) was added. The reaction mixture was stirred at room temperature for 2 days under nitrogen atmosphere. Then the reaction mixture was poured into water (15 ml), extracted with DCM (3 × 20 ml). The organic layers were combined together, washed with brine, dried with $MgSO_4$. The residue was purified by column chromatography to get brown solid (petroleum ether : ethyl acetate = 25 : 1, R_f = 0.6). Yield: 30%.

MS (ESI): m/z 1251.0325 ($[M]^+$, 100%)

EPR: a_{N1}= 6.89 G, a_{N1}= 4.56 G a_{N1}= 4.47 G

7.6 Experimental procedure from chapter 5

7.6.1 *N,N*-diphenylcarbodiimide derivatives 5.13, 5.44a and 5.44b

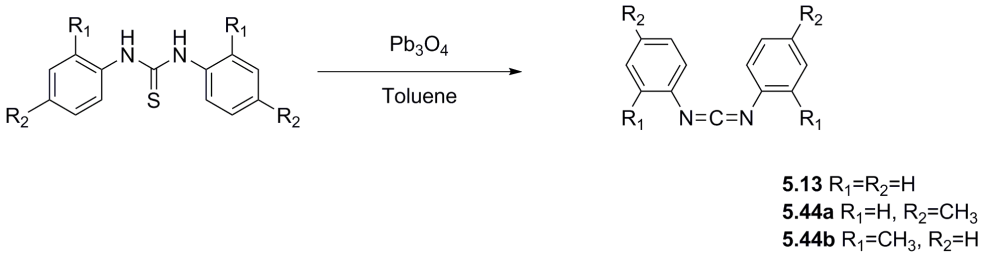

Figure 7.58 Preparation of *N*,*N*-diphenylcarbodiimide derivatives.

All the preparation of *N,N*-diphenylcarbodiimide derivatives (**5.13**, **5.44a** and **5.44b**) were carried out following literature procedure described below with the synthesis of **5.13** acting as a representative procedure.[169] Lead oxide (Pb_3O_4, 5 g, 7 mmol) was added to a solution of

diphenyl thiourea (5 g, 22 mmol) in toluene (50 ml). The mixture was refluxed until water ceased to liberate (Dean-Stark trap). Then, the mixture was filtered, and solvent was removed under reduced pressure. The residue was used for the next step without purification.

7.6.2 Triphenylaminoguanidine derivatives 5.14, 5.45a and 5.45b.

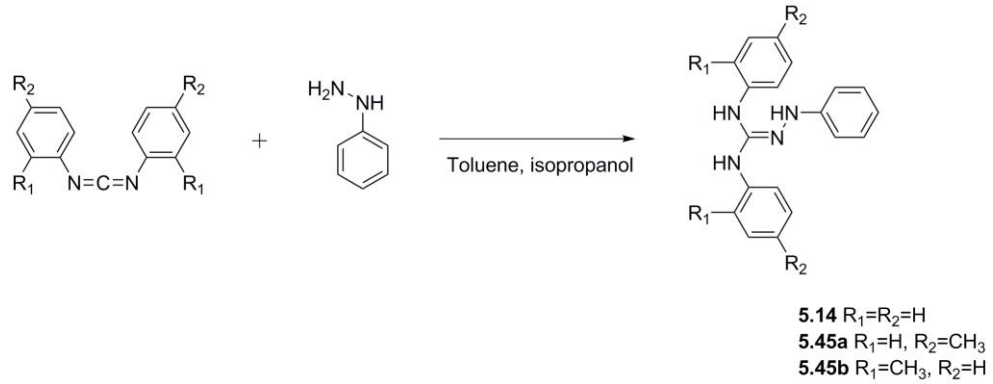

Figure 7.59 Preparation of triphenylaminoguanidine derivatives.

All the preparation of triphenylaminoguanidine derivatives (**5.14**, **5.45a** and **5.45b**) were carried out following literature procedure described below with the synthesis of **5.14** acting as a representative procedure.[169] To a solution of *N*,*N*-diphenylcarbodiimide in toluene (10 ml), 2.3 ml of phenylhydrazine was added dropwise at 0 °C. Then 30 ml of isopropanol was added to the mixture, and the resulting mixture was kept in fridge overnight. Then the crystalline product was filtered off and dried in air. The crude product was used directly for next step without further purification.

7.6.3 1,4-Diphenyl-3-phenylimino-5-propyl-1,2,4-triazole 5.25

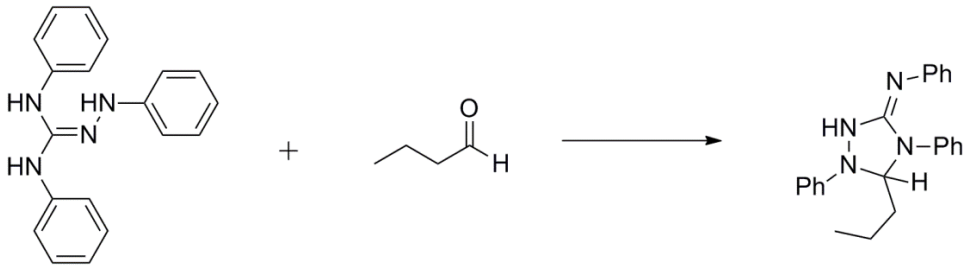

Figure 7.60 Preparation of 1,4-diphenyl-3-phenylimino-5-propyl-1,2,4-trizaole **5.25**.

To a suspension of triphenylaminoguanidine (2 g, 6.6 mmol) in isopropanol (10 ml),butylaldehyde (940 mg, 13 mmol) was added. Then the mixture was heated to 60 °C for 2 h; and then cooled to room temperature. The mixture was filtered off, washed with 10 ml isopropanol, and dried in air. Yield: 76%. The product was used directly for the next step without further purification.

7.6.4 1,4-Diphenyl-3-phenylimino-5-cyclopentyl-1,2,4-triazole 5.26

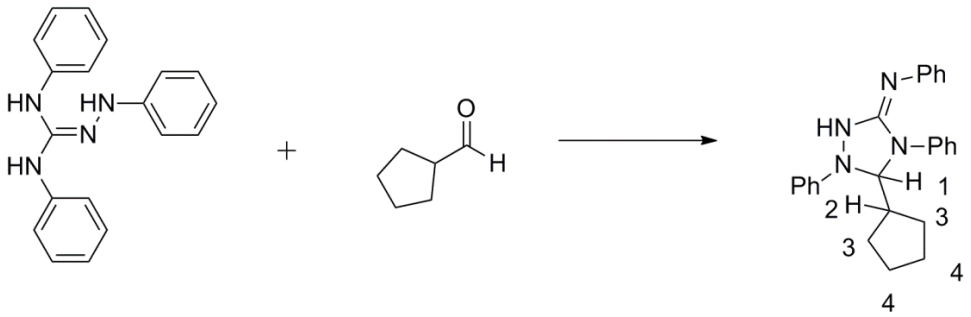

Figure 7.61 Preparation of 1,4-diphenyl-3-phenylimino-5-cyclopentyl-1,2,4-trizaole **5.26**.

To a suspension of triphenylaminoguanidine (500 mg, 1.7 mmol) in isopropanol (5 ml), cyclopentanecarboxaldehyde (400 mg, 4.1 mmol) was added. Then the mixture was heated to 70 °C for 2 h; and then cooled to room temperature. Solvent was removed, the residue was

purified by column chromatography (petroleum ether : ethyl acetate = 9 : 1, R_f = 0.4). Yield: 43%.

^{1}H-NMR (400 MHz; $CDCl_3$): δ 7.51-7.6 (m, 10H, aromatic protons), 7.38-7.36 (m, 2H, aromatic protons), 7.11-7.15 (m, 2H, aromatic protons), 6.71 (tt, J = 7, 1 Hz, 1H, aromatic protons), 5.27 (d, J = 5 Hz, 1H, H^1), 3.11 (m, 1H, H^2), 1.80-1.86 (m, 2H, H^3), 1.59-1.70 (m, 2H, H^3), 1.19-1.41 (m, 4H, H^4)

MS (ESI): m/z 383.2207 ($[M+H]^+$, 100%).

7.6.5 1,4-Diphenyl-3-phenylimino-5-propyl-1,2,4-trizazolium hydroxide 5.29

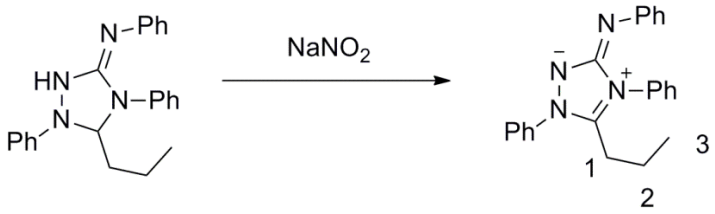

Figure 7.62 Preparation of 1,4-diphenyl-3-phenylimino-5-propyl-1,2,4-trizazolium hydroxide **5.29**.

To a suspension of 1,4-diphenyl-3-phenylimino-5-propyl-1,2,4-triazole (130 mg, 0.37 mmol) in isopropanol (0.6 ml), glacial acetic acid (0.1 ml) was added at 67 °C. Then a solution of sodium nitrite (48.8 mg, 0.7 mmol) in H_2O (110 µl) was added. The mixture was stirred for 10 min, and then 35% ammonia aqueous solution was added at 0 °C. The precipitate was collected by filtration, dried in a vacuum oven. Yield : 70%.

^{1}H-NMR (400 MHz; $CDCl_3$): δ 7.67-7.69 (m, 2H, aromatic protons), 7.42-7.60 (m, 10H, aromatic protons), 7.14-7.18 (m, 2H, aromatic protons), 6.73 (tt, J = 7, 1 Hz, 1H, aromatic protons), 2.73 (t, J = 8 Hz, 2H, H^1), 1.25-1.34 (m, 2H, H^2), 0.70 (t, J = 8 Hz, 3H, H^3).

^{13}C-NMR (400 MHz, $CDCl_3$): δ 155.9, 150.1, 145.4, 136.6, 133.3, 130.1, 129.8, 129.6, 128.4, 128.3, 125.7, 122.3, 118.3, 26.0, 20.0, 13.6.

MS (ESI): m/z 355.1895 ([M+H]$^+$, 100%).

7.6.6 1,4-Diphenyl-3-phenylimino-5-cyclopentyl-1,2,4- triazolium hydroxide 5.30

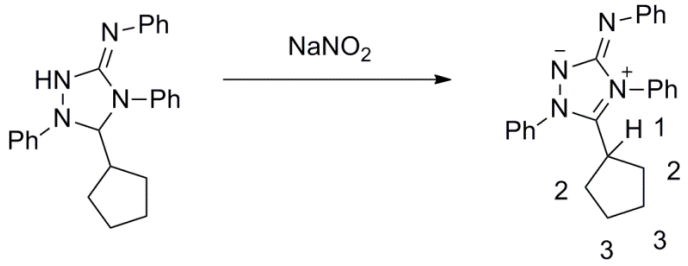

Figure 7.63 Preparation of 1,4-diphenyl-3-phenylimino-5-cyclopentyl-1,2,4- triazolium hydroxide **5.30**.

To a suspension of 1,4-diphenyl-3-phenylimino-5-cyclopentyl-1,2,4-triazole (130 mg, 0.37 mmol) in isopropanol (0.6 ml), glacial acetic acid (0.1 ml) was added at 67 °C. Then a solution of sodium nitrite (48.8 mg, 0.7 mmol) in H_2O (110 µl) was added. The mixture was stirred for 10 min, and then 35% ammonia aqueous solution was added at 0°C. The precipitate was collected by filtration, dried in a vacuum oven. Yield : 68%.

^{1}H-NMR (400 MHz; $CDCl_3$): δ 7.52-7.62 (m, 10H, aromatic protons), 7.38-7.40 (m, 2H, aromatic protons), 7.11-7.15 (m, 2H, aromatic protons), 6.71 (tt, J = 7, 1 Hz, 1H, aromatic protons), 3.11 (m 1H, H^1), 1.78-1.86 (m, 2H, H^2), 1.59-1.69 (m, 2H, H^2), 1.20-1.40 (m, 4H, H^3).

^{13}C-NMR (400 MHz, $CDCl_3$): δ 155.6, 149.0, 147.6, 136.7, 132.8, 130.7, 129.9, 129.8, 129.4, 128.4, 126.7, 121.7, 119.4, 35.6, 31.1, 25.9.

MS (ESI): m/z 381.2026 ([M+H]$^+$, 100%).

7.6.9 1,2,4-Triazole derivatives 5.46a and 5.46b.

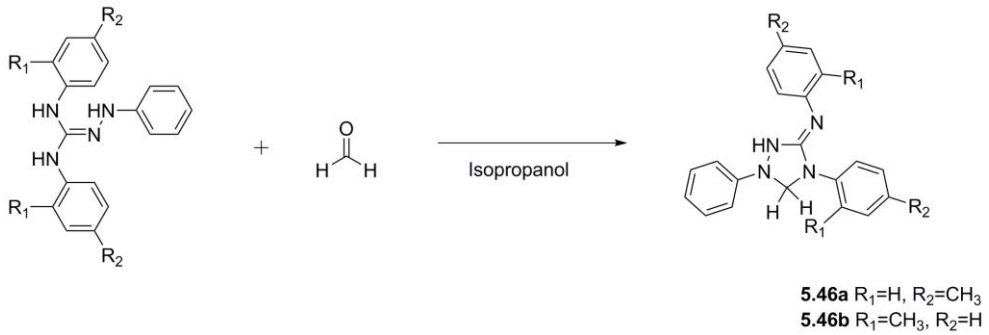

Figure 7.64 Preparation of 1,2,4-triazole derivatives **5.46a** and **5.46b**.

Preparation of 1,2,4-triazole derivatives **5.46a** and **5.46b** were carried out following the procedure described below with the synthesis of **5.46a** acting as a representative procedure. To a suspension of aminoguanidine **5.45a** (2 g, 6.6 mmol) in isopropanol (10 ml), 2 ml of 37% aqueous solution of formaldehyde was added. Then the mixture was heated to 60 °C for 2 h; and then cooled to room temperature. The mixture was filter off, washed with 10 ml isopropanol, and dried in air. The product was used directly for the next step without further purification.

5.46a: Yield: 75%. ^{1}H-NMR (400 MHz; $CDCl_3$): δ 7.20-7.34 (m, 6H, aromatic protons), 7.01-7.13 (m, 6H, aromatic protons), 6.86 (tt, J = 7, 1 Hz, 1H, aromatic protons), 5.19 (s 2H, CH_2), 2.35 (s, 3H, CH_3), 2.28 (s, 3H, CH_3).

MS (ESI): m/z 343.1899 ($[M+H]^+$, 100%).

5.46b: Yield: 79%. ^{1}H-NMR (400 MHz; $CDCl_3$): δ 7.18-7.32 (m, 6H, aromatic protons), 7.02-7.11 (m, 6H, aromatic protons), 6.92 (m, 1H, aromatic protons), 5.22 (s 2H, CH_2), 2.31 (s, 3H, CH_3), 2.23 (s, 3H, CH_3).

MS (ESI): m/z 343.1899 ($[M+H]^+$, 100%).

7.6.10 1,2,4-triazolium hydroxide derivatives 5.47a and 5.47b.

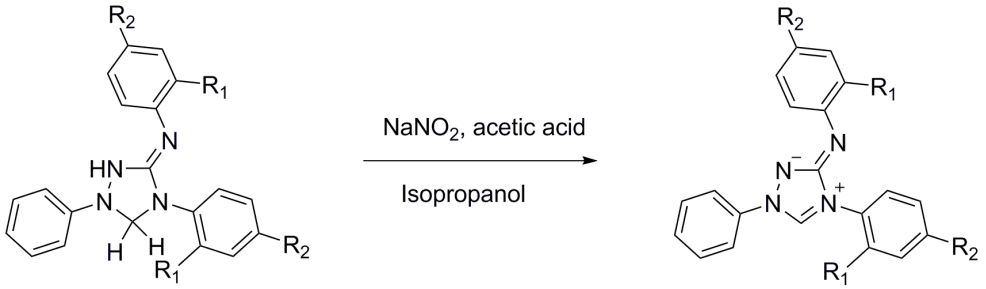

5.47a R_1=H, R_2=CH_3
5.47b R_1=CH_3, R_2=H

Figure 7.65 Preparation of 1,2,4-triazolium hydroxide derivatives **5.47a** and **5.47b**.

Preparation of 1,2,4-triazole derivatives **5.47a** and **5.47b** were carried out following the procedure described below with the synthesis of **5.47a** acting as a representative procedure. To a suspension of **5.46a** (130 mg, 0.37 mmol) in isopropanol (0.6 ml), glacial acetic acid (0.1 ml) was added at 67 °C. Then a solution of sodium nitrite (48.8 mg, 0.7 mmol) in H_2O (110 µl) was added. The mixture was stirred for 10 min, and then 35% ammonia aqueous solution was added at 0 °C. The precipitate was collected by filtration, dried in a vacuum oven.

5.47a: Yield: 63%. ^{1}H-NMR (400 MHz; $CDCl_3$): δ 6.99-7.86 (m, 14H, aromatic protons, CH), 2.25 (s, 3H, CH_3), 2.22 (s, 3H, CH_3). ^{13}C-NMR was not obtained due to the poor stability of the sample.

MS (ESI): m/z 341.1743 ($[M+H]^+$, 100%).

5.47b: Yield: 58%. ^{1}H-NMR with broad peaks was obtained. ^{13}C-NMR was not obtained due to the poor stability of the sample.

MS (ESI): m/z 341.1741 ($[M+H]^+$, 100%)

7.6.11 Nitrons 5.52, 5.53,5.54 and 5.55.

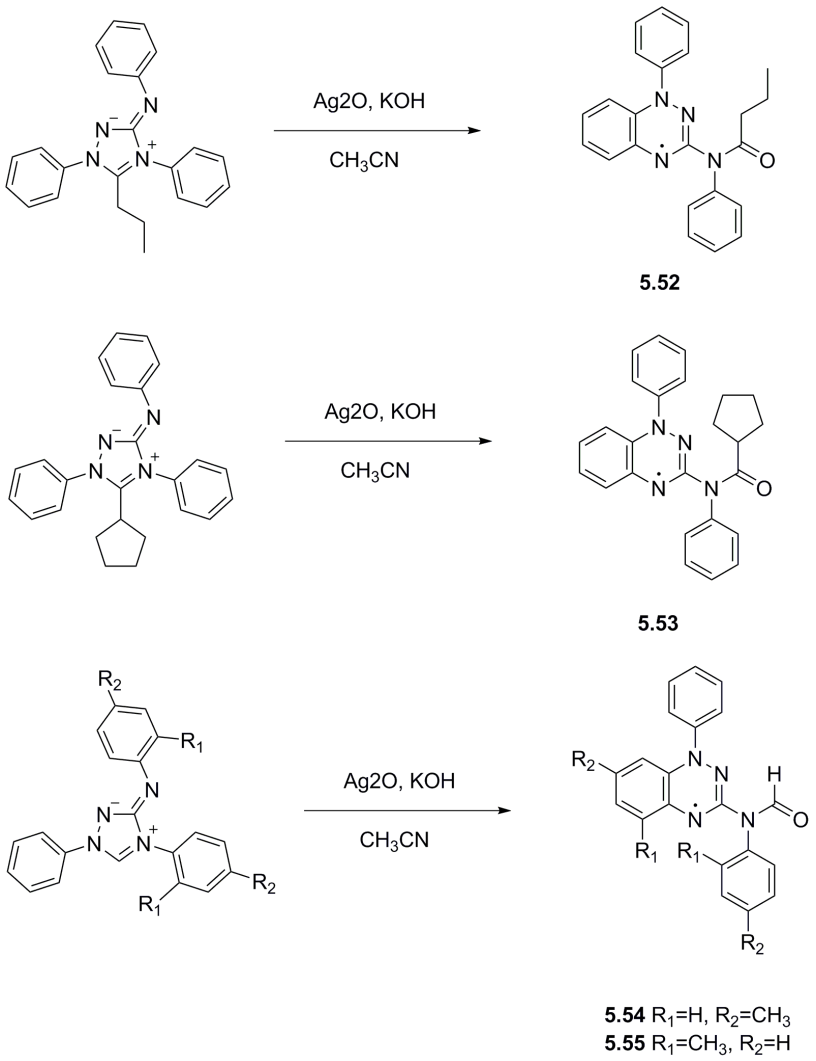

Figure 7.66 Preparation of Blatter-type radicals **5.52**, **5.53**, **5.54** and **5.55**.

All the preparation of Blatter's type radicals (**5.52**, **5.53**, **5.54** and **5.55**) were carried out following the procedure described below with the synthesis of **5.52** acting as a representative procedure. To a solution of 1,2,4-triazolium hydroxide **5.29** (0.3 mmol) in acetonitrile (20 ml), silver dioxide (75 mg, 0.3 mmol) and a aqueous KOH solution (0.5 M, 100µl) were added. The mixture was stirred at room temperature overnight. Then the mixture was filtered, solvent was removed under reduced pressure, the residue was purified by column chromatography ($CHCl_3$: MeOH = 30 : 1, Rf = 0.3).

5.52: Yield: 42%. MS (ESI): m/z 370.1771 ($[M+H]^+$, 100%).

EPR: a_{N1} = 8.05 G, a_{N2}= 4.98 G, a_{N3} = 4.76 G

Analysis for $C_{23}H_{21}N_4O$. Calcd (%): C 74.77 H 5.73 N 15.17; found: C 74.53 H 5.90 N 14.95.

5.53: Yield: 46%. MS (ESI): m/z 419.1834. ($[M+Na]^+$, 100%).

EPR: a_{N1} = 8.12 G, a_{N2}= 4.93 G, a_{N3} = 4.61 G

Analysis for C_{25}H23N4O. Calcd (%): C 75.93 H 5.86 N 14.17; found: C 75.77 H 5.45 N 13.89.

5.54: Yield: 67%. MS (ESI): m/z 356.1633 ($[M+H]^+$, 100%).

EPR: a_{N1} = 7.87 G, a_{N2}= 4.67 G, a_{N3} = 4.52 G

Analysis for $C_{22}H_{19}N_4O$. Calcd (%): C 74.35 H 5.39 N 15.76; found: C 73.87 H 5.41 N 15.70.

5.55: Yield: 62%. MS (ESI): m/z 356.1638 ($[M+H]^+$, 100%).

EPR: a_{N1} = 7.92 G, a_{N2}= 4.74 G, a_{N3} = 4.71 G

Analysis for $C_{22}H_{19}N_4O$. Calcd (%):C 74.35 H 5.39 N 15.76; found: C 74.47 H 5.41 N 15.69.

List of abbreviations

LC	Liquid crystal
Cr	Crystal
Iso	Isotropic
N	Nematic
SmC	Smectic C
SmA	Smectic A
Col_h	Columnar hexagonal
Col_r	Columnar rectangular
h	Hour
min	Minute
s	Second
TLC	Thin-layer chromatography
DCM	Dichloromethane
THF	Tetrahydrofuran
G	Gauss
Ar	Aromatic ring
ESI	Electrospray ionization
MALDI	Matrix-assisted laser desorption/ionization
n-BuLi	n-Butyllithium
DMF	Dimethylformamide

References

(1) Collings P. J.; Hird M. *Introduction to Liquid Crystals Chemistry and Physics*; Taylor & Francis Ltd, 1997.

(2) Chandrasekhar, S.; Sadashiva, B. K.; Suresh, K. A. *Pramana - J Phys* **1977**, *9*, 471.

(3) Kumar, S. *Chemistry of Discotic Liquid Crystals: From Monomers to Polymers*; Taylor & Francis Group, 2011.

(4) Nozary, H.; Piguet, C.; Rivera, J.-P.; Tissot, P.; Morgantini, P.-Y.; Weber, J.; Bernardinelli, G.; Bünzli, J.-C. G.; Deschenaux, R.; Donnio, B.; Guillon, D. *Chem. Mater.* **2002**, *14*, 1075.

(5) Blunk, D.; Praef, K.; Vill, V. *Hankbook of Liquid Crystals*; Wiley-VCH 1998.

(6) Cullity, B. D.; Graham, C. D. *Introduction to Magnetic Materials*; A JOHN WILEY & SONS, INC, 2009.

(7) Serrette, A.; Carroll, P. J.; Swager, T. M. *J. Am. Chem. Soc.* **1992**, *114*, 1887.

(8) Yuvaraj, A. R.; Yam, W. S.; Chan, T. N.; Goh, Y. P.; Hegde, G. *Spectrochimica Acta Part a-Molecular and Biomolecular Spectroscopy* **2015**, *135*, 1115.

(9) Tamura, R.; Uchida, Y.; Ikuma, N. *J. Mater. Chem.* **2008**, *18*, 2872.

(10) Kim, J.; Han, J. I. *Electronic Materials Letters* **2014**, *10*, 607.

(11) Giroudgodquin, A. M.; Latour, J. M.; Marchon, J. C. *Inorg Chem* **1985**, *24*, 4452.

(12) Ikuma, N.; Tamura, R.; Shimono, S.; Kawame, N.; Tamada, O.; Sakai, N.; Yamauchi, J.; Yamamoto, Y. *Angew. Chem. Int. Ed.* **2004**, *43*, 3677.

(13) Binnemans, K.; Galyametdinov, Y. G.; Van Deun, R.; Bruce, D. W.; Collinson, S. R.; Polishchuk, A. P.; Bikchantaev, I.; Haase, W.; Prosvirin, A. V.; Tinchurina, L.; Litvinov, I.; Gubajdullin, A.; Rakhmatullin, A.; Uytterhoeven, K.; Van Meervelt, L. *J. Am. Chem. Soc.* **2000**, *122*, 4335.

(14) Simon, J.; Sirlin, C. *Pure Appl. Chem.* **1989**, *61*, 1625.

(15) Ohta, K.; Watanabe, T.; Tanaka, S.; Fujimoto, T.; Yamamoto, I.; Bassoul, P.; Kucharczyk, N.; Simon, J. *Liq. Cryst.* **1991**, *10*, 357.

(16) Marcos, M.; Romero, P.; Serrano, J. L. *Chem. Mater.* **1990**, *2*, 495.

(17) Hudson, S. A.; Maitlis, P. M. *Chem. Rev.* **1993**, *93*, 861.

(18) Espinet, P.; Esteruelas, M. A.; Oro, L. A.; Serrano, J. L.; Sola, E. *Coord. Chem. Rev.* **1992**, *117*, 215.

(19) Giroud-Godquin, A.-M.; Maitlis, P. M. *Angew. Chem. Int. Ed. Engl.* **1991**, *30*, 375.

(20) Giroud-Godquin, A. M.; Latour, J. M.; Marchon, J. C. *Inorg Chem* **1985**, *24*, 4452.

(21) Andre, J. J.; Bernard, M.; Piechocki, C.; Simon, J. *J. Phys. Chem* **1986**, *90*, 1327.

(22) Galyametdinov, Y.; Ivanova, G.; Griesar, K.; Prosvirin, A.; Ovchinnikov, I.; Haase, W. *Adv. Mater.* **1992**, *4*, 739.

(23) Gehring, S.; Fleischhauer, P.; Haase, W.; Dietrich, M.; Witzel, H. *Biol. Chem. Hoppe-Seyler* **1990**, *371*, 786.

(24) Dvolaitzky, M.; Billard, J.; Poldy, F. *Tetrahedron* **1976**, *32*, 1835.

(25) Allgaier, J.; Finkelmann, H. *Macromol. Chem. Phys.* **1994**, *195*, 1017.

(26) Dvolaitzky, M.; Taupin, C.; Poldy, F. *Tetrahedron Lett* **1975**, 1469.

(27) Nakatsuji, S. i.; Mizumoto, M.; Ikemoto, H.; Akutsu, H.; Yamada, J.-i. *Eur. J. Org. Chem.* **2002**, *2002*, 1912.

(28) Yelamaggad, C. V.; Achalkumar, A. S.; Rao, D. S. S.; Nobusawa, M.; Akutsu, H.; Yamada, J.-i.; Nakatsuji, S. i. *J. Mater. Chem.* **2008**, *18*, 3433.

(29) Ikuma, N.; Tamura, R.; Masaki, K.; Uchida, Y.; Shimono, S.; Yamauchi, J.; Aoki, Y.; Nohira, H. *Ferroelectrics* **2006**, *343*, 119.

(30) Ikuma, N.; Tamura, R.; Shimono, S.; Uchida, Y.; Masaki, K.; Yamauchi, J.; Aoki, Y.; Nohira, H. *Adv. Mater.* **2006**, *18*, 477.

(31) Noda, Y.; Shimono, S.; Baba, M.; Yamauchi, J.; Ikuma, N.; Tamura, R. *J. Phys. Chem. B* **2006**, *110*, 23683.

(32) Uchida, Y.; Tamura, R.; Ikuma, N.; Shimono, S.; Yamauchi, J.; Aoki, Y.; Nohira, H. *Mol. Cryst. Liq. Cryst.* **2007**, *479*, 213/[1251].

(33) Uchida, Y.; Ikuma, N.; Tamura, R.; Shimono, S.; Noda, Y.; Yamauchi, J.; Aoki, Y.; Nohira, H. *J. Mater. Chem.* **2008**, *18*, 2950.

(34) Castellanos, S.; López-Calahorra, F.; Brillas, E.; Juliá, L.; Velasco, D. *Angew. Chem. Int. Ed.* **2009**, *48*, 6516.

(35) Uchida, Y.; Suzuki, K.; Tamura, R.; Ikuma, N.; Shimono, S.; Noda, Y.; Yamauchi, J. *J. Am.*

Chem. Soc. **2010**, *132*, 9746.

(36) An, Z. W.; Zheng, M. Y.; Wei, Y. S.; Li, J. L. *Mol. Cryst. Liq. Cryst.* **2012**, *557*, 28.

(37) Uchida, Y.; Suzuki, K.; Tamura, R. *J. Phys. Chem. B* **2012**, *116*, 9791.

(38) Jankowiak, A.; Pociecha, D.; Szczytko, J.; Monobe, H.; Kaszyński, P. *J. Am. Chem. Soc.* **2012**, *134*, 2465.

(39) Barmatov, E.; Grande, S.; Filippov, A.; Barmatova, M.; Kremer, F.; Shibaev, V. *Macromol. Chem. Phys.* **2000**, *201*, 2603.

(40) Filippov, A. P. *J. Opt. Technol.* **2001**, *68*, 700.

(41) Corvaja, C. *Electron Paramagnetic Resonance: A Practitioner's Toolkit*; A John Wiley & Sons, Inc., 2009.

(42) Weil, J. A.; Bolton, J. R. *Electron Paramagnetic Resonance: Elementary Theory and Practical Applications*; A John Wiley & Sons, Inc., 2007.

(43) Griffith, O. H.; Cornell, D. W.; McConnell, H. M. *J. Chem. Phys* **1965**, *43*, 2909.

(44) Piloty, O.; Schwerin, B. G. *Ber Dtsch Chem Ges* **1901**, *34*, 1870.

(45) Lebedev, O. L.; Khidekel, M. L.; Razuvaev, G. A. *Doklady Akademii Nauk Sssr* **1961**, *140*, 1327.

(46) Aurich, H. G.; Hahn, K.; Stork, K.; Weiss, W. *Tetrahedron* **1977**, *33*, 969.

(47) Einhorn, J.; Einhorn, C.; Ratajczak, F.; Durif, A.; Averbuch, M.-T.; Pierre, J.-L. *Tetrahedron Lett* **1998**, *39*, 2565.

(48) Blinco, J. P.; Hodgson, J. L.; Morrow, B. J.; Walker, J. R.; Will, G. D.; Coote, M. L.; Bottle, S. E. *J. Org. Chem.* **2008**, *73*, 6763.

(49) Hamilton, B. H.; Cardon, T. B.; Lorigan, G. A.; Ziegler, C. J. *Dalton Trans.* **2005**, 2941.

(50) Sümmermann, W.; Deffner, U. *Tetrahedron* **1975**, *31*, 593.

(51) Gomberg, M. *J. Am. Chem. Soc.* **1900**, *22*, 757.

(52) Neumann, W. P.; Uzick, W.; Zarkadis, A. K. *J. Am. Chem. Soc.* **1986**, *108*, 3762.

(53) Armet, O.; Veciana, J.; Rovira, C.; Riera, J.; Castaner, J.; Molins, E.; Rius, J.; Miravitlles, C.; Olivella, S.; Brichfeus, J. *J. Phys. Chem* **1987**, *91*, 5608.

(54) Guasch, J.; Grisanti, L.; Souto, M.; Lloveras, V.; Vidal-Gancedo, J.; Ratera, I.; Painelli, A.; Rovira, C.; Veciana, J. *J. Am. Chem. Soc.* **2013**, *135*, 6958.

(55) Mesa, J. A.; Velázquez-Palenzuela, A.; Brillas, E.; Coll, J.; Torres, J. L.; Juliá, L. *J. Org.*

Chem. **2011**, *77*, 1081.

(56) Katritzky, A. R.; Yang, B.; Dalal, N. S. *J. Org. Chem.* **1998**, *63*, 1467.

(57) Katritzky, A. R.; Yang, B.; Pleynet, D. P. M. *J. Org. Chem.* **1998**, *63*, 9992.

(58) Kuhn, R.; Trischmann, H. *Angew. Chem. Int. Ed. Engl.* **1963**, *2*, 155.

(59) Neugebauer, F. A.; Fischer, H.; Siegel, R. *Chem. Ber.* **1988**, *121*, 815.

(60) Jankowiak, A.; Pociecha, D.; Szczytko, J.; Monobe, H.; Kaszynski, P. *J. Mater. Chem. C* **2014**.

(61) Jankowiak, A.; Pociecha, D.; Szczytko, J.; Monobe, H.; Kaszyński, P. *Liq. Cryst.* **2013**, *41*, 385.

(62) Jankowiak, A.; Pociecha, D.; Szczytko, J.; Monobe, H.; Kaszynski, P. *J. Mater. Chem. C* **2014**, *2*, 319.

(63) Jankowiak, A.; Pociecha, D.; Monobe, H.; Szczytko, J.; Dębska, Ż.; Romański, J.; Kaszyński, P. *Phosphorus, Sulfur Silicon Relat. Elem.* **2012**, *188*, 418.

(64) Blatter, H. M.; Lukaszew.H *Tetrahedron Lett* **1968**, 2701.

(65) Vorlander, D. *Ber Dtsch Chem Ges* **1929**, *62*, 2831.

(66) Takezoe, H.; Takanishi, Y. *Jpn. J. Appl. Phys., Part 1* **2006**, *45*, 597.

(67) Sathyanarayana, P.; Radhika, S.; Sadashiva, B. K.; Dhara, S. *Soft Matter* **2012**, *8*, 2322.

(68) Cioanca, E.-R.; Epure, E. L.; Carlescu, I.; Lisa, G.; Wilson, D.; Hurduc, N.; Scutaru, D. *Mol. Cryst. Liq. Cryst.* **2011**, *537*, 51.

(69) Gimeno, N.; Martin-Rapun, R.; Rodriguez-Conde, S.; Serrano, J. L.; Folcia, C. L.; Pericas, M. A.; Ros, M. B. *J. Mater. Chem.* **2012**, *22*, 16791.

(70) Conte, G.; Cristiano, R.; Ely, F.; Gallardo, H. *Synth. Commun.* **2006**, *36*, 951.

(71) Dingemans, T. J.; Murthy, N. S.; Samulski, E. T. *J. Phys. Chem. B* **2001**, *105*, 8845.

(72) W., T. C.; Morten, M. In *Peptides: The Wave of the Future*; Houghten, R. A., Lebl, M., Eds.; American Peptide Society and Kluwer Academic Publishers; San Diego: 2002, p 263.

(73) Tornøe, C. W.; Christensen, C.; Meldal, M. *J. Org. Chem.* **2002**, *67*, 3057.

(74) Rostovtsev, V. V.; Green, L. G.; Fokin, V. V.; Sharpless, K. B. *Angew. Chem. Int. Ed.* **2002**, *41*, 2596.

(75) Gallardo, H.; Ely, F.; Bortoluzzi, A. J.; Conte, G. *Liq. Cryst.* **2005**, *32*, 667.

(76) Srividhya, D.; Manjunathan, S.; Thirumaran, S.; Saravanan, C.; Senthil, S. *J. Mol. Struct.*

2009, *927*, 7.

(77) Bilski, P.; Hideg, K.; Kálai, T.; Bilska, M. A.; Chignell, C. F. *Free Radical Biol. Med.* **2003**, *34*, 489.

(78) Hideg, É.; Kálai, T.; Hideg, K.; Vass, I. *Biochemistry* **1998**, *37*, 11405.

(79) Kalai, T.; Hubbell, W. L.; Hideg, K. *Synthesis-Stuttgart* **2009**, 1336.

(80) Ho, M.-S.; Hsu, C.-S. *Liq. Cryst.* **2010**, *37*, 293.

(81) Misharin, A. Y.; Bushmakina, N. G. *Synthesis-Stuttgart* **1985**, 656.

(82) Ding, P.; Wunnicke, D.; Steinhoff, H.-J.; Seela, F. *Chem. Eur. J.* **2010**, *16*, 14385.

(83) Kálai, T.; Fleissner, M. R.; Jekő, J.; Hubbell, W. L.; Hideg, K. *Tetrahedron Lett* **2011**, *52*, 2747.

(84) Hein, J. E.; Fokin, V. V. *Chem. Soc. Rev.* **2010**, *39*, 1302.

(85) Conte, G.; Ely, F.; Gallardo, H. *Liq. Cryst.* **2005**, *32*, 1213.

(86) Nordio, P. L.; Busolin, P. *J Chem Phys* **1971**, *55*, 5485.

(87) Chami, F.; Wilson, M. R.; Oganesyan, V. S. *Soft Matter* **2012**, *8*, 6823.

(88) Tiberio, G.; Muccioli, L.; Berardi, R.; Zannoni, C. *ChemPhysChem* **2009**, *10*, 125.

(89) Zhang, J.; Su, J.; Guo, H. *J. Phys. Chem. B* **2011**, *115*, 2214.

(90) Arcioni, A.; Bacchiocchi, C.; Vecchi, I.; Venditti, G.; Zannoni, C. *Chem. Phys. Lett.* **2004**, *396*, 433.

(91) Luckhurst, G. R. *Royal Institute of Chemistry, Reviews* **1970**, *3*, 61.

(92) Gomez, S. L.; Lenart, V. M.; Bechtold, I. H.; Figueiredo Neto, A. M. *Braz. J. Phys* **2012**, *42*, 355.

(93) De Sousa, F. A.; Michels, R. N.; Cardoso, P. M. M.; De Jesus, M. M. A. *Mol. Cryst. Liq. Cryst.* **2013**, *576*, 106.

(94) Rabenstein, M. D.; Shin, Y. K. *Proc. Natl. Acad. Sci.* **1995**, *92*, 8239.

(95) Misra, S. K.; Freed, J. H. In *Multifrequency Electron Paramagnetic Resonance*; Wiley-VCH Verlag GmbH & Co. KGaA: 2011, p 545.

(96) Osiecki, J. H.; Ullman, E. F. *J. Am. Chem. Soc.* **1968**, *90*, 1078.

(97) Wagner, B. E.; Linowski, J. W.; Potenza, J. A.; Bates, R. D.; Helbert, J. N.; Poindexter, E. H. *J. Am. Chem. Soc.* **1976**, *98*, 4405.

(98) Caneschi, A.; Gatteschi, D.; Laugier, J.; Rey, P.; Sessoli, R. *Inorg Chem* **1988**, *27*, 1553.

(99) Benelli, C.; Caneschi, A.; Gatteschi, D.; Guillou, O.; Pardi, L.; Rey, P. *Inorg. Chim. Acta* **1989**, *160*, 1.

(100) Takahashi, M.; Turek, P.; Nakazawa, Y.; Tamura, M.; Nozawa, K.; Shiomi, D.; Ishikawa, M.; Kinoshita, M. *Phys. Rev. Lett.* **1991**, *67*, 746.

(101) Greve, S.; Vill, V.; Friedrichsen, W. *Z Naturforsch B* **2002**, *57*, 677.

(102) Nakatsuji, S. i.; Ikemoto, H.; Akutsu, H.; Yamada, J.-i.; Mori, A. *J. Org. Chem.* **2003**, *68*, 1708.

(103) Ullman, E. F.; Osiecki, J. H.; Boocock, D. G. B.; Darcy, R. *J. Am. Chem. Soc.* **1972**, *94*, 7049.

(104) Hirel, C.; Vostrikova, K. E.; Pécaut, J.; Ovcharenko, V. I.; Rey, P. *Chem. Eur. J.* **2001**, *7*, 2007.

(105) Caneschi, A.; Gatteschi, D.; Rey, P. *Prog. Inorg. Chem.* **1991**, *39*, 331.

(106) Zhao, M.; Liu, J.; Wang, C.; Wang, L.; Liu, H.; Peng, S. *J Med Chem* **2005**, *48*, 4285.

(107) Ullman, E. F.; Call, L.; Osiecki, J. H. *J. Org. Chem.* **1970**, *35*, 3623.

(108) Harada, G.; Jin, T.; Izuoka, A.; Matsushita, M. M.; Sugawara, T. *Tetrahedron Lett* **2003**, *44*, 4415.

(109) Shimono, S.; Tamura, R.; Ikuma, N.; Takimoto, T.; Kawame, N.; Tamada, O.; Sakai, N.; Matsuura, H.; Yamauchi, J. *J. Org. Chem.* **2003**, *69*, 475.

(110) Perkins, M. J. *Annu. Rep. Prog. Chem. Sect. B: Org. Chem* **1968**, *65*, 171.

(111) Huisgen, R.; Wulff, J. *Chem Ber-Recl* **1969**, *102*, 1848.

(112) Gilchrist, T. L.; Harris, C. J.; Rees, C. W. *J Chem Soc Chem Comm* **1974**, 485.

(113) Barton, D. H. R.; Haynes, R. K.; Leclerc, G.; Magnus, P. D.; Menzies, I. D. *J. Chem. Soc., Perkin Trans. 1* **1975**, 2055.

(114) Barton, D. H. R.; Ducker, J. W.; Lord, W. A.; Magnus, P. D. *J. Chem. Soc., Perkin Trans. 1* **1976**, 38.

(115) Buzykin, B. I.; Gazetdinova, N. G. *B Acad Sci Ussr Ch+* **1980**, *29*, 1159.

(116) Neugebauer, F. A.; Umminger, I. *Chem. Ber.* **1980**, *113*, 1205.

(117) Neugebauer, F. A.; Umminger, I. *Chem Ber-Recl* **1980**, *113*, 1205.

(118) Constantinides, C. P.; Koutentis, P. A.; Krassos, H.; Rawson, J. M.; Tasiopoulos, A. J. *J. Org. Chem.* **2011**, *76*, 2798.

(119) Mukai, K.; Inoue, K.; Achiwa, N.; Jamali, J. B.; Krieger, C.; Neugebauer, F. A. *Chem. Phys. Lett.* **1994**, *224*, 569.

(120) Constantinides, C. P.; Koutentis, P. A.; Loizou, G. *Org. Biomol. Chem.* **2011**, *9*, 3122.

(121) Yan, B.; Cramen, J.; McDonald, R.; Frank, N. L. *Chem. Commun.* **2011**, *47*, 3201.

(122) Constantinides, C. P.; Koutentis, P. A.; Rawson, J. M. *Chem. Eur. J.* **2012**, *18*, 7109.

(123) Constantinides, C. P.; Koutentis, P. A.; Rawson, J. M. *Chem. Eur. J.* **2012**, *18*, 15433.

(124) Berezin, A. A.; Zissimou, G.; Constantinides, C. P.; Beldjoudi, Y.; Rawson, J. M.; Koutentis, P. A. *J Org Chem* **2014**, *79*, 314.

(125) Morgan, I. S.; Peuronen, A.; Hanninen, M. M.; Reed, R. W.; Clerac, R.; Tuononen, H. M. *Inorg Chem* **2014**, *53*, 33.

(126) Constantinides, C. P.; Koutentis, P. A.; Krassos, H.; Rawson, J. M.; Tasiopoulos, A. J. *J Org Chem* **2011**, *76*, 2798.

(127) P. Bandgar, B.; S. Uppalla, L. *Journal of Chemical Research Synopses* **1999**, 714.

(128) Steck, E. A.; Brundage, R. P.; Fletcher, L. T. *J. Am. Chem. Soc.* **1958**, *80*, 3929.

(129) Perkin, W. H.; Rubenstein, L. *J. Chem. Soc.* **1926**, *129*, 357.

(130) Beer, R. J. S.; McGrath, L.; Robertson, A.; Woodier, A. B. *J. Chem. Soc.* **1949**, 2061.

(131) Demers, J. P.; Klaubert, D. H. *Tetrahedron Lett* **1987**, *28*, 4933.

(132) Dufresne, C.; Leblanc, Y.; Berthelette, C.; McCooeye, C. *Synth. Commun.* **1997**, *27*, 3613.

(133) Mitchell, H.; Leblanc, Y. *J. Org. Chem.* **1994**, *59*, 682.

(134) DeBergh, J. R.; Spivey, K. M.; Ready, J. M. *J. Am. Chem. Soc.* **2008**, *130*, 7828.

(135) Jankowiak, A.; Kaszynski, P. *Beilstein J Org Chem* **2012**, *8*, 275.

(136) Nakanishi, T.; Miyashita, N.; Michinobu, T.; Wakayama, Y.; Tsuruoka, T.; Ariga, K.; Kurth, D. G. *J. Am. Chem. Soc.* **2006**, *128*, 6328.

(137) Nakanishi, T.; Schmitt, W.; Michinobu, T.; Kurth, D. G.; Ariga, K. *Chem. Commun.* **2005**, 5982.

(138) Contoret, A.; Eastwood, A.; Farrar, S.; Kelly, S. m.; Nicholls, E.; O'Neill, M.; Richards, G.; Wu, C. *Mol Cryst Liq Crys A* **2001**, *368*, 271.

(139) Nowak-Król, A.; Gryko, D.; Gryko, D. T. *Chemistry – An Asian Journal* **2010**, *5*, 904.

(140) Cardinaels, T.; Ramaekers, J.; Guillon, D.; Donnio, B.; Binnemans, K. *J. Am. Chem. Soc.*

2005, *127*, 17602.

(141) Holst, H. C.; Pakula, T.; Meier, H. *Tetrahedron* **2004**, *60*, 6765.

(142) Yelamaggad, C. V.; Achalkumar, A. S.; Rao, D. S. S.; Prasad, S. K. *J. Org. Chem.* **2007**, *72*, 8308.

(143) Gubaidullin, A. T.; Buzykin, B. I.; Litvinov, I. A.; Gazetdinova, N. G. *Russ. J. Gen. Chem.* **2004**, *74*, 939.

(144) Kadirov, M. K.; Buzykin, B. I.; Gazetdinova, N. G. *Russ. Chem. Bull.* **2002**, *51*, 1796.

(145) Koutentis, P. A.; Lo Re, D. *Synthesis-Stuttgart* **2010**, 2075.

(146) Hou, W.; Dehm, N. A.; Scott, R. W. J. *J Catal* **2008**, *253*, 22.

(147) Sheldon, R. A.; Dakka, J. *Catal. Today* **1994**, *19*, 215.

(148) Tiecco, M.; Testaferri, L.; Marini, F.; Santi, C.; Bagnoli, L.; Temperini, A. *Tetrahedron* **1997**, *53*, 10591.

(149) Li, G.; Liang, Y.; Antilla, J. C. *J. Am. Chem. Soc.* **2007**, *129*, 5830.

(150) Matsumoto, T.; Kakigi, H.; Suzuki, K. *Tetrahedron Lett* **1991**, *32*, 4337.

(151) Dierking, I. *Textures of Liquid Crystals*; Wiley-VCH Verlag GmbH & Co. KGaA, 2003.

(152) Richard J. Bushby; Boden, N. In *Handbook of Liquid Crystals*; John W. Goodby, Peter J. Collings, Takashi Kato, Carsten Tschierske, Helen Gleeson, Peter Raynes, Eds.; John Wiley & Sons, Inc.: 2014.

(153) Sergeyev, S.; Pisula, W.; Geerts, Y. H. *Chem. Soc. Rev.* **2007**, *36*, 1902.

(154) Adam, D.; Schuhmacher, P.; Simmerer, J.; Haussling, L.; Siemensmeyer, K.; Etzbachi, K. H.; Ringsdorf, H.; Haarer, D. *Nature* **1994**, *371*, 141.

(155) Sergeyev, S.; Levin, J.; Balandier, J.-Y.; Pouzet, E.; Geerts, Y. H. *Mendeleev Commun.* **2009**, *19*, 185.

(156) Noda, Y.; Shimono, S.; Baba, M.; Yamauchi, J.; Uchida, Y.; Ikuma, N.; Tamura, R. *Appl Magn Reson* **2008**, *33*, 251.

(157) Constantinides, C. P.; Carter, E.; Murphy, D. M.; Manoli, M.; Leitus, G. M.; Bendikov, M.; Rawson, J. M.; Koutentis, P. A. *Chem. Commun.* **2013**, *49*, 8662.

(158) Constantinides, C. P.; Koutentis, P. A.; Rawson, J. M. *Chem-Eur J* **2012**, *18*, 15433.

(159) Constantinides, C. P.; Koutentis, P. A.; Rawson, J. M. *Chem-Eur J* **2012**, *18*, 7109.

(160) Berezin, A. A.; Constantinides, C. P.; Drouza, C.; Manoli, M.; Koutentis, P. A. *Org. Lett.*

2012, *14*, 5586.

(161) Gopee, H.; Cammidge, A. N.; Oganesyan, V. S. *Angew Chem Int Edit* **2013**, *52*, 8917.

(162) Berezin, A. A.; Constantinides, C. P.; Mirallai, S. I.; Manoli, M.; Cao, L. L.; Rawson, J. M.; Koutentis, P. A. *Org. Biomol. Chem.* **2013**, *11*, 6780.

(163) Wanzlick, H. W.; Schönherr, H. J. *Angew. Chem. Int. Ed. Engl.* **1968**, *7*, 141.

(164) Öfele, K. *J. Organomet. Chem.* **1968**, *12*, P42.

(165) Arduengo, A. J.; Harlow, R. L.; Kline, M. *J. Am. Chem. Soc.* **1991**, *113*, 361.

(166) Farber, C.; Leibold, M.; Bruhn, C.; Maurer, M.; Siemeling, U. *Chem. Commun.* **2012**, *48*, 227.

(167) Massey, R. S.; Collett, C. J.; Lindsay, A. G.; Smith, A. D.; O'Donoghue, A. C. *J. Am. Chem. Soc.* **2012**, *134*, 20421.

(168) Busch, M. *Ber Dtsch Chem Ges* **1905**, *38*, 856.

(169) Kriven'ko, A. P.; Morozova, N. A. *Russ. J. Appl. Chem.* **2006**, *79*, 506.

(170) Kumar, J. A.; Saidachary, G.; Mallesham, G.; Sridhar, B.; Jain, N.; Kalivendi, S. V.; Rao, V. J.; Raju, B. C. *Eur. J. Med. Chem* **2013**, *65*, 389.

(171) Marcos, I. S.; Moro, R. F.; Costales, I.; Basabe, P.; Díez, D.; Mollinedo, F.; Urones, J. G. *Tetrahedron* **2012**, *68*, 7932.

(172) Guo, Y.; Yan, Y.-Y.; Yang, C.; Yu, X.; Zhi, X.-Y.; Xu, H. *Bioorg. Med. Chem. Lett.* **2012**, *22*, 5384.

(173) Busch, M. *J. Praket. Chem* **1906**, *74*, 533.

(174) Augstein, J.; Green, S. M.; Monro, A. M.; Wrigley, T. I.; Katritzky, A. R.; Tiddy, G. J. T. *J Med Chem* **1967**, *10*, 391.

(175) Montilla, F.; Pastor, A.; Galindo, A. n. *J. Organomet. Chem.* **2004**, *689*, 993.

(176) Hartke, K.; Radau, M. *Arch. Pharm.* **1972**, *305*, 708.

(177) Zhang, W.-X.; Nishiura, M.; Hou, Z. *Chem. Eur. J.* **2007**, *13*, 4037.

(178) Lachs, J. R.; Barrett, A. G. M.; Crimmin, M. R.; Kociok-Köhn, G.; Hill, M. S.; Mahon, M. F.; Procopiou, P. A. *Eur J Inorg Chem* **2008**, *2008*, 4173.

(179) Li, Q.; Wang, S.; Zhou, S.; Yang, G.; Zhu, X.; Liu, Y. *J. Org. Chem.* **2007**, *72*, 6763.

(180) Du, Z.; Li, W.; Zhu, X.; Xu, F.; Shen, Q. *J. Org. Chem.* **2008**, *73*, 8966.

(181) Zhu, X.; Du, Z.; Xu, F.; Shen, Q. *J. Org. Chem.* **2009**, *74*, 6347.

(182) Ong, T.-G.; O'Brien, J. S.; Korobkov, I.; Richeson, D. S. *Organometallics* **2006**, *25*, 4728.

(183) Alonso-Moreno, C.; Carrillo-Hermosilla, F.; Garcés, A. s.; Otero, A.; López-Solera, I.; Rodríguez, A. M.; Antiñolo, A. *Organometallics* **2010**, *29*, 2789.

(184) Koller, J. r.; Bergman, R. G. *Organometallics* **2010**, *29*, 5946.

(185) Ong, T.-G.; Yap, G. P. A.; Richeson, D. S. *J. Am. Chem. Soc.* **2003**, *125*, 8100.

(186) Schweizer, P. D.; Wadepohl, H.; Gade, L. H. *Organometallics* **2013**, *32*, 3697.

(187) Byrkit, G. D.; Michalek, G. A. *Ind. Eng. Chem.* **1950**, *42*, 1862.

(188) Kutsumizu, S.; Mori, H.; Fukatami, M.; Naito, S.; Sakajiri, K.; Saito, K. *Chem. Mater.* **2008**, *20*, 3675.

(189) Alvarez, S. G.; Alvarez, M. T. *Synthesis-Stuttgart* **1997**, 413.

(190) Zhao, M.; Liu, J. L.; Wang, C.; Wang, L. L.; Liu, H.; Peng, S. Q. *J Med Chem* **2005**, *48*, 4285.

(191) Zhao, M.; Li, Z.; Peng, L.; Tang, Y. R.; Wang, C.; Zhang, Z. D.; Peng, S. Q. *Biorg. Med. Chem.* **2007**, *15*, 2815.

(192) Klein, C.; Baranoff, E.; Nazeeruddin, M. K.; Grätzel, M. *Tetrahedron Lett* **2010**, *51*, 6161.

(193) Van Nostrum, C. F.; Picken, S. J.; Nolte, R. J. M. *Angew. Chem.* **1994**, *106*, 2298.

(194) Ravindran, J.; Subbaraju, G. V.; Ramani, M. V.; Sung, B.; Aggarwal, B. B. *Biochem. Pharmacol.* **2010**, *79*, 1658.

(195) Achalkumar, A. S.; Yelamaggad, C. V. *Tetrahedron Lett* **2012**, *53*, 7108.

(196) Steinke, N.; Frey, W.; Baro, A.; Laschat, S.; Drees, C.; Nimtz, M.; Hägele, C.; Giesselmann, F. *Chem. Eur. J.* **2006**, *12*, 1026.

(197) Jankowiak, A.; Kaszyńsk, P. *Beilstein J. Org. Chem.* **2012**, *8*, 275.